Contents

Chapter 1

Spatial beam structures

1.1 Beam axis and cross section definition

[1] A necessary condition for identifying a portion of deformable body as a beam – and hence applying the associated framework – is that its centroidal curve is at least loosely recognizable.

Once such centroidal line has been roughly defined, locally perpendicular planes may be derived whose intersection with the body itself defines the local beam cross section. Then, the G centroid position may be computed for each of the local cross sections, thus defining a second, refined centroidal line. A potentially iterative definition for the beam centroidal axis[2] is hence obtained. A rather arbitrary orientation may then be chosen for the centroidal curve.

A *local* cross-sectional reference system may be defined by aligning the normal z axis with the oriented centroidal curve, and by employing as the first in-section axis, namely x, the projection onto the cross-section plane of a given global $\hat{v}$ vector, that is assumed to be not parallel to the beam axis. The remaining in-section axis y is then derived, in order to obtain a local $Gxyz$ right-handed coordinate system, whose unit vectors are $\hat{\imath}, \hat{\jmath}, \hat{k}$.

Such construction of the local reference system for the beam branch is consistent with most the Finite Element (fe) codes.

If a thin walled profile is considered in place of a solid cross section member – i.e., the section wall midplane is recognizable too (see paragraph 2.1.1 below), then a curvilinear coordinate s may be defined that spans the in-cross-section wall midplane. Such in-cross-section wall midplane consists in a possibly multi-branched curve, which is parametrically defined by a pair of $x(s), y(s)$ functions, with s spanning the conventional $[0, l]$ interval.

In the case material is homogeneous along the wall thickness, the local thickness value $t(s)$ is some relevance, along with a local through-wall-thickness coordinate $r \in [-t(s)/2, +t(s)/2]$.

Such s, r, in-section coordinates based on the profile wall may be employed in place of their cartesian x, y counterparts, if favourable.

[2] here, centroidal curve, centroidal line, centroidal axis, or simply beam axis are treated as synonyms.

1.2 Joints and angular points

Beam axis may be discontinuous at sudden body geometry changes; a rigid body connection is ideally assumed to restrict the relative motion of the proximal segments.

Such rigid joint modeling may be extended to more complex n-way joints; if the joint finite stiffness is to be taken into account, it has to be described through the entries of a rank $6(n-1)$ symmetric square matrix [3].

At joints and at the beam axis angular points the cylindrical bodies obtained by sweeping the cross sections along the centroidal curve branches do usually overlap, and in general they only loosely mimic the actual deformable body geometry.

The results obtained through the local application of the elementary beam theory are of a problematic nature; they may at most be employed to scale the triaxial local stress/strain fields[4] that are evaluated resorting to more complex modelings.

1.3 Cross-sectional resultants for the spatial beam

The beam may be notionally split at any point along the axis, thus obtaining two facing cross sections, whose interaction is limited to three components of interfacial stresses, namely the axial normal stress σ_z and the two shear components τ_{yz}, τ_{zx}.

Three force resultant components may be defined by integration along the cross section area, namely the axial (normal) force, the y-

[3] i.e., joint stiffness is unfortunately not a scalar value.

[4] The peak stress values obtained through the elementary beam theory may be profitably employed as *nominal stresses* within the stress concentration effect framework.

and the x- oriented shear forces, respectively defined as

$$N = \int_{\mathcal{A}} \sigma_{zz} d\mathcal{A}$$
$$Q_y = \int_{\mathcal{A}} \tau_{yz} d\mathcal{A}$$
$$Q_x = \int_{\mathcal{A}} \tau_{zx} d\mathcal{A}$$

Three moment resultant components may be similarly defined, namely the x- and y- oriented bending moments, and the torsional moment. However, if the centroid is the preferred fulcrum for evaluating the bending moments, the below discussed C shear center is employed for evaluating the torsional moment; the two points might coincide, e.g. if the cross section is twice symmetric, but they are distinct in general. We hence define

$$M_x \equiv M_{(G,x)} = \int_{\mathcal{A}} \sigma_z y d\mathcal{A}$$
$$M_y \equiv M_{(G,y)} = -\int_{\mathcal{A}} \sigma_z x d\mathcal{A}$$
$$M_t \equiv M_{(C,z)} = \int_{\mathcal{A}} \left[\tau_{yz}(x - x_C) - \tau_{zx}(y - y_C)\right] d\mathcal{A}$$

The applied vector associated to the normal force component $(G, N\hat{k})$ is located at the section centroid , whereas the shear force $(C, Q_x\hat{\imath}+Q_y\hat{\jmath})$ is supposed to act at the shear center; such convention decouples the energy contribution of force and moment components for the straight beam.

Common alternative names for such resultants are *component of internal action*, *(beam) generalized stress components* etc.; they may also be interpreted as the reactions of an internal clamp constraint that joins the upstream and downstream portions of the structure, notionally severed at the cross section under scrutiny.

Most of the sign rules for the resultant force and moment components introduced for the plane problem lose their significance in the spatial realm.

The following convention is proposed for the few cases in which a sign characterization for the stress resultant components is required,

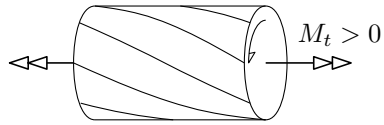

Figure 1.1: Right helix deformation of a cylinder subject to a conventionally positive torsional moment.

which originates from the definition of the local reference system, which in turn derives from the oriented nature of the beam branch, and from the $\hat{v}$ orientation vector, as discussed above; such rule is widely employed by FE codes.

Let's consider to the beam segment of Fig. 1.2 (a) and (b): positive resultant components adopt the direction of the associated local axis at the beam segment end that shows an outward-oriented local z axis; at beam segment ends characterized by an inward-oriented local z axis, the same positive stress resultant components are opposite to the respective local axes.

According to such a rule, axial load is positive if tractive, and the torsional moment is positive if deflects into a right helix a line traced parallel to the axis on the undeformed profile, see Fig. 1.1. No intuitive formulations are however available for the bending moment and shear components.

Cross section resultants may be obtained, based on equilibrium for a statically determinate structure. The ordinary procedure consists in

- notionally splitting the structure at the cross section whose resultants are under scrutiny;
- isolating a portion of the structure that ends at the cut, whose locally applied loads are all known; the structure has to be preliminarily solved for the all the constraint reactions that act on the isolated portion;
- setting the equilibrium equations for the isolated substructure, according to which the cross-sectional resultants are in equilibrium with all the loads locally applied to the isolated portion.

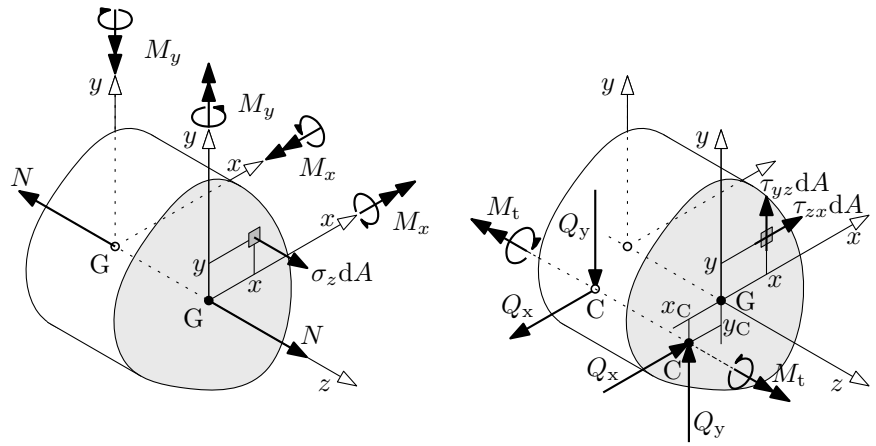

Figure 1.2: Stress resultants for the beam segment and the associated sign convention; for the sake of readability, symmetric and skew-symmetric components are split apart in Figure. Please remind that – even if visually applied at notable locations – the moment components have no definite application point within the cross section.

1.4 A worked example

The present paragraph is devoted to the evaluation of the stress resultants along the BD beam segment[5] of the simple structure of Figure 1.3c, which mimics from within the spatial beam framework boundaries the deformable body of Figure 1.3a.

The assumed distribution for the shear stress components τ_{zx} and τ_{yz} along the C-section thin wall, which is derived from a generalized application of the Jourawsky shear theory, locates its resultants in a shear center C which is external to the cross section convex envelope, as shown in Fig. 1.3b.

The shear center locus is represented in Fig. 1.3c as a dotted line, wherever distinct from the centroidal line.

The l distance from the B corner parametrically pinpoints a section along the BD segment, in correspondence of which the stress resultant components are evaluated.

[5]The more straightforward treatise of the AB segment is left to the reader; results will be here reported for discussion.

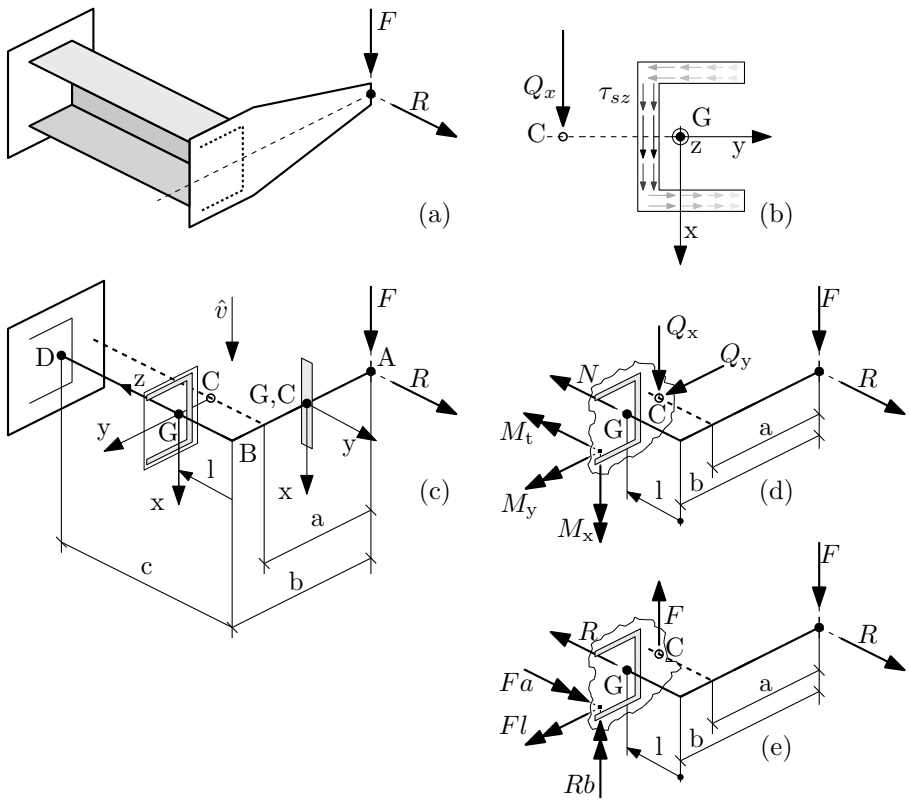

Figure 1.3: A planar beam structure, loaded both in-plane and out of plane. Please note that the plane the structure lies on is a symmetry plane for the material and for the constraints; the applied load may hence be decomposed into symmetric and skew-symmetric parts, leading to two uncoupled problems. A general spatial structure may be derived e.g. by turning the C-profile 90° on its axis.

The structure is then notionally partitioned in two substructures, and the portion spanning from the section under scrutiny to the free end is elected for further equilibrium analysis. Equilibrium equations for the other portion would involve the preliminary evaluation of the six constraint reaction components at D, based on global equilibrium.

Figure 1.3d collects the loads applied to such isolated substructure, including the six components of internal action at the section under scrutiny; the following equilibrium equations are set:

- translational equilibrium along the local x axis, namely

$$\mathrm{tx}: \ + F + Q_{\mathrm{x}} = 0;$$

- translational equilibrium along the local y axis, namely

$$\mathrm{ty}: \ + Q_{\mathrm{y}} = 0;$$

- translational equilibrium along the local z axis, namely

$$\mathrm{tz}: \ - R + N = 0;$$

- rotational equilibrium with respect to the centroidal, x-aligned axis, namely

$$\mathrm{rGx}: \ + Rb + M_{\mathrm{x}} = 0;$$

.

- rotational equilibrium with respect to the centroidal, y-aligned axis, namely

$$\mathrm{rGy}: \ - Fl + M_{\mathrm{y}} = 0;$$

.

- rotational equilibrium with respect to z-aligned axis passing through the shear center, namely

$$\mathrm{rCz}: \ + Fa + M_{\mathrm{t}} = 0;$$

from which the stress resultants may be trivially obtained.

The meditated choice for the rotational equilibrium axis makes the arm of the possibly unknown axial and shear forces vanish, thus decoupling the equations.

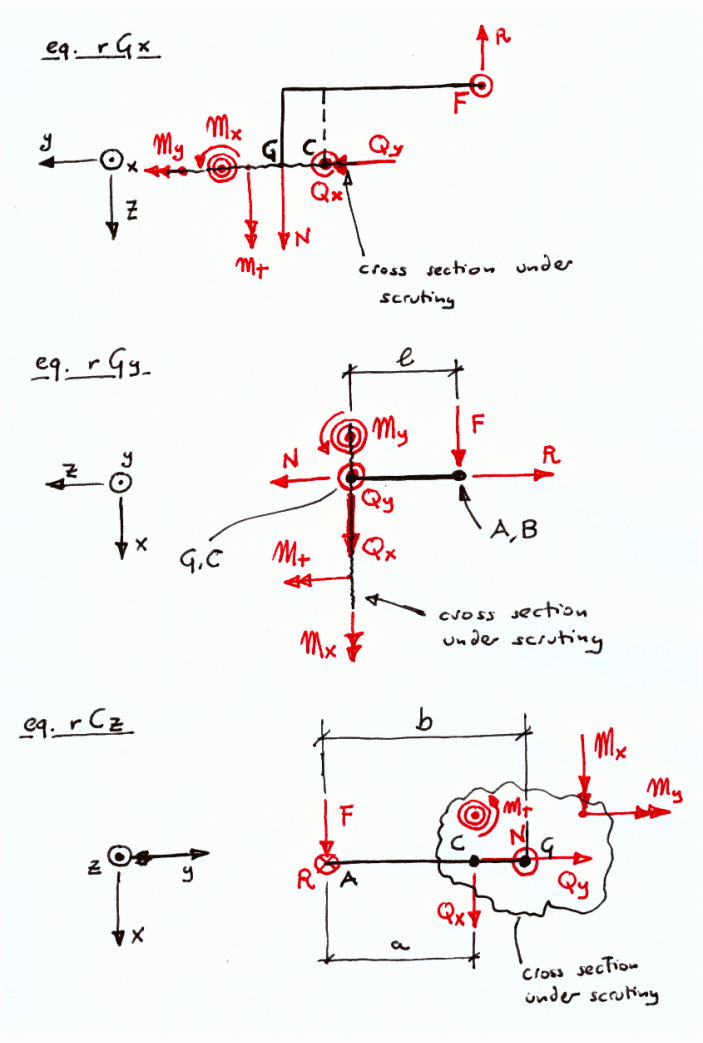

Figure 1.4: Projected views useful for discussing the isolated substructure rotational equilibrium. TODO.

Also, it is suggested to analyze the contributions to the rotational equilibrium with respect to a given axis by resorting to a projected view of the isolated substructure in which such axis is aligned with the line of sight[6], see Figure 1.4; the information lost in the projection are in fact of null relevance for the rotational equilibrium under scrutiny.

Figure 1.3e depicts the equilibrium state of the isolated substructure, and the visual comparison with its 1.3d counterpart offers an overview for the components of internal action.

Even if the described procedure is of general application within the spatial beam realm, the simple structure discussed exhibits elastic domain symmetry with respect to the plane the two centroidal segments lie on, a non-general property this, which is also respected by the specific constraints.

Such a peculiarity, along with the assumed linearity of the structure response, allows for the decomposition of the problem into a symmetric part, and into a skew-symmetric part. The symmetric portion of the applied load is embodied by the R force, whereas the skew-symmetric load portion is embodied by F.

Abetted by the fortunate orientation of the local axes[7] the three $N, Q_{\mathrm{y}}, M_{\mathrm{x}}$ in-plane resultants are produced by R alone, wherease the three $Q_{\mathrm{x}}, M_{\mathrm{y}}, M_{\mathrm{t}}$ out-of-plane resultants are induced by F alone. In-plane (out-of-plane) resultants are in fact symmetric (skew-symmetric) with respect to the plane the beam branches lies on, and the two symmetric and skew-symmetric parts of the problem are uncoupled.

Such property is useful in analyzing plane structures subject to mixed in-plane and out-of-plane loads, as the one under scrutiny.

It is finally noted that a general spatial structure may be derived from the proposed one e.g. by turning the C-profile 90° on its centroidal axis, and thus losing the elastic body symmetry.

1.5 Final remarks

The stress resultants at each section depend on the location of its center of axial elasticity and shear center, and on the orientation of the local reference system; any variation of the cross section design which

[6] i.e. a view in which such axis is exiting (or entering) the plane of view

[7] one parallel and one orthogonal to the symmetry plane

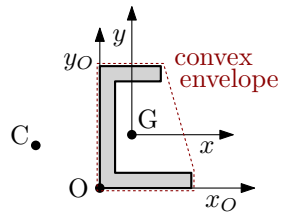

Figure 1.5: Notable points for a cross section. A reference point of convenience O may be defined, useful in providing a provisional reference system for pinning the section geometry independently from the possibly unknown elastic behavior, which defines instead the position of the G center of axial elasticity (aka. centroid), and the C shear center (aka. center of torsion). The latter, unlike the centroid, may fall outside the convex envelope of the section.

preserves the named elements does not require a reevaluation of the stress resultants.

In the case the actual cross section is still to be defined – and with it the two centers – they may both provisionally assumed coincident to an arbitrary located O point along the cross sections; the stress resultants are then evaluated based on equilibrium in terms of the three force resultants F_{Ox},F_{Oy},F_{Oz} – ideally applied at O, and the three moment resultants M_{Ox},M_{Oy},M_{Oz}, evaluated with respect to the O-centered pivot axes. Whilst the O-based force resultants de facto coincide with the $Q_{\mathrm{x}}, Q_{\mathrm{y}}, N$ internal action components, respectively, suitable transport moments are to be added to the O-based moment components in order to retrieve the usual moment resultants, as in

$$\begin{aligned} M_{\mathrm{x}} &= M_{\mathrm{Ox}} - F_{\mathrm{Oz}} \cdot y_{\mathrm{OG}} \\ M_{\mathrm{y}} &= M_{\mathrm{Oy}} + F_{\mathrm{Oz}} \cdot x_{\mathrm{OG}} \\ M_{\mathrm{t}} &= M_{\mathrm{Oz}} + F_{\mathrm{Ox}} \cdot y_{\mathrm{OC}} - F_{\mathrm{Oy}} \cdot x_{\mathrm{OC}} \end{aligned}$$

where $(x_{\mathrm{OG}}, y_{\mathrm{OG}})$ and $(x_{\mathrm{OC}}, y_{\mathrm{OC}})$ are the coordinates of the two notable centers, when eventually known, according to a Oxy reference system.

The center of axial elasticity may be determined as the *weighted* integral average of the material point coordinates along the cross section, i.e.

$$\{x_{\mathrm{OG}}, y_{\mathrm{OG}}\} = \frac{\int_{\mathcal{A}} E_z \{x_{\mathrm{O}}, y_{\mathrm{O}}\} \, d\mathcal{A}}{\int_{\mathcal{A}} E_z d\mathcal{A}} \tag{1.1}$$

where the weight consists in the pointwise axial elastic modulus E_z (vs. the density ρ as for the *center of gravity*, or just the unity when the aforementioned properties are uniform along the section), which is defined as the

$$E_z = \frac{\sigma_z}{\epsilon_z}$$

ratio between an applied axial stress σ_z and the resulting axial strain ϵ_z, in the absence of further stress components (uniaxial stress state, as along the gauge length of the customary tensile test specimen).

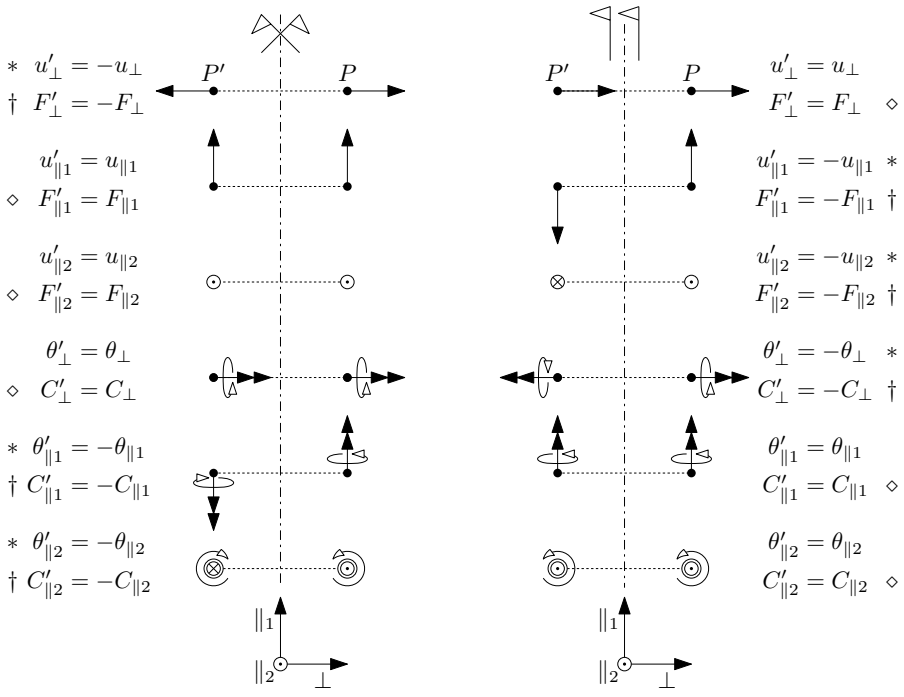

Figure 1.6: An overview of symmetrical and skew-symmetrical (generalized) loading and displacements.

1.6 Symmetry and skew-symmetry conditions

Symmetric and skew-symmetric loading conditions are mostly relevant for linearly-behaving systems; a nonlinear system may develop an asymmetric response to symmetric loading (e.g. column buckling).

Figure 1.6 collects symmetrical and skew-symmetrical pairs of vectors and moment vectors (moments); those (generalized) vectors are applied at symmetric points in space with respect to the reference plane. Vectors which are either normal or parallel to the plane are considered, that may embody the same named components of a generally oriented vector.

It may be observed that the symmetric/skew-symmetric condition for otherwise analogous pairs swaps in moving from vectors to moment vectors, and from the orthogonal to the parallel orientation.

The pair members may be moved towards the reference plane up

to a vanishing distance ϵ; for null ϵ both the point and the image lie on the plane, and they coincide. In the case different (in particular, opposite and nonzero) vectors are associated to the two coincident pair members, the physical field that such vectors are assumed to represent (displacements, applied forces, etc.) is not single-valued at the reference plane; such condition deserves an attentive rationalization.

Vector and moment pairs in Figure 1.6 may embody, depending on the context, displaments (denoted as u), rotations (θ), forces (F) and moments (M); the latters may be both related to internal and external actions; in the following, the feasibility of nonzero magnitude pairs is discussed as the members approach the reference plane ($\epsilon \to 0$).

The (generalized) displacement components decorated with the $*$ marker may induce material discontinuity at points laying on the [skew-]symmetry plane, if nonzero. Except for specific cases in which the discontinuity is expected – e.g. or notionally infinitesimal openings at the symmetry plane – they have to be constrained to zero at those points, thus introducing the so-called [skew-]symmetry constraints.

When an halved portion of the structure is modeled in place of the whole, since the response is expected to be [skew-]symmetric, these constraints act in place of the portion of the structure that is omitted from our model, and their reactions may be interpreted as internal action components at the coupling interface between the two halves.

In case of symmetry, a constraint equivalent to a planar joint is to be applied at points laying on the symmetry plane for ensuring displacement/rotation continuity between the modeled portion of the structure, and its image. In case of skew-symmetry, a constraint equivalent to a *doweled sphere - slotted cylinder* joint (see Figure 1.6), where the guide axis is orthogonal to the skew-symmetry plane, is applied at the points belonging to the intersection between the deformable body and the plane.

The $\diamond$ internal action components are null at points pertaining to the [skew-]symmetry plane, since they would otherwise violate the action-reaction law. The complementary $\dagger$ internal action components are generally nonzero at the [skew-]symmetry plane.

The $\dagger$ external action components are not allowed at points along the [skew-]symmetry plane; instead, the complementary $\diamond$ generalized force components are allowed, if they are due to locally applied external actions.

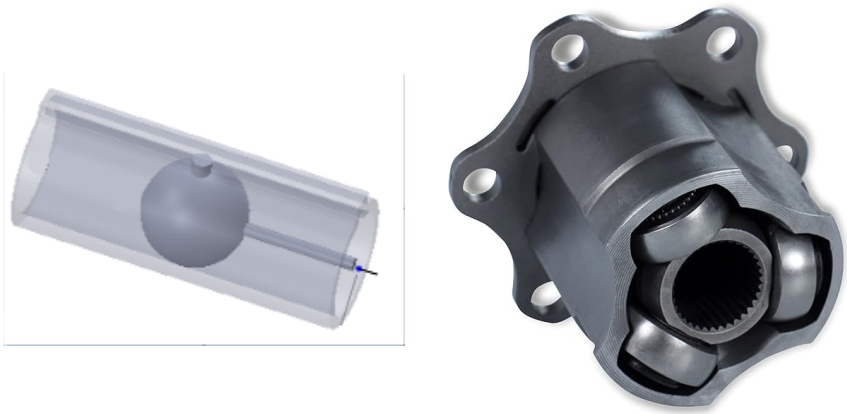

Figure 1.7: On the left, the doweled sphere - slotted cylinder joint, which is associated to the skew-symmetry constraint. On the right, an actual mechanical construction, the tripod joint.

In the case of a symmetric structure, generally asymmetric applied loads and imposed deflections may be decomposed in a symmetric part and in a skew-symmetric part; the problem may be solved by employing a half structure model for both the loadcases; the results may finally be superposed since the system is assumed linear.

1.7 Periodicity conditions

TODO, if required.

1.8 Axial load and uniform bending

It is preliminarily noted that the elementary extensional-flexural solution is exact with respect to the Theory of Elasticity if the following conditions hold:

- beam constant section;
- beam rectilinear axis;
- absence of locally applied loads;
- absence of shear resultants[8] (i.e. constant bending moments);
- principal material directions of orthotropy are uniform along the section, and one of them is aligned with the beam axis;
- the ν_{31} and the ν_{32} Poisson's ratios[9] are constant along the section, where 3 means the principal direction of orthotropy aligned with the axis. Please note that $E_i\nu_{ji} = E_j\nu_{ij}$, and hence $\nu_{ji} \neq \nu_{ij}$ for a generally orthotropic material.

Most of the above conditions are in fact violated in many textbook structural calculations, thus suggesting that the elementary beam theory is robust enough to be adapted to practical applications, i.e. limited error is expected if some laxity is used in circumscribing its scope[10].

The extensional-flexural solution builds on the basis of the following simplifying assumptions:

- the in-plane[11] stress components $\sigma_x, \sigma_y, \tau_{xy}$ are null;
- the out-of-plane shear stresses τ_{yz}, τ_{zx} are also null;

[8] A locally pure shear solution may be in fact superposed; such solution may however not be available for a general cross section.

[9] We recall that ν_{ij} is the Poisson's ratio that corresponds to a contraction in direction j, being a unitary extension applied in direction i in a manner that the elastic body is subject to a uniaxial stress state.

[10] Measures for both the error and the violation have to be supplied first in order to quantify the approximation.

[11] Both the *in-plane* and the *out-of-plane* expressions for the characterization of the stress/strain components refer to the cross sectional plane.

- the axial elongation ϵ_z linearly varies along the cross section, namely

$$\epsilon_z = a + bx + cy \tag{1.2}$$

or, equivalently[12], each cross section is assumed to remain planar in the deformed configuration.

The three general constants a, b and c possess a physical meaning; in particular a represents the axial elongation e as measured at the centroid[13], c represents the $1/\rho_x$ curvature[14] whereas b represent the $1/\rho_y$ curvature, apart from its sign.

Figure 1.8 (b) justifies the equality relation $c = 1/\rho_x$; the beam axial fibers with a Δz initial length are elongated by the curvature up to a $\Delta\theta\,(\rho_x + y)$ deformed length, where $\Delta\theta\rho_x$ equates Δz based on the length of the unextended fibre at the centroid. By evaluating the axial strain value for a general fiber, it follows that $\epsilon_z = 1/\rho_x\ y$.

In addition, Figure 1.8 (b) relates the $1/\rho_x$ curvature to the displacement component in the local y direction, namely v, and to the section rotation angle with respect to the local x axis, namely θ, thus obtaining

$$\frac{d\theta}{dz} = \frac{1}{\rho_x}, \quad \frac{dv}{dz} = -\theta\ + [g_y], \quad \frac{d^2v}{dz^2} = -\frac{1}{\rho_x} \tag{1.3}$$

For completeness, the influence of a possibly nonzero g_y shear deformation contribution, see Figure 1.8 (c), is added as a bracketed term, even if such contribution is assumed zero in the context of this paragraph.

Following analogous considerations, see 1.8 (d)-(f), we may similarly obtain

$$\frac{d\phi}{dz} = \frac{1}{\rho_y}, \quad \frac{du}{dz} = +\phi\ + [g_x], \quad \frac{d^2u}{dz^2} = +\frac{1}{\rho_y} \tag{1.4}$$

where ϕ is the cross section rotation about the local y axis, and u is the x displacement component.

[12]The axial, out-of-plane displacement $\Delta w = \int_{\Delta l} \epsilon_z dz = \Delta_l\,(a + bx + cy)$ accumulated between two contiguous cross sections with an Δl initial distance, is consistent with that of a relative rigid body motion.

[13]or, equivalently, the average elongation along the section, in an integral sense.

[14]namely the inverse of the beam curvature radii as observed with a line of sight aligned with the x axis. Curvature is assumed positive if the associated θ section rotation grows with increasing z, i.e. $d\theta/dz > 0$.

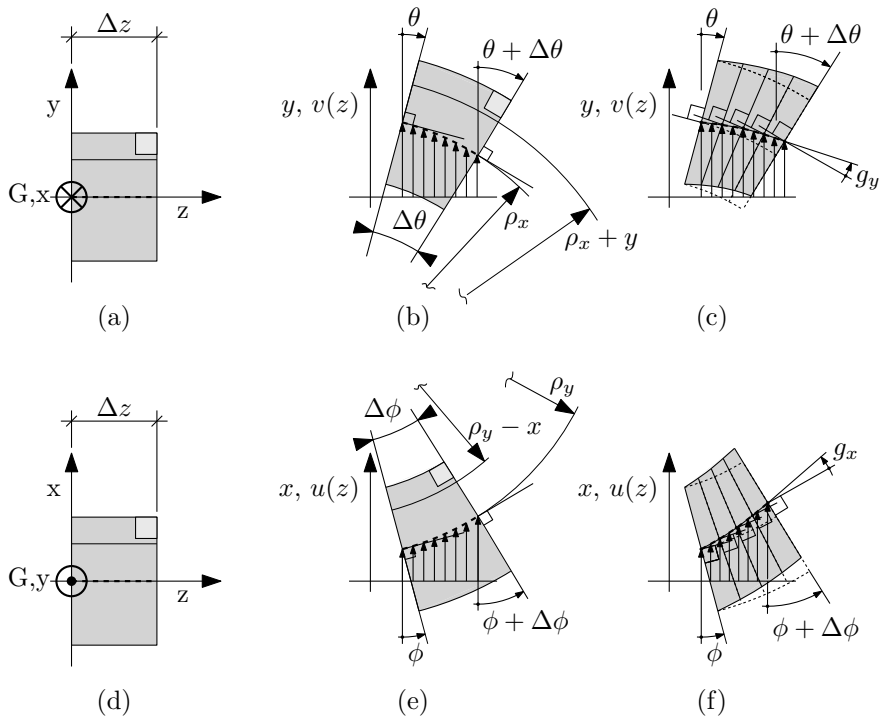

Figure 1.8: A differential fibre elongation proportional to the y coordinate induces a curvature $1/\rho_x$ on the normal plane with respect to the x axis, and a growth of the θ rotation in z, as in (b) with respect to (a). A differential fibre contraction proportional to the x coordinate induces a curvature $1/\rho_y$ on the normal plane with respect to the y axis, and a growth of the ϕ rotation in z, as in (e) with respect to (d). In (c) and (f), the further card-deck-like deformation associated to the g_y, g_x shear deflections, respectively, is represented.

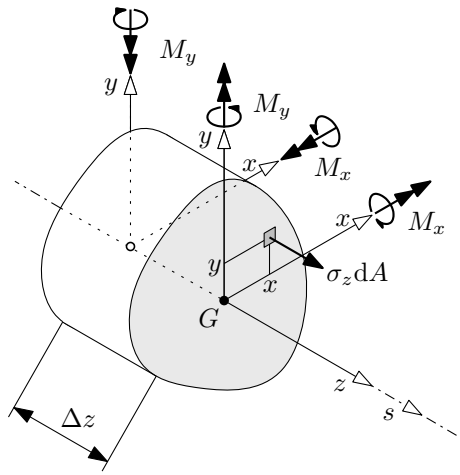

Figure 1.9: Positive x and y bending moment components adopt the same direction of the associated local axes at the beam segment end showing an outward-oriented arclength coordinate axis; at beam segment ends characterized by an inward-oriented local z axis, the same positive bending moment components are locally counter-oriented to the respective axes.

According to the assumptions in the preamble, a uniaxial stress state is assumed, where the only nonzero σ_z stress component may be determined as

$$\sigma_z = E_z \epsilon_z; \quad \epsilon_z = e - \frac{1}{\rho_y} x + \frac{1}{\rho_x} y \tag{1.5}$$

Stress resultants may easily be evaluated based on Fig. 1.9 as

$$N = \iint_{\mathcal{A}} E_z \epsilon_z dA = \overline{EA} e \tag{1.6}$$

$$M_x = \iint_{\mathcal{A}} E_z \epsilon_z y dA = \overline{EJ}_{xx} \frac{1}{\rho_x} - \overline{EJ}_{xy} \frac{1}{\rho_y} \tag{1.7}$$

$$M_y = -\iint_{\mathcal{A}} E_z \epsilon_z x dA = -\overline{EJ}_{xy} \frac{1}{\rho_x} + \overline{EJ}_{yy} \frac{1}{\rho_y} \tag{1.8}$$

where the combined material/cross-section stiffness moduli

$$\overline{EA} = \iint_{\mathcal{A}} E_z(x,y)\ dA \tag{1.9}$$

$$\overline{EJ}_{xx} = \iint_{\mathcal{A}} E_z(x,y) yy\ dA \tag{1.10}$$

$$\overline{EJ}_{xy} = \iint_{\mathcal{A}} E_z(x,y) yx\ dA \tag{1.11}$$

$$\overline{EJ}_{yy} = \iint_{\mathcal{A}} E_z(x,y) xx\ dA \tag{1.12}$$

may also be rationalized as the cross section area and moment of inertia, respectively, multiplied by a suitably averaged Young modulus, evaluated in the axial direction.

An equivalent form for Eqns. 1.7 and 1.8 is

$$\begin{bmatrix} M_x \\ M_y \end{bmatrix} = \underbrace{\begin{bmatrix} \overline{EJ}_{xx} & -\overline{EJ}_{xy} \\ -\overline{EJ}_{xy} & \overline{EJ}_{yy} \end{bmatrix}}_{[\overline{EJ}]} \begin{bmatrix} \frac{1}{\rho_x} \\ \frac{1}{\rho_y} \end{bmatrix} \tag{1.13}$$

from which the beam flexural stiffness $[\overline{EJ}]$ matrix may be derived.

Those moduli simplify to their usual $E_z A, E_z J_{**}$ analogues, where the influence of the material and of the geometry are separated if the former is homogeneous along the beam cross section.

From Eqn. 1.6 we obtain

$$e = \frac{N}{\overline{EA}}. \tag{1.14}$$

By concurrently solving Eqns. 1.7 and 1.8 with respect to the $1/\rho_x$ and $1/\rho_y$ curvatures, we obtain

$$\frac{1}{\rho_x} = \frac{M_x \overline{EJ}_{yy} + M_y \overline{EJ}_{xy}}{\overline{EJ}_{xx}\overline{EJ}_{yy} - \overline{EJ}_{xy}^2} \tag{1.15}$$

$$\frac{1}{\rho_y} = \frac{M_x \overline{EJ}_{xy} + M_y \overline{EJ}_{xx}}{\overline{EJ}_{xx}\overline{EJ}_{yy} - \overline{EJ}_{xy}^2} \tag{1.16}$$

or, equivalently

$$\begin{bmatrix} \frac{1}{\rho_x} \\ \frac{1}{\rho_y} \end{bmatrix} = [\overline{EJ}]^{-1} \begin{bmatrix} M_x \\ M_y \end{bmatrix} \tag{1.17}$$

where

$$[\overline{EJ}]^{-1} = \frac{1}{\overline{EJ}_{xx}\overline{EJ}_{yy} - \overline{EJ}_{xy}^2} \begin{bmatrix} \overline{EJ}_{yy} & \overline{EJ}_{xy} \\ \overline{EJ}_{xy} & \overline{EJ}_{xx} \end{bmatrix}$$

is the beam flexural compliance matrix. The equivalent curvature

$$\frac{1}{\rho_{\text{eq}}} = \sqrt{\frac{1}{\rho_x^2} + \frac{1}{\rho_y^2}}, \tag{1.18}$$

which is defined as the euclidean norm of the two curvature components, is also the inverse of the curvature radius as measured by an observer whose line of sight is aligned with the so called *neutral axis*, i.e. the $\epsilon_z = 0$ line.

Axial strain and stress components may then be obtained for any cross section point by substituting the above calculated generalized strain components e, $1/\rho_x$ and $1/\rho_y$ holding for the extensional-flexural beam into Eqn. 1.5, thus obtaining

$$\sigma_z = E_z\epsilon_z; \quad \epsilon_z = \begin{bmatrix} y & -x \end{bmatrix} [\overline{EJ}]^{-1} \begin{bmatrix} M_x \\ M_y \end{bmatrix} + \frac{1}{\overline{EA}} N \tag{1.19}$$

The peak axial strain is obtained at points farther from neutral axis of the stretched section; such neutral axis may be graphically defined as follows:

- the coordinate pair

  $$(x_N, y_N) \equiv e\rho_{\text{eq}}^2 \left(\frac{1}{\rho_y}, -\frac{1}{\rho_x} \right);$$

  with ρ_{eq} from 1.18, defines its nearest pass-through point with respect to the G centroid; the two points coincide in the case $e = 0$.

- its orientation is defined by the unit vector

  $$\hat{n}_{\parallel} = \rho_{\text{eq}} \left(\frac{1}{\rho_x}, \frac{1}{\rho_y} \right),$$

  whereas the direction

  $$\hat{n}_{\perp} = \rho_{\text{eq}} \left(-\frac{1}{\rho_y}, \frac{1}{\rho_x} \right),$$

  is orthogonal to the neutral axis, and oriented towards growing axial elongations.

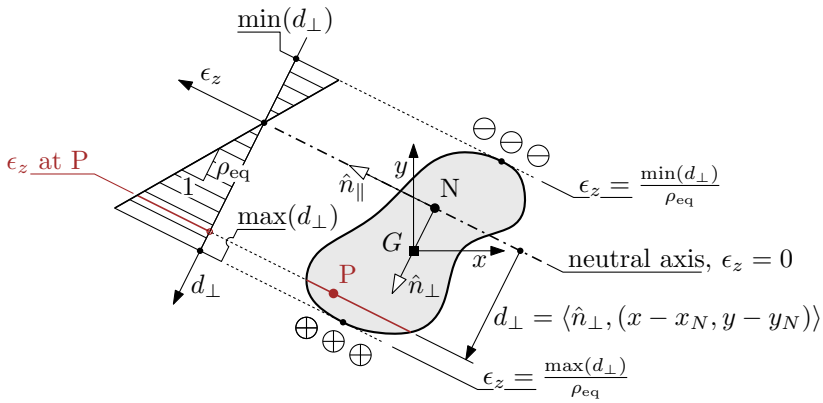

Figure 1.10: Graphical construction for retrieving the extremal strain values given an $N \equiv (x_N, y_N)$ point along the neutral axis, two $\hat{n}_\parallel$ and $\hat{n}_\perp$ unit vectors that are parallel and normal to neutral axis, respectively , and the ρ_{eq} curvature radius to retrieve strains from the $d_\perp$ projected distance measurements.

The cross section projection on on a generic $\hat{n}_\perp$-oriented line defines a segment whose ends are extremal with respect to the axial strain, since the axial strain may in fact be expressed – in the case of nonzero bending moment [15] – as

$$\epsilon_z = \frac{1}{\rho_{\text{eq}}} \underbrace{\langle \hat{n}_\perp, (x - x_N, y - y_N) \rangle}_{d_\perp} = \frac{1}{\rho_{\text{eq}}} d_\perp \tag{1.20}$$

where $d_\perp$ is the signed distance of the material point from the neutral axis.

The graphical construction for retrieving the extremal strain values along the cross section is shown in Figure 1.10.

If the bending moment vector $\vec{M}_f = (M_x, M_y)$ is imposed to be collinear to the neutral axis direction $\hat{n}_\parallel$, and hence – in turn – to the curvature component vector, we have

$$\begin{bmatrix} M_x \\ M_y \end{bmatrix} = \zeta \hat{n}_\parallel = \lambda \begin{bmatrix} \frac{1}{\rho_x} \\ \frac{1}{\rho_y} \end{bmatrix} \tag{1.21}$$

[15] $\epsilon_z = e$ otherwise

by resorting to the Eqn. 1.13, the following eigenpair problem is defined

$$\begin{bmatrix} M_x \\ M_y \end{bmatrix} = \underbrace{\begin{bmatrix} \overline{EJ}_{xx} & -\overline{EJ}_{xy} \\ -\overline{EJ}_{xy} & \overline{EJ}_{yy} \end{bmatrix}}_{[\overline{EJ}]} \begin{bmatrix} \frac{1}{\rho_x} \\ \frac{1}{\rho_y} \end{bmatrix} = \lambda \begin{bmatrix} \frac{1}{\rho_x} \\ \frac{1}{\rho_y} \end{bmatrix} \tag{1.22}$$

which leads to the definition of the principal directions for the cross sectional bending stiffness. In particolar, the (normalized) eigenvectors of the $[\overline{EJ}]$ matrix define the two principal bending stiffness directions

$$\hat{1} = \begin{bmatrix} 1_x \\ 1_y \end{bmatrix}, \quad \hat{2} = \begin{bmatrix} 2_x \\ 2_y \end{bmatrix},$$

and the associated $\overline{EJ}_{11}, \overline{EJ}_{22}$ eigenvalues constitute the associated bending stiffness moduli. Due to the property of the eigendecomposition with respect to the inverse, from

$$[\overline{EJ}] = \begin{bmatrix} 1_x & 2_x \\ 1_y & 2_y \end{bmatrix} \begin{bmatrix} \overline{EJ}_{11} & 0 \\ 0 & \overline{EJ}_{22} \end{bmatrix} \begin{bmatrix} 1_x & 1_y \\ 2_x & 2_y \end{bmatrix} \tag{1.23}$$

we have that

$$[\overline{EJ}]^{-1} = \begin{bmatrix} 1_x & 2_x \\ 1_y & 2_y \end{bmatrix} \begin{bmatrix} \frac{1}{\overline{EJ}_{11}} & 0 \\ 0 & \frac{1}{\overline{EJ}_{22}} \end{bmatrix} \begin{bmatrix} 1_x & 1_y \\ 2_x & 2_y \end{bmatrix}, \tag{1.24}$$

which leads to the following alternative expression for the 1.15, 1.16

$$\begin{bmatrix} \frac{1}{\rho_x} \\ \frac{1}{\rho_y} \end{bmatrix} = \underbrace{\underbrace{\begin{bmatrix} 1_x & 2_x \\ 1_y & 2_y \end{bmatrix} \underbrace{\begin{bmatrix} \frac{1}{\overline{EJ}_{11}} & 0 \\ 0 & \frac{1}{\overline{EJ}_{22}} \end{bmatrix}}_{\text{II}} \underbrace{\begin{bmatrix} 1_x & 1_y \\ 2_x & 2_y \end{bmatrix} \begin{bmatrix} M_x \\ M_y \end{bmatrix}}_{\text{I}}}_{\text{III}} \tag{1.25}$$

where the sequence of matrix-vector multiplication may be rationalized as follows:

- I leads to the (M_1, M_2) bending moment components with respect to the principal (with respect to bending) reference system 12;
- II scales the latter according to the two flexural compliance factors $1/\overline{EJ}_{11}$ and $1/\overline{EJ}_{22}$ in order to derive the associated, uncoupled, curvatures components;

- III finally translates those curvatures back to the original xy cartesian pair.

1.9 Stresses due to the shear cross section resultants, and torsion

In the presence of nonzero shear resultants, the bending moment exhibits a linear variation with the axial coordinate z in a straight beam. Based on the beam segment equilibrium we have

$$Q_y = \frac{dM_x}{dz}, \quad Q_x = -\frac{dM_y}{dz}, \tag{1.26}$$

as rationalized in Fig. 1.15, with $dz \to 0$ and M_x, M_y differentiable with respect to z.

The linear variation of the bending-induced curvature in z causes a likewise linear variation of the pointwise axial strain; stress variation is also linear in the case of constant E_z longitudinal elastic modulus.

In particular, the differentiation with respect to z of σ_z as espressed in Eqn. 1.19 returns

$$\frac{d\sigma_z}{dz} = E_z \begin{bmatrix} y & -x \end{bmatrix} \left[\overline{EJ}\right]^{-1} \begin{bmatrix} Q_y \\ -Q_x \end{bmatrix} \tag{1.27}$$

since its $E_z, [\overline{EJ}]$ terms are constant with respect to z; the bending moment derivatives are here expressed in terms of the shear resultants, as in Eqns. 1.26. Alternatively, we can write after some rearrangement

$$\frac{d\sigma_z}{dz} = E_z \begin{bmatrix} x & y \end{bmatrix} \frac{\left[\overline{EJ}\right]}{\det\left(\left[\overline{EJ}\right]\right)} \begin{bmatrix} Q_x \\ Q_y \end{bmatrix}. \tag{1.28}$$

Figure 1.11 rationalizes the axial equilibrium for an elementary volume of material; we have

$$\frac{d\tau_{zx}}{dx} + \frac{d\tau_{yz}}{dy} + \frac{d\sigma_z}{dz} + q_z = 0 \tag{1.29}$$

where, for the specific case, the distributed volumetric load q_z is natively zero.

It clearly emerges from such relation that the shear stresses τ_{zx}, τ_{yz}, that were null within the uniform bending framework, are non-uniform along the section – and hence not constantly zero – in the presence of shear resultants.

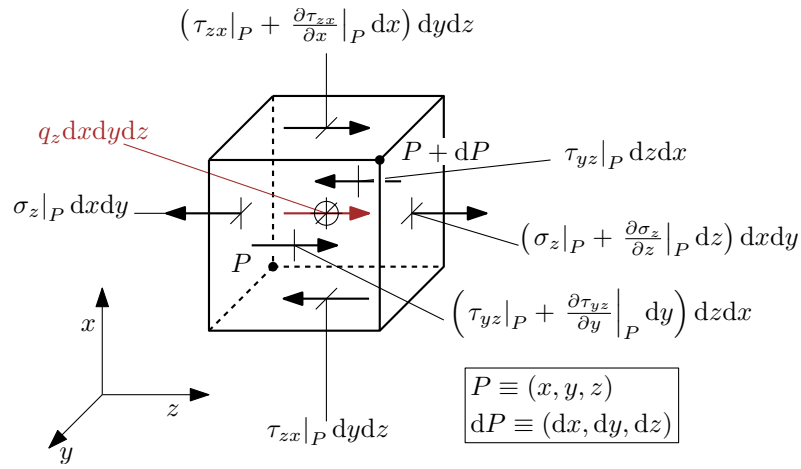

Figure 1.11: Equilibrium conditions with respect to the axial z translation for the infinitesimal volume extracted from the beam. In the case under scrutiny, the distributed volume action q_z is null.

An extensive treatise on the pointwise solution of a) the equilibrium equations 1.29, once coupled with b) the compatibility conditions and with c) the the material elastic response, is beyond the scope of the present contribution, although it has been derived for selected cross sections in e.g. [1].

However, some notes are presented in the present paragraph, that should provide a quick overview of the topic.

First, an artifice is introduced to analyze the shear straining in purity, i.e. to dissociate it from the nonuniform flexure, whose contribution may be latter superposed. From Eq. 1.29 we may observe that the $\frac{d\sigma_z}{dz}$ axial stress variation term is formally interchangeable with the q_z distributed volumetric load terms; in particular, a $\bar{q}_z$ defined as the Eq. 1.28 RHS, i.e.

$$\bar{q}_z = E_z \begin{bmatrix} x & y \end{bmatrix} \frac{[\overline{EJ}]}{\det\left([\overline{EJ}]\right)} \begin{bmatrix} Q_x \\ Q_y \end{bmatrix}. \tag{1.30}$$

may produce a shear stress/strain field analogous to that induced by transverse loads, but in the absence of actual flexure.

By accumulating those the $\bar{q}_z$ contributions along the the cross

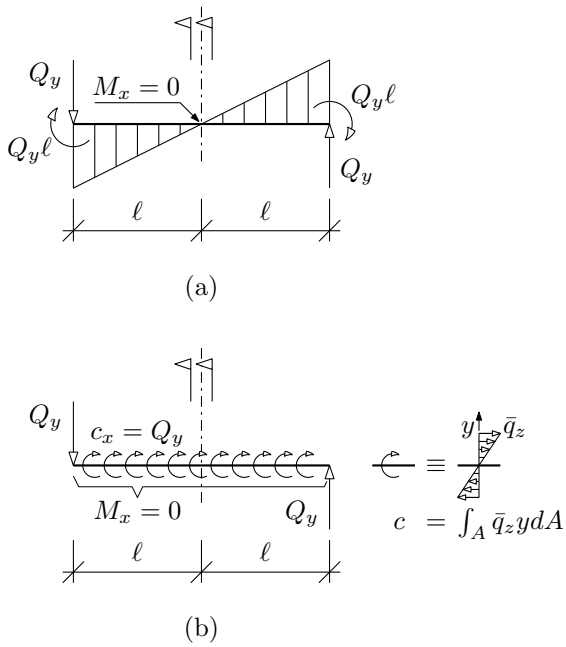

Figure 1.12: Transverse loads at a beam segment endpoints, and the necessary equilibrating moments: in (a), a pure shear condition is obtained at the midspan cross section, whereas in (b) such a condition is extended to the entire segment, by uniformly spreading the endpoint moments.

section, we obtain two components of moment lineic density[16] resultant

$$c_x = \int_{\mathcal{A}} \bar{q}_z y d\mathcal{A} = Q_y, \quad c_y = -\int_{\mathcal{A}} \bar{q}_z x d\mathcal{A} = -Q_x,$$

which equate in magnitude the shear components, see Fig. 1.12b, and a null force resultant

$$\int_{\mathcal{A}} \bar{q}_z d\mathcal{A} = 0.$$

By considering an unbounded beam subject to such $\bar{q}_z$ distributed load, with equilibrating Q_x, Q_y loads applied at both the infinitely far end faces, in correspondence of the shear center, holding a few

[16] i.e. moment per unit beam length

futher hypotheses[17] each cross sectional plane is a skew-symmetry plane for the prismatic solid and for the applied loads, leading to a skew-symmetric problem for which a translational self-similarity also holds in varying the cross section under scrutiny.

Since analogous properties are observed in the same infinite beam subject to torsion, we may consider an additional M_t torque applied at both the extremes, and hence combine the two pure shear and torsional skew-symmetric[18] loadcases in a single treatise.

The classical solution for the rectilinear beam subject to pure shear and torsion predicts a displacement field that is composed by the superposition of i) a rigid, in-plane cross section translation due to shear, in card-deck like sliding fashion, whose axial rates g_x, g_y are uniform ii) a rigid, in-plane[19] cross section rotation about the translated shear center, named twist, whose axial rate ψ' is uniform, and iii) an out-of-plane *warping* displacement $w(x, y)$ that is uniform in the axial direction, whereas it varies within the section; such warping displacement is zero only in the case of axisymmetric sections (e.g. solid and hollow circular cross sections) subject to torsion alone.

The resulting displacement field for the prismatic bar subject to shear and torsion may hence be cast as

$$\begin{aligned} u &= \left(g_x - (y - y_{\mathrm{C}})\,\psi'\right) z \\ v &= \left(g_y + (x - x_{\mathrm{C}})\,\psi'\right) z \\ w &= \bar{w}(x, y) \end{aligned} \tag{1.31}$$

Such a displacement field is represented in Figs. 1.18a and 1.18b.

Due to the rigid nature of the in-plane displacements, the in-plane strain components ϵ_x, ϵ_y, ϵ_{xy} are zero, along with the ϵ_z axial strain component, due to the axially constant nature of the warping displacement. The in-plane stress components σ_x, σ_y, τ_{xy}, and the normal stress σ_z are also zero, based on the associated strain components, and the material elastic symmetry.

The residual out-of-plane (oop) shear strain components may then

[17] if the cross section is constant and the material exhibits a symmetric elastic behavior (i.e. monoclinic) with respect to the cross-sectional plane

[18] with respect to the cross sectional plane

[19] the rotation vector is actually normal to the cross sectional plane; the *in-plane* motion characterization refers to the associated displacement field.

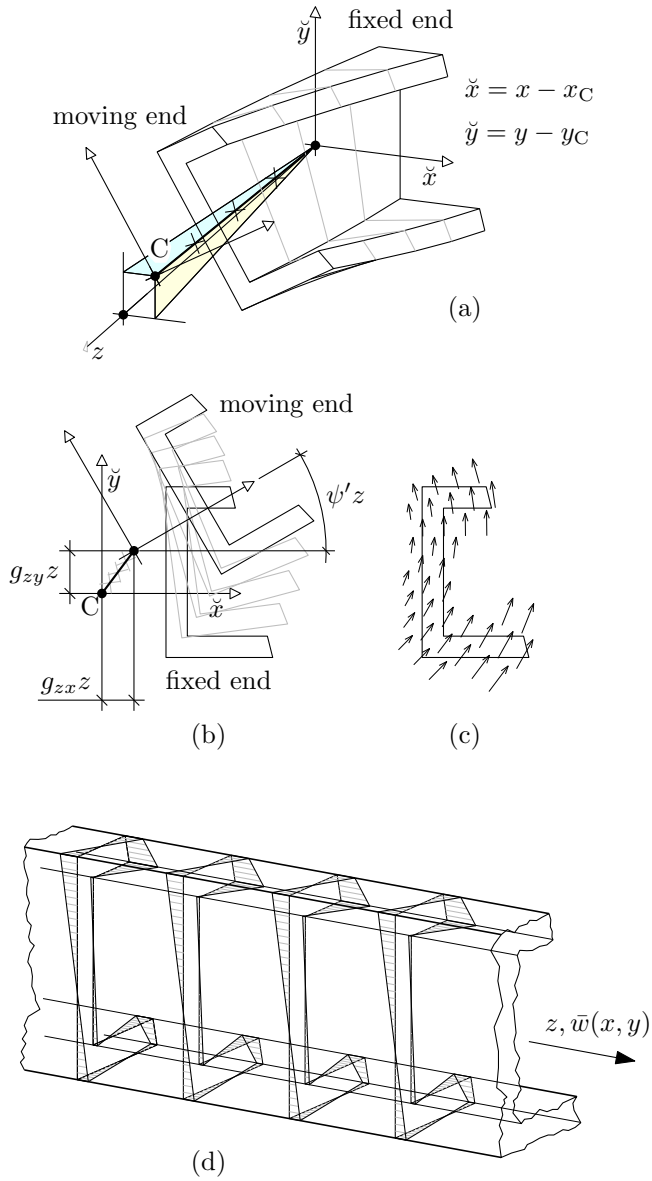

Figure 1.13: In (a) and (b), the u, v deflection induced by the g_x, g_y, ψ' generalized strain components, and in (c) the associated γ_{zx}, γ_{zy} shear strain field, which may credibly produce a substantially aligned τ_{zx}, τ_{zy} shear stress field that violates the free lateral surface condition. In (d), the warping displacement field for a purely torsional (no shear) loadcase.

be derived from the displacement field as

$$\gamma_{zx} = \underbrace{g_x - (y - y_C)\,\psi'}_{\frac{\partial u}{\partial z}} + \frac{\partial \bar{w}}{\partial x}, \quad \gamma_{zy} = \underbrace{g_y + (x - x_C)\,\psi'}_{\frac{\partial v}{\partial z}} + \frac{\partial \bar{w}}{\partial y} \tag{1.32}$$

and, in turn, oop shear stress components may be derived from the material transverse shear constitutive law, namely

$$\begin{bmatrix} \tau_{zx} \\ \tau_{zy} \end{bmatrix} = \underbrace{\begin{bmatrix} G_{zx} & H_{zxzy} \\ H_{zxzy} & G_{zy} \end{bmatrix}}_{\underline{\underline{\mathrm{G}}}_{z*}} \begin{bmatrix} \gamma_{zx} \\ \gamma_{zy} \end{bmatrix} \tag{1.33}$$

where the coupling term H_{zxzy} is null if x, y are principal directions of orthotropy, and in the case of isotropic materials where we also have that both G_{zx}, G_{zy} coincide with the material shear modulus $G = \frac{E}{2(1+\nu)}$.

In order to respect the stress-free condition of the lateral surface, the normal component of the (τ_{zx}, τ_{zy}) vector must vanish at the cross-section shape boundary, i.e.

$$\langle \hat{n}, (\tau_{zx}, \tau_{zy}) \rangle = 0 \quad (x, y) \in \mathrm{bd}(\mathcal{A}) \tag{1.34}$$

where $\hat{n}$ is the locally normal unit vector.

The $\left(\frac{\partial u}{\partial z}, \frac{\partial v}{\partial z}\right)$ contributions of the rigid card-deck-like roto-translation to the oop strain field – i.e. the oop strain field in the supposed absence of warping motion – is shown in Fig. 1.18c, and it is clearly far from being aligned with the cross-section shape border; even if the (τ_{zx}, τ_{zy}) oop shear stress field is strictly aligned to its strain counterpart only in the case of isotropic materials, the misalignment between the two fields is limited[20] . Hence, the warping contribution to the oop shear strain and – in turn – stress fields is fundamental in reorienting the latter in order to make Eq. 1.34 hold.

[20]In the general case, the angle between the two oop stress/strain vectors is bounded by a limit $0 \leq \arccos \frac{2\sqrt{\eta}}{1+\eta} < \frac{\pi}{2}$ aperture, where $0 < \eta \leq 1$ is the ratio between the lowest and the highest eigenvalues of the $\underline{\underline{\mathrm{G}}}_{z*}$ oop shear constitutive matrix. In the allegedly extremal case of a $[\pm 45\mathrm{F}]_{\mathrm{n}}$ twill high modulus CFRP laminated beam, where the in-ply shear modulus is much higher than the transverse counterpart ($\eta \approx 0.08$), a limit angle of $\approx 58.5°$ is obtained.

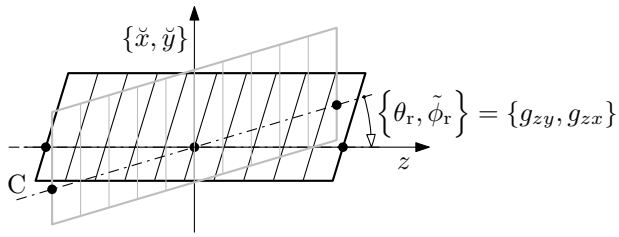

Figure 1.14: FIXME

By further superposing the rotation depicted in Fig. 1.14, namely

$$\begin{aligned} \{\theta_{\mathrm{r}}, \phi_{\mathrm{r}}\} &= \{g_{zy}, -g_{zx}\} \\ \{u_{\mathrm{r}}, v_{\mathrm{r}}\} &= -\{g_{zx}, g_{zy}\} z \\ w_{\mathrm{r}} &= g_{zx}(x - x_C) + g_{zy}(y - y_C) \end{aligned}$$

we realign the C shear centers with their original position, thus obtaining

$$\begin{aligned} u &= \left(g_x - (y - y_{\mathrm{C}})\,\psi'\right) z + u_{\mathrm{r}} = -(y - y_{\mathrm{C}})\,\psi' z \\ v &= \left(g_y + (x - x_{\mathrm{C}})\,\psi'\right) z + v_{\mathrm{r}} = +(x - x_{\mathrm{C}})\,\psi' z \\ w &= \bar{w} + w_{\mathrm{r}} \end{aligned} \tag{1.35}$$

and reducing the whole in-plane (ip) motion to a pure, progressive rotation around the shear center line, at the cost of an added contribution to w. Such a displacement field will be later obtained in the fe modeling of the profile segment in order to retrieve the beam elastic properties.

Also, by differentiating the Eq. 1.35 displacement field, we obtain an oop shear strain formulation

$$\gamma_{zx} = \underbrace{-(y - y_{\mathrm{C}})\,\psi'}_{\frac{\partial u}{\partial z}} + \frac{\partial \bar{w}}{\partial x}, \quad \gamma_{zy} = \underbrace{+(x - x_{\mathrm{C}})\,\psi'}_{\frac{\partial v}{\partial z}} + \frac{\partial \bar{w}}{\partial y} \tag{1.36}$$

lacking of the g_{zx}, g_{zy} unknown terms.

By substituting the Eq. 1.36 strains withing Eq. 1.33 we obtain oop the shear stresses which may in turn be substituted within the

$$\frac{d\tau_{zx}}{dx} + \frac{d\tau_{yz}}{dy} + \bar{q}_z = 0 \tag{1.37}$$

equilibrium equation along the cross-section domain, and within the Eq. 1.34 boundary condition, we obtain an anisotropic, inhomogeneous Poisson problem[21] in the $\bar{w}(x, y)$ unknown function.

Then, the problem may be split in a pure shear subproblem, with $\psi' = 0$, which is solved first, where the two Q_x, Q_y shear resultants within the $\bar{q}_z$ term act as load parameters, the (x_C, y_C) shear center coordinates are obtained from the (τ_{zx}, τ_{zy}) resultant lines of action, and the $\{\chi_x, \chi_y, \chi_{xy}\}/\overline{GA}$ terms are obtained from the strain energy induced by three different shear load combinations (e.g. $Q_x > 0$ alone, $Q_y > 0$ alone, combined $Q_x = Q_y > 0$).

A second, torsional only subproblem is then approached by putting $Q_x = Q_y = 0$, and in turn $\bar{q}_z = 0$, and employing the ψ' twist rate as the load parameter. Once obtained the solution in terms of (τ_{zx}, τ_{zy}) stresses, the torsional moment M_t may then be retrieved as their moment resultant.

[21] a second order partial differential equation, plus b.c.

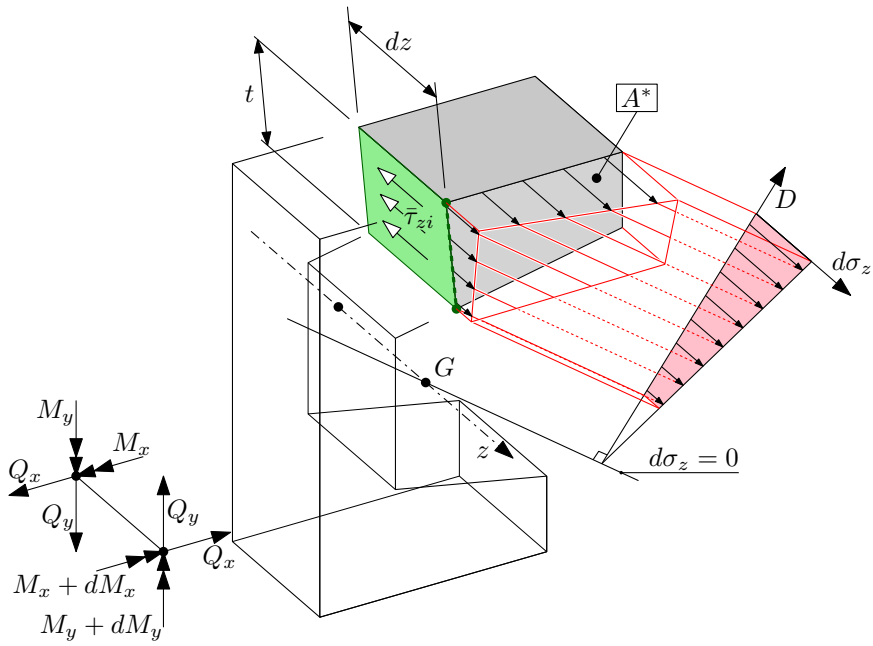

Figure 1.15: Equilibrium conditions for the isolated beam segment portion. It is noted that the null σ_z variation locus, $d\sigma_z = 0$, does not coincide with the bending neutral axis in general. Also, the depicted linear variation of $d\sigma_z$ with the D distance from such null $d\sigma_z$ locus does not hold in the case of non-uniform E_z modulus.

1.9.1 The Jourawsky approach and its extension for a general section

The aforementioned axial equilibrium condition, whose treatise is cumbersome for the infinitesimal volume, may be more conveniently dealt with if a finite portion of the beam segment is taken into account, as in Figure 1.15.

A beam segment is considered whose axial extent is dz; the beam cross section is partitioned based on a (possibly curve, see Fig. 1.16) line that isolates an area portion A^* – and the related beam segment portion – for further scrutiny; axial equilibrium equation may then be

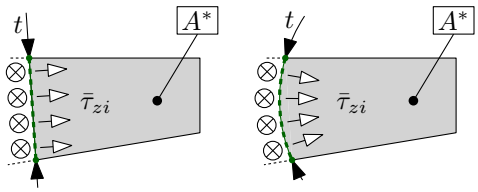

Figure 1.16: The curve employed for isolating the beam segment portion defines the direction of the τ_{zi} components whose average value is evaluated.

stated for the isolated beam segment portion as follows

$$\bar{\tau}_{zi} t = \int_{A^*} \frac{d\sigma_z}{dz} dA, \tag{1.38}$$

where

$$\bar{\tau}_{zi} = \frac{1}{t} \int_t \tau_{zi} dr \tag{1.39}$$

is the average shear stress acting in the z direction along the cutting surface; i is the (locally normal) inward direction with respect to such a surface. Due to the reciprocal nature of the shear stresses, the same $\bar{\tau}_{zi}$ shear stress acts along the cross sectional plane, and locally at the cutting curve itself. These shear actions are assumed positive if inward directed with respect to A^*.

The $\bar{\tau}_{zi} t$ product is named *shear flow*, and may be evaluated along a general cutting curve.

It is noted that, according to Eqn. 1.38, no information is provided with regard to a) the τ_{zr} shear stress that acts parallel to the cutting curve, nor b) the pointwise variation of τ_{zi} with respect of its average value $\bar{\tau}_{zi}$. If the resorting to more cumbersome calculation frameworks is not an option, those quantities are usually just neglected; an informed choice for the cutting curve is thus critical for a reliable application of the method.

In the simplified case of a) uniform material and b) local x, y axes that are principal axes of inertia (i.e. $J_{xy} = 0$), the usual formula is obtained

$$\bar{\tau}_{zi} t = \int_{A^*} \left(\frac{y Q_y}{J_{xx}} + \frac{x Q_x}{J_{yy}} \right) dA = \frac{\bar{y}^* A^*}{J_{xx}} Q_y + \frac{\bar{x}^* A^*}{J_{yy}} Q_x, \tag{1.40}$$

where $\bar{y}^* A^*$ and $\bar{x}^* A^*$ are the first order area moments of the A^* section portion with respect to the x and y axes, respectively[22].

1.9.2 Shear induced stresses in an open section, thin walled beam

In the case of thin walled profiles, the integral along the isolated area in Eqn. 1.38 may be performed with respect to the arclength coordinate alone; the value the $d\sigma_z/dz$ integrand assumes at the wall midplane is supposed representative of its integral average along the wall thickness, thus obtaining

$$\bar{\tau}_{zi} t = q_{zi} = \int_0^s \int_{-t/2}^{t/2} \frac{d\sigma_z}{dz} dr d\varsigma \approx \int_0^s \left.\frac{d\sigma_z}{dz}\right|_{r=0} t d\varsigma. \tag{1.41}$$

Such assumed equivalence strictly holds for a) straight wall segments[23] and b) a linear variation of the integrand along the wall, a condition, the latter, that holds if the material properties are homogeneous with respect to the wall midplane[24]; in the more general case, the error incurred by this approach vanishes with vanishing thickness for what concerns assumption a), whereas if the material is inhomogeneous, through-thickness averaged $\bar{E}_z, \bar{G}_{zi}$ moduli may be employed in place of their pointwise counterpart.

If a thin walled section segment is considered such that it is not possible to infer that the interfacial shear stress is zero at at least one of its extremities, a further term needs to be considered for the equilibrium, thus obtaining

$$\bar{\tau}_{zi}(s) t(s) = q(s) = \int_a^s \frac{d\sigma_z}{dz} t d\varsigma + \underbrace{\bar{\tau}_{zi}(a) t(a)}_{q_A}. \tag{1.42}$$

In the case of open thin walled profiles, however, such a choice for the isolated section portion is suboptimal, unless the q_A term is known.

[22] According to the employed notation, $(\bar{x}^*, \bar{y}^*)$ are the centre of gravity coordinates for the A^* area.

[23] i.e. the Jacobian of the $(s, r) \mapsto (x, y)$ mapping is constant with r.

[24] a linear $d\epsilon_z/dz$ axial strain variation is in fact associated to the curvature variation in z, and not an axial stress variation;

1.9.3 Shear induced stresses in an closed section, thin walled beam

In the case of a closed thin walled, generally asymmetric section, the search for a point along the wall at which the shear flow may be assumed zero is normally not viable, and the employment of Eq. 1.42 in place of the simpler Eq. 1.41 is unavoidable.

In this case, a parametric value for the $\bar{\tau}_{iz}$ shear stress is assumed for a set of points along the cross section midcurve – one for each elementary closed loop[25] if the points are non-redundantly chosen[26].

In the multicellular cross section example shown in Figure 1.17, two elementary loops are detected; shear flows at the A, B points are parametrically defined as $\tau_A t_A$ and $\tau_B t_B$, respectively.

The $\tau(s)$ shear stress at each point along the profile wall may then be determined based on Eqn. 1.42 as a function a) of the shear resultant components Q_x and Q_y, and b) of the parametrically defined shear stresses at the A,B points.

Due to the assumed linear response for the profile, superposition principle may be employed in isolating the four elementary contributions to the shear stress flow along the section.

The first two elementary contributions $f_{;Qx}(s)$ and $f_{;Qy}(s)$ are respectively due to the action alone of the x and y shear force components, whose magnitudes Q_x^{u} and Q_y^{u} is assumed equal the product of the stress unit (e.g. 1 MPa) and of the cross sectional area. Those forces are assumed to act in the ideal absence of shear flow at points where the latter is assumed as a parameter (points A and B in Figure 1.17).

Since the condition of zero shear flow is stress-compatible with an opening in the closed section loop, the cross section may be idealized as severed at the assumed shear flow points, and hence open. The equilibrium-based solution procedure derived for the open thin-walled section may hence be profitably applied.

A family of further elementary contributions, one for each of the assumed shear stress points, may be derived by imposing zero para-

[25] i.e. a closed loop not enclosing any other closed loop.

[26] Redundancy may be pointed out by ideally cutting the cross section at these points: if a monolithic open cross section is obtained, the point choice is not redundant; if a portion of the section is completely isolated, and a loop remains closed, the location of these points causes redundancy.

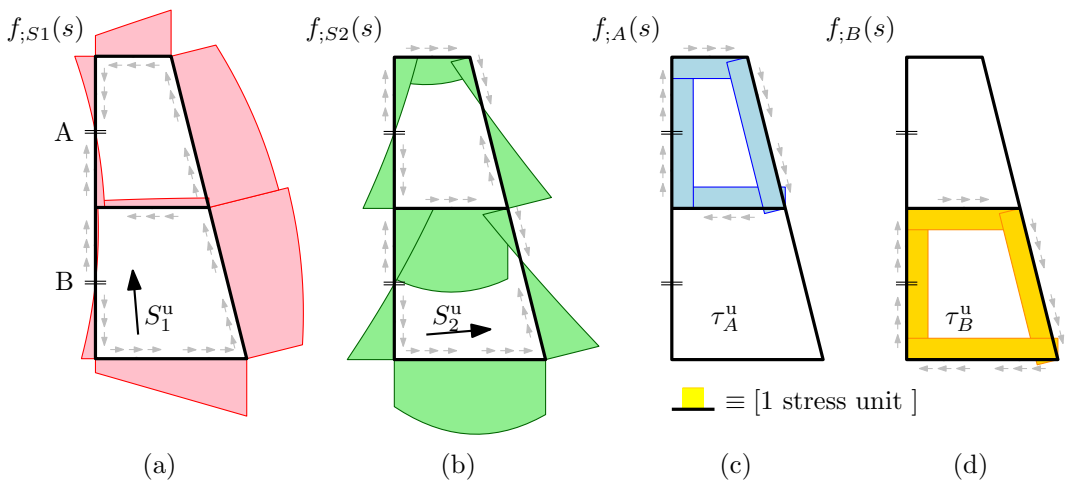

Figure 1.17: Contributions to the $\tau_{zi}(s)$ shear stress along the profile walls associated to a) a unit shear force component Q_1^{u} applied along the first principal axis of inertia, whose magnitude equals the product of the cross section area and the unit stress, b) an analogous shear force component Q_2^{u} aligned with the second principal axis of inertia, c) a unit shear stress τ_A^{u} applied at the opposite fictitious cut surfaces at A, and d) a unit shear stress τ_B^{u} applied at the opposite fictitious cut surfaces at B. Profile wall thickness is constant in the presented example, thus producing a continuous shear stress diagram, whereas continuity is rather aa unit shear stress τ_A^{u} applied at the opposite fictitious cut surfaces at a property of the shear flow.

metric shear flow at all the points but the one under scrutiny, and in the absence of externally applied shear resultants. The elastic problem may be rationalized as an open – initially closed, then ideally severed – thin walled profile, that is loaded by an internal constraint action whose magnitude is unity in terms of stresses. Equilibrium considerations reduce to the conservation of the shear flow due to the absence of $d\sigma_z/dz$ differential axial stress, as in the case of a closed profile under torsion discussed below.

Figures 1.17 (a) and (b) show the shear stress contributions $f_{;S1}(s)$ and $f_{;S2}(s)$ induced in the ideally opened (i.e. zero redundant shear flows at the A,B points) multicellar profile by the first and the second shear force components, respectively; due to the author distraction, such figure refers to shear components aligned with the principal directions of bending stiffness, and not to the usual x,y axes.

Figures 1.17 (c) and (d) show the shear stress contributions $f_{;A}(s)$ and $f_{;B}(s)$ associated to unity values for the parametric shear flows at the A, B segmentation points, respectively.

The cumulative shear stress distribution for the section in Figure 1.17 is

$$\tau(s) = \frac{Q_1}{\mathcal{A}} f_{;S1}(s) + \frac{Q_2}{\mathcal{A}} f_{;S2}(s) + \tau_A f_{;A}(s) + \tau_B f_{;B}(s) \tag{1.43}$$

where s is a suitable arclength coordinate.

The associated elastic potential energy may then be integrated over a Δz beam axial portion, thus obtaining

$$\Delta U = \int_s \frac{\tau^2}{2G_{sz}} t \Delta z ds \tag{1.44}$$

According to the Castigliano second theorem, the ΔU derivative with respect to the $\bar{\tau}_i$ assumed shear stress value at the i-th segmentation point equates the generalized displacement with respect to which the internal constraint reaction works, i.e. the $t\Delta z\bar{\delta}_i$ integral of the relative longitudinal displacement between the cut surfaces; we hence have

$$\frac{\partial \Delta U}{\partial \bar{\tau}_i} = \bar{\delta}_i t \Delta z \tag{1.45}$$

The $\bar{\delta}_i$ symbol refers to the average value along the $t\Delta z$ area of such axial relative displacement.

Material continuity requires zero $\bar{\delta}_i$ value at each segmentation point, thus defining a set of equations, one for each $\bar{\tau}_i$ unknown parameter, whose solution leads to the definition of the actual shear stress distribution along the closed wall profile.

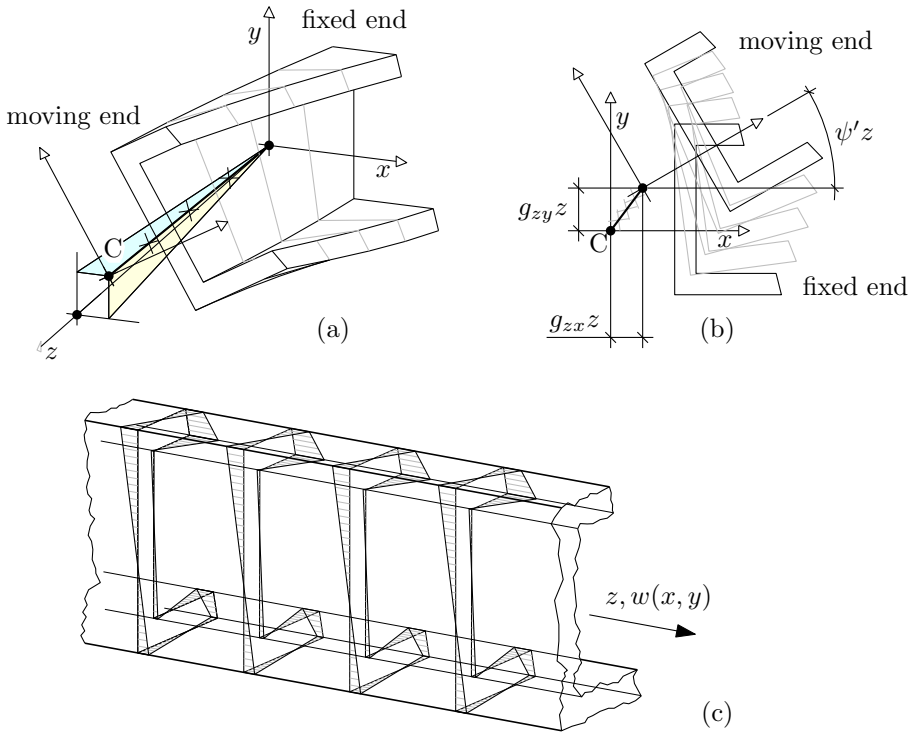

Figure 1.18: TODO

1.9.4 Shear stresses due to the St. Venant torsion

FIXME

The classical solution for the rectilinear beam subject to uniform torsion predicts a displacement field that is composed by the superposition of i) a rigid, in-plane[27] cross section rotation about the shear centre, named twist, whose axial rate is uniform, and ii) an out-of-plane *warping* displacement that is uniform in the axial direction, whereas it varies within the section; such warping displacement is zero in the case of axisymmetric sections only (e.g. solid and hollow circular cross sections).

Due to the rigid nature of the in-plane displacements, the in-plane strain components ϵ_x, ϵ_y, ϵ_{xy} are zero; the in-plane stress components

[27] the rotation vector is actually normal to the cross sectional plane; the *in-plane* motion characterization refers to the associated displacement field.

σ_x, σ_y, τ_{xy}, and the normal stress σ_z are also zero if z is a direction of orthotropy for the material – as it is assumed in the following. The motion is internally restricted only due to the nonzero out-of-plane shear stresses τ_{yz} and τ_{zx}, that develop as an elastic reaction to the associated strain components.

A more in-depth treatise of the topic involves the solution of an plane, inhomogeneous Laplace partial differential equation with essential conditions imposed at the cross section boundary, which is beyond the scope of the present contribution.

However, in the case of open- and closed- section, thin walled beams, simplified solutions are available based on the assumptions that a) the out-of-plane shear stresses are locally aligned to the wall midsurface - i.e. $\tau_{zr} = 0$ leaving τ_{zs} as the only nonzero stress component[28], and b) the residual τ_{zs} shear component is either constant by moving through the wall thickness (closed section case), or it linearly varies with the through-thickness coordinate r.

FIXME

1.9.5 Solid section beam

TODO.

1.9.6 Closed section, single-celled thin walled beam

The τ_{sz} component is assumed uniform along the wall thickness, or, equivalently, its deviation from the average value is neglected in calculations.

In the case the material is non-uniform across the thickness, the γ_{sz} shear strain is assumed uniform, whereas the τ_{sz} varies with the varying G_{sz} shear modulus.

In the absence of σ_z, the axial equilibrium of a portion of beam segment dictates that the shear flow $t\tau$ remains constant along the wall, i.e.

$$t_1\tau_1 = t_2\tau_2$$

as depicted in Figure 1.19.

[28] Here, the notation introduced in paragraph XXX for the thin walled section is employed.

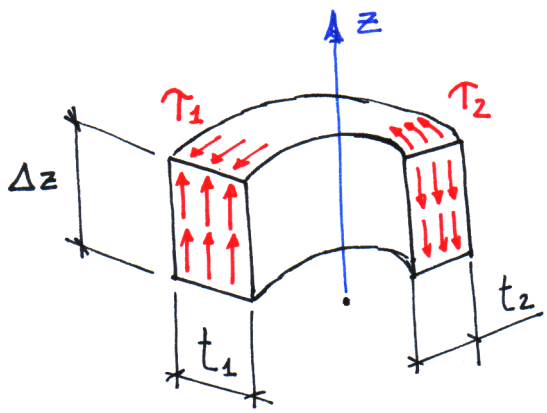

Figure 1.19: Axial equilibrium for a portion of profile wall, in the case of a closed, thin-walled profile subject to torsion.

By skipping some further interesting observations (TODO) we may just introduce the Bredt formula for the cross-section torsional stiffness

$$K_t = \frac{4A^2}{\oint \frac{1}{t} dl} \tag{1.46}$$

which is valid for single-celled, closed thin wall sections.

The peak stress is located at thinnest point along the wall, and equals

$$\tau_{\max} = \frac{M_t}{2t_{\min}A} \tag{1.47}$$

.

1.9.7 Closed section, multi-celled thin walled beam

TODO. However, a lower bound for the stiffness of the multi-celled thin walled beam may be obtained by fictitiosly severing the inner walls, thus obtaining a single cell defined by the outer wall alone.

An upper bound for the stiffness is obtained by assuming each shared inner wall as shear-rigid, and then by summing the stiffnesses of each elementary closed loop, as they constituted independent profiles. The shear-rigid nature of the inner walls is enforced by neglecting their contribution to the circuital integral at the Bredt formula denominator.

1.9.8 Open section, thin walled beam

The shear strain component γ_{zs} is assumed linearly varying across the thickness; if the G_{sz} shear modulus is assumed uniform, such linear variation characterizes the τ_{zs} stress components too.

The average value along the thickness of the τ_{zs} stress component is zero, as zero is the shear flow as defined in the previous paragraph.

For thin enough open sections of uniform and isotropic material we have

$$K_T \approx \frac{1}{3} \int_0^l t^3(s) ds \tag{1.48}$$

If the thin-walled cross section may be described as a sequence of constant thickness wall segments, the simplified formula

$$K_T \approx \frac{1}{3} \sum_i l_i t_i^3 \tag{1.49}$$

is obtained where t_i and l_i are respectively the length and the thickness of each segment.

The peak value for the τ_{zs} stress component is observed in correspondence to thickest wall section point and it equates

$$\tau_{\max} = \frac{M_t t_{\max}}{K_T} \tag{1.50}$$

By applying the reported formulas to a rectangular section whose span length is ten times the wall thickness, the torsional stiffness is overestimated by slightly less than 7%; a similar relative error is reported in terms of shear stress underestimation.

1.9.9 Torsional stiffening due to restrained warping at profile ends: Vlasov torsion theory

As a pedagogical introduction to the restrained warping torsion, an open, thin-walled I-section beam[29] is considered where its ends are both butt-welded to massive plates, see Fig. 1.20, that locally impede the warping deformation at the base of the de Saint Venant torsion theory.

[29] also named H-section, double-T, based on normalized profile codes, e.g. IPN, IPE, or UC beams

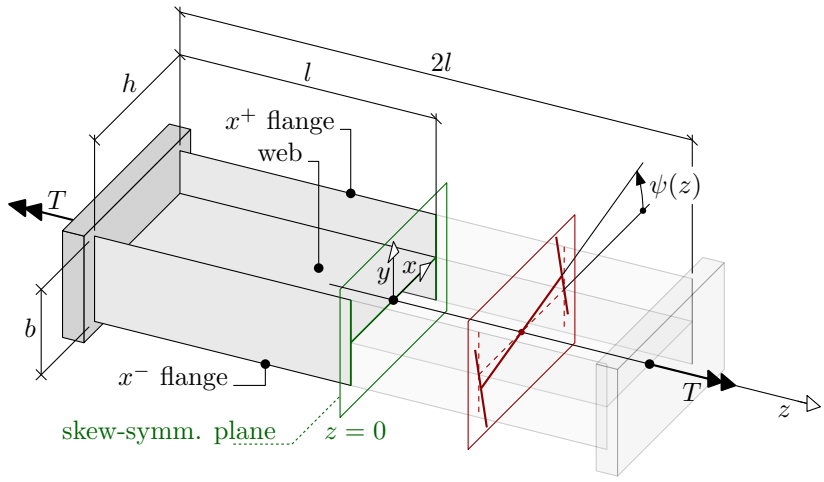

Figure 1.20: The problem under scrutiny.

Two opposite T torques are applied that induce an axial counter-rotation $2rl$ of the beam extremities, and hence a twist deformation of the profile, which is locally quantified through the $\psi(z)$ section twist angle, and whose average rate along the $2l$ overall span length is r.

Due to the skew-symmetric nature of the problem with respect to the three xy, yz and zx planes, the cross sectional motion is limited to a twist rotation about the z axis, which is centroidal with respect to shear, plus the restrained warping out-of-plane displacement.

In Figure 1.21 the profile walls are ideally partitioned into a set of limited width rectangular blades; the profile section rotation locally induces at each blade section three distinct motions, i.e. a) a twist rotation, b) a widthwise translation, and c) a transverse translation with respect to the blade width.

The axial rate of the twist motion a) is at the base of the de St. Venant torsional model for open thin walled sections, which covers it exhaustively; conversely, the second order axial rate of the b) and c) translations induce bending curvatures at the blades, whose contribution to the internal energy increases the profile stiffness in torsion with respect to twist alone.

In particular, while the c) contribution acts along the blade bending weak axis and it is usually neglected, the b) contribution is considerable

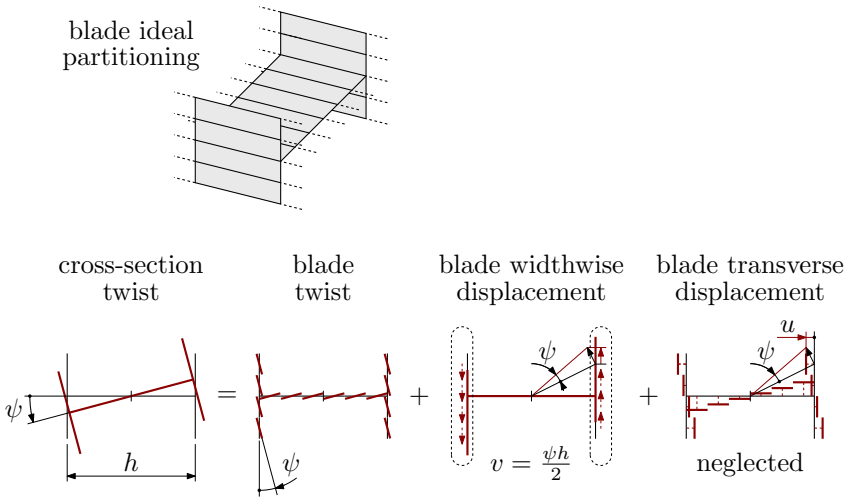

Figure 1.21: Cross section partitioning into limited width blades, and analysis of their twist/deflective motion.

and it constitutes the basis of the Vlasov restrained torsion theory for thin walled profiles. Due to the mutual interaction occurring at the blade flanks which are not free surfaces, the general treatise is cumbersome.

Limiting our discussion to the Fig. 1.20 didactic example, according to Fig. 1.21 the blades extracted from the central web undergo a purely c) transverse deflection, and their contribution is neglected. The b) widthwise relevant deflection occurs instead at the two x^+, x^- flanges, which are treated as two independent, rectangular cross section beams, thus effectively resembling the two profile assembly of the Par. 1.13 simplified ladder frame example.

In the unconstrained warping case, a reference $T_{\text{ref}} = GK_t r$ torque is produced, which is fully ascribable to the flange and web twisting. Here, the GK_t constant is the usual torsional stiffness for the profile, with

$$G = \frac{E}{2(1-\nu)}, \quad K_t = \frac{1}{3}\int_\ell t^3(s)ds = \frac{(2b+h)\,t^3}{3}.$$

As underlined in Fig. 1.22a, the two twisted flanges undergo a further rigid body rotation $\check{\theta} = \frac{rh}{2}$ about the x axis, whose associated axial displacement is incompatible with the end plate rigidity. As a

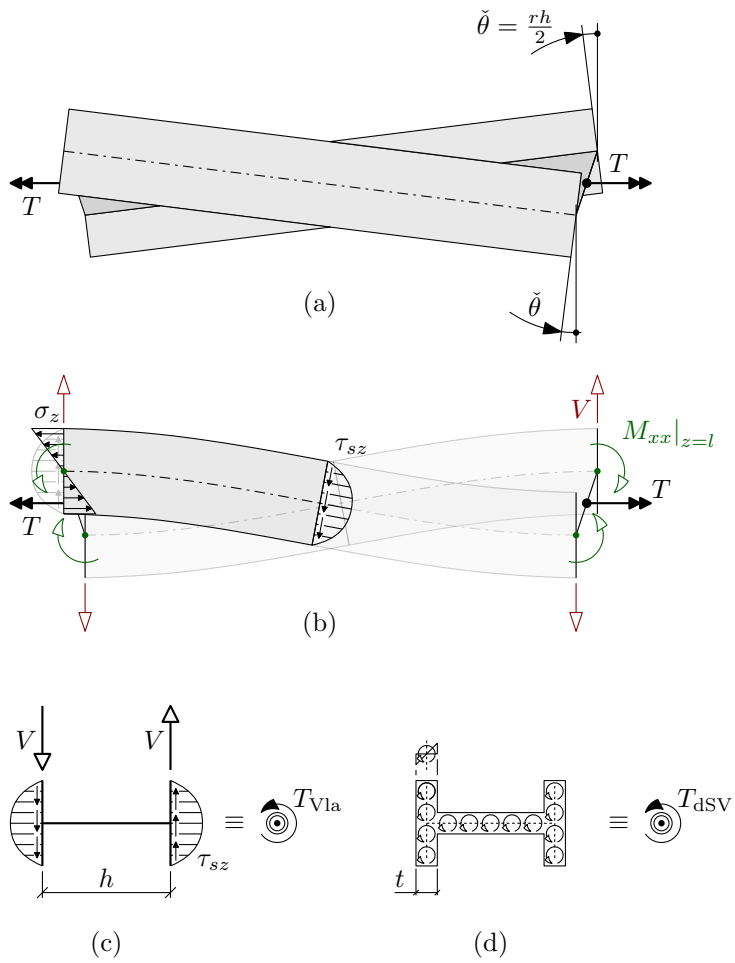

Figure 1.22: In b), the skew-symmetric, S-shaped bending deflection of the two flanges, as the profile undergoes to torsional twist; the τ_{sz} shear stresses (uniform in z) are pointed out at the midspan cross section, whereas the σ_z flexural stress distribution peak out at the restrained-warping extremities. In a), the same overall twist is applied, under free warping conditions; the transverse displacement of the flange extremities is absorbed by a mere rotation. In c) and d), the contribution to the overall torsional moment due to the flange shear forces, T_{Vla}, and of the wall twist reactions, T_{dSV}, respectively.

.

reaction, two opposite moments are expected to occur.

By considering the bending of the x^+ flange alone[30], the V flange shear force is retrieved as the axial rate of the M_x flexural moment,

$$V = \frac{dM_x}{dz}.$$

According to Fig. 1.22c, the contribution of the flange bending to the profile torsional torque equates the shear force couple

$$T_{\mathrm{Vla}} = hV = h\frac{dM_x}{dz};$$

based on the flange flexural compliance

$$M_x = \frac{EJ_{xx}}{\rho_x} = -EJ_{xx}\frac{d^2v}{dz^2}, \quad EJ_{xx} = \frac{Eb^3t}{12}$$

we obtain

$$T_{\mathrm{Vla}} = -h\overline{EJ}_{xx}\frac{d^3v}{dz^3},$$

where the v transverse displacement may in turn be determined as

$$v = \frac{h}{2}\psi,$$

where ψ is the local twist angle, see Fig. 1.21.

Such a contribution of the flange bending to the overall torsional torque transmission may hence be expressed as a function of the (third derivative of) twist angle as

$$T_{\mathrm{Vla}} = -\frac{h^2}{2}EJ_{xx}\frac{d^3\psi}{dz^3} = -EC_w\frac{d^3\psi}{dz^3}$$

where

$$EC_w = EJ_{xx}\frac{h^2}{2} = \frac{Eb^3th^2}{24}$$

embodies the I-beam cross-sectional constant for the restrained warping torsion. Different expressions may be obtained for different cross-sections.

[30] the x^- flange behaves skew-symmetrically

Besides that, the torsional moment transmitted according to the de St. Venant torsion theory is

$$T_{\mathrm{dSV}} = GK_t \frac{d\psi}{dz},$$

By dimensionally comparing the two EC_w, GK_t constants, a characteristic length of the cross section with respect to the Vlasov (restrained warping) torsion theory may be defined as follows

$$d = \sqrt{\frac{EC_w}{GK_t}}, \quad EC_w = d^2 GK_t$$

Since the overall torsional torque is constant along the beam in the absence of distributed twisting actions, the sum of its two T_{Vla} and T_{dSV} constituents remains stationary in z, thus obtaining

$$0 = \frac{dT_{\mathrm{dSV}}}{dz} + \frac{dT_{\mathrm{Vla}}}{dz} = -EC_w \frac{d^4\psi}{dz^4} + GK_t \frac{d^2\psi}{dz^2}$$

$$0 = -d^2 \frac{d^4\psi}{dz^4} + \frac{d^2\psi}{dz^2}$$

which is a 4th-order differential equation in the ψ unknown function, whose solutions take the general form

$$\psi(z) = C_1 \sinh\frac{z}{d} + C_2 \cosh\frac{z}{d} + C_3 \frac{z}{d} + C_4 \tag{1.51}$$

where the C_i constants are defined based on the boundary conditions.

In the theory of restrained warping torsion, an auxiliary, higher order resultant moment quantity named *bimoment* is introduced; in the case of the pedagogical I-section example under scrutiny, the bimoment appears as the product of the two flange bending moments M_x, times their h distance, which acts as a further, higher order arm, i.e.

$$B = M_x \cdot h$$

whereas in general it is defined based on the EC_w constant and the second rate of twist as in

$$B = -EC_w \frac{d^2\psi}{dz^2};$$

axial stresses along the cross section linearly scale with the above bimoment quantity, provided that the material behaves elastically.

Warping related boundary conditions may be stated as follows:

- free warping: $\frac{d^2\psi}{dz^2} = 0$, i.e. absence of bimoment, $B = 0$;
- no warping: $\frac{d\psi}{dz} = 0$, i.e. absence of de St. Venant transmitted moment, $T_{\mathrm{dSV}} = 0$;

whereas the customary boundary conditions

- imposed rotation, $\psi = c$;
- imposed overall torque, $T_{\mathrm{dSV}} + T_{\mathrm{Vla}} = C$;

are defined as usual.

In the case under scrutiny, see Fig. 1.20, the even C_2, C_4 coefficients of Eq. 1.51 are null by skew-symmetry, whereas the remaining odd C_1, C_3 coefficients are obtained as

$$\{C_1, C_3\} = rl \cdot \frac{\left\{-1, \cosh\left(\frac{l}{d}\right)\right\}}{\frac{l}{d}\cosh\left(\frac{l}{d}\right) - \sinh\left(\frac{l}{d}\right)} \tag{1.52}$$

by imposing at both ends a given amount of twist and no warping, i.e.

$$\psi|_{z=l} = rl, \quad \left.\frac{d\psi}{dz}\right|_{z=l} = 0.$$

Relevant results are reported in Fig. 1.23, where the overall torque and the isolated contribution of its constituents – sampled at the midspan – are plotted as a function of the η ratio between the overall span length $2l$ and the characteristic length d. Due to normalization, such a Figure encompasses the general case of an arbitrary cross-sectional shape and a generally elastic material.

It clearly appears from the Fig. 1.23 that i) the stiffening effect of the constrained warping at ends is extremely relevant, and ii) the Vlasov thin wall bending is the preferential torque transmission mechanism, when the $2l$ overall span length is of same the order of the d characteristic length, or lower (i.e. *not* $\eta \gg 1$).

The classical de St. Venant torsion theory is only applicable when the overall span length $2l$ becomes considerably greater than the characteristic length d, i.e. $\eta \gg 1$.

The analytical expression obtained for the stiffening factor due to constrained warping at ends (this is a further interpretation for the

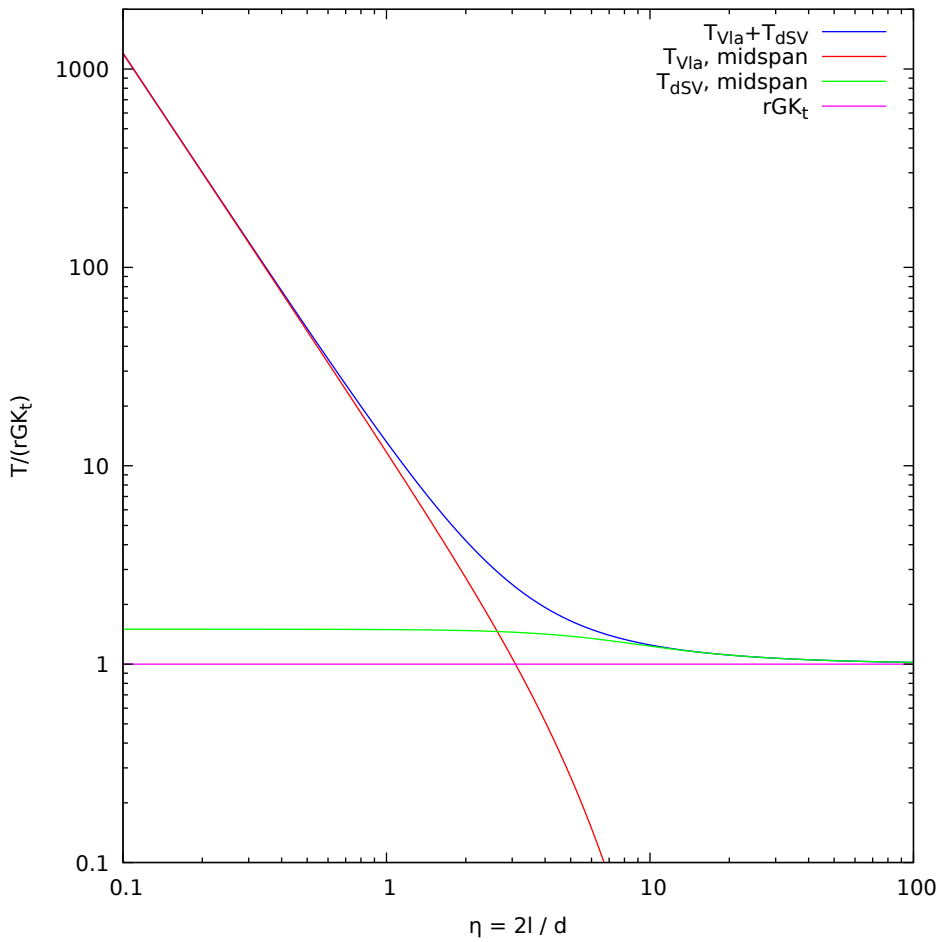

Figure 1.23: Relevant results for the problem under scrutiny. The overall torque ("$T_{\mathrm{Vla}} + T_{\mathrm{dSV}}$" labeled blue line) is plotted as a function of the η ratio between the overall span length $2l$ and the characteristic length d. The isolated contribution of its two constituents is sampled at the midspan ("T_{Vla}, midspan" labeled red line, and "T_{dSV}, midspan" labeled green line), and the GK_tr reference torque proper of the unconstrained warping case is added for comparison (purple line). The ordinate axis is normalized with respect to the GK_tr reference torque proper of the unconstrained warping torsion.

"$T_{\mathrm{Vla}} + T_{\mathrm{dSV}}$" labeled blue curve in Fig. 1.23) is

$$\frac{T_{\mathrm{Vla}} + T_{\mathrm{dSV}}}{GK_t r} = \frac{\eta}{\eta - 2\tanh\left(\frac{\eta}{2}\right)} = S(\eta). \tag{1.53}$$

Such a stiffening factor may usefully be employed to evaluate the d characteristic length of a given, arbitrary profile cross section from, e.g., FE simulations or experiments.

The torsional stiffness of a $2\bar{l}$ long specimen may in fact be evaluated in both i) restrained warping at both ends conditions – k_{i} value – and ii) free warping conditions – k_{ii} value. Then, the measured ratio

$$\bar{S} = \frac{k_{\mathrm{i}}}{k_{\mathrm{ii}}}$$

may be compared with the ordinate values of the Fig. 1.23, "$T_{\mathrm{Vla}} + T_{\mathrm{dSV}}$" labeled, blue curve, thus obtaining the ratio between the $2\bar{l}$ specimen length and the $\bar{d}$ characteristic length as the associated abscissa.

Alternatively, the Newton iteration

$$\eta_{i+1} = \eta_i + \frac{\bar{S} - S_i}{S'_i}, \quad S_i = S(\eta_i), \quad S'_i = \left.\frac{\partial S}{\partial \eta}\right|_{\eta=\eta_i}$$

converges to the η^* solution when initialized with $\eta_0 = 1$; then the $\bar{d}$ characteristic length may be obtained as

$$\bar{d} = \frac{2\bar{l}}{\eta^*}.$$

Such a d characteristic length for the Vlasov restrained torsion theory is usually much greater than the a cross-section characteristic size in the case of open thin-walled cross sections as the one under scrutiny, thus leading to high S stiffening ratios even for apparently long (with respect to a, but not to d) profiles; d is usually much smaller than a in the case of closed thin-walled cross section, thus producing a substantial negligibility of the stiffening effect due to restrained warping at ends.

1.10 Castigliano's second theorem and its applications

Castigliano's second theorem may be employed for calculating deflections and rotations, and it states:

> Once the strain energy of a linear elastic structure is expressed as a function of a set of generalized loads[31] Q_i , the partial derivative of the strain energy with respect to each generalized load supplies the generalized displacement[32] q_i on which such a load performs work.

In equation form,

$$q_i = \frac{\partial U}{\partial Q_i}$$

where U is the strain energy.

In case of elastically nonlinear structures, the second Castigliano theorem may still be employed[33], provided that the complementary elastic strain energy U^* is used in place of the strain energy U, see Fig. 1.24. The two energy terms coincide in linearly behaving structures.

1.11 Internal energy for the spatial straight beam

The lineic[34] elastic strain energy density for the spatial rectilinear beam may be expressed as a quadratic function of its cross section resultants,

[31] namely, forces or moments, but also a pressure load etc.

[32] namely displacements and rotations, or, in the case of a pressure load, the volume spanned with deformation by the pressurized surface.

[33] this nonlinear extension of the Castigliano theorem is however referred to in literature as the Crotti-Engesser theorem.

[34] i.e. per unit length; the far more customary *linear* adjective is so overloaded of meanings that I rather prefer such an exotic alternative.

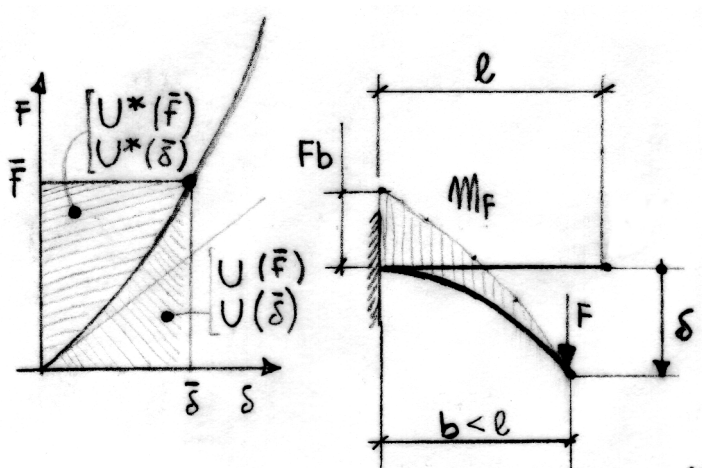

Figure 1.24: An elastic structure subject to large rotations, which shows a nonlinear stiffening behaviour; the bending moment diagram is evaluated based on the beam portion equilibrium in its *deformed* configuration. The complementary elastic strain energy U^* is plotted for a given applied load $\bar{f}$ or assumed displacement $\bar{\delta}$, alongside the elastic strain energy U.

thus leading to the general form

$$\frac{dU}{dl} = \frac{1}{2} \begin{pmatrix} N \\ M_{\mathrm{x}} \\ M_{\mathrm{y}} \\ Q_{\mathrm{x}} \\ Q_{\mathrm{y}} \\ M_{\mathrm{t}} \end{pmatrix}^{\top} \begin{pmatrix} a_{1,1} & g_{1,2} & g_{1,3} & i_{1,4} & i_{1,5} & i_{1,6} \\ 0 & b_{2,2} & e_{2,3} & i_{2,4} & i_{2,5} & i_{2,6} \\ 0 & 0 & b_{3,3} & i_{3,4} & i_{3,5} & i_{3,6} \\ 0 & 0 & 0 & c_{4,4} & f_{4,5} & h_{4,6} \\ 0 & 0 & 0 & 0 & c_{5,5} & h_{5,6} \\ 0 & 0 & 0 & 0 & 0 & d_{6,6} \end{pmatrix}_{\mathrm{Sym}} \begin{pmatrix} N \\ M_{\mathrm{x}} \\ M_{\mathrm{y}} \\ Q_{\mathrm{x}} \\ Q_{\mathrm{y}} \\ M_{\mathrm{t}} \end{pmatrix}, \tag{1.54}$$

where the coefficient matrix may be equivalently defined as an upper triangular matrix, or as its symmetric part; the symmetric part of such coefficient matrix also embodies the *compliance matrix* for the unit length beam segment.

Most of the 21 independent matrix coefficients are zero if a few properties hold for the beam cross section and material; in particular:

- the i coefficients are null if the material is symmetric with respect to the cross-sectional plane, i.e. if the material is *monoclinic* with respect to such a plane. An orthotropic material falls within this category if one of the principal directions is aligned with the beam axis. An isotropic material always falls within this category. Local scale material homogeneization may be considered for composite materials which are pointwisely not compliant, but compliant in average (e.g. through-thickness balanced laminates);

- the g and the h coefficients are also zeroed if, as it ordinarily happens, the poles employed in evaluating the bending moments and the torsional moment coincide with the centroid and with the shear center, respectively. Moreover, the coordinates of such two points, if not already known, may be derived by imposing null g and h coefficients.

- the e coefficient is zero if the local x, y axes are aligned with the principal directions of inertia of the cross section;

- the f coefficient is zero for a dedicated orientation choice for the shear force components, which does not in general coincide with the principal directions of inertia; those directions however

coincide with the symmetry axis and its perpendicular direction for a symmetric cross section.

In the case of a homogeneus, isotropic material, the residual nonzero coefficients are defined as follows.

$$a_{1,1} = \frac{1}{EA} \qquad \{b_{2,2}, b_{3,3}, e_{2,3}\} = \frac{\{J_{\mathrm{yy}}, J_{\mathrm{xx}}, 2J_{\mathrm{xy}}\}}{E\left(J_{\mathrm{xx}}J_{\mathrm{yy}} - J_{\mathrm{xy}}^2\right)}$$
$$d_{6,6} = \frac{1}{GK_t} \qquad \{c_{4,4}, c_{5,5}, f_{4,5}\} = \frac{\{\chi_{\mathrm{x}}, \chi_{\mathrm{y}}, \chi_{\mathrm{xy}}\},}{GA}$$

where

- A, J_{yy}, J_{xx} and J_{xy} are the section area and moments of inertia, respectively;
- K_{t} is the section torsional stiffness (**not** generally equivalent to its polar moment of inertia);
- E and G are the material Young Modulus and Shear Modulus, respectively.

The shear energy normalized coefficients χ_{y},χ_{x},χ_{xy} are specific to the cross section geometry, and may be collected from the expression of the shear strain energy due to the concurrent action of the $Q_{\mathrm{x}}, Q_{\mathrm{y}}$ shear forces.

In the case the strain energy contribution of any of the stress resultants is to be neglected, the associated matrix coefficients may be set to zero; such manipulation makes the beam *rigid* with respect to the stress resultant whose contribution to the strain energy is nullified.

Finally, the quadratic form matrix[35] in Eq. 1.55 may be used to derive from the generalized stress components $\{N, M_{\mathrm{x}}, M_{\mathrm{y}}, Q_{\mathrm{x}}, Q_{\mathrm{y}}, M_{\mathrm{t}}\}$ for the beam cross section the energetically associated generalized strain

[35] here the symmetric part, and not the matrix itself, has to be strictly employed, as underlined.

components

$$\begin{pmatrix} e \\ \frac{1}{\rho_{\mathrm{x}}} \\ \frac{1}{\rho_{\mathrm{y}}} \\ g_{\mathrm{x}} \\ g_{\mathrm{y}} \\ \psi' \end{pmatrix} = \begin{pmatrix} a_{1,1} & g_{1,2} & g_{1,3} & i_{1,4} & i_{1,5} & i_{1,6} \\ 0 & b_{2,2} & e_{2,3} & i_{2,4} & i_{2,5} & i_{2,6} \\ 0 & 0 & b_{3,3} & i_{3,4} & i_{3,5} & i_{3,6} \\ 0 & 0 & 0 & c_{4,4} & f_{4,5} & h_{4,6} \\ 0 & 0 & 0 & 0 & c_{5,5} & h_{5,6} \\ 0 & 0 & 0 & 0 & 0 & d_{6,6} \end{pmatrix}_{\underline{\mathrm{Sym}}} \begin{pmatrix} N \\ M_{\mathrm{x}} \\ M_{\mathrm{y}} \\ Q_{\mathrm{x}} \\ Q_{\mathrm{y}} \\ M_{\mathrm{t}} \end{pmatrix}, \qquad (1.55)$$

where

- e is the axial elongation at the centroid;
- $\frac{1}{\rho_{\mathrm{x}}}$, $\frac{1}{\rho_{\mathrm{y}}}$ are the flexural curvatures;
- g_{x}, g_{y} are the average shear strain components;
- ψ' is the torsional twist rate.

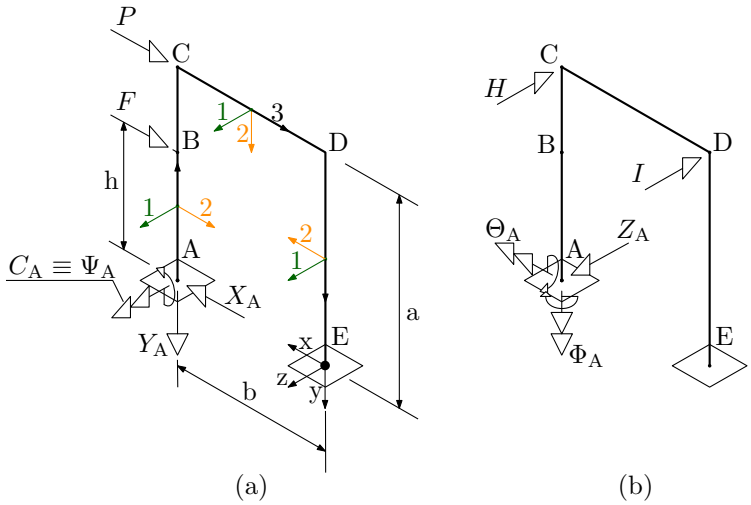

Figure 1.25: A rollbar-like frame; Figures a) and b) collect the considered in-plane and out-of-plane actions, respectively, which are split for added readability.

1.12 A semi-worked example: a rollbar-like frame

Let's considered the plane frame structure depicted in Fig. 1.25, representing a simplified rollbar; a thin-walled, circular steel profile is employed for both the upright and the cross members, whose median diameter and thickness are d and t, respectively [36].

A global (E, xyz) reference system is employed[37] to represent the frame nodal coordinates, if required, and the constraint reaction components.

A local reference system $(G, 123)$ is set along the beam segments, whose third axis follows the beam branch orientation, and whose first axis is everywhere aligned with the global z direction.

The rollbar frame is clamped at both the A and E ends, and it is

[36] The present treatise is applicable to a generic material and cross section, provided that symmetry holds with respect to the plane the frame lies on; such further condition may be overcome coupling terms are considered between the otherwise uncoupled in-plane to out-of-plane problems.

[37] sorry for its unusual orientation, it has been inherited from some legacy lecture notes of mine.

loaded i) by a lateral force P, and ii) by a transverse force H, both applied at node C.

Expected results of the analysis are i) the internal action components at each frame node, and wherever they are maximal ii) the constraint reactions at the A and E clamps, iii) the lateral, inward[38] deflections $\tilde{u}_{\mathrm{B}}, \tilde{u}_{\mathrm{C}}$ at B and C, respectively, and iv) the transverse[39] deflections $\tilde{w}_{\mathrm{C}}, \tilde{w}_{\mathrm{D}}$ at both C and D.

The second Castigliano theorem is resorted to for deflection calculation, thus requiring the application of auxiliary, fictitious external forces F and I, that may perform work with the monitored deflection, if not already set (see the H force).

The structure is six times statically indeterminate; the clamp at A is removed, and the associated six components of constraint reaction, see Fig. 1.25, are set as further, parametrically defined external loads; a statically determinate *principal* stucture is hence obtained, which preserves the clamp at E as its only connection to ground.

The expression of the structure internal strain energy, namely

$$U\left(P, F, X_{\mathrm{A}}, Y_{\mathrm{A}}, \Psi_{\mathrm{A}}, H, I, Z_{\mathrm{A}}, \Theta_{\mathrm{A}}, \Phi_{\mathrm{A}}\right) \tag{1.56}$$

is obtained as a function of i) the applied loads and ii) of the parametrically defined reactions by integration of the lineic strain energy density along the structure; such energy density depends in turn on the pointwise value of the internal action components, see Eq. 1.55.

The actual value of those parametrically defined loads is obtained by imposing a null deflection along each of the six d.o.f.s at node A, and thus casting a linear (due to the assumed structure behaviour) system of six equations in the aforementioned six unknown parameters. Again, the second Castigliano theorem is employed in evaluating the node A generalized displacements.

Please note that Eq. 1.56 strain energy is deliberately *not* a function of the reactions at E. If the strain energy expression contains any of the reaction components associated to the principal structure residual constraints, their dependence (due to equilibrium) on external loads and parametrically defined reactions must be made explicit before applying the partial derivative operator [40]

[38] i.e. counter-oriented with respect to the x global axis

[39] i.e., oriented along the negative global z direction

[40] The contribution of the external loads and parametric reactions to the structure

The simplest way to do so is to substitute within U their expression according to the equilibrium equation solution.

Due to the symmetric nature of the structure under scrutiny, and to its assumed linear behavior, the overall problem may be partitioned into two uncoupled symmetric (or *in-plane*) and skew-symmetric(or *out-of-plane*) subproblems, that might be solved separately.

In order to streamline the treatise, the contribution alone is considered of the moment kind of stress resultants, thus neglecting the profile compliance with respect to axial and shear internal actions; such customary approximation - consistent with an *inextensible* Euler beam model - is justified by the supposed profile slenderness.

Figure 1.26 collects the contribution of each the in-plane external actions to the M_1 bending moment, plotted along the beam flank in tension. Such bending moment diagrams are obtained by considering the equilibrium of the portion of principal structure that spans from the A free end to each section which in turn is under scrutiny; please try to derive those diagrams on your own, since they *might hide some errors*.

We also notice that, consistently with the local axis orientation, M_1 is assumed positive if it stretches the profile fibers that are inner with respect to the frame.

Similarly, Fig. 1.27 collects the M_2 bending moment component, assumed positive if it stretches the fibers on the "back" of the frame (i.e. the cross section points whose z or 1 coordinates are the most negative), along with the M_t torsional moment, whose sign is explicitly reported. Again, please derive them independently, since *some mistakes might be present*.

We observe that all the diagrams are branchwise linear, due to the piecewise straight centroidal segment nature, and the absence of distributed actions. In such condition, a generic M moment components may be conveniently expresses as

$$M(s) = M_0 \, f\left(\frac{s}{l}\right) + M_l \, g\left(\frac{s}{l}\right), \qquad f(\xi) = 1 - \xi, \qquad g(\xi) = \xi$$

strain energy could otherwise remain nested within the constraint reaction symbols, at the risk of leaving them behind while performing the differentiation. Such loss of legitimate contributes actually occurs on the Maxima algebraic manipulator if the constraint reaction components are not *explicitly* declared dependent on the aforementioned actions.

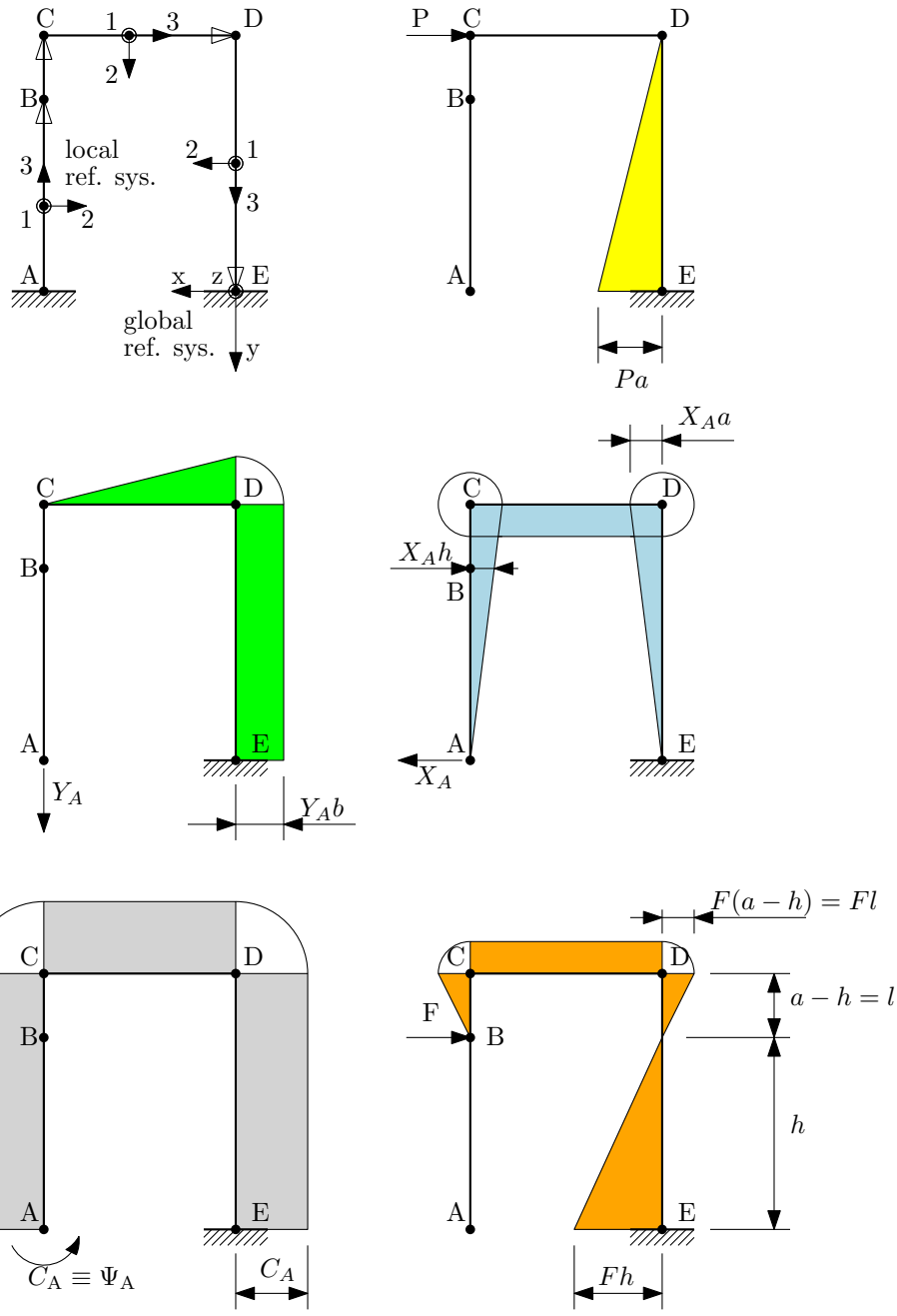

Figure 1.26: XXX

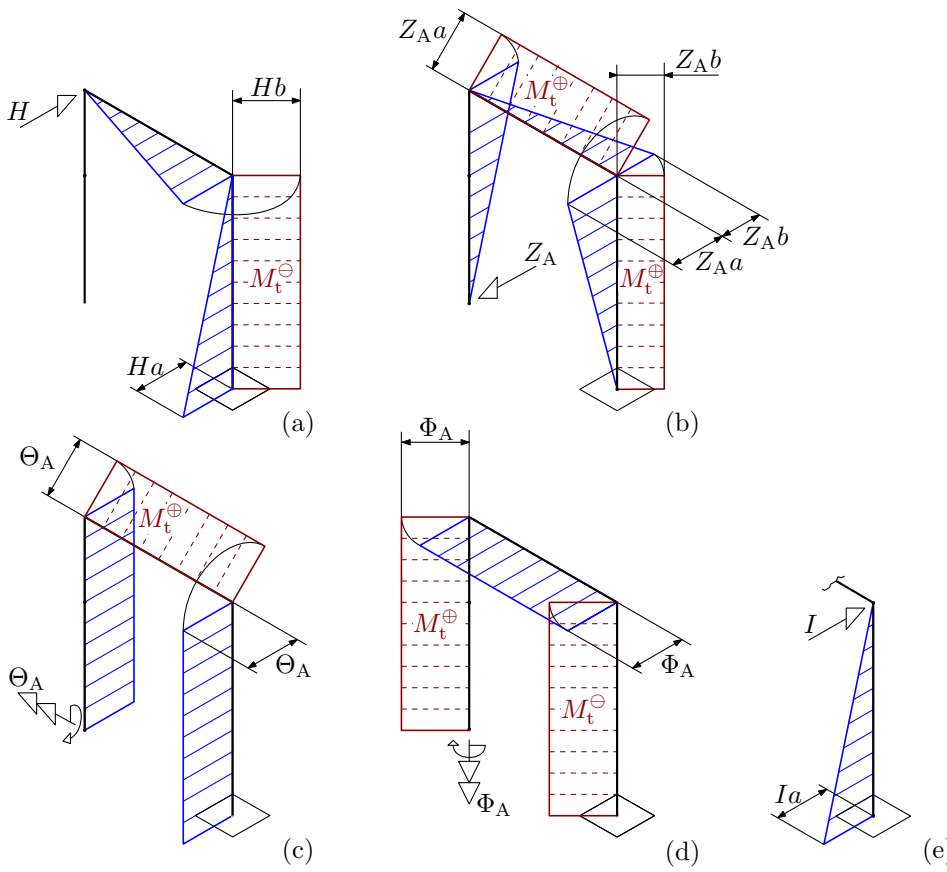

Figure 1.27: XXX

where $s \in [0, l]$ is a dimensional abscissa which spans through the l extension of each oriented segment, M_0 and M_l are the moment values at the extremities, and $\{f, g\}$ are two weight function whose aim is to linearly interpolate the moment extremal values along the beam segment interior.

For each segment, the associated strain energy is evaluated as

$$U = \int_0^l \underbrace{\frac{M_1^2(s)}{2EJ}}_{\text{symm.}} + \underbrace{\frac{M_2^2(s)}{2EJ} + \frac{M_{\text{t}}^2(s)}{2GK_{\text{t}}}}_{\text{skew-symm.}} ds, \tag{1.57}$$

where

$$J = \frac{\pi d^3 t}{8}, \qquad K_{\text{t}} = \frac{\pi d^3 t}{4}, \qquad G = \frac{E}{2\,(1+\nu)};$$

each beam branch contribution is finally accumulated to obtain the overall structure strain energy, possibly split into its symmetric and skew-symmetric parts.

Once the structure strain energy has been evaluated, we may proceed in evaluating the requested deflections as

$$\begin{aligned} \tilde{u}_{\text{B}} &= \frac{\partial U}{\partial F} & \tilde{u}_{\text{C}} &= \frac{\partial U}{\partial P} \\ \tilde{w}_{\text{C}} &= \frac{\partial U}{\partial H} & \tilde{w}_{\text{D}} &= \frac{\partial U}{\partial I}; \end{aligned}$$

similarly, we may derive the deflections at A, and cast a system of equations to enforce kinematic compatibility with the original constraints, namely

$$\begin{aligned} u_{\text{A}} &= \frac{\partial U}{\partial X_{\text{A}}} = 0 & v_{\text{A}} &= \frac{\partial U}{\partial Y_{\text{A}}} = 0 & \psi_{\text{A}} &= \frac{\partial U}{\partial \Psi_{\text{A}}} = 0 \\ w_{\text{A}} &= \frac{\partial U}{\partial Z_{\text{A}}} = 0 & \theta_{\text{A}} &= \frac{\partial U}{\partial \Theta_{\text{A}}} = 0 & \phi_{\text{A}} &= \frac{\partial U}{\partial \Phi_{\text{A}}} = 0. \end{aligned}$$

The value of the six unknown reactions at A may be then derived as a (linear) function of the remaining loads, e.g.

$$\begin{aligned} X_{\text{A}} &= X_{\text{A}}\,(F, P, H, I) = \alpha F + \beta P \underbrace{+\gamma H + \delta I}_{=0} \\ Y_{\text{A}} &= Y_{\text{A}}\,(F, P, H, I) = \dots \\ \Psi_{\text{A}} &= \dots \end{aligned}$$

etc., where the linear combination coefficients are placeholders for their actual counterparts which derive from the system solution. The fictitious nature of the H and I load is now explicited by assuming for them a null magnitude. Unless done before, the constraint reaction components at E may now be derived by solving the equilibrium equations for the whole principal structure.

Finally, we may substitute within the previously obtained $\tilde{u}_{\mathrm{B}}$, $\tilde{u}_{\mathrm{C}}$, $\tilde{w}_{\mathrm{C}}$, and $\tilde{w}_{\mathrm{D}}$ displacements the now available expressions for the parametric reaction forces, thus obtaining their dependence on the F, P external loads alone.

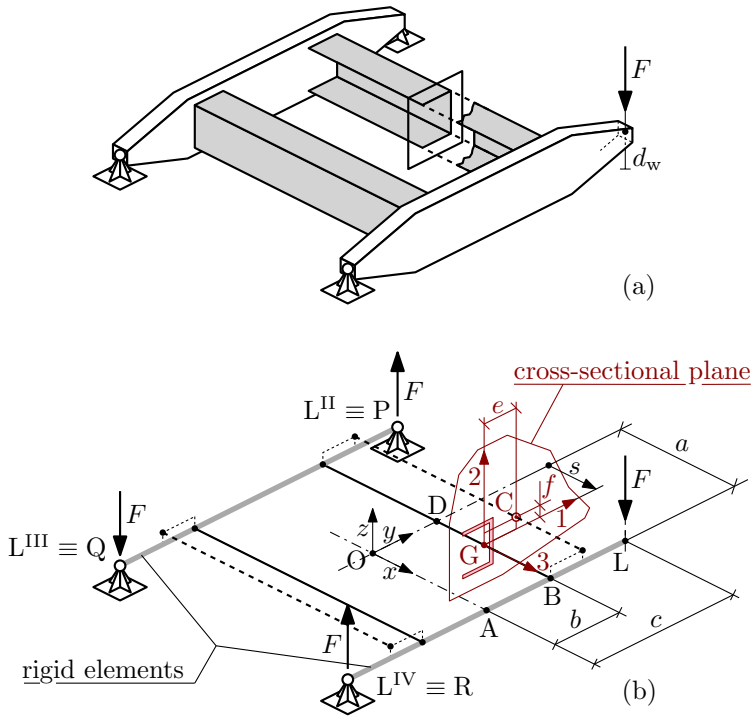

Figure 1.28: A simplified ladder-frame chassis, consisting in two longitudinal channel-section beams spanning along the wheelbase; their connection to the axles are assumed as rigid for simplicity, and the three supports are such to exert a purely vertical reaction force.

1.13 A semi-worked example: a simplified ladder frame chassis

The present contribution concerns the *torsional stiffness*[41] evaluation for the simplified ladder-frame chassis depicted in Fig. 1.28, whose track width is $2c$ for both the axles, and whose wheelbase is $2a$; the length of the two rail profiles is nominally assumed equal to the wheelbase.

Torsional stiffness is an established chassis structure conventional property, which is significant for the suspension tuning practicability

[41] a.k.a. torsional *rigidity*

with respect to under-/oversteering control; still, it is simplistic to assume that a high enough torsional stiffness may prevent handling issues in general, since, e.g. it is pretty uncoupled with the structure response to dynamic lateral forces. Nevertheless, the measurement procedure is straightforward, and the test rig is cheap.

Fig. 1.28a represents a formally correct test setting for the torsional stiffness; the chassis is *simply* supported at three of the wheel centers, whereas a vertical force F is applied at the fourth one, at which the d_{w} vertical deflection is also measured.

The vertical supports allow for three residual rigid body motions along the (O,xy) horizontal plane; a statically determinate set of further constraint is required for uniquely positioning the structure in space.

It is of the most importance to grant the statically determinate nature of the overall constraining system, since any further restraint might unduly support the loaded structure, and thus spuriously raising its observed stiffness.

A straightforward analysis of the chassis structure global equilibrium[42] returns that each axle is loaded by a pair of equal and opposite vertical forces - i.e. by a pure, longitudinally oriented moment vector, and that those two front and rear moments are self compensating. In the case of equal track widths, four vertical forces of equal magnitude F are applied at the four wheel centers, whose orientation switches along the axles, and from the axle to axle; in the case of different track widths, forces of equal magnitude are applied at each wheel of the axle, and they scale from the front to the rear with the inverse of the track width.

Once obtained the experimental ratio between the F force and the d_{w} deflection, the torsional stiffness k may be derived as the ratio between the magnitude of the torque applied to each axle, and the relative twist angle, namely

$$k = \frac{2cF}{\frac{d_{\mathrm{w}}}{2c}} = \frac{F(2c)^2}{d_{\mathrm{w}}}, \tag{1.58}$$

[42] with reference to Fig. 1.28b, i) rotational equilibrium with respect to the rear PQ axle requires a downward F force at R, ii) rotational equilibrium with respect to the front LR axle requires that the two rear supports exert equal and opposite vertical reactions, whose magnitude is set by iii) the rotational equilibrium with respect to the longitudinal chassis axis.

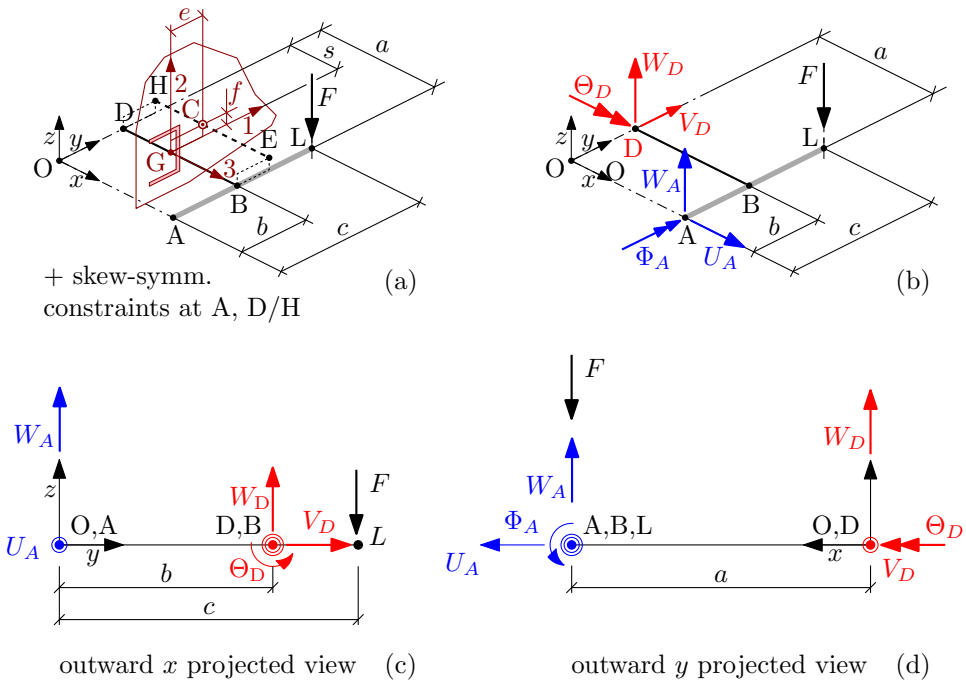

Figure 1.29: A quarter portion of the ladder frame, which is the minimal portion to be modeled due to the dual skew-symmetry. Please note that the (O,xyz) reference system of the present figure coincides with its fixed counterpart as in Fig. 1.28 in the undeformed configuration only. The present figure reference frame partly follows, in fact, the structure deflection.

where the $2c$ track width pertains to the axle that includes the loaded (and monitored in deflection) wheel center.

In the case under scrutiny of equal track widths, the twice-symmetric structure is loaded by a system of four forces which are skew-symmetrically arranged with respect to both the (O,zx) and the (O,yz) planes[43].

A twice skew-symmetric problem is thus obtained, whose representative portion - a quarter of the whole structure - is represented Figure 1.29a.

[43] a third skew-symmetry plane, namely the (O,xz) exists if the profiles are consistently symmetric; however, limited benefit is attained in considering such a third skew-symmetry plane in the treatise.

Skew-symmetry constraints are required at the intersection of the front axle rigid member with the (O,zx) plane - a point, this, which is *nominally* embodied by the A location[44], and at the intersection of the longitudinal rails with the (O,yz) plane, nominally taken at the D centroid of the interested cross section. Those constraints are set in order to grant material - or rigid body motion law - continuity between the modeled, representative portion of the structure, and its images, and they lead to the reaction forces and moments listed in Fig. 1.29b.

It worth to mention that the problem depicted in Fig. 1.28 is *not* twice skew-symmetric in itself, due to the unsimmetric nature of the support arrangement; however, the problem acquires such a property once the exerted reaction forces are considered, in place of the originating constraints.

In such cases, the problem solutions obtained i) for the complete structure, subject to the original constraints, and ii) for the representative portion, and duly mirrored, are consistent in terms of strains, stresses and with regard to their resultants, whereas they differ by a rigid body motion in terms of absolute displacement and rotations. Such a behavior can be rationalised by considering that a moving frame exists, according to which a [skew-]symmetric structure behavior is observed; this moving reference system is ideally pinned to the structure at the same d.o.f.s that are affected by the [skew-]symmetry constraints.

Most of the skew-symm. constraint reaction forces may be set based on the equilibrium equations for the quarter ladder-frame structure, see Fig. 1.29b; U_{A} and V_{D} are set null based on the translational equilibrium with respect to the global x and y axes, respectively. By casting a system of equations which involves the translational equilibrium with respect to z, and the rotational equilibrium with respect to the (O,x) and the (O,y) axes - see Figs 1.29c and 1.29d, other three unknown reactions amongst W_{A}, Φ_{A}, W_{D} and Θ_{D} may be defined; the remaining independent equilibrium equation - a rotational one, and associated to the (O,z) axis - is trivially satisfied in the absence of any contribution, thus making the overall system of equations rank deficient of degree one.

The [quarter] ladder-frame structure, loaded according to the torsional stiffness test, appears hence once *internally* statically indeter-

[44] any point of the (O,zx) plane may equally serve the purpose

minate[45]; we then define a principal structure by fictively releasing the z oriented constraint at A, and thus allowing for a z-oriented slippage at the interface between the ABL rigid member and its image. As usual, the associated W_{A} reaction force is treated as a parameter, whose value is tuned to reinstate continuity at A; the remaining constraint reactions are then obtained as a linear combination of the F and W_{A} load parameters.

The second Castigliano theorem is employed to evaluate the w_{A} vertical deflection at A, which in turn requires the expression for the internal strain energy to be cast as a function of the same aforementioned load parameters.

Since the contribution of a rigid member to the structure strain energy is zero by definition, we proceed to the evaluation of the internal action components for the channel section rail; by considering the equilibrium of a DG rail segment, where G is a centroidal point taken at a s distance from D - see Fig. 1.29a, we obtain

$$N = 0 \qquad Q_1 = -V_{\mathrm{D}} = 0 \qquad Q_2 = -W_{\mathrm{D}} = W_{\mathrm{A}} - F$$

and

$$\begin{aligned} M_1 &= -sW_{\mathrm{D}} = -s\left(W_{\mathrm{A}} - F\right) \\ M_2 &= +sV_{\mathrm{D}} = 0 \\ M_{\mathrm{t}} &= -\Theta_{\mathrm{D}} + eW_{\mathrm{D}} - fV_{\mathrm{D}} = \left(F - W_{\mathrm{A}}\right)(e+b) - Fc. \end{aligned}$$

The torsional moment M_{t} does not coincide with $-\Theta_{\mathrm{D}}$ since the $V_{\mathrm{D}}, W_{\mathrm{D}}$ shear aligned forces are assumed as applied at the D - which is a centroid, and they result shifted with respect to the cross-sectional shear center.

The following expression for the strain energy lineic density is employed – cfr. Eq.1.55 – which preserves the contribution of all the internal action components

$$\begin{aligned} \frac{dU}{dl} = \; & \frac{N^2}{2EA\alpha_{\mathrm{axl}}} + \frac{J_{22}M_1^2 + J_{11}M_2^2 + 2J_{12}M_1M_2}{2E\left(J_{11}J_{22} - J_{12}^2\right)\alpha_{\mathrm{flx}}} \\ & + \frac{M_{\mathrm{t}}^2}{2GK_t\alpha_{\mathrm{trs}}} + \frac{\chi_1 Q_1^2 + \chi_2 Q_2^2 + \chi_{12}Q_1Q_2}{2GA\alpha_{\mathrm{shr}}}. \end{aligned}$$

[45]Please note that, apart from the peculiar [skew-]symmetric condition, a spatial closed ring is in general six times statically indeterminate.

Also, the cross section elastic characteristic with respect to each internal action component is scaled by a normally unit auxiliary factor $\alpha_\square$, which may steer the elastic response towards infinite compliance ($\alpha_\square \to 0$) or infinite stiffness ($\alpha_\square \to \infty$); those stiffness multipliers will be employed in the discussion of the results below, and may be ignored otherwise.

We may now integrate such a lineic strain energy density over the interval $s \in [0, a]$, thus obtaining the U internal strain energy for the quarter frame as a quadratic function of F and W_A.

The vertical deflection at A may then be derived according to the Castigliano theorem, and may be set to zero in order to obtain the expression of W_A as a linear function of F.

As in the previous worked example, such $W_\mathrm{A}(F)$ is substituted within the $U\left(F, W_\mathrm{A}\right)$ quarter frame internal energy expression, which becomes a function of the sole external load F.

A further applications of the Castigliano theorem let us derive the d deflection of the F force application point for the quarter ladder-frame structure, i.e. with respect to the aforementioned moving reference system, according to which the displacement field is twice skew-symmetric.

The absolute d_w deflection of the L wheel center, i.e. the deflection observed according to a reference system consistent with the three supports of Fig. 1.28, may be derived based on the observation that the internal energy for the *whole* chassis is four times the one evaluated for the quarter structure; we thus obtain

$$d_\mathrm{w} = \frac{d(4U)}{dF} = 4d. \tag{1.59}$$

Such a result may be rationalized considering the $(-d, +d, -d, +d)$ vertical deflections of the (L,P,Q,R) points, respectively, derived from the mirrored quarter structure response. A downward, uniform, translation of magnitude d reestablishes the congruence with the fixed supports at points P,R, with overall deflections $(-2d, 0, -2d, 0)$. Finally, a suitable rotation with respect to the PR diagonal raises of a $2d$ quantity the vertical position of the Q point, thus reinstating compliance with the third support. Since the L and the Q points are located at an equal distance from the pivot line, the same rotation lowers the L point of an equal $2d$ quantity, thus leading to the absolute deflection configuration $(-4d, 0, 0, 0)$.

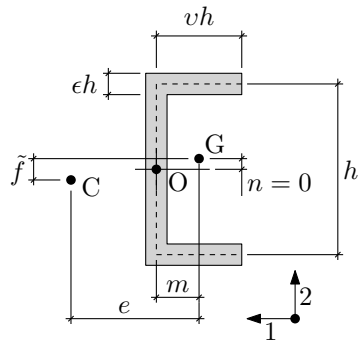

Figure 1.30: Dimensions for the channel section employed in calculations. The web height h is the relevant dimensional parameter, whereas υ is the ratio between the flange width and the web height, and ϵ sets the ratio between the wall thickness – assumed uniform – and the web height. Centroidal coordinates (m, n) are measured with respect to the web midspan, whereas the shear center coordinates (e, f) are measured with respect to the centroid. Please note that the cross-section properties reported in the maxima worksheet are evaluated according to a small thickness hypothesis, i.e. their expressions is consistent with a vanishing ϵ, first order Taylor expansion.

The ladder-frame chassis torsional stiffness may be then evaluated according to Eqn. 1.58, which leads to a pretty composite expression whose rationalization is complicated.

In order to isolate the influence of the various parameters, a reference configuration is defined in terms of channel section and global chassis dimensions. In particular, the worked example provided in form of a maxima worksheet employs the channel section of Fig.1.30 for both the rails. Also, all the $\alpha_\square$ auxiliary stiffness multipliers are bonded to unity in the reference case.

The response of the structure to the variation of one or more parameters is assessed based on the torsional stiffness ratio between the altered configuration, and the reference one.

Leaving to the willing reader the influence analysis of the various parameters[46], we focus on how the three main sources of compliance

[46]Consider in particular the influence of the rail span length a, of their mutual distance b, and the influence of the cross section size h and thickness t. Since the

– namely, the rail compliance to the torsional moment, to the bending moment, and to shear actions – interact in defining the overall compliance of the simple structure under scrutiny.

The ratio is hence considered between the chassis torsional stiffness for the reference configuration, namely k_{ref}, and its $k\left(\alpha_{\mathrm{trs}}, \alpha_{\mathrm{flx}}, \alpha_{\mathrm{shr}}\right)$ counterpart obtained with given α_{trs}, α_{flx} and α_{shr} profile torsional, bending a shear stiffness multipliers, respectively.

If we speculate the profile flexural[47] and shear stiffness to vanish, i.e. the longitudinal rail torsional stiffness is fictitiously left alone in elastically connecting the two rigid elements, we may consider the limit

$$\lim_{\alpha_{\mathrm{flx}}, \alpha_{\mathrm{shr}} \to 0} \frac{k\left(1, \alpha_{\mathrm{flx}}, \alpha_{\mathrm{shr}}\right)}{k_{\mathrm{ref}}} = p > 0 \tag{1.60}$$

which returns a nonzero fraction of the unity, whose value is pretty small for the open thin-walled section under scrutiny, but that might become relevant for bulky closed section profiles. Each profile is in fact twisted by the same amount of relative rotation that occurs between the two front and rear rigid members, thus accumulating internal strain energy, and thus requiring a finite work-supplying external force.

We now consider the complementary condition, in which the two rails lose their capability to elastically react to torsion, whilst retaining their full shear and flexural stiffness; we hence consider the limit

$$\lim_{\alpha_{\mathrm{trs}} \to 0} \frac{k\left(\alpha_{\mathrm{trs}}, 1, 1\right)}{k_{\mathrm{ref}}} = 1 - p > 0 \tag{1.61}$$

which also returns a nonzero fraction of the unity, complementary to the former one, as expected. Such a fraction of the overall stiffness may be observed to vanish e.g. with vanishing spacing between the two rails; it is in fact associated to the vertical misalignment of the longitudinal beam ends, which equates the product of the relative rigid member rotation by an arm that is equal to half the rail spacing. Such

material is homogeneous and isotropic, the stiffness varies linearly with the Young modulus, you don't really have to check. For a cleaner analysis, try also to isolate the various sources of compliance, i.e. compliance with respect to bending moments, torsional moment, and shear actions alone.

[47] Here, we follow for added clarity the academic distinction between *bending*, which – in consistency with to the general *nonuniform* bending meaning – may be employed as an umbrella term for both flexure and shear, and *flexure*, which excludes shear contributions.

a vertical misalignment may not be achieved through a profile rigid motion, and hence a further contribution is due to the overall strain energy.

The complementary nature of the two above quantities hints for a in parallel disposition of the two means the profile may react to the relative rotation of the rigid members they are clamped to.

The latter contribution may be further scrutinized by splitting the two distinct shear and flexural contributions; we consider in particular the two limits

$$\lim_{\alpha_{\text{shr}}\to 0}\lim_{\alpha_{\text{trs}}\to 0}\frac{k\left(\alpha_{\text{trs}},1,\alpha_{\text{shr}}\right)}{k_{\text{ref}}}=0\qquad\lim_{\alpha_{\text{flx}}\to 0}\lim_{\alpha_{\text{trs}}\to 0}\frac{k\left(\alpha_{\text{trs}},\alpha_{\text{flx}},1\right)}{k_{\text{ref}}}=0 \tag{1.62}$$

which both vanish, thus indicating that none of the two isolated elastic reactions may be activated alone. By turning into rigid the profile with respect to either shear or flexure, i.e.

$$\lim_{\alpha_{\text{shr}}\to\infty}\lim_{\alpha_{\text{trs}}\to 0}\frac{k\left(\alpha_{\text{trs}},1,\alpha_{\text{shr}}\right)}{k_{\text{ref}}}=q>1-p>0 \tag{1.63}$$

$$\lim_{\alpha_{\text{flx}}\to\infty}\lim_{\alpha_{\text{trs}}\to 0}\frac{k\left(\alpha_{\text{trs}},\alpha_{\text{flx}},1\right)}{k_{\text{ref}}}=r>1-p>0, \tag{1.64}$$

we obtain finite normalized flexural and shear compliances, $1/q$ and $1/r$ respectively, whose sum equates the cumulative compliance $1/(1-p)$ attributable to the overall bending. An in-series arrangement of the two flexural and shear compliances is thus suggested, which finds rationalization in the fact that the same end transverse shift may be accomodated both through i) an S-shaped, purely flexural deflection, ii) through a card-deck pure shear inclination, or iii) a combination of the two.

The compliance components' arrangement for the simplified ladder-frame chassis under scrutiny is shown in Figure 1.31; in a general structure, the mutual interaction of the elastic members may not be pigeonholed within the simplistic "many in parallel" or "many in-series" models; a complex combination of those two elementary modes may be considered even for the simple, single d.o.f. case treated in the present paragraph.

It is finally noted that, in the case of struts manufactured from composite laminates, the speculative selective deactivation of one or

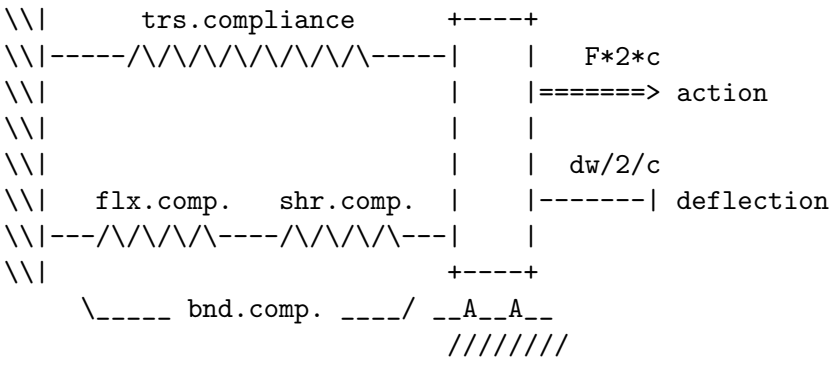

Figure 1.31: An ASCII art rationalization of the compliance components' arrangement for the simplified ladder frame chassis under scrutiny; the torsional elastic compliance of the profiles acts in parallel with their combined in-series flexural and shear compliance.

the other mean of elastic response earns actual significance, since the simple lack of dedicated laminae may suffice in obtaining such a tricky behavior; as an example, the absence of axially oriented fibers in a CFRP laminated profile may lead to a condition which is very similar to the $\alpha_{\text{flx}} \to 0$ case.

Chapter 2

Fundamentals of Finite Element Method for structural applications

2.1 Basic formulation for plates and shells

2.1.1 Some assumptions for the kinematic model of the plate

A necessary condition for applying the plate/shell model framework to a deformable body is that a geometrical midsurface might be, if only loosely, recognized for such a body. Then, an iterative refinement procedure[1] may be applied to such tentative midsurface guess.

Then, material should be observed as *[piecewise-]*homogeneous, or slowly varying in mechanical properties while moving at a fixed distance from the midsurface.

Of the two outer surfaces, one has to be defined as the *upper* or *top* surface, whereas the other is named lower ot *bottom*, thus implicitly orienting the midsurface normal towards the top.

Finally, the body should result fully determined based on a) its midsurface, b) its pointwise thickness, and c) the through-thickness (tt) distribution of the constituent materials.

The geometrical midsurface is of little significance if the material distribution is not symmetric[2]; such midsurface, in fact, exhibits no relevant properties in general. Its definition is nevertheless pretty straighforward.

In the present treatise, a more general *reference* surface definition is preferred to its median geometric counterpart; in particular, an *offset* term o is considered that pointwisely shifts the geometric midsurface with respect to the reference surface. A positive offset shifts the midsurface towards the top.

With the introduction of the offset term, the reference surface may be arbitrarily positioned with respect to the body itself; as an example, an offset set equal to plus or minus half the thickness makes the reference surface correspondent to the bottom or top surfaces, respectively.

Such offset term becomes fundamental in the Finite Element (FE) shell implementation, where, in fact, the reference plane is uniquely

[1] Normal segments may be cast from each point along the midsurface, that end on the outer body surfaces. The midpoint locus of these segments redefines the midsurface itself.

[2] If the unsimmetric laminate is composed by isotropic layers, a reference plane may be obtained for which the $\underline{\underline{b}}$ membrane-to-bending coupling matrix vanishes; a similar condition may not be verified in the presence of orthotropic layers.

defined by the position of the nodes, whereas the offset arbitrarily shifts the geometrical midsurface.

In the case of limited[3] curvatures, and for considerations whose scope is local, the tangent reference plane may be employed in place of the possibly curve reference surface, thus locally reducing the general shell treatise to its planar, plate counterpart.

Figure 2.1 shows the basic kinematic relations for the shear deformable (Mindlin) plate model; in the undeformed configuration, P is a generic material point along the plate thickness, and Q is its normal projection on the reference plane. Such Q point is named *reference point* for the tt normal segment it belongs to.

A local reference system is defined, whose third axis z is normal to the undeformed midsurface; the first ip x axis may be arbitrarily oriented, e.g. by projecting a global $\hat{v}$ unit vector, and the remaining y axis may be construed such that it finalizes the right xyz triad.

Then, the deformed configuration is considered, and the motion of both the points is monitored according to two mutually orthogonal views. The P displacement components $(u_{\mathrm{P}}, v_{\mathrm{P}}, w_{\mathrm{P}})$ may be defined as a function of the motion of its reference point Q, described in terms of its displacement components (u, v, w), plus the two θ, ϕ rotation components with respect to the x, y ip local axes, respectively. Those angular displacements are defined with respect to the normal segment orientation, as measured on the orthogonally projected views. After some cumbersome trigonometric manipulations[4] we obtain

$$
\begin{aligned}
u_P &= u + z\,(1+\check{\epsilon}_z)\,\frac{\cos\theta}{\sqrt{1-\sin^2\phi\sin^2\theta}}\sin\phi \\
v_P &= v - z\,(1+\check{\epsilon}_z)\,\frac{\cos\phi}{\sqrt{1-\sin^2\phi\sin^2\theta}}\sin\theta \\
w_P &= w + z\left((1+\check{\epsilon}_z)\,\frac{\cos\phi\cos\theta}{\sqrt{1-\sin^2\phi\sin^2\theta}} - 1\right),
\end{aligned}
$$

where $z\,(1+\check{\epsilon}_z)$ is the length of the PQ segment on the deformed configuration, which is further scaled by the fractional factors due to projection along Fig. 2.1 views.

[3] with respect to thickness

[4] in which it may happen to miss some higher order terms, as the author persistently did in previous versions of the present notes

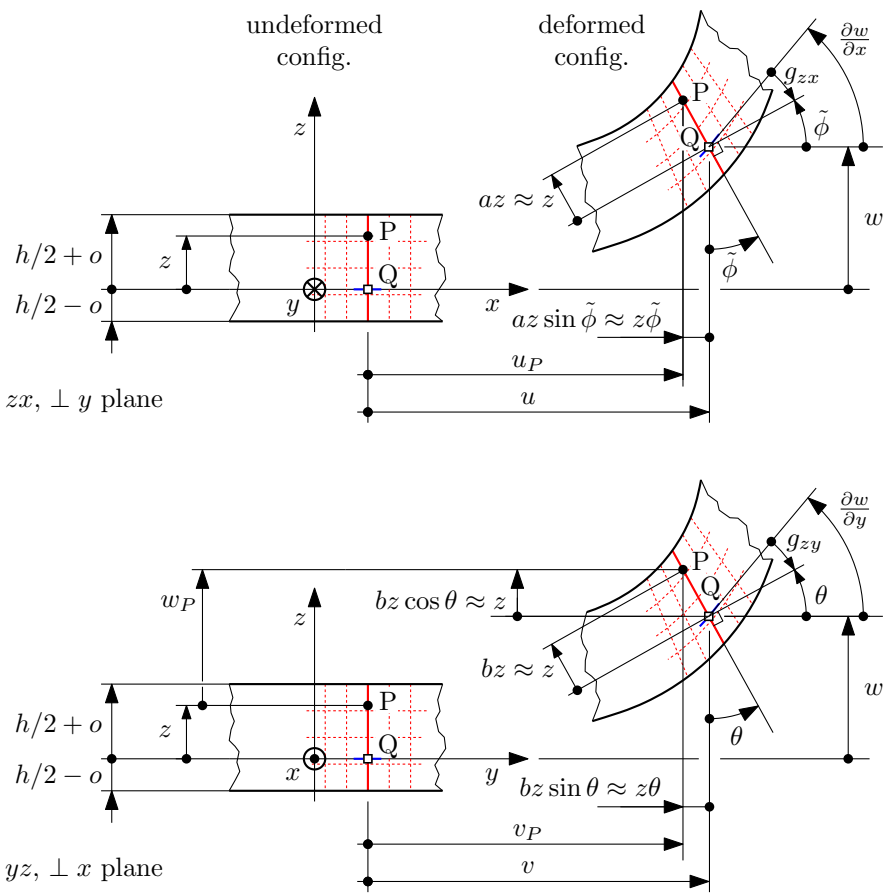

$$\{a,b\} = \frac{(1+\check{\epsilon})}{\sqrt{1-\sin^2\phi\sin^2\theta}}\{\cos\theta,\cos\phi\} \approx 1$$

Figure 2.1: Relevant dimensions for describing the deformable plate kinematics. Here, two a, b factors are introduced which reduce to unity for small rotations and strain.

The $\check{\epsilon}_z$ average z strain term is defined based on the accumulation of the Poisson shrinkage (or elongation) along the PQ segment, i.e.

$$\begin{aligned}\check{\epsilon}_z(z) &= \frac{1}{z}\int_0^z \epsilon_z d\varsigma \\ &= \frac{1}{z}\int_0^z -\frac{\nu}{1-\nu}\left(\epsilon_x+\epsilon_y\right)d\varsigma,\end{aligned}$$

the second expression holding in the case of isotropic materials only.

The stress component σ_z which is normal to the reference surface is in fact assumed to be either zero or negligible. Being a full discussion[5] of such a plane stress assumption beyond the scope of the present contribution (bspc), we limit our treatise to the observation that, in the inevitably anecdotal case of Fig. 2.2, the ratio between the oop σ_z stress component and its ip counterparts varies with the square of the ratio between the thickness and an in plane significant length. The engineering relevance of such a normal stress component rapidly vanishes with increasing plate thinness. The Fig. 2.2 examples also points out the intermediate magnitude decay of the oop shear stresses, whose normalized form linearly varies with the same thinness ratio.

Such displacement components may be linarized with respect to i) the small rotations and ii) small ϵ_z strain hypotheses, thus obtaining the following expressions

$$u_P = u + z\phi \tag{2.1}$$

$$v_P = v - z\theta \tag{2.2}$$

$$w_P = w. \tag{2.3}$$

A treatise of the large rotation and/or large strain nonlinear case is, again, bspc.

[5]Such assumption is coherent with the free surface conditions at the top and the bottom skins, and with the moderate thickness of the elastic body, that allows only a narrow deviation from the boundary values. In fact, the equilibrium of a partitioned, tt material segment requires that

$$\sigma_z(z) = -\int_{-h/2+o}^{z} \frac{\partial \tau_{zx}}{\partial x} + \frac{\partial \tau_{yz}}{\partial y} dz = +\int_{z}^{+h/2-o} \frac{\partial \tau_{zx}}{\partial x} + \frac{\partial \tau_{yz}}{\partial y} dz,$$

where τ_{zx}, τ_{yz} are the interlaminar, oop shear stress components, whose ip gradient is limited.

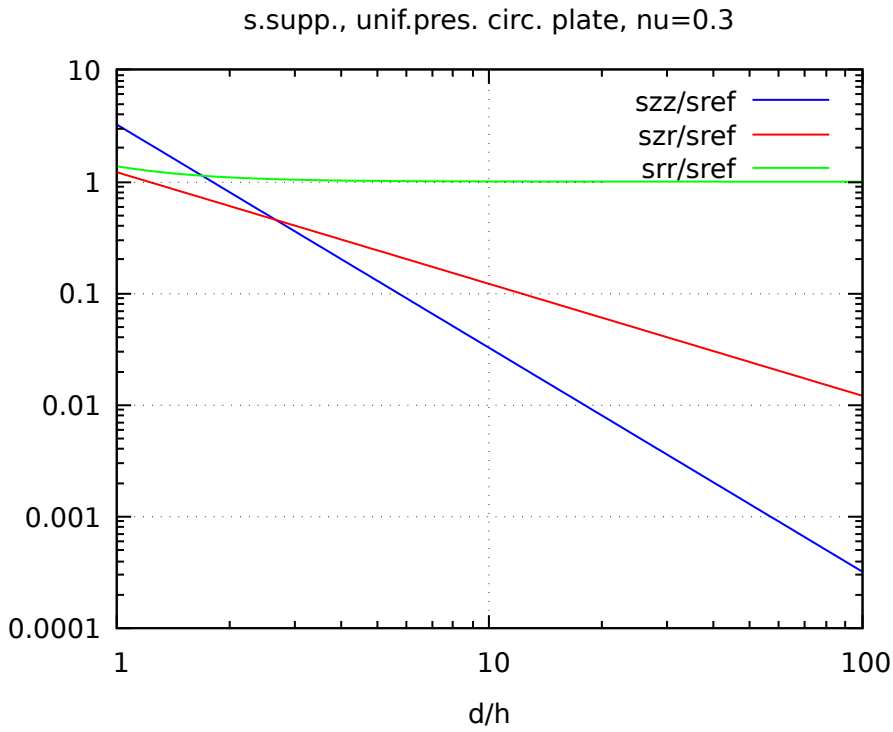

Figure 2.2: Normalized stress component magnitude in the case of a simply supported circular plate subject to normal pressure, according to the spatial theory of elasticity, see [2, p.349]. A homogeneous and isotropically elastic circular plate of diameter d and thickness h is simply supported along its perimeter (i.e. apart from the their transverse component, displacements are free, and so are rotations), and it is loaded by a unit pressure at its upper surface. The peak magnitude of the transverse stress σ_{z} falls at the pressurized surface, and it equates the pressure value. The oop shear stress τ_{zr} is maximal at the lateral surface median curve, and it equates $\frac{3}{8}\left(\frac{d}{h}\right)$. The two ip direct stress components $\sigma_{\mathrm{r}}, \sigma_{\theta}$ reach the common peak value of $\frac{3(\nu+3)}{32}\left(\frac{d}{h}\right)^2 + \frac{\nu+2}{20}$ in correspondence of the plate center, at the stretched surface; the thin plate peak stress counterpart, $\sigma_{\mathrm{ref}} = \frac{3(\nu+3)}{32}\left(\frac{d}{h}\right)^2$, which lacks the $O\left(\left(\frac{d}{h}\right)^0\right)$ second term, is taken as the normalizing stress value for the ordinate. The remaining $\tau_{\mathrm{r}\theta}$, $\tau_{\theta\mathrm{z}}$ stress components are zero due to axisymmetry. The commonwise $\nu = 0.3$ Poisson ratio value is used in tracing the Figure.

According to such linearized expression, the kinematics of the P points originally[6] laying on a tt segment that is normal at Q to the reference surface may be described as that of a rigid body.

The intrinsic shear related warping is either negated or neglected, along with any sliding motion of the P points along the segment[7].

Also, the behaviour of such a segment is coherent with its rigid body modeling from the external loads point of view; in particular the external actions act on the plate deformable body only through their tt resultants, and no stress/strain components, or work, are associated by the shell framework to wall squeezing actions, e.g. laminations.

We thus observe that, according to the shell framework, the following external actions are not distinguishable: i) a q pressure applied at the upper surface, ii) a $-q$ traction applied at the lower surface, iii) a q differential pressure between the outer surfaces, with $p+q$ applied at the top, and a generic p applied at the bottom, and iv) a transverse inertial force whose area density is q, namely due to a oppositely oriented $\frac{q}{\rho h}$ acceleration, where ρ is the material density. Also, a fp, friction induced, x-oriented shear action at the upper surface is not distinguishable from an analogous distributed force for unit area applied at the reference surface, plus a y-oriented distributed moment per unit area, whose magnitude is $fp(h/2+o)$.

By observing the deformed configurations in Fig. 2.1, the normal displacement $\left(\frac{\partial w}{\partial x}, \frac{\partial w}{\partial y}\right)$ gradient – i.e. the gained slope of the deformed reference surface, with respect to its original orientation – is made up of two terms, namely the rotation of the normal segment, which originates from the accumulation of the flexural curvature, and the shear compliance, which resembles the transverse slippage typical of a card deck. The following expressions are derived

$$\frac{\partial w}{\partial x} = g_{zx} - \phi \tag{2.4}$$

$$\frac{\partial w}{\partial y} = g_{yz} + \theta \tag{2.5}$$

[6] i.e. in the undeformed configuration

[7] The elision of higher order terms renders the laminate kinematically – but not elastically – indistinguishable from its counterpart that might derive from a plane *strain* assumption.

in which the latin g_{z*} employed for the oop shear components emphasizes their tt average[8] nature.

2.1.2 Local and generalized strains

The ip strain components may hence be derived at the P point through differentiation, and in particular we have

$$\epsilon_x = \frac{\partial u_P}{\partial x} = \frac{\partial u}{\partial x} + z\frac{\partial \phi}{\partial x} \tag{2.6}$$

$$\epsilon_y = \frac{\partial v_P}{\partial y} = \frac{\partial v}{\partial y} - z\frac{\partial \theta}{\partial y} \tag{2.7}$$

$$\gamma_{xy} = \frac{\partial u_P}{\partial y} + \frac{\partial v_P}{\partial x} \tag{2.8}$$

$$= \left(\frac{\partial u}{\partial y} + \frac{\partial v}{\partial x}\right) + z\left(+\frac{\partial \phi}{\partial y} - \frac{\partial \theta}{\partial x}\right) \tag{2.9}$$

It clearly appears from the expressions above that the pointwise strain values are due to the sum of i) the strain components as observed at the reference plane,

$$\underline{\mathrm{e}} = \begin{bmatrix} \frac{\partial u}{\partial x} \\ \frac{\partial v}{\partial y} \\ \frac{\partial u}{\partial y} + \frac{\partial v}{\partial x} \end{bmatrix} = \begin{bmatrix} e_x \\ e_y \\ g_{xy} \end{bmatrix} \equiv \underline{\epsilon}_{\mathrm{Q}} \tag{2.10}$$

which are named *membrane* strains[9] in the customary case in which the material is symmetric[10] with respect to the reference plane, plus ii) terms that linearly scale with the z distance from such a plane, whose coefficients

$$\underline{\kappa} = \begin{bmatrix} +\frac{\partial \phi}{\partial x} \\ -\frac{\partial \theta}{\partial y} \\ +\frac{\partial \phi}{\partial y} - \frac{\partial \theta}{\partial x} \end{bmatrix} = \begin{bmatrix} \kappa_x \\ \kappa_y \\ \kappa_{xy} \end{bmatrix} \tag{2.11}$$

[8] in strain energy

[9] $\underline{\mathrm{e}}$ is an alternative symbol for the more natural, and previously employed $\underline{\bar{\epsilon}}$, whose double barred appearance is however terrible. To complete the transition, also the $\bar{\epsilon}_x$, $\bar{\epsilon}_y$ and g_{xy} symbols have been changed onto their e_x, e_y, g_{xy} counterpart.

[10] or, more generally, elastically balanced

are named *curvatures*.[11] The strains at the reference surface, and the curvatures constitute the ip subset[12] of plate [shell] *generalized strain components*, which are e.g. usually returned by fe solvers; those components allow for the following compact representation of the ip strains at P

$$\underline{\epsilon}_{\mathrm{P}} \equiv \underline{\epsilon} = \underline{\mathrm{e}} + z\,\underline{\kappa}\,. \tag{2.12}$$

It worth to be stressed that the kinematic assumptions for the plate model impose a linear tt profile for each single ip strain component; those components may hence be sampled at the outer surfaces alone, without loss of information. It is here anticipated that an analogous behaviour is proper of the ip stress components if and only if (iif) the material is elastically homogeneous along the thickness .

The two κ_x and κ_y curvatures equate to the inverse of the normal curvature radii, as probed at the reference surface along the respective local directions; those curvatures are positive if the upper plate fibers are stretched, or, equivalently, if the reference surface acquires convexity if observed from above – i.e. from a point on the positive z axis.

Figure 2.3 clarifies the nature of the *mixed* curvature term κ_{xy}, which is e.g. typical of open thin walled members – and flat plates as a particular case – subject to torsion[13].

[11] Please note that in the case of shells, the bare *curvature* name may be confusing, since it might refer to either

- the initial, original, geometric, undeformed curvature, which is proper of the shell before the application of some external loads, or to the
- strain, strain-induced, elastic[-plastic], bending, flexural curvature, or curvature change, which consist in the variation of the thin wall curvature due to the effect of the applied loads.

Except for [locally] flat panels, the author suggests to always specify which kind of curvature we refer to. Here, *curvature* is used with reference to *curvature change*.

[12] the (g_{zx}, g_{zy}) oop subset of generalized strain components will be introduced in paragraph 2.1.5 .

[13] the *torsional* curvature denomination for the κ_{xy} term, that the present author has widely employed in the past, is not so proper nor widespread, so it might be better avoided. Flexure and torsion are in fact not as uncoupled in the plate realm as they are in beam theory, and *flexure* might be conveniently employed as an umbrella term that also encompass profile (open and thin) wall deformation due to pure torsion.

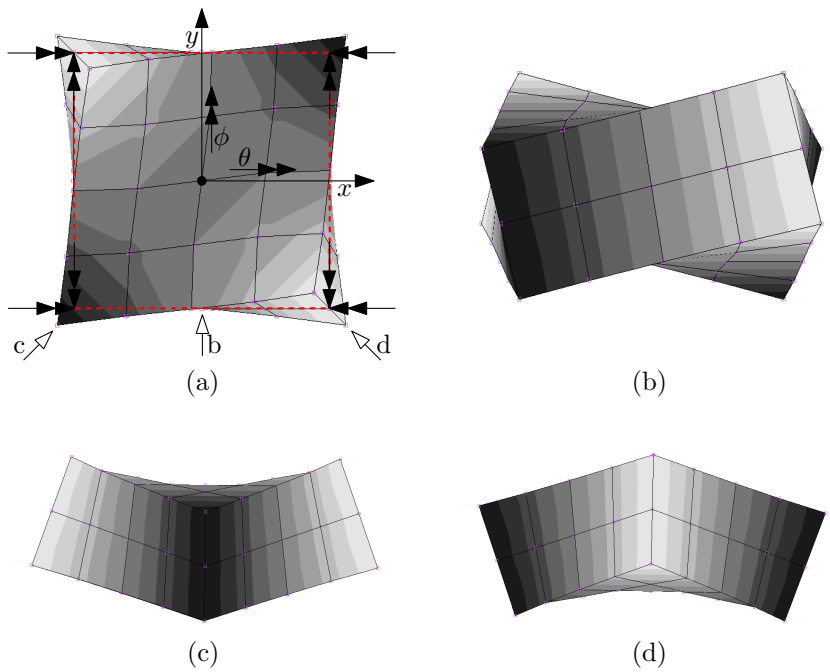

Figure 2.3: Positive κ_{xy} mixed curvature for the plate element. The grayscale coloring is proportional to the normal displacement w, which spans from an extremal downward deflection (black), to an equal in modulus extremal upward deflection (white). The gray level at the centroid is associated to zero. Subfigure (a) shows the positive γ_{xy} shear strain at the upper surface, the ip undeformed midsurface, and the negative γ_{xy} at the lower surface; the point of sight related to subfigures (b) to (d) are also evidenced. θ and ϕ rotation components decrease with x and increase with y, respectively, thus leading to positive κ_{xy} contributions. As shown in subfigures (c) and (d), the mixed curvature of subfigure (b) evolves into two anticlastic bending curvatures if the reference system is aligned with the square plate element diagonals, and hence rotated by 45° with respect to z.

2.1.3 Stresses, and their through-thickness resultants

The ip stress components at P are derived from strains by referring to the material elastic constants, and to the plane stress hypothesis. We hence have

$$\begin{bmatrix} \sigma_x \\ \sigma_y \\ \tau_{xy} \end{bmatrix} = \underline{\sigma} = \underline{\underline{\mathrm{D}}}\, \underline{\epsilon} = \underline{\underline{\mathrm{D}}}\, \underline{\mathrm{e}} + z\, \underline{\underline{\mathrm{D}}}\, \underline{\kappa}\,, \tag{2.13}$$

where $\underline{\underline{\mathrm{D}}}$ embodies the material constitutive law which elastically relates to ip stress/strain components, and which is derived according to the plane stress hypothesis.

In the particular case of an isotropic material – the generally orthotropic case is treated below – such a matrix takes the form

$$\underline{\underline{\mathrm{D}}} = \frac{E}{1-\nu^2} \begin{bmatrix} 1 & \nu & 0 \\ \nu & 1 & 0 \\ 0 & 0 & \frac{1-\nu}{2} \end{bmatrix}, \tag{2.14}$$

whereas the normal component of strain, which is due to the Poisson shrinkage alone, may be evaluated as

$$\epsilon_z = -\frac{\nu}{1-\nu}\left(\epsilon_x + \epsilon_y\right). \tag{2.15}$$

The attentive reader may observe that no mention is made to the oop shear stresses, to which paragraph 2.1.5 is devoted below.

Moreover, the absence of transverse shear terms in current paragraph formulation, and in particular in Eq. 2.13, hints for the ip and the oop stress/strain components to be elastically uncoupled; the material has evidently been *implicitly* assumed as monoclinic with respect to the reference surface. Such a condition holds e.g. for isotropic materials, and for the orthotropic plies usually employed in laminates.

As in the classical theory of beams, stress components are integrated along the relevant unit of analysis, namely the cross section there, and the tt normal segment here, to obtain suitable internal action resultants.

According to the thin plate framework, stress resultants take the form of forces per unit length along the surface, and they may be

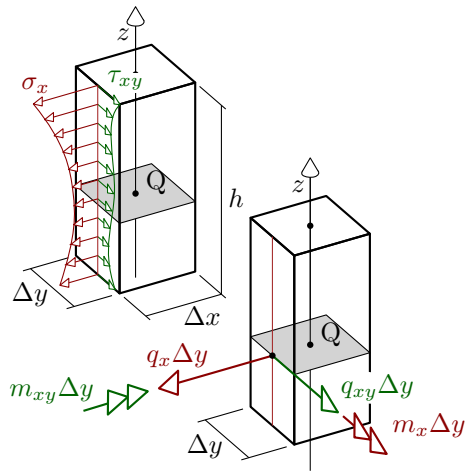

Figure 2.4: XXX

expressed as

$$\underline{\mathrm{q}} = \begin{bmatrix} q_x \\ q_y \\ q_{xy} \end{bmatrix} = \int_h \underline{\sigma}\, dz$$
$$= \underbrace{\int_h \underline{\underline{\mathrm{D}}}\, dz}_{\underline{\underline{\mathrm{a}}}}\ \underline{\mathrm{e}} + \underbrace{\int_h \underline{\underline{\mathrm{D}}}\, z dz}_{\underline{\underline{\mathrm{b}}}}\ \underline{\kappa} \tag{2.16}$$

in the case of the ip components, whereas for the oop components we have

$$\underline{\mathrm{q}}_z = \begin{bmatrix} q_{xz} \\ q_{yz} \end{bmatrix} \qquad q_{xz} = \int_h \tau_{zx} dz \qquad q_{yz} = \int_h \tau_{yz} dz. \tag{2.17}$$

Those quantities may be interpreted with respect to their (doubled if single) subscripts as follows: q_{ab} is the b component of internal action that is transmitted through a tt imaginary gate, whose in plane width is unit and whose normal is oriented along a. According to this rationalization, the $\underline{\mathrm{q}}$ components are also called *stress flows*.

Besides the internal action resultants of the force kind, by weighting the stress component contribution based on their z lever arm we obtain

the moment stress resultants (or *moment flows*), whose expressions follow

$$\underline{\mathrm{m}} = \left[\begin{array}{c} m_x \\ m_y \\ m_{xy} \end{array} \right] = \int_h \underline{\sigma}\, z dz$$

$$= \underbrace{\int_h \underline{\underline{\mathrm{D}}}\, z dz}_{\underline{\underline{\mathrm{b}}} \equiv \underline{\underline{\mathrm{b}}}^{\mathrm{T}}}\, \underline{\mathrm{e}} + \underbrace{\int_h \underline{\underline{\mathrm{D}}}\, z^2 dz}_{\underline{\underline{\mathrm{c}}}}\, \underline{\kappa}\,. \tag{2.18}$$

A selection of internal action components is represented in Fig. 2.4 shows, along with the stress distributions they arise from.

2.1.4 Constitutive equations for the plate

By employing the matrices defined in Eqs. 2.16 and 2.18, the cumulative generalized strain - stress resultants relations for the plate (or for the laminate) may be summarized in the following expressions

$$\left[\begin{array}{c} \underline{\mathrm{q}} \\ \underline{\mathrm{m}} \end{array} \right] = \left[\begin{array}{cc} \underline{\underline{\mathrm{a}}} & \underline{\underline{\mathrm{b}}} \\ \underline{\underline{\mathrm{b}}}^{\mathrm{T}} & \underline{\underline{\mathrm{c}}} \end{array} \right] \left[\begin{array}{c} \underline{\mathrm{e}} \\ \underline{\kappa} \end{array} \right] \tag{2.19}$$

which are usually referred to as the *constitutive equations* of the [laminate] plate, and the coefficient matrix, named *constitutive matrix* for the laminate, summarizes the elastic response of the latter.

The contribution of the ip stress/strain components to the elastic strain energy area density[14] is defined based on the previous relation as

$$\upsilon^{\dagger} = \frac{1}{2} \left[\begin{array}{c} \underline{\mathrm{q}} \\ \underline{\mathrm{m}} \end{array} \right]^{\top} \left[\begin{array}{c} \underline{\mathrm{e}} \\ \underline{\kappa} \end{array} \right] \tag{2.20}$$

$$= \frac{1}{2} \left[\begin{array}{c} \underline{\mathrm{e}} \\ \underline{\kappa} \end{array} \right]^{\top} \left[\begin{array}{cc} \underline{\underline{\mathrm{a}}} & \underline{\underline{\mathrm{b}}} \\ \underline{\underline{\mathrm{b}}}^{\mathrm{T}} & \underline{\underline{\mathrm{c}}} \end{array} \right] \left[\begin{array}{c} \underline{\mathrm{e}} \\ \underline{\kappa} \end{array} \right]. \tag{2.21}$$

The $\underline{\underline{\mathrm{a}}}$ and the $\underline{\underline{\mathrm{c}}}$ minors of the constitutive matrix characterize the plate stiffness with respect to membrane and flexural load case families respectively; the membrane/flexural coupling stiffness minor

[14] i.e. strain energy per unit reference surface area

$\underline{\underline{\mathrm{b}}}$, which is in general nonzero, vanishes if the material is symmetrically distributed with respect to the reference surface.

In the commonwise case of tt homogeneous material, and null offset[15] we have

$$\underline{\underline{\mathrm{a}}} = h\,\underline{\underline{\mathrm{D}}} \qquad\qquad \underline{\underline{\mathrm{b}}} = \underline{\underline{0}} \qquad\qquad \underline{\underline{\mathrm{c}}} = \frac{h^3}{12}\,\underline{\underline{\mathrm{D}}},$$

i.e. the membrane stiffness varies linearly with the wall thickness, the flexural stiffness varies with the cube of the thickness, and the membrane and the flexural loadings are mutually uncoupled. Such a laminate elastic properties dependence on thickness essentially holds also for laminates, if the tt distribution of the various materials is kept comparable.

2.1.5 The transverse shear stress/strain components

A full treatise on the title topic is, due to its complexity, bspc; starting points for further investigation my be found in [3], [4] or in the theory manual of your favourite fe solver[16].

The two transverse shear components

$$\underline{\mathrm{g}}_z = \begin{bmatrix} g_{yz} \\ g_{zx} \end{bmatrix}$$

are in fact more directly recognizable as further contributions to the $\left(\frac{\partial w}{\partial x}, \frac{\partial w}{\partial y}\right)$ normal deflection gradient, with respect to what is attributable to flexure alone, than tt averages of actual, pointwise shear strains – see e.g. Figure 2.1.

Since no direct procedure is available[17] for directly probing the g_{yz} and g_{zx} quantities in a deflected plate, their definition is inevitably nebulous.

The two transverse shear stress resultants defined in Eq. 2.17

$$\underline{\mathrm{q}}_z = \begin{bmatrix} q_{xz} \\ q_{yz} \end{bmatrix}$$

[15] In the presence of a nonzero offset between the reference and the median planes, the uncoupled nature of the plate membrane/flexural loadings is only *formally* lost. If the same problem is considered based on a median reference plane, in fact, such a property is obviously restored.

[16] See e.g. MSC.Marc 2013.1 Documentation, Vol. A, pp. 433-436

[17] as far as the writer knows

are assumed to perform work[18] on the same g_{yz} and g_{zx} transverse shear components, respectively; the transverse shear contribution to the elastic strain energy per unit ref. surface area is hence

$$\upsilon^{\ddagger} = \frac{1}{2}\,\underline{\mathrm{g}}_{z}^{\top}\,\underline{\mathrm{q}}_{z} = \frac{1}{2}g_{xz}q_{xz} + \frac{1}{2}g_{yz}q_{yz}. \tag{2.22}$$

The constitutive equation for the transverse shear is set at tt normal segment (vs. punctual) level, with the declared aim of collecting the elastic strain energy contributions along the thickness, and they are usually formulated as

$$\upsilon^{\ddagger} = \frac{1}{2}\,\underline{\mathrm{g}}_{z}^{\top}\,\underbrace{\left[\chi\left(\frac{1}{h}\int_{h}\underline{\underline{\mathrm{G}}}^{-1}dz\right)^{-1}\right]}_{\underline{\underline{\Gamma}}}\,\underline{\mathrm{g}}_{z} \tag{2.23}$$

where $\underline{\underline{\mathrm{G}}}$ is the pointwise constitutive matrix for the transverse shear components[19] – which is considered in terms of its tt harmonic average[20], χ is a *shear correction factor* – which accommodates for possibly any incongruence in the formulation, and $\underline{\underline{\Gamma}}$ is an emended transverse shear constitutive matrix for the whole plate.

In the case of isotropic materials, $\underline{\underline{\mathrm{G}}}$ is a diagonal matrix whose terms equate the shear modulus, i.e.

$$\underline{\underline{\mathrm{G}}} = \frac{E}{2\,(1+\nu)}\begin{bmatrix} 1 & 0 \\ 0 & 1 \end{bmatrix},$$

whereas the χ shear correction factor is usually assumed as $\frac{5}{6}$ if the material is tt uniform[21]; different χ values are however proposed in literature, see e.g. [5], along with different procedures[22] for evaluating

[18] in particular, work for unit reference surface area

[19] $\underline{\underline{\mathrm{G}}}$ is the 2 by 2 matrix s.t., pointwisely, $\begin{bmatrix} \tau_{zx} \\ \tau_{yz} \end{bmatrix} = \underline{\underline{\mathrm{G}}}\begin{bmatrix} \gamma_{zx} \\ \gamma_{yz} \end{bmatrix}$.

[20] the shear sliding - rather than the elastic reactions, is accumulated across the various layers, thus assuming an *in series* layout of equivalent springs

[21] please note the parallel with the inverse 1.2 correction factor for the shear contribution to the beam elastic strain energy, proper of the solid rectangular cross section.

[22] we report as an example the notable case of of sandwich panels – whose transverse shear compliance is rarely negligible, in which Γ is defined as the $\underline{\underline{\mathrm{G}}}_{\mathrm{foam}}$ transverse shear constitutive matrix for the foam/honeycomb material interposed between the outer skins, multiplied by the overall panel thickness h; in this case the χ transverse shear correction factor is implicitly defined as unity.

$\underline{\underline{\Gamma}}$. By comparing Eqns. 2.22 and 2.23 we also derive the *de facto* transverse shear constitutive relation

$$\underline{\mathrm{q}}_z = \underline{\underline{\Gamma}}\, \underline{\mathrm{g}}_z. \tag{2.24}$$

for the Mindlin shear deformable plate.

In the case pointwise values are requested for the τ_{zx} and τ_{yz} stress components – e.g. in the analysis of interlaminar stresses in composite laminates, those quantities are derived from the assumed absence of shear stresses on the lower surface, and by accumulating the ip stress component contributions to the x and y translational equilibria up to the desired z sampling height, see Fig. 2.5. We hence obtain

$$\tau_{zx}(z) = -\int_{-\frac{h}{2}+o}^{z} \frac{\partial \sigma_x}{\partial x} + \frac{\partial \tau_{xy}}{\partial y} dz = \int_{z}^{+o+\frac{h}{2}} \frac{\partial \sigma_x}{\partial x} + \frac{\partial \tau_{xy}}{\partial y} dz \tag{2.25}$$

$$\tau_{yz}(z) = -\int_{-\frac{h}{2}+o}^{z} \frac{\partial \tau_{xy}}{\partial x} + \frac{\partial \sigma_y}{\partial y} dz = \int_{z}^{+o+\frac{h}{2}} \frac{\partial \tau_{xy}}{\partial x} + \frac{\partial \sigma_y}{\partial y} dz. \tag{2.26}$$

The parallel is evident with the Jourawsky shear theory for beams.

A complete form for the constitutive equations for the (oop) shear-deformable plate may be finally cast as

$$\begin{bmatrix} \underline{\mathrm{q}} \\ \underline{\mathrm{m}} \\ \underline{\mathrm{q}}_z \end{bmatrix} = \begin{bmatrix} \underline{\underline{\mathrm{a}}} & \underline{\underline{\mathrm{b}}} & \underline{\underline{0}} \\ \underline{\underline{\mathrm{b}}}^{\mathrm{T}} & \underline{\underline{\mathrm{c}}} & \underline{\underline{0}} \\ \underline{\underline{0}} & \underline{\underline{0}} & \underline{\underline{\Gamma}} \end{bmatrix} \begin{bmatrix} \underline{\mathrm{e}} \\ \underline{\kappa} \\ \underline{\gamma}_z \end{bmatrix} \tag{2.27}$$

where the null, uncoupling minors are again due to the assumed material pointwise elastic symmetry with respect to the $\perp z$ plane.

2.1.6 Hooke's law for the orthotropic lamina

Hooke's law for the orthotropic material ip stress conditions, with respect to principal axes of orthotropy;

$$\underline{\underline{\mathrm{D}}}_{123} = \begin{bmatrix} \frac{E_1}{1-\nu_{12}\nu_{21}} & \frac{\nu_{21}E_1}{1-\nu_{12}\nu_{21}} & 0 \\ \frac{\nu_{12}E_2}{1-\nu_{12}\nu_{21}} & \frac{E_2}{1-\nu_{12}\nu_{21}} & 0 \\ 0 & 0 & G_{12} \end{bmatrix} \tag{2.28}$$

$$\begin{bmatrix} \sigma_1 \\ \sigma_2 \\ \tau_{12} \end{bmatrix} = \underline{\underline{\mathrm{T}}}_1 \begin{bmatrix} \sigma_x \\ \sigma_y \\ \tau_{xy} \end{bmatrix} \qquad \begin{bmatrix} \epsilon_1 \\ \epsilon_2 \\ \gamma_{12} \end{bmatrix} = \underline{\underline{\mathrm{T}}}_2 \begin{bmatrix} \epsilon_x \\ \epsilon_y \\ \gamma_{xy} \end{bmatrix} \tag{2.29}$$

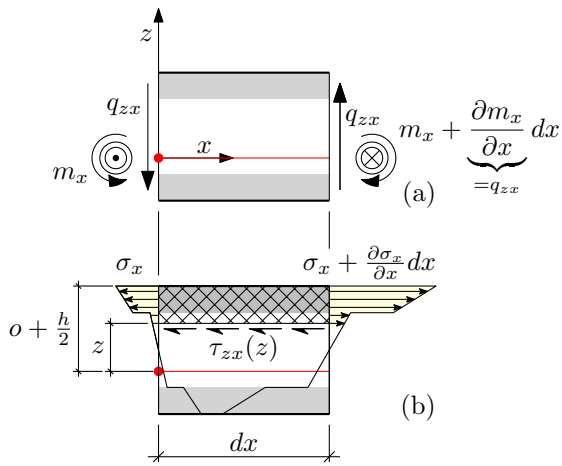

Figure 2.5: *à la* Jourawski approach for determining the pointwise $\tau_{zx}(z)$ stress component from the q_{zx} resultant. In deriving the σ_x stress distribution, along with its $\frac{\partial \sigma_x}{\partial x}$ grow rate, curvature components other than κ_x are assumed zero, thus mimicking the cylindrical bending condition proper of a transversely infinite plate; also, the τ_{xy} are assumed constant in y, and their contribution to the x translational equilibrium is cumulatively zero.

where

$$\underline{\underline{\mathrm{T}}}_1 = \begin{bmatrix} m^2 & n^2 & 2mn \\ n^2 & m^2 & -2mn \\ -mn & mn & m^2 - n^2 \end{bmatrix} \tag{2.30}$$

$$\underline{\underline{\mathrm{T}}}_2 = \begin{bmatrix} m^2 & n^2 & mn \\ n^2 & m^2 & -mn \\ -2mn & 2mn & m^2 - n^2 \end{bmatrix} \tag{2.31}$$

α is the angle between 1 and x;

$$m = \cos(\alpha) \qquad\qquad n = \sin(\alpha) \tag{2.32}$$

The inverse transformations may be obtained based on the relations

$$\underline{\underline{\mathrm{T}}}_1^{-1}(+\alpha) = \underline{\underline{\mathrm{T}}}_1(-\alpha) \qquad\qquad \underline{\underline{\mathrm{T}}}_2^{-1}(+\alpha) = \underline{\underline{\mathrm{T}}}_2(-\alpha) \tag{2.33}$$

Finally

$$\underline{\sigma} = \underline{\underline{\mathrm{D}}}\,\underline{\epsilon} \qquad\qquad \underline{\underline{\mathrm{D}}} \equiv \underline{\underline{\mathrm{D}}}_{xyz} = \underline{\underline{\mathrm{T}}}_1^{-1}\,\underline{\underline{\mathrm{D}}}_{123}\,\underline{\underline{\mathrm{T}}}_2 \tag{2.34}$$

With regard to the transverse shear constitutive relation, in the case of an orthotropic material whose oop shear moduli are G_{z1} and G_{2z} we have

$$\underline{\underline{\mathrm{G}}} = \begin{bmatrix} n^2 G_{z1} + m^2 G_{2z} & mnG_{z1} - mnG_{2z} \\ mnG_{z1} - mnG_{2z} & m^2 G_{z1} + n^2 G_{2z} \end{bmatrix}.$$

2.1.7 An application: the four point bending test specimen.

The case of the four point bending test is considered, see Figure 2.6a, with an isotropic and homogeneous specimen material. Specimen dimensions are defined as in Figure, where the b the specimen width is taken as the relevant unit of length.

The width to length ratio of the specimen is less than unity, but far from being negligible; a treatise according to the plate theory would hence be more appropriate than the beam model which is usually proposed by normative.

Such a test is based on the assumption that the bending moment – a beam framework quantity – is constant along the gauge length, and

equal to Fl; such a quantity equates the through-width (tw) integral of the m_{x} moment resultant, whose value is assumed tw constant and equal to $m_{\mathrm{x}}^* = Fl/b$. The specimen curvature along the gauge length is

$$k_{\mathrm{x}}^* = \frac{12Fl}{Ebh^3} \tag{2.35}$$

according to the beam theory; such a value is taken as a reference.

The treatise according to the plate theory is far less straightforward that its trivial beam counterpart, since e.g. we may consider the two opposite extremal cases of i) unconstrained anticlastic secondary curvature, or, equivalently, null m_{y} transverse (in the sense of tw, not tt) moment resultant, and ii) cylindrical bending, i.e. null transverse κ_{y} curvature. The membrane generalized stress/strain components are zero, as the transverse shear terms along the gauge length. The mixed moment resultant and curvature are zero in both the cases, since they are null at the xz symmetry plane, and they are assumed tw constant[23]. By applying the constitutive relations proper of the homogeneous, isotropic plates, we derive for the unconstrained anticlastic curvature case i)

$$m_{\mathrm{x}} = m_{\mathrm{x}}^* \qquad m_{\mathrm{y}} = 0 \qquad \kappa_{\mathrm{x}} = k_{\mathrm{x}}^* \qquad \kappa_{\mathrm{y}} = -\nu k_{\mathrm{x}}^*,$$

whereas for the cylindrical bending case ii) we have

$$m_{\mathrm{x}} = m_{\mathrm{x}}^* \qquad m_{\mathrm{y}} = \nu m_{\mathrm{x}}^* \qquad \kappa_{\mathrm{x}} = \left(1-\nu^2\right) k_{\mathrm{x}}^* \qquad \kappa_{\mathrm{y}} = 0.$$

We then observe that the nonzero κ_{y} transverse curvature predicted by i) is inconsistent with the hypothesis of a full width line contact at the supports, whose cylindrical surface is transversely flat; the unconstrained anticlastic curvature confines the specimen contact interaction with the inner supports to a point in correspondence of the width midspan, whereas the outer supports touch the specimen at its edges only. Such a tw inhomogeneous loading condition induces contact actions which may effectively oppose the anticlastic curvature, which locally appears not "unconstrained" anymore.

On the other hand, a m_{y} moment resultant which is predicted according to cylindrical bending not to vanish at the specimen flanks

[23] the mixed moment resultant m_{xy} is moreover expected to vanish at the specimen flanks, in continuity with the free surface boundary condition (bc)

is incompatible with the free surface boundary condition; continuity conditions require in fact that a distributed moment external action is applied at the specimen flanks, which apparently is not the case.

The actual response of the specimen in terms of moment resultants and curvatures, as probed at its centroidal axis, is plotted in Fig. 2.6b in the case of bilateral support condition, i.e. $w = 0$ and $w = d$ at the outer and inner indenters, respectively, being d displacement of the inner, moving, support. The cylindrical bending solution ii) is observed at the supports, whereas a progressive transition to the unconstrained anticlastic curvature solution i) is observed while moving away from those supported areas. In particular, the central portion of the gauge length behaves consistently with i).

In Fig. 2.6c, the same quantities are reported in the actual case of unilateral contact at supports, i.e. the Signorini conditions[24] are imposed which consist in

$$g(y) \geq 0 \tag{2.36}$$

$$f(y) \geq 0 \tag{2.37}$$

$$g(y) \cdot f(y) = 0, \tag{2.38}$$

where $f(y)$ is the lineic contact force along the width, positive if compressive, and $g(y)$ is the gap between specimen and indenter, namely $g(y) = -w(y)$ and $g(y) = w(y) - d$ at the outer and inner supports, respectively.

According to this second model, supports are less effective in locally imposing a null secondary curvature, thus extending the validity of the unconstrained anticlastic curvature solution i) to most of the gauge length.

2.1.8 Notes on membrane and flexural regimes, and thin walled profiles

In the present paragraph a symmetric (if not uniform) material distribution is assumed with respect to the profile midsurface, which acts as reference surface, in order to have $\underline{\underline{b}} = 0$ and then a proper decoupling

[24] Those conditions consist in turn in a no compenetration inequality 2.36, in a no tractive contact action inequality 2.37, and in the mutual local exclusion of nozero gap and nonzero contact force, 2.38.

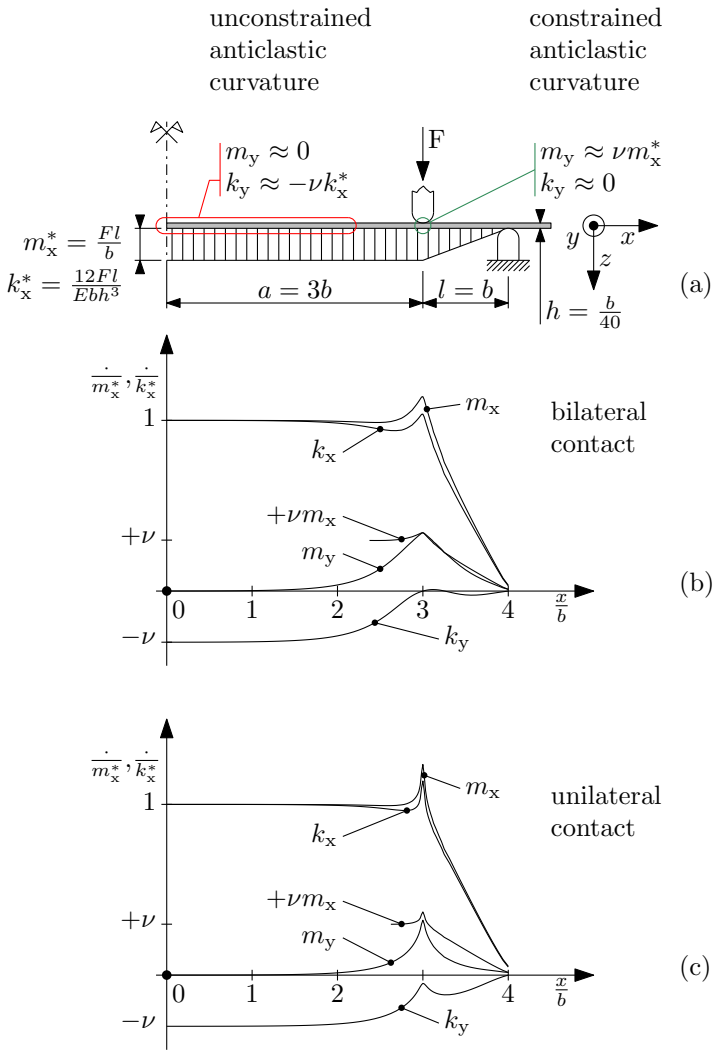

Figure 2.6: The *not-so-trivial* four point bending case, where b is the specimen out-of-sketch-plane width (we might call it *depth*). Moment fluxes and curvatures are sampled at the specimen midwidth, whereas they may vary while moving towards the flanks; the average value of m_x along the width must in fact coincide with m_x^* in correspondence with the load span.

between the membrane – i.e. tt uniform, $\{\underline{\mathrm{e}}, \underline{\mathrm{q}}\}$ dominated – strain regime, and the flexural – i.e. linear in z, $\{\underline{\mathrm{m}}, \underline{\kappa}\}$ dominated – strain regime.

The two regimes exhibit characteristic behaviors in terms of strain magnitude variation while updating the h wall thickness – and the material distribution consistently – at design stage.

In particular, if the walls of a thin-walled part are subject to a purely membrane regime, and the thicknesses are all scaled by a common λ factor while holding the midsurface fixed, the part stiffness (i.e. the full set of relevant load/deflection ratios) grows linearly with λ; on the other hand, if the part's walls are subject to a purely flexural regime, the part stiffness grows with the third power of λ.

From the strain magnitude variation point of view, two extremal loadcases are considered.

According to the first loadcase – named *imposed load* condition, the loads applied to the part (forces, moments, pressures..) are assumed as invariant with the part stiffness, as in the case they are applied by external load-controlled devices; also, the strain energy decreases with the inverse of an increasing part stiffness.

According to the second loadcase – named *imposed displacement* condition – the part is globally stretched by a fixed amount, which is invariant with the part stiffness, as in the case of displacement-controlled loading devices. In this loadcase, the loads applied to the part grow consistently with the part stiffness, in order to reach the given deflections; also, the strain increases linearly with the part stiffness.

This is also the case of a not directly loaded deformable subframe, that is attached to a relatively stiff, autonomously load bearing main frame; ideally, the subframe accomodates for the displacement of its attachment points, while the main deflects under load.

If the part walls are subject to a purely membrane regime, the strain magnitude is inversely proportional to the wall thickness under imposed-load conditions, whereas they are invariant with the thickness under imposed-displacement (and hence imposed membrane stretching) conditions. In the case of a purely flexural regime, the strain magnitude is inversely proportional to the square of the wall thickness under imposed-load conditions, whereas it paradoxically increases with the thickness under imposed-displacement (and hence immposed curvatures) conditions. See also the summarizing Table 2.1.

regime	membrane	flexural
stiffness	$\propto h^1$	$\propto h^3$
strain mag., imp.-load	$\propto h^{-1}$	$\propto h^{-2}$
strain mag., imp.-disp.s	$\propto h^0$	$\propto h^1$

Table 2.1: Power law influence of the h wall thickness on the plate membrane/flexural stiffness and induced strain magnitude.

With reference to thin walled profiles, the profile wall undergoes a substantially membrane strain regime when loaded by the symmetric components of internal action, namely axial load and flexural moments, and also when shear loads are applied, in accordance with the Jourawsky theory.

In the case of torsion, closed thin-walled (ctw) profiles still exhibit a membrane strain regime along the profile walls, whereas the flexural strain distribution is characteristic of the twisted open thin-walled (otw) profiles, according to the De Saint Venant torsion theory. The axial stretching further induced by the retained warping according to the Vlasov theory of torsion, follows the membrane regime.

The flexural regime may also be produced by concentrated actions that locally deflect the profile walls, see e.g. Fig. 2.7 joint, and by the development of local plate buckling modes at the axially compressed portion of profile walls, or in shear panels along the compressed diagonal; in particular, local buckling critical loads are ruled by the $\underline{\underline{c}}$ minor of the plate constitutive matrix, and they hence scale with the third power of the wall thickness.

2.1.9 Final Notes.

A few sparse notes:

- If the unsymmetric laminate is composed by isotropic layers, a reference plane may be obtained for which the $\underline{\underline{b}}$ membrane-to-bending coupling matrix vanishes; a similar condition may not be verified in the presence of orthotropic layers.

- Thermally induced distortion is not self-compensated in an unsymmetric laminate even if the temperature is held constant

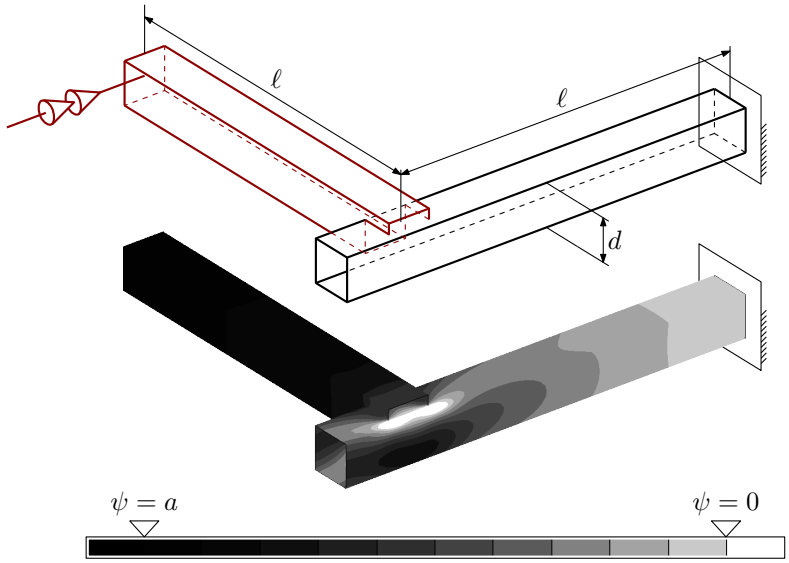

Figure 2.7: FIXME

through the thickness. Such fact, united to the unavoidable thermal cycles that occurs during manufacturing if not during operation, makes such configurations pretty undesirable.

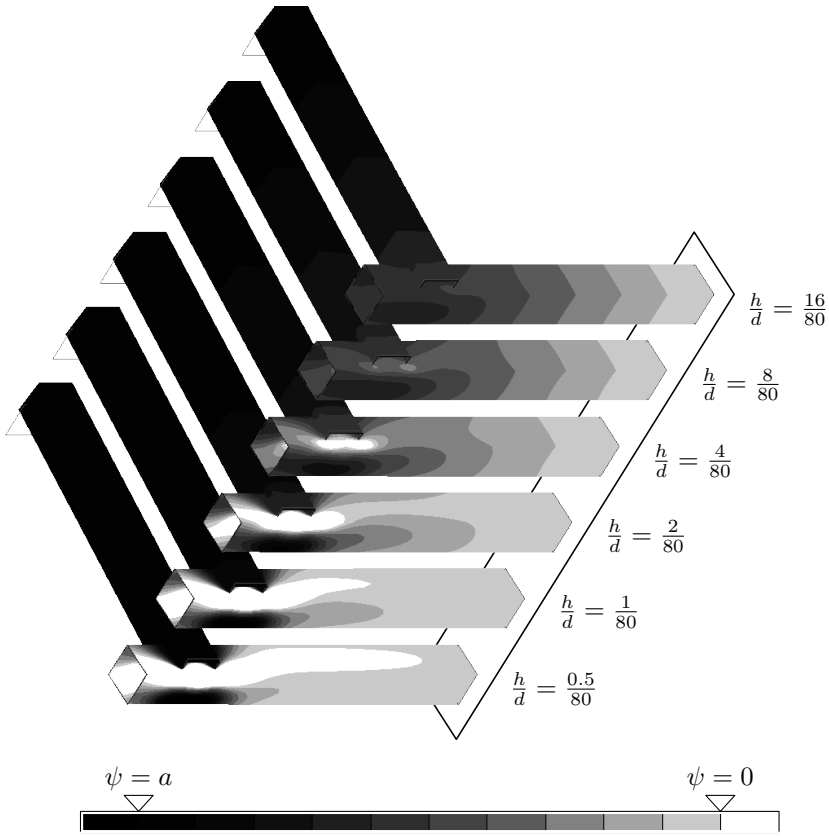

Figure 2.8: FIXME

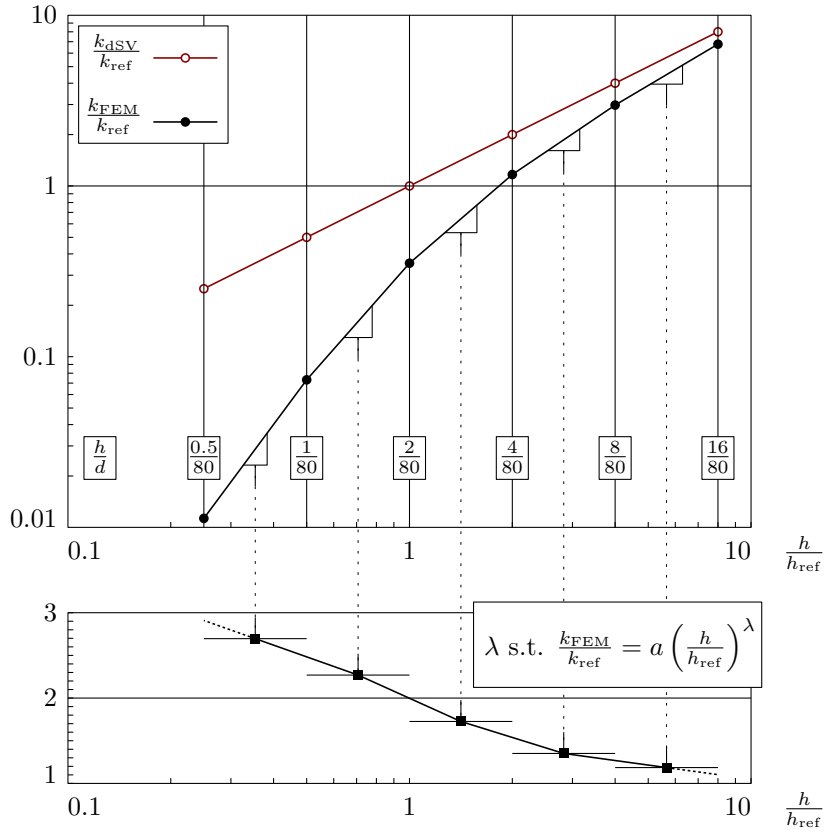

Figure 2.9: FIXME

2.2 Preliminary results

2.2.1 Interpolation functions for the quadrilateral domain

The elementary quadrilateral domain. A quadrilateral domain is considered whose vertices are conventionally located at the $(\pm 1, \pm 1)$ points of an adimensional (ξ, η) plane coordinate system, see Figure 2.10. Scalar values f_i are associated to a set of *nodal* points $\mathrm{P}_i \equiv [\xi_i, \eta_i]$, which for the present case coincide with the quadrangle vertices, numbered as in Figure.

A $f(\xi, \eta)$ interpolation function may be devised by defining a set of nodal influence functions $N_i(\xi, \eta)$ to be employed as the coefficients (weights) of a moving weighted average

$$f(\xi, \eta) \stackrel{\text{def}}{=} \sum_i N_i(\xi, \eta) f_i \tag{2.39}$$

Requisites for such weight functions are:

- for each point of the domain, the sum of the weights is unitary

$$\sum_i N_i(\xi, \eta) = 1, \ \forall [\xi, \eta] \tag{2.40}$$

- to grant continuity of the $f(\xi, \eta)$ function with the nodal samples, the influence of a node is unitary at its location, whereas the influence of the others vanishes there, i.e.

$$N_i(\xi_j, \eta_j) = \delta_{ij} \tag{2.41}$$

  where δ_{ij} is the Kronecker delta function.

Moreover, suitable functions should be continuous and straightforwardly differentiable up to any required degree.

Low order polynomials are ideal candidates for the application; for the particular domain, the nodal weight functions may be stated as

$$N_i(\xi, \eta) \stackrel{\text{def}}{=} \frac{1}{4} (1 \pm \xi) (1 \pm \eta), \tag{2.42}$$

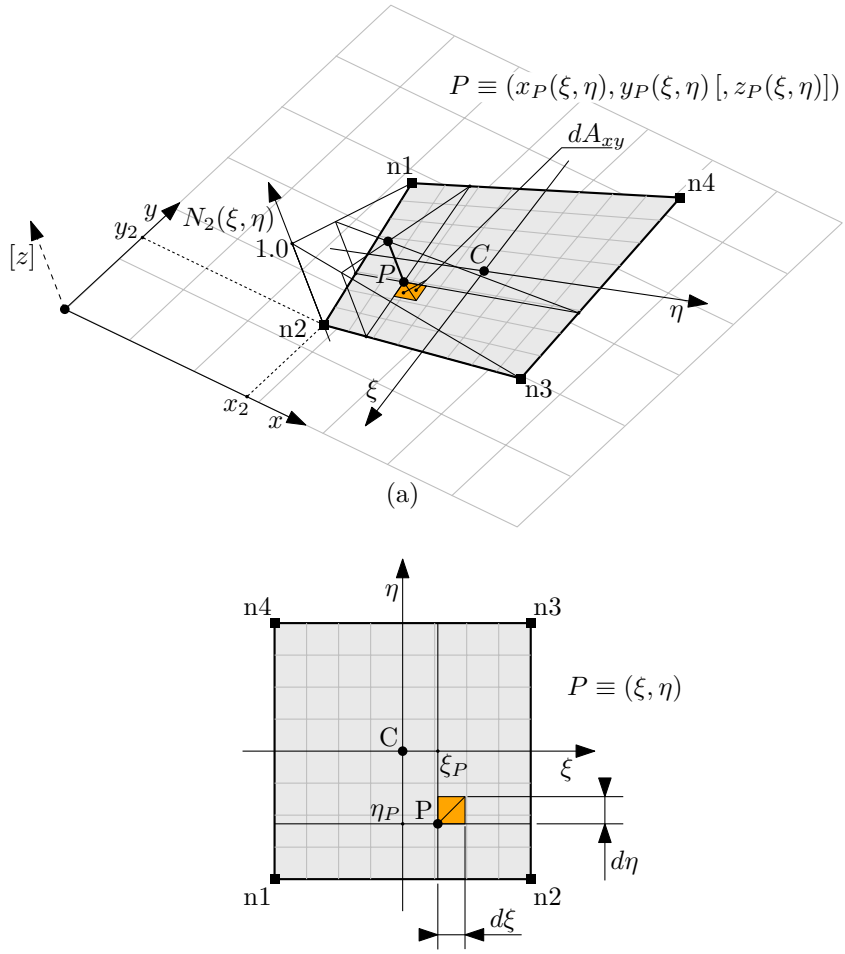

Figure 2.10: Quadrilateral elementary domain (a), and a representative weight function (b).

where sign ambiguity is resolved[25] for each i-th node by enforcing Eqn. 2.41.

The bilinear interpolation function defined by Eqs. 2.39 and 2.42 turns into a general linear relation with (ξ, η) if the four sample points (ξ_i, η_i, f_i) are coplanar – but otherwise arbitrary – in the ξ, η, f space.

Further generality may be introduced by *not* enforcing coplanarity.

The weight functions for the four-node quadrilateral are in fact quadratic although incomplete[26] in nature, due to the presence of the $\xi\eta$ product, and the absence of any ξ^2, η^2 term.

Each $N_i(\xi, \eta)$ term, and the combined $f(\xi, \eta)$ function, defined as in Eqn. 2.39, behave linearly if restricted to $\xi = \text{const.}$ or $\eta = \text{const.}$ loci – and in particular along the four edges; quadratic behaviour may instead arise along a general direction, e.g. along the diagonals, as in Fig. 2.10b example. Such behaviour is called *bilinear*.

We now consider the $f(\xi, \eta)$ interpolation function partial derivatives. The partial derivative

$$\frac{\partial f}{\partial \xi} = \underbrace{\left(\frac{f_2 - f_1}{2}\right)}_{[\Delta f/\Delta \xi]_{12}} \underbrace{\left(\frac{1-\eta}{2}\right)}_{N_1+N_2} + \underbrace{\left(\frac{f_3 - f_4}{2}\right)}_{[\Delta f/\Delta \xi]_{43}} \underbrace{\left(\frac{1+\eta}{2}\right)}_{N_4+N_3} = a\eta + b \quad (2.43)$$

linearly varies in η from the incremental ratio value measured at the $\eta = -1$ lower edge, to the value measured at the $\eta = 1$ upper edge; the other partial derivative

$$\frac{\partial f}{\partial \eta} = \left(\frac{f_4 - f_1}{2}\right)\left(\frac{1-\xi}{2}\right) + \left(\frac{f_3 - f_2}{2}\right)\left(\frac{1+\xi}{2}\right) = c\xi + d. \quad (2.44)$$

behaves similarly, with $c = a$. Partial derivatives in ξ, η remain constant while moving along the corresponding differentiation direction[27].

[25] the formula may be alternatively cast in the definite form

$$N_i(\xi, \eta) \stackrel{\text{def}}{=} \frac{1}{4}\left(1 + \xi\xi_i\right)\left(1 + \eta\eta_i\right),$$

where ξ_i, η_i are the coordinates of the i-th node.

[26] or, equivalently, *enriched linear*, as discussed above and in the following

[27] The relevance of such partial derivative orders will appear clearer to the reader once the strain field will have been derived in paragraph XXX.

An equivalent expression for Eq. 2.39 is the following

$$f(\xi,\eta) = \begin{bmatrix} N_1(\xi,\eta) & \cdots & N_i(\xi,\eta) & \cdots & N_n(\xi,\eta) \end{bmatrix} \begin{bmatrix} f_1 \\ \vdots \\ f_i \\ \vdots \\ f_n \end{bmatrix}$$

$$= \underline{\underline{\mathrm{N}}}\,(\xi,\eta)\,\underline{\mathrm{f}}\,, \tag{2.45}$$

which resorts to the inner mechanics of the matrix-vector product for performing the summation; the $\underline{\mathrm{f}}$ vector collects the function nodal values, whereas the $\underline{\underline{\mathrm{N}}}\,(\xi,\eta)$ weigth function row matrix collects their influence coefficient at the provided (ξ,η) location.

The general planar quadrilateral domain. The interpolation functions introduced above for the natural quadrilateral may be profitably employed in defining a coordinate mapping between a general quadrangular domain – see Fig. 2.11a – and its reference counterpart, see Figures 2.10 or 2.11b.

In particular, we first define the $\underline{\xi}_i \mapsto \underline{\mathrm{x}}_i$ coordinate mapping for the four vertices[28] alone, where ξ,η are the reference (or natural, or elementary) coordinates and x,y are their physical counterpart.

Then, a mapping for the inner points may be derived by interpolation, namely

$$\underline{\mathrm{x}}\,(\underline{\xi}) = \underline{\mathrm{m}}\,(\underline{\xi}) = \sum_{i=1}^{4} N_i\,(\underline{\xi})\;\underline{\mathrm{x}}_i, \tag{2.46}$$

or, by expliciting the $\underline{\mathrm{m}} \equiv \underline{\mathrm{x}}$ components,

$$\underline{\mathrm{m}}\,(\underline{\xi}) = \begin{bmatrix} x(\xi,\eta) \\ y(\xi,\eta) \end{bmatrix}$$

with

$$x(\xi,\eta) = \sum_{i=1}^{4} N_i(\xi,\eta)x_i \qquad\qquad y(\xi,\eta) = \sum_{i=1}^{4} N_i(\xi,\eta)y_i.$$

[28]The condensed notation $\underline{\xi}_i \equiv (\xi_i,\eta_i)$, $\underline{\mathrm{x}}_i \equiv (x_i,y_i)$ for coordinate vectors is employed.

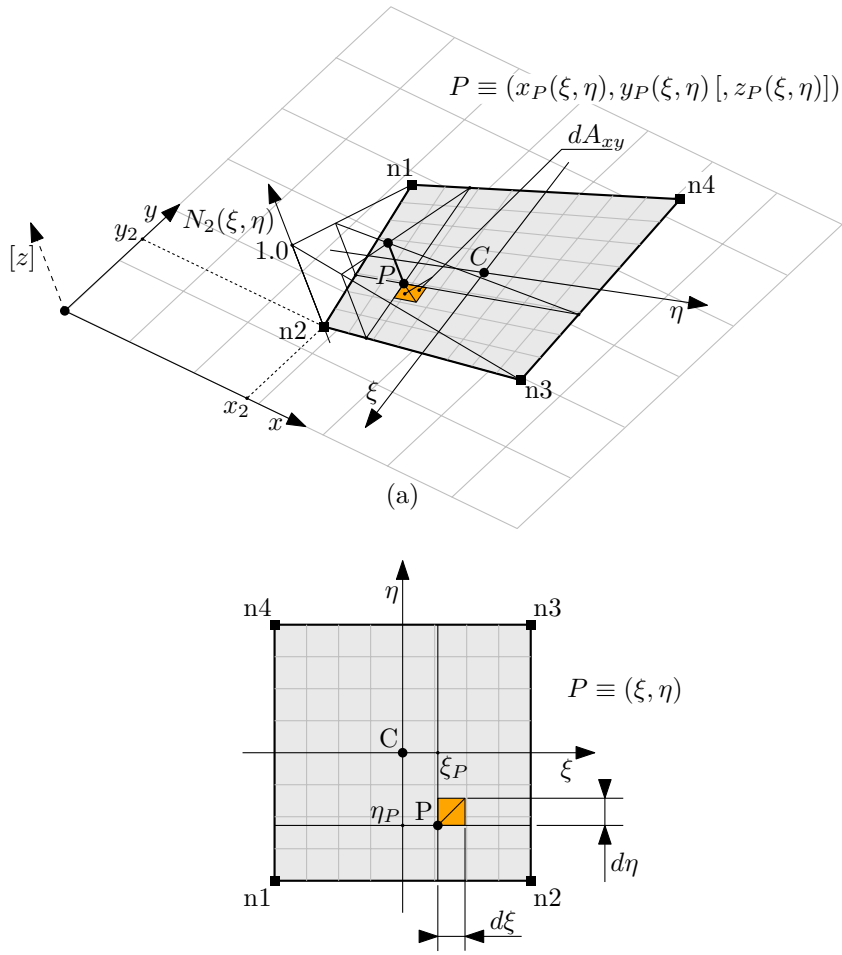

Figure 2.11: Quadrilateral general domain, (a), and its reference counterpart (b). If the general quadrangle is defined within a spatial environment, and not as a figure lying on the xy plane, limited z_i offsets are allowed at nodes with respect to such plane, which are not considered in Figure.

In the employed notation, the parametric dependence of the $\underline{\mathrm{m}}\,(\xi,\eta)$ mapping on the nodal coordinates is not explicit, but clearly unavoidable; the complete notation $\underline{\mathrm{m}}\,(\xi,\eta;\,\underline{\mathrm{x}}_i)$ might be alternatively employed, where $\underline{\mathrm{x}}_i$ is a placeholder for the physical coordinates of each node.

The availability of an inverse $\underline{\mathrm{m}}^{-1} : \underline{\mathrm{x}} \mapsto \underline{\xi}$ mapping is not granted; in particular, a closed form representation for such inverse is not generally available[29].

In the absence of an handy inverse mapping function, it is convenient to reinstate the interpolation procedure obtained for the natural domain, i.e.

$$f(\xi,\eta) \stackrel{\text{def}}{=} \sum_i N_i(\xi,\eta) f_i \tag{2.47}$$

The four f_i nodal values are interpolated based on the *natural* ξ,η coordinates of an inner P point, and not as a function of its physical x,y coordinates, that are never promoted to the independent variable role.

The interpolation scheme behind the $\underline{\mathrm{m}}$ mapping – and the mapping itself – behaves linearly along η =const. and ξ =const. one dimensional subdomains, and in particular along the quadrangle edges[30]; the inverse mapping $\underline{\mathrm{m}}^{-1}$ exists and it is a linear function[31] along the image of those line segments on the physical plane, under the further

[29] Inverse relations are derived in [6], which however are case-defined and based on a selection table; for a given $\bar{\underline{\mathrm{x}}}$ physical point, however, Newton-Raphson iterations rapidly converge to the $\bar{\underline{\xi}} = \underline{\mathrm{m}}^{-1}(\bar{\underline{\mathrm{x}}})$ solution if the centroid is chosen for algorithm initialization, see Section XXX

[30] see paragraph XXX

[31] A constructive proof may be defined for each edge as follows. We consider a generic Q point along such edge whose physical coordinates are (x_Q, y_Q). Of the two natural coordinates of Q, one is trivial to be derived since its value is constant along the edge. The other, for which we employ the λ placeholder symbol, may be defined through the expression

$$\lambda = 2\frac{(x_Q - x_i)(x_j - x_i) + (y_Q - y_i)(y_j - y_i)}{(x_j - x_i)^2 + (y_j - y_i)^2} - 1,$$

where i,j are the two subdomain endpoints at which λ equates -1 and $+1$, respectively, and $(x_i, y_i), (x_j, y_j)$ the associated physical coordinates. A similar function may be defined for any segment for which either ξ or η is constant, and not only for the quadrangle edges. Please note that the above inverse mapping formula is not applicable iif the segment physical length at the denominator is zero.

condition that its length is nonzero[32]. Being a composition of linear functions, the interpolation function $f(\underline{\mathrm{m}}^{-1}(x,y))$ is also linear along the aforementioned subdomains, and in particular along the quadrangle edges.

The directional derivatives of f with respect to x or y are obtained based the indirect relation

$$\begin{bmatrix} \frac{\partial f}{\partial \xi} \\ \frac{\partial f}{\partial \eta} \end{bmatrix} = \underbrace{\begin{bmatrix} \frac{\partial x}{\partial \xi} & \frac{\partial y}{\partial \xi} \\ \frac{\partial x}{\partial \eta} & \frac{\partial y}{\partial \eta} \end{bmatrix}}_{\underline{\underline{\mathrm{J}}}^{\top}(\xi,\eta;\underline{\mathrm{x}}_i)} \begin{bmatrix} \frac{\partial f}{\partial x} \\ \frac{\partial f}{\partial y} \end{bmatrix} \tag{2.48}$$

The function derivatives with respect to ξ, η are obtained as

$$\begin{bmatrix} \frac{\partial f}{\partial \xi} \\ \frac{\partial f}{\partial \eta} \end{bmatrix} = \sum_i \begin{bmatrix} \frac{\partial N_i}{\partial \xi} \\ \frac{\partial N_i}{\partial \eta} \end{bmatrix} f_i. \tag{2.49}$$

The *transposed* Jacobian matrix of the mapping function that appears in 2.48 is

$$\underline{\underline{\mathrm{J}}}^{\top}(\xi,\eta) = \begin{bmatrix} \frac{\partial x}{\partial \xi} & \frac{\partial y}{\partial \xi} \\ \frac{\partial x}{\partial \eta} & \frac{\partial y}{\partial \eta} \end{bmatrix} \tag{2.50}$$

$$= \sum_i \left(\begin{bmatrix} \frac{\partial N_i}{\partial \xi} & 0 \\ \frac{\partial N_i}{\partial \eta} & 0 \end{bmatrix} x_i + \begin{bmatrix} 0 & \frac{\partial N_i}{\partial \xi} \\ 0 & \frac{\partial N_i}{\partial \eta} \end{bmatrix} y_i \right) \tag{2.51}$$

If the latter matrix is assumed nonsingular – condition, this, that pairs the bijective nature of the $\underline{\mathrm{m}}$ mapping, equation 2.48 may be inverted, thus leading to the form

$$\begin{bmatrix} \frac{\partial f}{\partial x} \\ \frac{\partial f}{\partial y} \end{bmatrix} = \left(\underline{\underline{\mathrm{J}}}^{\top}\right)^{-1} \begin{bmatrix} \cdots & \frac{\partial N_i}{\partial \xi} & \cdots \\ \cdots & \frac{\partial N_i}{\partial \eta} & \cdots \end{bmatrix} \begin{bmatrix} \vdots \\ f_i \\ \vdots \end{bmatrix} \tag{2.52}$$

$$= \underbrace{\left(\underline{\underline{\mathrm{J}}}^{\top}\right)^{-1} \begin{bmatrix} \frac{\partial \underline{\underline{\mathrm{N}}}}{\partial \xi} \\ \frac{\partial \underline{\underline{\mathrm{N}}}}{\partial \eta} \end{bmatrix}}_{\underline{\underline{\mathrm{L}}}(\xi,\eta;\underline{\mathrm{x}}_i), \text{ or just } \underline{\underline{\mathrm{L}}}(\xi,\eta)} \underline{\mathrm{f}} \tag{2.53}$$

[32]The case exists of an edge whose endpoints are superposed, i.e. the edge collapses to a point.

where the inner mechanics of the matrix-vector product are appointed for the Eq. 2.49 summation; the differential operator $\underline{\mathrm{L}}(\xi, \eta; \underline{\mathrm{x}}_i)$ – or just $\underline{\mathrm{L}}(\xi, \eta)$ if, again, we disregard its parametric dependence on the nodal coordinates – is also defined that extract the x, y directional derivatives of the interpolation function from its nodal values.

The general spatial quadrilateral domain. TODO.

2.2.2 Gaussian quadrature rules for some relevant domains.

Reference one dimensional domain. The gaussian quadrature rule for approximating the definite integral of a $f(\xi)$ function over the $[-1, 1]$ reference interval is constructed as the customary weighted sum of internal function samples, namely

$$\int_{-1}^{1} f(\xi) d\xi \approx \sum_{i=1}^{n} f(\xi_i) w_i; \tag{2.54}$$

Its peculiarity is to employ location-weight pairs (ξ_i, w_i) that are optimal with respect to the polynomial class of functions. Nevertheless, such choice has revealed itself robust enough for for a more general employment.

Let's consider a m-th order polynomial

$$p(\xi) \stackrel{\text{def}}{=} a_m \xi^m + a_{m-1} \xi^{m-1} + \ldots + a_1 \xi + a_0$$

whose exact integral is

$$\int_{-1}^{1} p(\xi) d\xi = \sum_{j=0}^{m} \frac{(-1)^j + 1}{j+1} a_j$$

The integration residual between the exact definite integral and the weighted sample sum is defined as

$$r\left(a_j, (\xi_i, w_i)\right) \stackrel{\text{def}}{=} \sum_{i=1}^{n} p(\xi_i) w_i - \int_{-1}^{1} p(\xi) d\xi \tag{2.55}$$

The optimality condition is stated as follows: the quadrature rule involving n sample points (ξ_i, w_i), $i = 1 \ldots n$ is optimal for the m-th order polynomial if a) the integration residual is null for general

a_j values , and b) such condition does not hold for any lower-order sampling rule.

Once observed that the zero residual requirement is satisfied by any sampling rule when the a_j polynomial coefficients are all null, condition a) may be enforced by imposing that such zero residual value remains constant with varying a_j terms, i.e.

$$\begin{cases} \dfrac{\partial r\left(a_j,(\xi_i,w_i)\right)}{\partial a_j}=0, \quad j=0\dots m \end{cases} \tag{2.56}$$

A system of $m+1$ polynomial equations of degree[33] $m+1$ is hence obtained in the $2n$ (ξ_i, w_i) unknowns; in the assumed absence of redundant equations, solutions do not exist if the constraints outnumber the unknowns, i.e. $m > 2n-1$. Limiting our discussion to the threshold condition $m = 2n-1$, an attentive algebraic manipulation of Eqns. 2.56 may be performed in order to extract the (ξ_i, w_i) solutions, which are unique apart from the pair permutations[34].

Eqns. 2.56 solutions are reported in Table 2.2 for quadrature rules

[33] the $(m+1)$-th order $w_m\xi^m$ term appears in equations

[34] In this note, location-weight pairs are obtained for the gaussian quadrature rule of order $n = 2$, aiming at illustrating the general procedure. The general $m = 2n-1 = 3$rd order polynomial is stated in the form

$$p(\xi)=a_3\xi^3+a_2\xi^2+a_1\xi+a_0, \quad \int_{-1}^{1}p(\xi)d\xi=\frac{2}{3}a_2+2a_0,$$

whereas the integral residual is

$$r=a_3\left(w_1\xi_1^3+w_2\xi_2^3\right)+a_2\left(w_1\xi_1^2+w_2\xi_2^2-\frac{2}{3}\right)+a_1\left(w_1\xi_1+w_2\xi_2\right)+a_0\left(w_1+w_2-2\right)$$

Eqns 2.56 may be derived as

$$\begin{cases} 0=\frac{\partial r}{\partial a_3}=w_1\xi_1^3+w_2\xi_2^3 & (e_1)\\ 0=\frac{\partial r}{\partial a_2}=w_1\xi_1^2+w_2\xi_2^2-\frac{2}{3} & (e_2)\\ 0=\frac{\partial r}{\partial a_1}=w_1\xi_1+w_2\xi_2 & (e_3)\\ 0=\frac{\partial r}{\partial a_0}=w_1+w_2-2 & (e_4) \end{cases}$$

which are independent of the a_j coefficients.

By composing $\left(e_1-\xi_1^2e_3\right)/(w_2\xi_2)$ it is obtained that $\xi_2^2=\xi_1^2$; e_2 may then be written as $(w_1+w_2)\xi_1^2=2/3$, and then as $2\xi_1^2=2/3$, according to e_4. It derives that $\xi_{1,2}=\pm1/\sqrt{3}$. Due to the opposite nature of the roots, e_3 implies $w_2=w_1$, relation, this, that turns e_4 into $2w_1=2w_2=2$, and hence $w_{1,2}=1$.

n	ξ_i	w_i
1	0	2
2	$\pm\frac{1}{\sqrt{3}}$	1
3	0	$\frac{8}{9}$
	$\pm\sqrt{\frac{3}{5}}$	$\frac{5}{9}$
4	$\pm\sqrt{\frac{3}{7}-\frac{2}{7}\sqrt{\frac{6}{5}}}$	$\frac{18+\sqrt{30}}{36}$
	$\pm\sqrt{\frac{3}{7}+\frac{2}{7}\sqrt{\frac{6}{5}}}$	$\frac{18-\sqrt{30}}{36}$

Table 2.2: Integration points for the lower order gaussian quadrature rules.

with up to $n = 4$ sample points[35].

It is noted that the integration points are symmetrically distributed with respect to the origin, and that the function is never sampled at the $\{-1, 1\}$ extremal points.

General one dimensional domain. The extension of the one dimensional quadrature rule from the reference domain $[-1, 1]$ to a general $[a, b]$ domain is pretty straightforward, requiring just a change of integration variable – i.e. a mapping function $x = m(\xi)$ s.t. $a = m(-1)$ and $b = m(1)$ – to obtain the following

$$\int_a^b g(x)dx = \int_{-1}^{1} g\left(m(\xi)\right) \frac{dm}{d\xi} d\xi \approx \sum_{i=1}^{n} g\left(m(\xi_i)\right) \left.\frac{dm}{d\xi}\right|_{\xi=\xi_i} w_i. \quad (2.57)$$

Such a mapping function may be conveniently defined along the same lines as the weight (or shape) function based interpolation, thus obtaining

$$m(x) = \underbrace{\left(\frac{1-\xi}{2}\right)}_{N_1} a + \underbrace{\left(\frac{1+\xi}{2}\right)}_{N_2} b.$$

[35] see `https://pomax.github.io/bezierinfo/legendre-gauss.html` for higher order gaussian quadrature rule sample points.

The first order derivative may be evaluated as

$$\frac{dm}{d\xi} = \frac{dN_1}{d\xi}a + \frac{dN_2}{d\xi}b = \frac{b-a}{2}$$

and it is constant along the interval, so that it may be collected outside of the summation, thus leading to

$$\int_a^b g(x)dx \approx \frac{b-a}{2}\sum_{i=1}^{n} g\left(\frac{b+a}{2} + \frac{b-a}{2}\xi_i\right) w_i. \tag{2.58}$$

Reference quadrangular domain. A quadrature rule for the reference quadrangular domain of Figure 2.10a may be derived by nesting the quadrature rule defined for the reference interval, see Eqn. 2.54, thus obtaining

$$\int_{-1}^{1}\int_{-1}^{1} f(\xi,\eta)\, d\xi d\eta \approx \sum_{i=1}^{p}\sum_{j=1}^{q} f(\xi_i,\eta_j)\, w_i w_j \tag{2.59}$$

where (ξ_i, w_i) and (η_j, w_j) are the coordinate-weight pairs of the two quadrature rules of p and q order, respectively, employed for spanning the two coordinate axes. The equivalent notation

$$\int_{-1}^{1}\int_{-1}^{1} f(\xi,\eta)\, d\xi d\eta \approx \sum_{l=1}^{pq} f\left(\underline{\xi}_l\right) w_l \tag{2.60}$$

emphasises the characteristic nature of the pq point/weight pairs for the domain and for the quadrature rule employed; a general integer bijection[36] $\{1\dots pq\} \leftrightarrow \{1\dots p\} \times \{1\dots q\}$, $l \leftrightarrow (i,j)$ may be utilized to formally derive the two-dimensional quadrature rule pairs

$$\underline{\xi}_l = (\xi_i, \eta_j), \quad w_l = w_i w_j, \quad l = 1\dots pq \tag{2.61}$$

from their uniaxial counterparts.

[36] e.g.

$$\{i-1; j-1\} = (l-1) \bmod (p,q), \quad l-1 = (j-1)q + (i-1)$$

where the operator

$$\{a_n; \dots; a_3; a_2; a_1\} = m \bmod (b_n, \dots, b_3, b_2, b_1)$$

consists in the extraction of the n least significant a_i digits of a mixed radix representation of the integer m with respect to the sequence of b_i bases, with $i = 1\dots n$.

General quadrangular domain. The rectangular infinitesimal area $dA_{\xi\eta} = d\xi d\eta$ in the neighborhood of a ξ_P, η_P location, see Figure 2.11b, is mapped to the dA_{xy} quadrangle of Figure 2.11a, which is composed by the two triangular areas

$$dA_{xy} = \frac{1}{2!}\begin{vmatrix} 1 & x\,(\xi_P & ,\eta_P &) & y\,(\xi_P & ,\eta_P &) \\ 1 & x\,(\xi_P + d\xi, & \eta_P &) & y\,(\xi_P + d\xi, & \eta_P &) \\ 1 & x\,(\xi_P + d\xi, & \eta_P + d\eta) & & y\,(\xi_P + d\xi, & \eta_P + d\eta) \end{vmatrix} + \\ + \frac{1}{2!}\begin{vmatrix} 1 & x\,(\xi_P + d\xi, & \eta_P + d\eta) & & y\,(\xi_P + d\xi, & \eta_P + d\eta) \\ 1 & x\,(\xi_P & ,\eta_P + d\eta) & & y\,(\xi_P & ,\eta_P + d\eta) \\ 1 & x\,(\xi_P & ,\eta_P &) & y\,(\xi_P & ,\eta_P &) \end{vmatrix}. \quad (2.62)$$

The determinant formula for the area of a triangle, shown below along with its n-dimensional symplex hypervolume generalization,

$$\mathcal{A} = \frac{1}{2!}\begin{vmatrix} 1 & x_1 & y_1 \\ 1 & x_2 & y_2 \\ 1 & x_3 & y_3 \end{vmatrix}, \quad \mathcal{H} = \frac{1}{n!}\begin{vmatrix} 1 & \underline{\mathrm{x}}_1 \\ 1 & \underline{\mathrm{x}}_2 \\ \vdots & \vdots \\ 1 & \underline{\mathrm{x}}_{n+1} \end{vmatrix} \quad (2.63)$$

has been employed above[37].

By operating a local multivariate linearization of the 2.62 matrix terms, the relation

$$dA_{xy} \approx \frac{1}{2!}\begin{vmatrix} 1 & x & y \\ 1 & x + x_{,\xi}d\xi & y + y_{,\xi}d\xi \\ 1 & x + x_{,\xi}d\xi + x_{,\eta}d\eta & y + y_{,\xi}d\xi + y_{,\eta}d\eta \end{vmatrix} + \\ + \frac{1}{2!}\begin{vmatrix} 1 & x + x_{,\xi}d\xi + x_{,\eta}d\eta & y + y_{,\xi}d\xi + y_{,\eta}d\eta \\ 1 & x + x_{,\eta}d\eta & y + y_{,\eta}d\eta \\ 1 & x & y \end{vmatrix}$$

is obtained, where $x, y, x_{,\xi}, x_{,\eta}, y_{,\xi}$, and $y_{,\eta}$ are the x, y functions and their first order partial derivatives, evaluated at the (ξ_P, η_P) point; infinitesimal terms of order higher than $d\xi, d\eta$ are neglected.

[37] A direct formula for the area of the polygon given the vertex coordinates is also available, see `https://en.wikipedia.org/wiki/Shoelace_formula`

After some matrix manipulations[38], the following expression is obtained

$$dA_{xy} = \underbrace{\begin{vmatrix} x_{,\xi} & y_{,\xi} \\ x_{,\eta} & y_{,\eta} \end{vmatrix}}_{\left|J^{\mathrm{T}}(\xi_P,\eta_P;\underline{\mathrm{x}},\underline{\mathrm{y}})\right|} dA_{\xi\eta} \tag{2.64}$$

that equates the ratio of the mapped and of the reference areas to the determinant of the transformation (transpose) Jacobian matrix[39].

After the preparatory passages above, we obtain

$$\iint_{A_{xy}} g(x,y)dA_{xy} = \int_{-1}^{1}\int_{-1}^{1} g\left(x\left(\xi,\eta\right), y\left(\xi,\eta\right)\right)\left|J(\xi,\eta)\right| d\xi d\eta, \tag{2.65}$$

thus reducing the quadrature over a general domain to its reference domain counterpart, which has been discussed in the paragraph above.

Based on Eqn. 2.60, the quadrature rule

$$\iint_{A_{xy}} g(\underline{\mathrm{x}})dA_{xy} \approx \sum_{l=1}^{pq} g\left(\underline{\mathrm{x}}\left(\underline{\xi}_l\right)\right)\left|J(\underline{\xi}_l)\right| w_l \tag{2.66}$$

[38]In the first determinant, the second row is subtracted from the third one, and the first row is subtracted from the second one. The $d\xi$, $d\eta$ factors are then collected from the second and the third row respectively. In the second determinant, the second row is subtracted from the first one, and the third row is subtracted from the second one. The $d\xi$, $d\eta$ factors are then collected from the first and the second row respectively. We now have

$$dA_{xy} = \frac{1}{2}\begin{vmatrix} 1 & x & y \\ 0 & x_{,\xi} & y_{,\xi} \\ 0 & x_{,\eta} & y_{,\eta} \end{vmatrix} d\xi d\eta + \frac{1}{2}\begin{vmatrix} 0 & x_{,\xi} & y_{,\xi} \\ 0 & x_{,\eta} & y_{,\eta} \\ 1 & x & y \end{vmatrix} d\xi d\eta$$

The first column of both the determinants contains a single, unitary, nonzero term, whose row and column indexes are even once added up; the determinants of the associated complementary minors hence equate their whole matrix counterpart. We hence obtain

$$dA_{xy} = \frac{1}{2}\begin{vmatrix} x_{,\xi} & y_{,\xi} \\ x_{,\eta} & y_{,\eta} \end{vmatrix} d\xi d\eta + \frac{1}{2}\begin{vmatrix} x_{,\xi} & y_{,\xi} \\ x_{,\eta} & y_{,\eta} \end{vmatrix} d\xi d\eta$$

from which Eq.2.64 may be straightforwardly derived.

[39]The Jacobian matrix for a general $\underline{\xi} \mapsto \underline{\mathrm{x}}$ mapping is in fact defined according to

$$[J(\underline{\xi}_P)]_{ij} \stackrel{\mathrm{def}}{=} \left.\frac{\partial x_i}{\partial \xi_j}\right|_{\underline{\xi}=\underline{\xi}_P} \qquad i,j = 1\ldots n$$

being i the generic matrix term row index, and j the column index

is derived, stating that the definite integral of a g integrand over a quadrangular domain pertaining to the physical x, y plane (x, y are dimensional quantities, namely lengths) may be approximated as follows:

1. a reference-to-physical domain mapping is defined, that is based on the vertex physical coordinate interpolation;

2. the function is sampled at the physical locations that are the images of the Gaussian integration points previously obtained for the reference domain;

3. a weighted sum of the collected samples is performed, where the weights consist in the product of i) the adimensional w_l Gauss point weight (suitable for integrating on the reference domain), and ii) a dimensional area scaling term, that equals the determinant of the transformation Jacobian matrix, locally evaluated at the Gauss points.

General, spatial quadrangular domain. TODO... but, in the meantime

$$dA_{xyz} = \sqrt{\begin{vmatrix} x_{,\xi} & x_{,\eta} \\ y_{,\xi} & y_{,\eta} \end{vmatrix}^2 + \begin{vmatrix} y_{,\xi} & y_{,\eta} \\ z_{,\xi} & z_{,\eta} \end{vmatrix}^2 + \begin{vmatrix} z_{,\xi} & z_{,\eta} \\ x_{,\xi} & x_{,\eta} \end{vmatrix}^2} d\xi d\eta \tag{2.67}$$

$$\underline{\mathrm{L}}\left(\xi, \eta; \underline{\mathrm{x}}_i\right) \approx ... \tag{2.68}$$

2.3 The bilinear isoparametric shear-deformable shell element

> This is a four-node, thick-shell element with global displacements and rotations as degrees of freedom. Bilinear interpolation is used for the coordinates, displacements and the rotations. The membrane strains are obtained from the displacement field; the curvatures from the rotation field. The transverse shear strains are calculated at the middle of the edges and interpolated to the integration points. In this way, a very efficient and simple element is obtained which exhibits correct behavior in the limiting case of thin shells. The element can be used in curved shell analysis as well as in the analysis of complicated plate structures. For the latter case, the element is easy to use since connections between intersecting plates can be modeled without tying. Due to its simple formulation when compared to the standard higher order shell elements, it is less expensive and, therefore, very attractive in nonlinear analysis. The element is not very sensitive to distortion, particularly if the corner nodes lie in the same plane. All constitutive relations can be used with this element.
>
> — MSC.Marc 2013.1 Documentation, vol. B, Element library.

2.3.1 Element geometry

Once introduced the required algebraic paraphernalia, the definition of a quadrilateral bilinear isoparametric shear-deformable shell element is straightforward.

The quadrilateral element geometry is defined by the position in space of its four vertices, which constitute the set of *nodal points*, or *nodes*, i.e. the set of locations at which field components are primarily, parametrically, defined; interpolation is employed in deriving the field values elsewhere.

A suitable interpolation scheme, named *bilinear*, has been introduced in paragraph 2.2.1; the related functions depend on the normalized coordinate pair $\xi, \eta \in [-1, 1]$ that spans the elementary quadrilateral of Figure 2.10.

A global reference system OXYZ is employed for concurrently dealing with multiple elements (i.e. at a whole model scale); a more convenient, local Cxyz reference system, z being locally normal to the shell, is used when a single element is under scrutiny – e.g. in the current paragraph.

Nodal coordinates define the element initial, undeformed, geometry[40], or, alternatively, the portion of thin-walled body reference surface that pertains to the current element; physical, spatial coordinates for each other element point may be retrieved by interpolation based on the associated pair of natural ξ, η coordinates, namely

$$\begin{bmatrix} X(\xi,\eta) \\ Y(\xi,\eta) \\ Z(\xi,\eta) \end{bmatrix} = \sum_{i=1}^{n} N_i(\xi,\eta) \begin{bmatrix} X_i \\ Y_i \\ Z_i \end{bmatrix}, \qquad \begin{bmatrix} x(\xi,\eta) \\ y(\xi,\eta) \\ z(\xi,\eta) \end{bmatrix} = \sum_{i=1}^{n} N_i(\xi,\eta) \begin{bmatrix} x_i \\ y_i \\ z_i \end{bmatrix} \tag{2.69}$$

with reference to both the global and the local systems.

In particular, the C centroid is the image within the physical space of the $\xi = 0, \eta = 0$ natural coordinate system origin.

The in-plane orientation of the local Cxyz reference system is somewhat arbitrary and implementation-specific; the MSC.Marc approach is used as an example, and it is described in the following. The in-plane x, y axes are tentatively defined[41] based on the physical directions that are associated with the ξ, η natural axes, i.e. the oriented segments spanning a) from the midpoint of the n4-n1 edge to the midpoint of the n2-n3 edge, and b) from the midpoint of the n1-n2 edge to the midpoint of the n3-n4 edge, respectively; however, these two tentative axes are not mutually orthogonal in general. The mutual Cxy angle is then amended by rotating those interim axes with respect to a third, binormal axis Cz, while preserving their initial bisectrix.

[40] They are however continuosly updated within most common nonlinear analysis frameworks, where *initial* usually refers to the last computed, aka *previous* step of an iterative scheme.

[41] The MSC.Marc element library documentation defines them as a normalized form of the

$$\left(\frac{\partial X}{\partial \xi}, \frac{\partial Y}{\partial \xi}, \frac{\partial Z}{\partial \xi}, \right) \Bigg|_{\xi=0,\eta=0}, \left(\frac{\partial X}{\partial \eta}, \frac{\partial Y}{\partial \eta}, \frac{\partial Z}{\partial \eta}, \right) \Bigg|_{\xi=0,\eta=0},$$

vectors, which are evaluated at the centroid. The two definitions may be proved equivalent based on the bilinear interpolation properties.

The resulting quadrilateral shell element has limited capabilities of representing a curve surface; it is in fact flat, apart from a (suggestedly limited) anticlastic curvature of the element diagonals, which is associated to the quadratic $\xi\eta$ term of the interpolation functions. It is e.g. not capable of representing a single curvature surface.

The curve nature of a thin-walled body midsurface may thus be reproduced by recurring to a tessellation of essentially flat, but mutually angled elements.

2.3.2 Displacement and rotation fields

The element degrees of freedom consist in the displacements and the rotations of the four quadrilateral vertices, i.e. *nodes*.

By interpolating the nodal values, displacement and rotation functions may be derived along the element as

$$\begin{bmatrix} u(\xi,\eta) \\ v(\xi,\eta) \\ w(\xi,\eta) \end{bmatrix} = \sum_{i=1}^{4} N_i(\xi,\eta) \begin{bmatrix} u_i \\ v_i \\ w_i \end{bmatrix} \tag{2.70}$$

$$\begin{bmatrix} \theta(\xi,\eta) \\ \phi(\xi,\eta) \\ \psi(\xi,\eta) \end{bmatrix} = \sum_{i=1}^{4} N_i(\xi,\eta) \begin{bmatrix} \theta_i \\ \phi_i \\ \psi_i \end{bmatrix} \tag{2.71}$$

with $i = 1 \ldots 4$ cycling along the element nodes. If we collect the element nodal dofs within the six column vectors

$$\underline{\mathrm{u}} = \begin{bmatrix} \vdots \\ u_i \\ \vdots \end{bmatrix} \qquad \underline{\mathrm{v}} = \begin{bmatrix} \vdots \\ v_i \\ \vdots \end{bmatrix} \qquad \underline{\mathrm{w}} = \begin{bmatrix} \vdots \\ w_i \\ \vdots \end{bmatrix}$$

$$\underline{\theta} = \begin{bmatrix} \vdots \\ \theta_i \\ \vdots \end{bmatrix} \qquad \underline{\phi} = \begin{bmatrix} \vdots \\ \phi_i \\ \vdots \end{bmatrix} \qquad \underline{\psi} = \begin{bmatrix} \vdots \\ \psi_i \\ \vdots \end{bmatrix}$$

we may resort to compact notations in the form

$$u(\xi,\eta) = \underline{\underline{\mathrm{N}}}\,(\xi,\eta)\,\underline{\mathrm{u}} \qquad\qquad v(\xi,\eta) = \underline{\underline{\mathrm{N}}}\,(\xi,\eta)\,\underline{\mathrm{v}}$$

et cetera.

Those column vectors are in turn stacked to form the cumulative

$$\underline{\mathrm{d}}^{\top} = \left[\underline{\mathrm{u}}^{\top} \quad \underline{\mathrm{v}}^{\top} \quad \underline{\mathrm{w}}^{\top} \quad \underline{\theta}^{\top} \quad \underline{\phi}^{\top} \quad \underline{\psi}^{\top} \right] \tag{2.72}$$

dof column vector for the title element.

The $\underline{\psi}$ vector associated with the drilling degree of freedom – i.e. the rotation with respect to the normal z axis – is *not* omitted, although its contribution to the element strain energy deserves some discussion, see the dedicated paragraph below.

2.3.3 Strains

By recalling Eqn. 2.52, we have e.g.

$$\begin{bmatrix} \frac{\partial u}{\partial x} \\ \frac{\partial u}{\partial y} \end{bmatrix} = \underbrace{\left(\underline{\underline{\mathrm{J}}}' \right)^{-1} \begin{bmatrix} \cdots & \frac{\partial N_i}{\partial \xi} & \cdots \\ \cdots & \frac{\partial N_i}{\partial \eta} & \cdots \end{bmatrix}}_{\underline{\underline{\mathrm{L}}}(\xi,\eta;\underline{\mathrm{x}}_i) \text{ or just } \underline{\underline{\mathrm{L}}}(\xi,\eta)} \begin{bmatrix} \vdots \\ u_i \\ \vdots \end{bmatrix} \tag{2.73}$$

for the x-oriented displacement component; the differential operator $\underline{\underline{\mathrm{L}}}(\xi, \eta; \underline{\mathrm{x}}_i)$, which extracts the x, y directional derivatives from the nodal values of a given field component, is employed.

A block defined $\underline{\underline{\mathrm{Q}}}(\xi, \eta)$ matrix is thus obtained that cumulatively relates the in-plane displacement component derivatives to the associated nodal values

$$\begin{bmatrix} \frac{\partial u}{\partial x} \\ \frac{\partial u}{\partial y} \\ \frac{\partial v}{\partial x} \\ \frac{\partial v}{\partial y} \end{bmatrix} = \underbrace{\begin{bmatrix} \underline{\underline{\mathrm{L}}}(\xi,\eta) & \underline{\underline{0}} \\ \underline{\underline{0}} & \underline{\underline{\mathrm{L}}}(\xi,\eta) \end{bmatrix}}_{\underline{\underline{\mathrm{Q}}}(\xi,\eta)} \begin{bmatrix} \underline{\mathrm{u}} \\ \underline{\mathrm{v}} \end{bmatrix} \tag{2.74}$$

An equivalent relation may then be obtained for the rotation field

$$\begin{bmatrix} \frac{\partial \theta}{\partial x} \\ \frac{\partial \theta}{\partial y} \\ \frac{\partial \phi}{\partial x} \\ \frac{\partial \phi}{\partial y} \end{bmatrix} = \underline{\underline{\mathrm{Q}}}(\xi, \eta) \begin{bmatrix} \underline{\theta} \\ \underline{\phi} \end{bmatrix} \tag{2.75}$$

By making use of two auxiliary matrices $\underline{\underline{\mathrm{H}}}'$ and $\underline{\underline{\mathrm{H}}}''$ that collect the $\{0, \pm 1\}$ coefficients in Eqns. 2.10 and 2.11, we obtain that the ip

strain components at the reference surface, and the curvatures equate respectively

$$\begin{bmatrix} e_x \\ e_y \\ g_{xy} \end{bmatrix} = \underbrace{\begin{bmatrix} +1 & 0 & 0 & 0 \\ 0 & 0 & 0 & +1 \\ 0 & +1 & +1 & 0 \end{bmatrix}}_{\underline{\underline{\mathrm{H}}}'} \begin{bmatrix} \frac{\partial u}{\partial x} \\ \frac{\partial u}{\partial y} \\ \frac{\partial v}{\partial x} \\ \frac{\partial v}{\partial y} \end{bmatrix} = \underline{\underline{\mathrm{H}}}' \underline{\underline{\mathrm{Q}}}(\xi,\eta) \begin{bmatrix} \underline{\mathrm{u}} \\ \underline{\mathrm{v}} \end{bmatrix} \quad (2.76)$$

$$\begin{bmatrix} \kappa_x \\ \kappa_y \\ \kappa_{xy} \end{bmatrix} = \underbrace{\begin{bmatrix} 0 & 0 & +1 & 0 \\ 0 & -1 & 0 & 0 \\ -1 & 0 & 0 & +1 \end{bmatrix}}_{\underline{\underline{\mathrm{H}}}''} \begin{bmatrix} \frac{\partial \theta}{\partial x} \\ \frac{\partial \theta}{\partial y} \\ \frac{\partial \phi}{\partial x} \\ \frac{\partial \phi}{\partial y} \end{bmatrix} = \underline{\underline{\mathrm{H}}}'' \underline{\underline{\mathrm{Q}}}(\xi,\eta) \begin{bmatrix} \underline{\theta} \\ \underline{\phi} \end{bmatrix} \quad (2.77)$$

or, by referring to the whole set of nodal dofs,

$$\underline{\mathrm{e}} = \underbrace{\begin{bmatrix} \underline{\underline{\mathrm{H}}}' \underline{\underline{\mathrm{Q}}}(\xi,\eta) & \underline{\underline{0}} & \underline{\underline{0}} & \underline{\underline{0}} & \underline{\underline{0}} \end{bmatrix}}_{\underline{\underline{\mathrm{B}}}_e(\xi,\eta)} \underline{\mathrm{d}} \quad (2.78)$$

$$\underline{\kappa} = \underbrace{\begin{bmatrix} \underline{\underline{0}} & \underline{\underline{0}} & \underline{\underline{0}} & \underline{\underline{\mathrm{H}}}'' \underline{\underline{\mathrm{Q}}}(\xi,\eta) & \underline{\underline{0}} \end{bmatrix}}_{\underline{\underline{\mathrm{B}}}_\kappa(\xi,\eta)} \underline{\mathrm{d}}\,. \quad (2.79)$$

The $\underline{\underline{\mathrm{B}}}_e$ and $\underline{\underline{\mathrm{B}}}_\kappa$ matrices are block-defined by appending to the 3x8 blocks introduced in Eqn. 2.76 and 2.77, respectively, a suitable set of 3x4 null block placeholders.

The ip strain components at a generic ξ, η, z point along the element thickness may then be derived according to Eqn. 2.12 as a (linear) function of the nodal degrees of freedom

$$\underline{\epsilon}(\xi,\eta,z) = \left(\underline{\underline{\mathrm{B}}}_e(\xi,\eta) + z\,\underline{\underline{\mathrm{B}}}_\kappa(\xi,\eta)\right) \underline{\mathrm{d}}\,; \quad (2.80)$$

the oop shear strain components, as defined in Eqns. 2.4 and 2.5, become instead

$$\begin{bmatrix} g_{zx} \\ g_{yz} \end{bmatrix} = \underline{\underline{\mathrm{L}}}(\xi,\eta)\,\underline{\mathrm{w}} + \begin{bmatrix} \underline{\underline{0}} & +\underline{\underline{\mathrm{N}}}(\xi,\eta) \\ -\underline{\underline{\mathrm{N}}}(\xi,\eta) & \underline{\underline{0}} \end{bmatrix} \begin{bmatrix} \underline{\theta} \\ \underline{\phi} \end{bmatrix}, \quad (2.81)$$

and thus, by employing a notation consistent with **??**,

$$\begin{bmatrix} g_{zx} \\ g_{yz} \end{bmatrix} = \underbrace{\begin{bmatrix} \underline{\underline{0}} & \underline{\underline{0}} & \underline{\underline{\mathrm{L}}}(\xi,\eta) & 0 & \underline{\underline{\mathrm{N}}}(\xi,\eta) & \underline{\underline{0}} \\ & & & -\underline{\underline{\mathrm{N}}}(\xi,\eta) & 0 & \end{bmatrix}}_{\underline{\underline{\mathrm{B}}}_{\gamma}(\xi,\eta)} \underline{\mathrm{d}} \tag{2.82}$$

where the transformation matrix that derives the out-of-plane, interlaminar strains from the nodal degrees of freedom vector is constituted by six 2×4 blocks.

2.3.4 Stresses

In general, material constitutive laws are employed in deriving stress components from their strain counterpart.

In the case of a shell element, the plane stress relations discussed in Paragraph 2.1, see Eqns. 2.13, may be employed in deriving the pointwise ip stress components from the associated strains.

Also, the plate constitutive laws reported as Eqns. 2.19 may be employed in deriving the tt force and moment ip stress resultants from the generalized strains obtained in Eqns. 2.78, 2.79. The oop shear stress resultants may be derived from the associated Eqns. 2.82 generalized strains by resorting to Eq. 2.24.

2.3.5 The element stiffness matrix.

In this paragraph, the elastic behaviour of the finite element under scrutiny is derived.

The element is considered in its deformed configuration, being

$$\underline{\mathrm{d}}^{\top} = \begin{bmatrix} \underline{\mathrm{u}}^{\top} & \underline{\mathrm{v}}^{\top} & \underline{\mathrm{w}}^{\top} & \underline{\theta}^{\top} & \underline{\phi}^{\top} & \underline{\psi}^{\top} \end{bmatrix} \tag{2.83}$$

the dof vector associated with such condition.

A virtual displacement field perturbs such deformed configuration; as usual, those virtual displacements are infinitesimal, they do occur while time is held constant, and, being otherwise arbitrary, they respect the existing kinematic constraints.

Whilst, in fact, no external constrains are applied to the element, the motion of the pertaining material points is prescribed based on a) the assumed plate kinematics, and b) on the bilinear, isoparametric

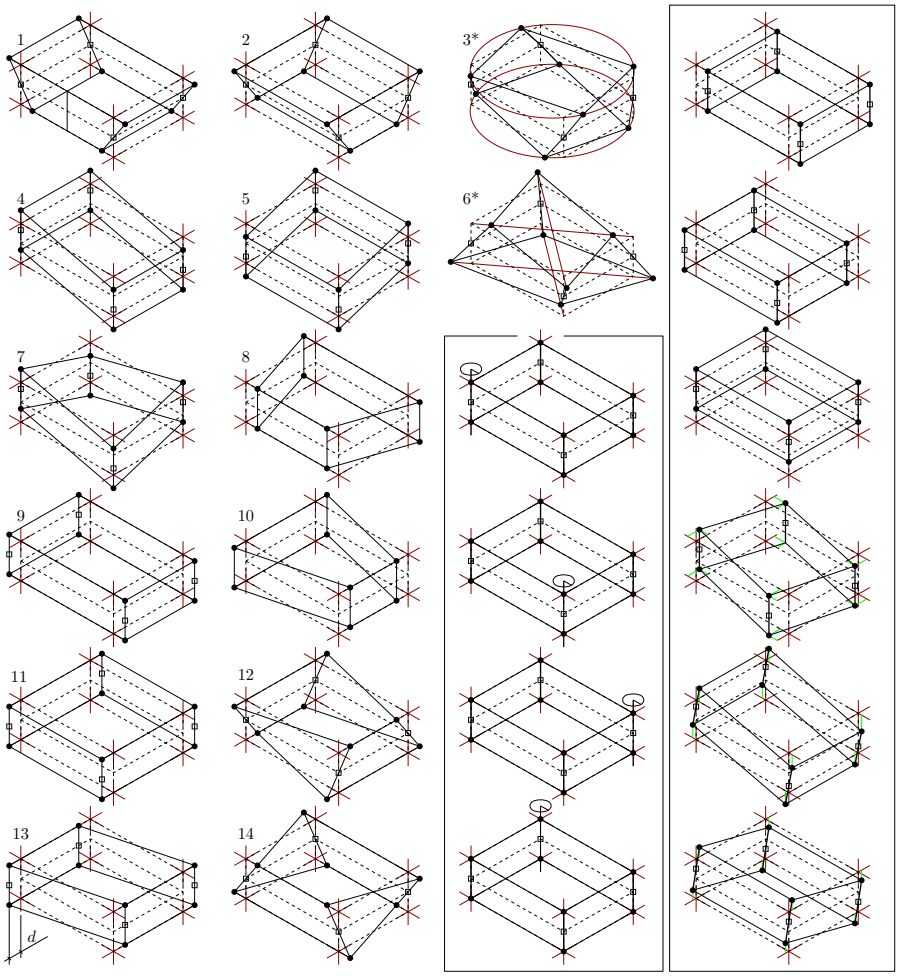

Figure 2.12: Elementary modes for the four-noded Mindlin plate element. The six rigid body modes, and the four pure drilling modes, are framed in Figure. The pure κ_{xy} mixed curvature mode represented in Fig. 2.3 is obtained as a combination of modes 6* and 7. The element behaves as stiff for any motion that is not a linear combination of these elementary modes.

interpolation laws that propagate the generalized nodal displacements $\delta\,\underline{\mathrm{d}}$ towards the quadrilateral's interior.

Since the element is supposed to elastically react to such $\underline{\mathrm{d}}$ deformed configuration, a set of external actions

$$\underline{\mathrm{G}}^{\top} = \begin{bmatrix} \underline{\mathrm{U}}^{\top} & \underline{\mathrm{V}}^{\top} & \underline{\mathrm{W}}^{\top} & \underline{\Theta}^{\top} & \underline{\Phi}^{\top} & \underline{\Psi}^{\top} \end{bmatrix} \tag{2.84}$$

is applied at nodes[42] – one each dof, that equilibrate the stretched element reactions.

The nature of each $\underline{\mathrm{G}}$ generalized force component is defined based on the nature of the associated generalized displacement, such that the overall virtual work they perform on any $\delta\,\underline{\mathrm{d}}$ motion is

$$\delta\,\Upsilon_{\mathrm{e}} = \delta\,\underline{\mathrm{d}}^{\top}\,\underline{\mathrm{G}}\,. \tag{2.85}$$

Let's now consider the internal virtual work produced by the same $\delta\,\underline{\mathrm{d}}$ displacements.

The ip stress components that are induced by the $\underline{\mathrm{d}}$ generalized displacements equal

$$\underline{\sigma} = \underline{\underline{\mathrm{D}}}\,(z)\,\left(\underline{\underline{\mathrm{B}}}_{e}(\xi,\eta) + \underline{\underline{\mathrm{B}}}_{\kappa}(\xi,\eta)z\right)\,\underline{\mathrm{d}} \tag{2.86}$$

according to the previous paragraphs,and they perform [volumic density of] internal work on the

$$\delta\,\underline{\epsilon} = \left(\underline{\underline{\mathrm{B}}}_{e}(\xi,\eta) + \underline{\underline{\mathrm{B}}}_{\kappa}(\xi,\eta)z\right)\,\delta\,\underline{\mathrm{d}} \tag{2.87}$$

virtual elongations.

Similar considerations may be assessed with reference to the plate theory framework; in particular, the internal action stress and moment resultants may be derived from the element dof as

$$\underline{\mathrm{q}} = \left(\underline{\mathrm{a}}\,\underline{\underline{\mathrm{B}}}_{e}(\xi,\eta) + \underline{\mathrm{b}}\,\underline{\underline{\mathrm{B}}}_{\kappa}(\xi,\eta)\right)\,\underline{\mathrm{d}} \tag{2.88}$$

$$\underline{\mathrm{m}} = \left(\underline{\mathrm{b}}^{\top}\,\underline{\underline{\mathrm{B}}}_{e}(\xi,\eta) + \underline{\mathrm{c}}\,\underline{\underline{\mathrm{B}}}_{\kappa}(\xi,\eta)\right)\,\underline{\mathrm{d}}\,, \tag{2.89}$$

and they perform [surficial density of] virtual work on the virtual variation of the generalized strain components

$$\delta\,\underline{\mathrm{e}} = \underline{\underline{\mathrm{B}}}_{e}(\xi,\eta)\,\delta\,\underline{\mathrm{d}} \tag{2.90}$$

$$\delta\,\underline{\kappa} = \underline{\underline{\mathrm{B}}}_{\kappa}(\xi,\eta)\,\delta\,\underline{\mathrm{d}}\,, \tag{2.91}$$

[42] There is no lack of generality in assuming the equilibrating external actions applied at dofs only, as discussed in Par. XXX below.

The associated internal virtual work may be derived by integration along the element volume, i.e. along the thickness, and along the quadrilateral portion of reference surface that pertains to the element. We thus obtain a first contribution to the overall internal virtual work

$$\begin{aligned}
\delta\,\Upsilon_{\mathrm{i}}^{\dagger} &= \iint_{\mathcal{A}}\int_{h} \delta\,\underline{\epsilon}^{\top}\,\underline{\sigma}\,dzd\mathcal{A} \\
&= \iint_{\mathcal{A}}\int_{h} \left(\left(\underline{\underline{\mathrm{B}}}_{e}+\underline{\underline{\mathrm{B}}}_{\kappa}z\right)\,\delta\,\underline{\mathrm{d}}\right)^{\top}\,\underline{\underline{\mathrm{D}}}\,\left(\underline{\underline{\mathrm{B}}}_{e}+\underline{\underline{\mathrm{B}}}_{\kappa}z\right)\,\underline{\mathrm{d}}\,dzd\mathcal{A} \\
&= \delta\,\underline{\mathrm{d}}^{\top}\left[\iint_{\mathcal{A}}\int_{h}\left(\underline{\underline{\mathrm{B}}}_{e}^{\top}+\underline{\underline{\mathrm{B}}}_{\kappa}^{\top}z\right)\,\underline{\underline{\mathrm{D}}}\,\left(\underline{\underline{\mathrm{B}}}_{e}+\underline{\underline{\mathrm{B}}}_{\kappa}z\right)dzd\mathcal{A}\right]\,\underline{\mathrm{d}} \\
&= \delta\,\underline{\mathrm{d}}^{\top}\,\underline{\underline{\mathrm{K}}}^{\dagger}\,\underline{\mathrm{d}}\,, \qquad (2.92)
\end{aligned}$$

which may equivalently be expressed based on the plate/laminate constitutive matrix minors as

$$\begin{aligned}
\delta\,\Upsilon_{\mathrm{i}}^{\dagger} &= \iint_{\mathcal{A}}\left(\delta\,\underline{\mathrm{e}}^{\top}\,\underline{\mathrm{q}}+\delta\,\underline{\kappa}^{\top}\,\underline{\mathrm{m}}\right)d\mathcal{A} \\
&= \delta\,\underline{\mathrm{d}}^{\top}\left[\iint_{\mathcal{A}}\begin{bmatrix}\underline{\underline{\mathrm{B}}}_{e}\\ \underline{\underline{\mathrm{B}}}_{\kappa}\end{bmatrix}^{\top}\begin{bmatrix}\underline{\underline{\mathrm{a}}} & \underline{\underline{\mathrm{b}}}\\ \underline{\underline{\mathrm{b}}}^{\mathrm{T}} & \underline{\underline{\mathrm{c}}}\end{bmatrix}\begin{bmatrix}\underline{\underline{\mathrm{B}}}_{e}\\ \underline{\underline{\mathrm{B}}}_{\kappa}\end{bmatrix}d\mathcal{A}\right]\,\underline{\mathrm{d}} \\
&= \delta\,\underline{\mathrm{d}}^{\top}\,\underline{\underline{\mathrm{K}}}^{\dagger}\,\underline{\mathrm{d}}\,, \qquad (2.93)
\end{aligned}$$

since we recall that

$$\left\{\underline{\underline{\mathrm{a}}},\,\underline{\underline{\mathrm{b}}},\,\underline{\underline{\mathrm{c}}}\right\}=\int_{h}\underline{\underline{\mathrm{D}}}\,\left\{1,z,z^{2}\right\}dz,$$

and that the $\underline{\underline{\mathrm{B}}}_{\{e,\kappa\}}$ matrices are constant in z.

Integration along i) the reference surface, and ii) along the thickness is numerically performed through potentially distinct quadrature rules; in particular, contributions are collected along the surface according to the two points per axis (four points overall) Gaussian quadrature formula introduced in Par. 2.2.2, whilst a (composite) Simpson rule is applied in z, being each material layer sampled at its outer and middle points. In general, any volume integral along the element, i.e.

$$\begin{aligned}
&\iiint_{\Omega} g(\xi,\eta,x,y,z)d\Omega = \qquad (2.94)\\
&=\int_{-1}^{+1}\int_{-1}^{+1}\int_{-\frac{h}{2}+o}^{+\frac{h}{2}+o} g(\xi,\eta,x(\xi,\eta),y(\xi,\eta),z)dz\,\left|\,\underline{\mathrm{J}}\,(\xi,\eta)\right|\,d\xi d\eta,
\end{aligned}$$

where g is a generic function of the isoparametric or physical coordinates, will be numerically performed according to such scheme.

the outer integrals in the isoparametric coordinates (ξ, η) are evaluated according to the usual two points per axis gaussian quadrature rule, whereas a [composite] Simpson rule is employed along the tt coordinate z.

The two points per axis quadrature rule is the lowest order rule that returns an exact integral evaluation in the case of *distortion-free*[43] elements, i.e. planar elements whose peculiar (parallelogram) shape also determines a linear (vs. bilinear) isoparametric mapping. Since the associated Jacobian matrix is constant with respect to ξ, η, the $\underline{\underline{\mathrm{L}}}$ matrix defined in 2.73 linearly varies with such isoparametric coordinates, and so do the $\underline{\underline{\mathrm{B}}}_e$, $\underline{\underline{\mathrm{B}}}_\kappa$ matrices. The integrand of Eqn. 2.92 is thus a quadratic function of the ξ, η integration variables, as the Jacobian matrix determinant that scales the physical and the natural infinitesimal areas, see Eq. 2.64, is also constant.

A second contribution to the internal virtual work, which is due to the out-of-plane shear components, may be obtained with similar considerations based on Eqns. 2.82 and 2.23; such contribution may be cast as

$$\begin{aligned}
\delta \Upsilon_{\mathrm{i}}^{\ddagger} &= \iint_{\mathcal{A}} \delta \underline{\gamma}_z^{\top} \underline{\mathrm{q}}_z d\mathcal{A} \\
&= \delta \underline{\mathrm{d}}^{\top} \left[\iint_{\mathcal{A}} \underline{\underline{\mathrm{B}}}_\gamma^{\top} \underline{\underline{\Gamma}} \underline{\underline{\mathrm{B}}}_\gamma d\mathcal{A} \right] \underline{\mathrm{d}} \\
&= \delta \underline{\mathrm{d}}^{\top} \underline{\underline{\mathrm{K}}}^{\ddagger} \underline{\mathrm{d}} . \qquad (2.95)
\end{aligned}$$

The overall internal work is thus

$$\begin{aligned}
\delta \Upsilon_{\mathrm{i}} &= \delta \Upsilon_{\mathrm{i}}^{\dagger} + \delta \Upsilon_{\mathrm{i}}^{\ddagger} \\
&= \delta \underline{\mathrm{d}}^{\top} \left(\underline{\underline{\mathrm{K}}}^{\dagger} + \underline{\underline{\mathrm{K}}}^{\ddagger} \right) \underline{\mathrm{d}} \\
&= \delta \underline{\mathrm{d}}^{\top} \underline{\underline{\mathrm{K}}} \, \underline{\mathrm{d}} . \qquad (2.96)
\end{aligned}$$

The principle of virtual works states that the external and the internal virtual works are equal for a general virtual displacement $\delta \underline{\mathrm{d}}$, namely

$$\delta \underline{\mathrm{d}}^{\top} \underline{\mathrm{G}} = \delta \Upsilon_{\mathrm{e}} = \delta \Upsilon_{\mathrm{i}} = \delta \underline{\mathrm{d}}^{\top} \underline{\underline{\mathrm{K}}} \, \underline{\mathrm{d}} , \quad \forall \delta \underline{\mathrm{d}} , \qquad (2.97)$$

[43] Many distinct definitions are associated to the element distortion concept, being the one reported relevant for the specific dissertation passage.

if and only if the applied external actions $\underline{\mathrm{G}}$ are in equilibrium with the elastic reactions due to the displacements $\underline{\mathrm{d}}$; the following equality thus holds

$$\underline{\mathrm{G}} = \underline{\underline{\mathrm{K}}}\,\underline{\mathrm{d}}\,; \tag{2.98}$$

the $\underline{\underline{\mathrm{K}}}$ *stiffness matrix* relates a deformed element configuration, which is defined based on the generalized displacement vector $\underline{\mathrm{d}}$, with the $\underline{\mathrm{G}}$ generalized forces that have to be applied at the element nodes to keep the element in such a stretched state.

2.3.6 The shear locking flaw

Figures 3.4 rationalize the shear locking phenomenon that plagues the plain bilinear isoparametric element in its mimicking the pure bending deformation modes; the case of an in-plane constant curvature bending is presented, but an analogous behaviour is observed in the out-of-plane bending case.

In Figure 3.4a, a rectangular[44] planar element is presented, whose geometry is defined by the a/b side length ratio, being the thickness not relevant for the treatise. The material is assumed linearly elastic, homogeneous and isotropic.

In Figure 3.4b, the exact solution for an equivalent prismatic body subject to pure bending is presented in terms of strain components and strain energy area density, as a function of the imposed angular displacement of the ends. The first Castigliano theorem may be employed in deriving the applied bending moment C_{b}, as predicted by the exact solution.

In Figure 3.4c, the same angular displacement is imposed to the flanks of a four-noded, isoparametric element of the kind described in the present treatise. The trapezoidal (or *keystoning*) deformation shown in Figure is the best-effort exact solution mimicking we may obtain with a single element.

In the absence of oop displacements and ip rotations, a pure membrane deformation is obtained; the drilling dof is not considered. Strain components are derived according to the proposed formulation, and reported along with the strain energy area density; apart from the ϵ_x longitudinal strain, inconsistencies are observed with respect to the exact solution. Again, the first Castigliano theorem may be employed in deriving the bending moment C_{iso4}, as predicted by the element formulation.

In Figure 3.4d, the exact solution is subtracted from its finite element counterpart, thus revealing a spurious residual strain field, whose most notable characteristic is a generally nonzero ip shear strain component γ_{xy}. Such a component is constant in the transverse to bending direction y, whereas it linearly varies in the axial direction x from $+\alpha/2$ to $-\alpha/2$, being null at the $x = 0$ (or $\xi = 0$) locus alone.

Such a spurious shear component contributes to the element strain

[44] vs. generally quadrangular, for the sake of treatise simplicity

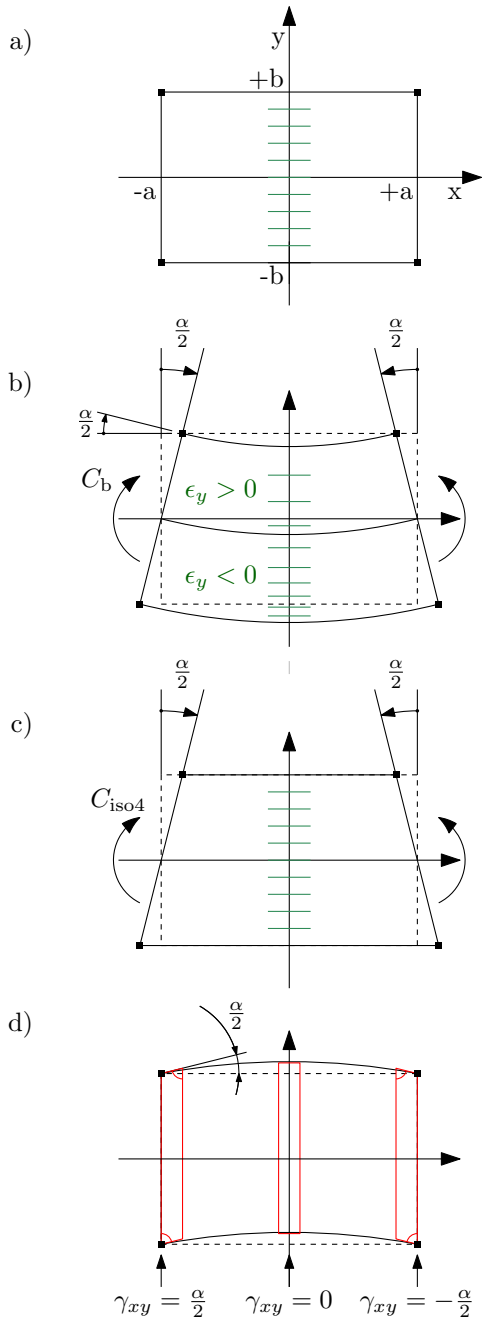

Figure 2.13: Rationalization of the [ip] shear locking phenomenon, in the case of a rectangular plate element. An analogous construction may be derived for the oop counterpart.

energy thus stiffening the element with respect to the exact solution; the ratio between the bending moments to be applied to induce a given curvature is also reported, which reveals that a $\approx +48\%$ bogus stiffening is to be expected for the geometrically regular element, and the commonest structural materials.

In particular the error grows with the a/b ratio, and it becomes consistent with that due the sole $\sigma_y = 0$ vs. $\epsilon_y = 0$ incongruity ($\approx +9.8\%$) in the limit case of $a/b \to 0$.

If such a spurious stiffening is tolerable for the in-plane bending – which is a secondary loadcase for a thin walled body, the analogous results obtained in the more significant transverse deflection (out-of-plane) bending case makes the element under scrutiny not compliant with the Irons patch test[45] for plates – i.e., some error due to discretization is noticed even in the uniform curvature bending loadcase.

Many workarounds are proposed in literature, see e.g. the chapters devoted to the topic in [9]; in the following, two emending techniques are presented, which are (apparently[46]) employed for the MSC.Marc Element 75.

A solution for the oop plate bending

An ingenious sampling and interpolation technique has been developed in [10] that overcomes the locking effect due to the spurious transverse shear strain that develops when the element is subject to out-of-plane bending. Such technique, however, does not correct the element behaviour with respect to in-plane bending.

Eqn. 2.82 is employed in obtaining the tranverse shear strain components g_{zx} and g_{yz} at the edge midpoints; the edge-aligned component $g_{z\widehat{ij}}$ is derived by projection along the $\widehat{ij}$ direction, whereas the orthogonal component is neglected.

Figure 2.14a evidences that a null spurious tranverse shear is measured at the midpoint of the 12 and of the 41 edges when a constant,

[45] in summary: a finite element formulation passes the patch test if an arbitrarily coarse discretization still exactly forecasts any uniform [generalized] strain solution, given a conformable set of boundary conditions; see [7], and [8] for some further developments.

[46] Documentation is not as detailed, and the source code is not available; some literature search and some reverse engineering hints for the usage of such techniques.

out-of-plane curvature is locally enforced that develops along the $\widehat{12}$ and the $\widehat{41}$ directions, respectively. Such property holds for all edges.

In Figure 2.14b, a differential out-of-plane displacement is added to the initial pure bending configuration of Fig. 2.14a, and in the absence of further rotations at nodes; a proper (vs. spurious) transverse shear strain field is thus induced in the element, that the sampling scheme must properly evaluate.

The edge aligned, transverse shear components sampled at the side midpoints are then assigned to the whole edge, and in particular to both its extremal nodes.

As shown in Figure 2.14b (and in the related enlarged view), two independent transverse shear components $g_{z\widehat{12}}$ and $g_{z\widehat{41}}$ are associated to the n1 node, which is taken as an example.

A vector is uniquely determined, whose projections on the $\widehat{12}$ and $\widehat{41}$ directions coincide with the associated transverse shear components; the components of such vector with respect to the x, y axes define the $g_{zx,\mathrm{n1}}$ and $g_{yz,\mathrm{n1}}$ tranverse shear terms at the n1 node.

Such procedure is repeated for all the element vertices; the obtained nodal values for the transverse shear components are then interpolated to the element interior, according to the customary bilinear scheme.

Due to the peculiarity of the initial sampling points, the obtained tranverse shear strain field is amended with respect to the spurious contribution that previously led to the shear locking effect; the usual quadrature scheme may now be employed.

Equation 2.82 still formalizes the passage from nodal dofs to the out-of-plane shear field, since the procedure described in the present paragraph may be easily cast in the form of a revised $\underline{\underline{\mathrm{B}}}_\gamma$ matrix.

A solution for the ip plate bending, which also mitigates the drilling mode quirks.

TODO.

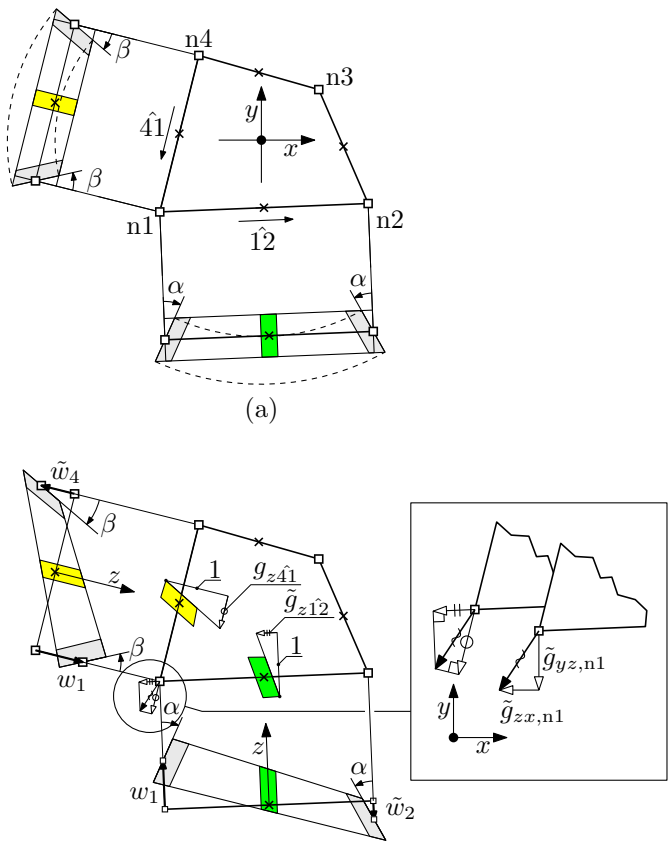

Figure 2.14: A transverse shear sampling technique employed in the four-noded isoparametric element for preventing shear locking in the oop plate bending.

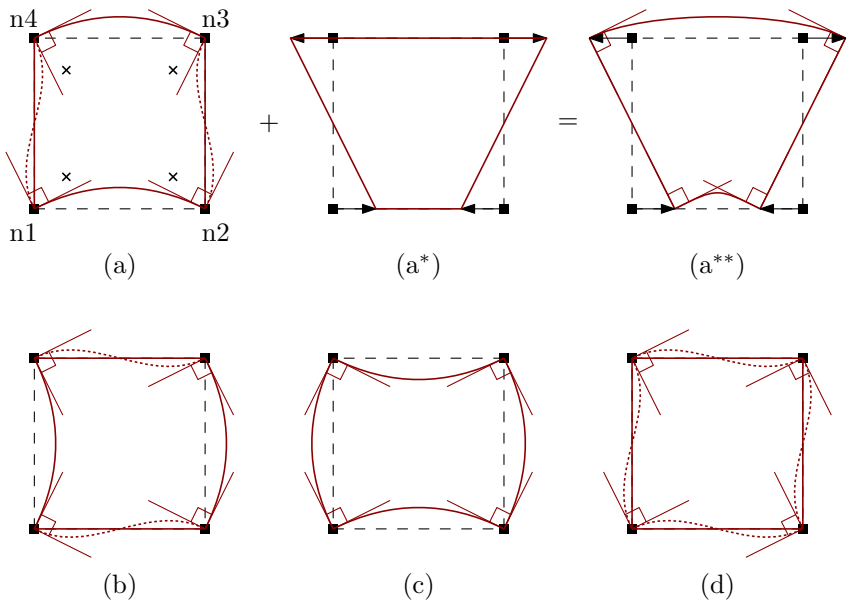

Figure 2.15: Four elementary combinations of the drilling dofs, and the displacement modes produced based on a partial – due to the abatement of the S shaped cubic term – slope-continuity at the rotated corners. The (a) and the (b) modes reproduce – in a displacement continuity preserving manner – the two Wilson's incompatible modes; in particular, the (a) mode may be superposed to the (a*) keystoning deformation in order to conserve the right angle of the element corners in pure flexure, in order to avoid the insurgence of the spurious ip shear component. Two remaining modes, the (c) mixed pincushion-barrel mode and the (d) uniform rotation mode, are of limited interest; the latter (d) mode, in particolar, is nullified by the aforementioned abatement and it may be regarded as the only residual strain energy free drilling motion.

2.4 Mass matrix for the finite element

2.4.1 Energy consistent formulation for the mass matrix

The Ω volume of material associated to a finite element is considered, along with the local, physical reference system (x, y, z), and its isoparametric counterpart that, for the quadrilateral plate element under scrutiny, is embodied by the (ξ, η, z) triad.

The *vector* shape function array

$$\underline{\underline{\mathrm{S}}}\,(\xi,\eta,z) = \begin{bmatrix} \dots & \hat{u}_i(\xi,\eta,z) & \dots \\ \dots & \hat{v}_i(\xi,\eta,z) & \dots \\ \dots & \hat{w}_i(\xi,\eta,z) & \dots \end{bmatrix} \tag{2.99}$$

is defined based on the elementary motions $\underline{\hat{\mathrm{u}}}_i \equiv [\hat{u}_i, \hat{v}_i, \hat{w}_i]^\top$ induced to the element material points by imposing a unit value to the i-th degree of freedom d_i, while keeping the others fixed.

The displacement field is then defined as a linear combination of the elementary motions above, where the $\underline{\mathrm{d}}$ element dofs serve as coefficients, namely

$$\underline{\mathrm{u}}\,(\xi,\eta,z) = \underline{\underline{\mathrm{S}}}\,(\xi,\eta,z)\,\underline{\mathrm{d}}\,. \tag{2.100}$$

Deriving with respect to time the equation above, the velocity field

$$\dot{\underline{\mathrm{u}}}\,(\xi,\eta,z) = \underline{\underline{\mathrm{S}}}\,(\xi,\eta,z)\,\dot{\underline{\mathrm{d}}} \tag{2.101}$$

is obtained as a function of the first variation in time of element dofs. Expression 2.101 is simplified by the constant-in-time nature of $\underline{\underline{\mathrm{S}}}$.

The kinetic energy contribution associated to the deformable element material points may be integrated, thus obtaining

$$E_{\mathrm{kin}} = \frac{1}{2}\iiint_\Omega \dot{\underline{\mathrm{u}}}^{\top}\,\dot{\underline{\mathrm{u}}}\,\rho d\Omega \tag{2.102}$$

where ρ is the material mass density, that may vary across the domain. By substituting the velocity field definition of Eq. 2.101 we obtain

$$E_{\mathrm{kin}} = \frac{1}{2}\iiint_\Omega \left[\underline{\underline{\mathrm{S}}}\;\dot{\underline{\mathrm{d}}}\right]^{\top}\left[\underline{\underline{\mathrm{S}}}\;\dot{\underline{\mathrm{d}}}\right]\rho d\Omega, \tag{2.103}$$

and finally

$$E_{\mathrm{kin}} = \frac{1}{2}\,\dot{\underline{\mathrm{d}}}^{\top}\left[\iiint_\Omega \underline{\underline{\mathrm{S}}}^{\top}\,\underline{\underline{\mathrm{S}}}\,\rho d\Omega\right]\,\dot{\underline{\mathrm{d}}} = \frac{1}{2}\,\dot{\underline{\mathrm{d}}}^{\top}\,\underline{\underline{\mathrm{M}}}\,\dot{\underline{\mathrm{d}}}\,. \tag{2.104}$$

The integral term that defines the $\underline{\underline{\mathrm{M}}}$ *mass* matrix is evaluated by resorting to the same quadrature technique introduced for its stiffness counterpart.

The actual nature of the mass matrix terms varies based on the type of the dofs that are associated to the term row and column; in particular, the diagonal terms that are related to displacements and rotations are dimensionally consistent with a mass and a moment of inertia, respectively.

The mass matrix quantifies the inertial response of the finite element; according to its definition

$$\underline{\underline{\mathrm{M}}} = \iiint_{\Omega} \underline{\underline{\mathrm{S}}}^{\top} \underline{\underline{\mathrm{S}}} \, \rho d\Omega, \tag{2.105}$$

it is merely a function of the material density, and of the kinematic laws that constrain the motion of the material particles within the element.

If a set of external (generalized) forces $\underline{\mathrm{G}}$ is applied to the element dofs in the fictitious absence of elastic reactions, a purely inertial response is expected. The $\dot{\underline{\mathrm{d}}}$ vector defines the instantaneous first derivative in time of the dofs (i.e. nodal translational and rotational velocities); the instantaneous power supplied by the external forces is then evaluated as $\dot{\underline{\mathrm{d}}}^{\top} \underline{\mathrm{G}}$, that induces an equal time derivative of the kinetic energy, quantified as [47]

$$\begin{aligned} \dot{\underline{\mathrm{d}}}^{\top} \underline{\mathrm{G}} = \frac{dE_{\mathrm{kin}}}{dt} &= \frac{d}{dt} \left(\frac{1}{2} \dot{\underline{\mathrm{d}}}^{\top} \underline{\underline{\mathrm{M}}} \, \dot{\underline{\mathrm{d}}} \right) \\ &= \frac{1}{2} \left(\ddot{\underline{\mathrm{d}}}^{\top} \underline{\underline{\mathrm{M}}} \, \dot{\underline{\mathrm{d}}} + \dot{\underline{\mathrm{d}}}^{\top} \underline{\underline{\mathrm{M}}} \, \ddot{\underline{\mathrm{d}}} \right) \\ &= \dot{\underline{\mathrm{d}}}^{\top} \underline{\underline{\mathrm{M}}} \, \ddot{\underline{\mathrm{d}}}. \end{aligned}$$

Due to the general nature of $\dot{\underline{\mathrm{d}}}$, equality

$$\underline{\mathrm{G}} = \underline{\underline{\mathrm{M}}} \, \ddot{\underline{\mathrm{d}}} \tag{2.106}$$

is implied, which points out the mass matrix role in transforming the dof vector second derivative in time (i.e. nodal translational and rota-

[47] The symmetric matrix characterizing property

$$\underline{\mathrm{x}}^{\top} \underline{\underline{\mathrm{A}}} \, \underline{\mathrm{y}} = \underline{\mathrm{y}}^{\top} \underline{\underline{\mathrm{A}}} \, \underline{\mathrm{x}} \quad \forall \underline{\mathrm{x}}, \underline{\mathrm{y}} \in \mathbb{R}^n$$

is used in deriving the last passage.

tional accelerations) into the generalized force components that are to be applied in order to sustain such variation of motion.

2.4.2 Lumped mass matrix formulation

In a few applications, a diagonal form for the mass matrix is preferred at the expense of a) a strict adherence to energy consistency with regard to rotational motions, and b) some arbitrariness in its definition.

The finite element volume is ideally partitioned into a set of influence domains, one each node. In the case of the four-noded quadrilateral, material points whose ξ, η isoparametric coordinates fall within the first, second, third and fourth quadrant are associated to nodes n3, n4, n1 and n2, respectively; those distributed masses are then ideally accumulated at the associated node.

A group of four concentrated nodal masses is thus defined, whose motion is defined based on single translational dofs, and not on the plurality of weighted contributions that induces the nonzero, nondiagonal terms at the consistent mass matrix.

This undue material accumulation at the element periphery produces a spurious increase of the moment of inertia, condition, this, that may only be worsened if (positive) rotational inertias are introduced at nodes.

Those nodal rotational inertias are however required in associating a bounded angular acceleration to unbalanced nodal torques; solution methods based on the mass matrix inversion, e.g. explicit dynamic procedures, are precluded otherwise. Since there is no consensus on the quantification those inertial terms, the reader is addressed to specialized literature.

The effect of this elemental overestimation on the rotational inertia of the modeled structures decreases with mesh refinement, and it vanishes for a theoretically vanishing element size.

2.5 External forces

Energetically consistent external actions may be applied at the nodal dofs, that may be interpreted as *concentrated* forces and moments; their physical rationalization outside the discretized structure framework –

and in particular back to the underlying elastic continua theory – is far from being trivial.

Surface tractions and volumetric loads are instead naturally tied with the continuum formulation, and are usually employed in formalizing the load condition of structural components.

The present paragraph derives the equivalent nodal representation of distributed actions acting on the domain of a single finite element; the inverse relation provides a finite, distributed traction counterpart to concentrated actions applied at the nodes of a discretized FE model.

The $\underline{\underline{\mathrm{S}}}$ set of elementary deformation modes that is introduced in the context of the element mass matrix derivation, see Eqn. 2.99, is employed to define a virtual displacement field within the element domain based on the virtual variation $\delta\,\underline{\mathrm{d}}$ of its nodal dofs values, i.e.

$$\delta\,\underline{\mathrm{u}}\,(\xi,\eta,z) = \underline{\underline{\mathrm{S}}}\,(\xi,\eta,z)\delta\,\underline{\mathrm{d}}\,, \tag{2.107}$$

see also Eq. 2.100.

A volumetric external load is considered, whose components $\underline{\mathrm{p}} = [p_x, p_y, p_z]$ are consistent with the $\underline{\underline{\mathrm{S}}}$ matrix reference system, i.e. the local to the element, physical Cxyz one. If external load components are defined in the context of a global reference system, straightforward reference frame transformations are to be applied.

The virtual work performed by those distributed actions is first integrated along the element domain, and then equalled to its nodal counterpart $\delta\,\underline{\mathrm{d}}^{\top}\,\underline{\mathrm{F}}$, thus leading to

$$\begin{aligned}
\delta\,\underline{\mathrm{d}}^{\top}\,\underline{\mathrm{F}} &= \iiint_{\Omega} (\delta\,\underline{\mathrm{u}})^{\top}\;\underline{\mathrm{p}}\,d\Omega \\
&= \iiint_{\Omega} \left(\underline{\underline{\mathrm{S}}}\,\delta\,\underline{\mathrm{d}}\right)^{\top}\;\underline{\mathrm{p}}\,d\Omega \\
&= \delta\,\underline{\mathrm{d}}^{\top} \iiint_{\Omega} \underline{\underline{\mathrm{S}}}^{\top}\,\underline{\mathrm{p}}\,d\Omega,
\end{aligned}$$

and finally to

$$\underline{\mathrm{F}} = \iiint_{\Omega} \underline{\underline{\mathrm{S}}}^{\top}\,\underline{\mathrm{p}}\,d\Omega \tag{2.108}$$

due to the general nature of $\delta\,\underline{\mathrm{d}}$.

In the case of the plate element under scrutiny, we recall that the volume integral of Eq. 2.108 is numerically evaluated according to Eq. 2.94 quadrature scheme.

In general, the quadrature along the domain is performed according to the methods introduced for deriving the element stiffness matrix. If a surface or an edge load are supplied in place of the volumetric load vector $\underline{p}$, Eq. 2.108 integral may be adapted to span each loaded element face, or edge.

In the case of low order isoparametric elements – e.g. the four-noded quadrilateral shell element, an alternative, simplified procedure for the consolidation of the distributed loads into nodal forces becomes viable. According to such procedure, the element domain is partitioned into influence volumes, one each node; the external load contributions are then accumulated within each partition, and the resultant force vector is applied to the associated node.

By moving such resultant force from the distribution center of gravity (cog) to the corner node, momentum balance is naively disregarded; the induced error however decreases with the load field variance across the element, and hence with the element size. Such error vanishes for uniform distributed loads.

In the presence of a better established, work consistent counterpart, such simplified procedure is mostly employed to set a rule-of-thumb equivalence between distributed and nodal loads; in particular, the stress-singular nature of a set of nodal loads may be easily pointed out if it is observed that a finite load resultant is applied to influence areas that cumulatively vanish with vanishing element size.

2.6 Joining elements into structures.

2.6.1 Displacement and rotation field continuity

Displacement and rotation fields are continuous at the isoparametric quadrilateral inter-element interfaces; they are in fact continuous at nodes since the associated nodal dofs are shared by adjacent elements, and the field interpolations that occur within each quadrilateral domain a) they both reduce to the same linear relation along the shared edge, and b) they are performed in the absence of any contributions related to unshared nodes or dofs.

A similar result does not hold for the [generalized] strain and stress components, which are in general discontinuous across the element boundaries; such a discontinuity – which vanishes with mesh refinement except at singularities[48] – constitutes an indicator of the fe discretization error.

2.6.2 Expressing the element stiffness matrix in terms of global dofs

As seen in Par. 2.3.5, the stiffness matrix of each j-th element defines the elastic relation between the associated generalized forces and displacements, i.e.

$$\underline{\mathrm{G}}_{\mathrm{e}j} = \underline{\underline{\mathrm{K}}}_{\mathrm{e}j}\, \underline{\mathrm{d}}_{\mathrm{e}j} \tag{2.109}$$

where the dofs definition is local with respect to the element under scrutiny.

In order to investigate the mutual interaction between elements in a structure, a common set of *global* dofs is required; in particular, generalized displacement dofs are defined at each l-th global node, i.e., for nodes interacting with the shell element formulation under scrutiny,

$$\underline{\mathrm{d}}_{\mathrm{g}l} = \begin{bmatrix} u_{\mathrm{g}l} \\ v_{\mathrm{g}l} \\ w_{\mathrm{g}l} \\ \theta_{\mathrm{g}l} \\ \varphi_{\mathrm{g}l} \\ \psi_{\mathrm{g}l} \end{bmatrix} . \tag{2.110}$$

[48] i.e. at locations at which a singularity (or a discontinuity) of the *exact* solution may be theoretically predicted

The global reference system $OXYZ$ is typically employed in projecting nodal vector components. However, each l-th global node may be supplied with a specific reference system, whose unit vectors are $\hat{\imath}_{gl}, \hat{\jmath}_{gl}, \hat{k}_{gl}$, thus permitting the employment of non uniformly aligned (e.g. cylindrical) global reference systems.

Those nodal degrees of freedom may be collected in a global dofs vector

$$\underline{\mathrm{d}}_{\mathrm{g}}^{\top} = \left[\underline{\mathrm{d}}_{\mathrm{g1}}^{\top} \quad \underline{\mathrm{d}}_{\mathrm{g2}}^{\top} \quad \dots \quad \underline{\mathrm{d}}_{\mathrm{g}l}^{\top} \quad \dots \quad \underline{\mathrm{d}}_{\mathrm{g}n}^{\top} \right] \tag{2.111}$$

that parametrically defines any deformed configuration of the structure.

Analogously, a global, external (generalized[49]) forces vector may be defined, that assumes the form

$$\underline{\mathrm{F}}_{\mathrm{g}}^{\top} = \left[\underline{\mathrm{F}}_{\mathrm{g1}}^{\top} \quad \underline{\mathrm{F}}_{\mathrm{g2}}^{\top} \quad \dots \quad \underline{\mathrm{F}}_{\mathrm{g}l}^{\top} \quad \dots \quad \underline{\mathrm{F}}_{\mathrm{g}n}^{\top} \right]; \tag{2.112}$$

since single dof (or single-dof constraint (spc)) and multi dof (or multi-dof constraint (mpc)) kinematic constraints[50] are expected to be applied to the structure dofs, the following vector of reaction forces

$$\underline{\mathrm{R}}_{\mathrm{g}}^{\top} = \left[\underline{\mathrm{R}}_{\mathrm{g1}}^{\top} \quad \underline{\mathrm{R}}_{\mathrm{g2}}^{\top} \quad \dots \quad \underline{\mathrm{R}}_{\mathrm{g}l}^{\top} \quad \dots \quad \underline{\mathrm{R}}_{\mathrm{g}n}^{\top} \right] \tag{2.113}$$

is introduced. Many FE softwares – and MSC.Marc in particular – treat spc and mpc constraints separately, thus leading to two set of constraint actions, namely the (strictly named) *reaction forces*, and the *tying forces*, respectively; for the sake of simplicity, the constraint treatise is unified in the present contribution.

The simple four element, roof-like structure of Fig. 2.16 is employed in the following to discuss the procedure that derives the elastic response characterization for the structure from its elemental counterparts.

The structure comprises nine nodes, whose location in space is defined according to a global reference system $OXYZ$, see Table 2.3.

[49] Unless otherwise specified, the *displacement* and *force* terms refer to the dofs, and the suitable actions that perform work with their variation, respectively. They are in fact *generalized* forces and displacements.

[50] in a previous version of this contribution, an equivalency was proposed between the single dof vs. multi dof constraint characterization, and the *external* – i.e. *to ground* – vs. *internal* classification. In fact, those classifications are disjoint, since, if ground reactions are expected in the single dof case, legitimate multi dof constraint exist – e.g. the hypothetical $u_{g2} = v_{g5}$ – whose reactions are not self-equilibrated, and hence require an external, ground intervention for their balancing.

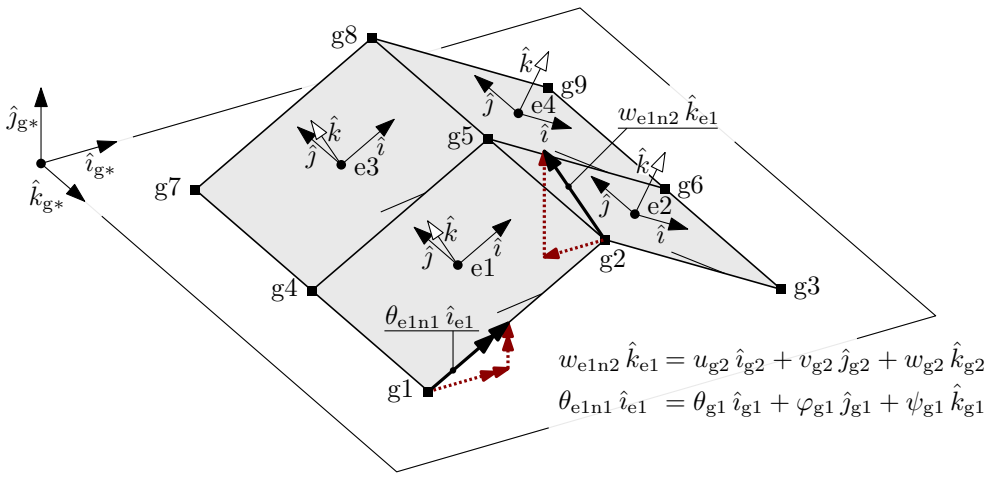

Figure 2.16: A simple four-element, roof-like structure employed in discussing the assembly procedures. The elements are square, thick plates whose angle with respect to the global XY plane is 30°

node	X	Y	Z
g1	$-ac$	0	$+a$
g2	0	$+as$	$+a$
g3	$+ac$	0	$+a$
g4	$-ac$	0	0
g5	0	$+as$	0
g6	$+ac$	0	0
g7	$-ac$	0	$-a$
g8	0	$+as$	$-a$
g9	$+ac$	0	$-a$

Table 2.3: Nodal coordinates for the roof-like structure of Figure 2.16. a is the element side length, $c = \cos 30°$ and $s = \sin 30°$

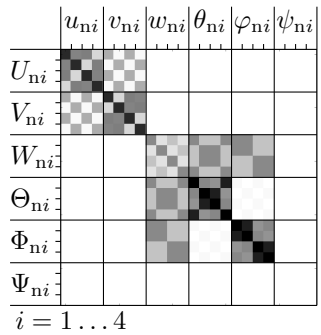

Figure 2.17: A representation of the stiffness matrix terms for each element in the example structure; the term magnitude is represented through a linear grayscale, spanning from zero (white) to the peak value (black).

	n1	n2	n3	n4
e1	g1	g2	g5	g4
e2	g2	g3	g6	g5
e3	g4	g5	g8	g7
e4	g5	g6	g9	g8

Table 2.4: Element connectivity for the roof-like structure of Figure 2.16. As an example, the node described by the local numbering e3n2 is mapped to the global node g5.

The structure is composed by four, identical, four noded isoparametric shell elements, whose formulation is described in the preceding section 2.3.

A grayscale, normalized representation of the element stiffness matrix is shown in Figure 2.17, where the white to black colormap spans from zero to the maximum in absolute value term.

The mapping between local, element based node numbering and the global node numbering is reported in the connectivity Table 2.4.

Such i) local to global node numbering mapping, together with ii) the change in reference system mentioned above, defines a set of elemental dof mapping matrices, $\underline{\underline{\mathrm{P}}}_{ej}$, one each j-th element. Such matrices are defined as follows: the i-th row the $\underline{\underline{\mathrm{P}}}_{ej}$ matrix contains the coefficients of the linear combination of global dofs that equates the

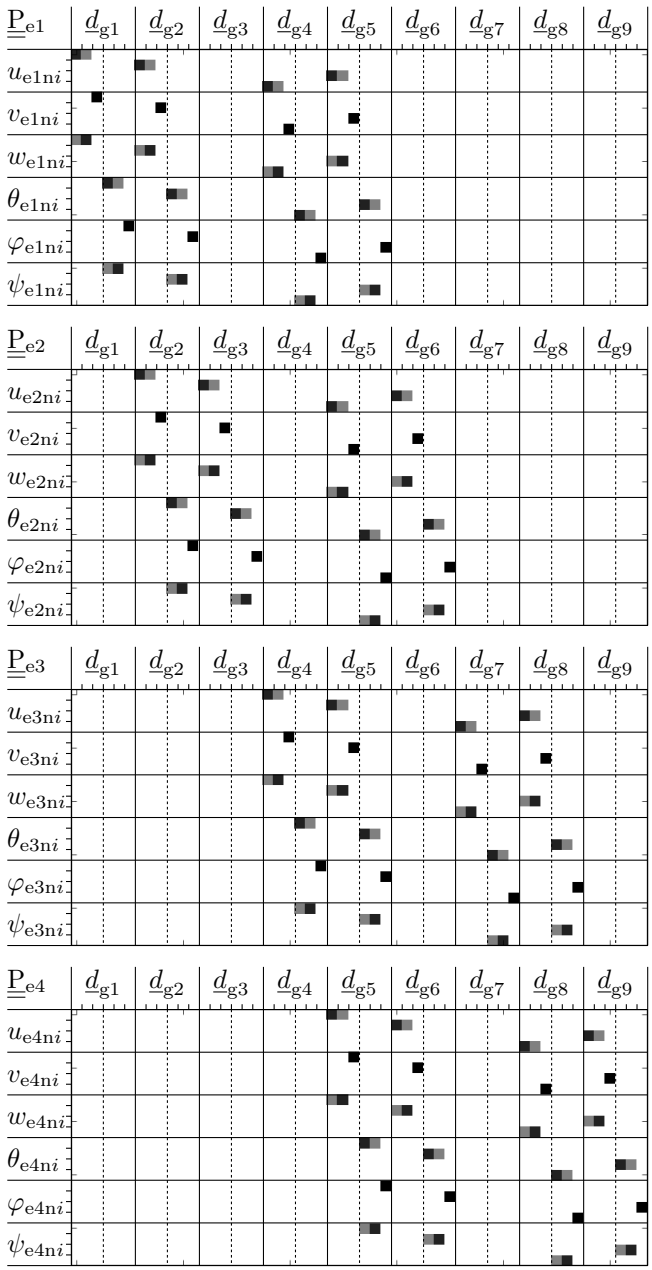

Figure 2.18: A grayscale representation of the terms of the four $\underline{\underline{P}}_{ej}$ mapping matrices associated the elements of Fig. 2.16. The colormap spans from white (zero) to black (one); the lighter and the darker grey colors represent terms that equate in modulus $\sin 30°$ and $\cos 30°$, respectively.

i local dof of the j-th element; an example is proposed in the following to illustrate such relation.

With reference to the structure of Figure 2.16, w_{e1n2} and θ_{e1n1} respectively represent the 10th and the 13th local degrees of freedom of element 1.

Their global representation involves a subset of the g2 and g1 global nodes dofs, respectively, namely

$$w_{\mathrm{e1n2}} = \langle \hat{i}_{\mathrm{e1}}, \hat{i}_{\mathrm{g2}} \rangle u_{\mathrm{g2}} + \langle \hat{k}_{\mathrm{e1}}, \hat{j}_{\mathrm{g2}} \rangle v_{\mathrm{g2}} + \langle \hat{k}_{\mathrm{e1}}, \hat{k}_{\mathrm{g2}} \rangle w_{\mathrm{g2}} \tag{2.114}$$

$$\theta_{\mathrm{e1n1}} = \langle \hat{i}_{\mathrm{e1}}, \hat{i}_{\mathrm{g1}} \rangle \theta_{\mathrm{g1}} + \langle \hat{i}_{\mathrm{e1}}, \hat{j}_{\mathrm{g1}} \rangle \phi_{\mathrm{g1}} + \langle \hat{i}_{\mathrm{e1}}, \hat{k}_{\mathrm{g1}} \rangle \psi_{\mathrm{g1}} \tag{2.115}$$

where $\hat{i}_{\mathrm{e1}}$,$\hat{j}_{\mathrm{e1}}$, $\hat{k}_{\mathrm{e1}}$ are the orientation vectors of the element 1 local reference system, $\hat{i}_{\mathrm{g1}}$,$\hat{j}_{\mathrm{g1}}$,$\hat{k}_{\mathrm{g1}}$ and $\hat{i}_{\mathrm{g2}}$,$\hat{j}_{\mathrm{g2}}$,$\hat{k}_{\mathrm{g2}}$ are the orientation vectors of the global nodes 1 and 2 reference systems, and $\langle \cdot, \cdot \rangle$ represents their mutual scalar product, or, equivalently, the cosinus of the angle between two unit vectors.

The 10th and the 13th row of the $\underline{\underline{\mathrm{P}}}_{\mathrm{e1}}$ mapping matrix are defined based on Eqs.2.114 and 2.115, respectively, and they are null except for the elements

$$\left[\underline{\underline{\mathrm{P}}}_{\mathrm{e1}}\right]_{10,7} = \langle \hat{k}_{\mathrm{e1}}, \hat{i}_{\mathrm{g2}} \rangle \qquad \left[\underline{\underline{\mathrm{P}}}_{\mathrm{e1}}\right]_{13,4} = \langle \hat{i}_{\mathrm{e1}}, \hat{i}_{\mathrm{g1}} \rangle$$

$$\left[\underline{\underline{\mathrm{P}}}_{\mathrm{e1}}\right]_{10,8} = \langle \hat{k}_{\mathrm{e1}}, \hat{j}_{\mathrm{g2}} \rangle \qquad \left[\underline{\underline{\mathrm{P}}}_{\mathrm{e1}}\right]_{13,5} = \langle \hat{i}_{\mathrm{e1}}, \hat{j}_{\mathrm{g1}} \rangle$$

$$\left[\underline{\underline{\mathrm{P}}}_{\mathrm{e1}}\right]_{10,9} = \langle \hat{k}_{\mathrm{e1}}, \hat{k}_{\mathrm{g2}} \rangle \qquad \left[\underline{\underline{\mathrm{P}}}_{\mathrm{e1}}\right]_{13,6} = \langle \hat{i}_{\mathrm{e1}}, \hat{k}_{\mathrm{g1}} \rangle,$$

being u_{g2},v_{g2},w_{g2},θ_{g1},ϕ_{g1} and ψ_{g1} the 7th, 8th, 9th, 4th, 5th and 6th global degrees of freedom according to their position in $\underline{\mathrm{d}}_{\mathrm{g}}$.

Figure 2.18 presents a grayscale representation of the four $\underline{\underline{\mathrm{P}}}_{\mathrm{e}j}$ matrices; please note the extremely sparse nature of those matrices, whose number of nonzero terms scales with the single element dof cardinality, whereas the total number of terms scale with the whole structure dof cardinality.

The rows of the rectangular $\underline{\underline{\mathrm{P}}}_{\mathrm{e}j}$ mapping matrix are mutually orthonormal; the mapping matrix is orthogonal in the sense of the Moore-Penrose pseudoinverse, since its transpose and its pseudoinverse coincide.

By resorting to the elemental dof mapping matrix artifice, the j-th element dofs may be derived from their global counterpart as

$$\underline{\mathrm{d}}_{\mathrm{e}j} = \underline{\underline{\mathrm{P}}}_{\mathrm{e}j} \, \underline{\mathrm{d}}_{\mathrm{g}}, \quad \forall j. \tag{2.116}$$

Eq. 2.109 let us further derive the component of external actions that are required by each j-th stretched element to oppose the its own elastic reactions as

$$\underline{\mathrm{G}}_{\mathrm{e}j} = \underline{\underline{\mathrm{K}}}_{\mathrm{e}j}\, \underline{\underline{\mathrm{P}}}_{\mathrm{e}j}\, \underline{\mathrm{d}}_{\mathrm{g}}, \quad \forall j; \tag{2.117}$$

such a external action vector, which is still expressed in terms of the local set of dofs, is now formulated as a function of the global displacement vector. Those elemental external action components $\underline{\mathrm{G}}_{\mathrm{e}j}$ may be cast in terms of the global dof set based on the following virtual work equivalency

$$\delta\, \underline{\mathrm{d}}_{\mathrm{g}}^{\top}\, \underline{\mathrm{G}}_{\mathrm{g}\leftarrow\mathrm{e}j} = \left(\underline{\underline{\mathrm{P}}}_{\mathrm{e}j}\, \delta\, \underline{\mathrm{d}}_{\mathrm{g}}\right)^{\top}\, \underline{\mathrm{G}}_{\mathrm{e}j}, \quad \forall\ \delta\, \underline{\mathrm{d}}_{\mathrm{g}} \tag{2.118}$$

where $\delta\, \underline{\mathrm{d}}_{\mathrm{g}}$ is a generic global virtual displacement, $\underline{\underline{\mathrm{P}}}_{\mathrm{e}j}\, \delta\, \underline{\mathrm{d}}_{\mathrm{g}}$ is the associated virtual variation of the j-th element dofs, see Eq.2.116, and

$$\underline{\mathrm{G}}_{\mathrm{g}\leftarrow\mathrm{e}j} = \underline{\underline{\mathrm{P}}}_{\mathrm{e}j}^{\top}\, \underline{\mathrm{G}}_{\mathrm{e}j} \tag{2.119}$$

is the global counterpart of the local $\underline{\mathrm{G}}_{\mathrm{e}j}$ nodal action vector.

Based on 2.109, 2.116 and 2.119, the contribution of the j-th element to the elastic response of the structure may finally be described as the vector of global force components

$$\underline{\mathrm{G}}_{\mathrm{g}\leftarrow\mathrm{e}j} = \underline{\underline{\mathrm{P}}}_{\mathrm{e}j}^{\top}\, \underline{\underline{\mathrm{K}}}_{\mathrm{e}j}\, \underline{\underline{\mathrm{P}}}_{\mathrm{e}j}\, \underline{\mathrm{d}}_{\mathrm{g}}; \tag{2.120}$$

that have to be applied at the structure dofs in order to equilibrate the elastic reactions that arise at the nodes of the j-th element, if a deformed configuration is prescribed for the latter according to the $\underline{\mathrm{d}}_{\mathrm{g}}$ global displacement mode.

By accumulating the contribution of the various elements in a structure, the overall relation is obtained

$$\underline{\mathrm{G}}_{\mathrm{g}} = \sum_{j} \underline{\mathrm{G}}_{\mathrm{g}\leftarrow\mathrm{e}j} = \left(\sum_{j} \underbrace{\underline{\underline{\mathrm{P}}}_{\mathrm{e}j}^{\top}\, \underline{\underline{\mathrm{K}}}_{\mathrm{e}j}\, \underline{\underline{\mathrm{P}}}_{\mathrm{e}j}}_{\underline{\underline{\mathrm{K}}}_{\mathrm{g}\leftarrow\mathrm{e}j}} \right) \underline{\mathrm{d}}_{\mathrm{g}} = \underline{\underline{\mathrm{K}}}_{\mathrm{g}}\, \underline{\mathrm{d}}_{\mathrm{g}}, \tag{2.121}$$

that defines the $\underline{\underline{\mathrm{K}}}_{\mathrm{g}}$ global stiffness matrix as an assembly of the $\underline{\underline{\mathrm{K}}}_{\mathrm{g}\leftarrow\mathrm{e}j}$ elemental contributions. The contribute accumulation at each summatory step is graphically represented in Fig. 2.19, in the case of the example structure of Fig. 2.16.

The global stiffness matrix is symmetric, and it shows nonzero terms at cells whose row and column indices are associate to two dofs that are bridged by a direct elastic link – i.e., an element exists, that insists on both the nodes those dofs pertain; since only a limited number of elements insist on each given node, the matrix is sparse, as shown in Fig. 2.19d.

An favourable numbering of the global nodes may be searched for, such that the nonzero terms are clustered within a (possibly) narrow band around the diagonal; the resulting stiffness matrix is hence *banded*, condition this that reduces both the storage memory requirements, and the computational effort in applying the various algebraic operators to the matrix.

The stiffness matrix (half-)bandwidth may be predicted by evaluating the bandwidth required for storing each element contribution

$$b_{\mathrm{e}j} = (i_{\max} - i_{\min} + 1)\, l, \tag{2.122}$$

and retaining the

$$b = \max_{\mathrm{e}j} b_{\mathrm{e}j} \tag{2.123}$$

peak value; in the formula 2.122, l is the number of dof per element node, whereas $i_{\max}$ and $i_{\max}$ are the extremal integer labels associated to the element nodes, according to the global numbering.

2.6.3 External forces assembly

The element vector forces are accumulated to derive global external forces vector $\underline{\mathrm{F}}_{\mathrm{g}}$, as in

$$\underline{\mathrm{F}}_{\mathrm{g}} = \sum_{j} \underline{\underline{\mathrm{P}}}_{\mathrm{e}j}^{\top} \underline{\mathrm{F}}_{\mathrm{e}j}; \tag{2.124}$$

the transposed $\underline{\underline{\mathrm{P}}}_{\mathrm{e}j}^{\top}$ mapping matrix is employed to translate the actions on the local dofs to their global counterpart.

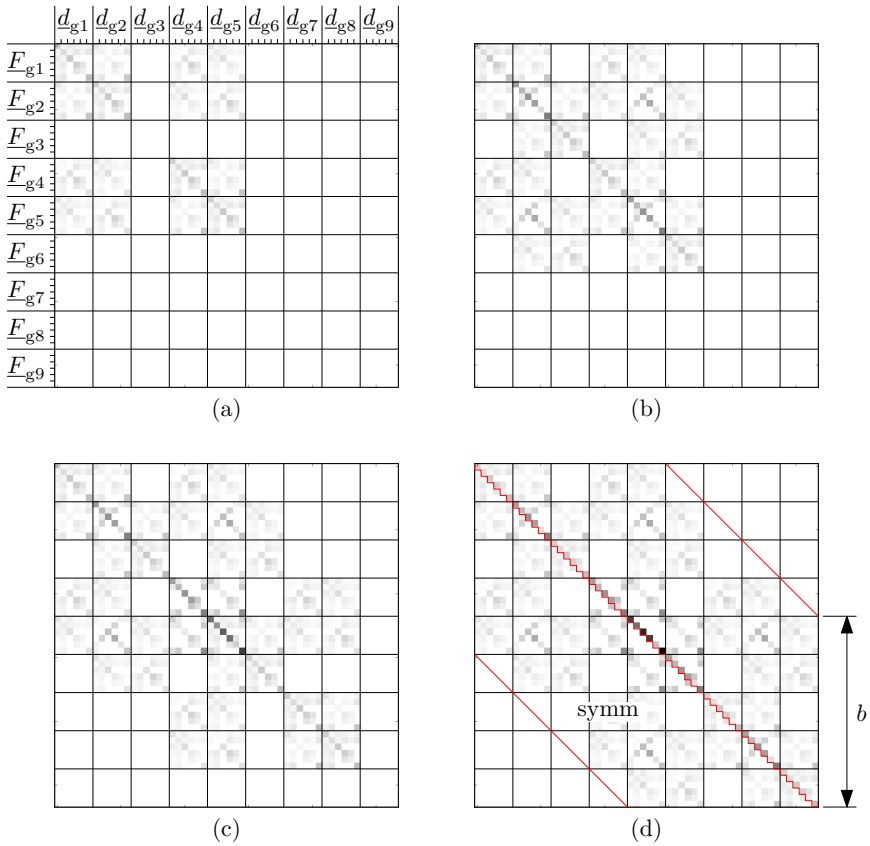

Figure 2.19: Graphical representation of the assembly steps for the stiffness matrix of the Fig. 2.16 structure. In (a), the $\underline{\underline{\mathrm{K}}}_{\mathrm{g}\leftarrow\mathrm{e}1}$ term is presented alone; the $\underline{\underline{\mathrm{K}}}_{\mathrm{g}\leftarrow\mathrm{e}2}$, $\underline{\underline{\mathrm{K}}}_{\mathrm{g}\leftarrow\mathrm{e}3}$ and $\underline{\underline{\mathrm{K}}}_{\mathrm{g}\leftarrow\mathrm{e}4}$ are sequentially accumulated, thus leading to (b), (c) and (d). In (d), the symmetric and banded nature of the matrix is evidenced. The zero-initialized form for the matrix that precedes the (a) step is omitted.

2.7 Constraints.

2.7.1 A pedagogical example.

Figure 2.20 represents a simple, pedagogical example of a three d.o.f. elastic system subject to a set of two kinematic constraints. The first, I, embodies a typical multi d.o.f. constraint[51], namely a 3:1 leverage between the vertical displacements d_3 and d_1. The second, II, consists in a single d.o.f., inhomogeneous constraint that imposes a fixed value to the d_2 vertical displacement.

Both the kinematic constraint may be cast in the same algebraic form of a linear *variation*[52] constraint

$$\sum_i \alpha_{ji} d_i = \underline{\alpha}_j^{\top} \underline{\mathrm{d}} = \beta_j$$

where $j = I, II$ and $i = 1 \dots 3$ the indexes span through the constraints and the model d.o.f.s, respectively, and the $\underline{\alpha}_j$ equation coefficient vectors and inhomogeneous terms are

$$\underline{\alpha}_{\mathrm{I}}^{\top} = \begin{bmatrix} 3 & 0 & 1 \end{bmatrix} \qquad \beta_{\mathrm{I}} = 0$$
$$\underline{\alpha}_{\mathrm{II}}^{\top} = \begin{bmatrix} 0 & 1 & 0 \end{bmatrix} \qquad \beta_{\mathrm{II}} = 0.2$$

In the absence of constraints, viable system configurations span the whole $\mathbb{R}^3$ space of Fig. 2.21 (a); viable configurations with respect to the first constraint alone span the *hyper*-plane/subspace[53] I, whereas the subspace II collects the feasible configurations with respect to the second constraint.

It is relevant to underline that the feasible configuration hyperplanes I and II are normal to the associated coefficient vectors $\underline{\alpha}_{\mathrm{I}}$ and $\underline{\alpha}_{\mathrm{II}}$, respectively.

The $\mathrm{I} \cap \mathrm{II}$ intersection subspace collects the configurations that satisfies both the constraints; such subspace is orthogonal to both $\underline{\alpha}_{\mathrm{I}}$ and $\underline{\alpha}_{\mathrm{II}}$.

[51] usually, and rather improperly, named *multipoint* constraint (MPC)

[52] due to the presence of the inhomogeneous term β_j

[53] The subspace of the feasible configurations with respect to a single, scalar linear equation is an hyperplane in the configuration space; due to the limited d.o.f. set cardinality, Figure 2.21 (a) represents a 2d plane within a 3d space. The *hyper*-nomenclature is preserved for generality.

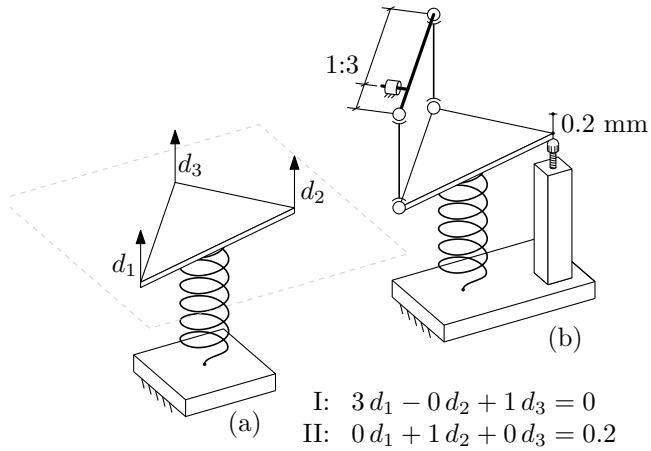

Figure 2.20: A pedagogical elastic three d.o.f. system, (a), subject to a few kinematic constraints (b).

If the constraints are assumed as ideal[54], the exerted reactions are orthogonal to the allowed virtual displacements – i.e. feasible displacements departing from a feasible configuration; reaction forces are confined on a subspace of the reaction space that corresponds to[55] the orthogonal complement of the feasible virtual displacement subspace. By moving on the constraint reaction space shown in 2.21 (b), the reaction forces associated to constraint I and II are thus proportional to the $\underline{\alpha}_{\mathrm{I}}$ and $\underline{\alpha}_{\mathrm{II}}$ vectors, respectively; the cumulative constraint reactions lie on the linear span of those two vectors, namely span$(\underline{\alpha}_{\mathrm{I}}, \underline{\alpha}_{\mathrm{II}})$.

2.7.2 General formulation

Purpose of the present paragraph is to define a set of m linear, possibly inhomogeneous[56] (i.e. linear *variation*) constraint equations amongst

[54] or, namely, frictionless

[55] i.e. the two subspaces share, with adjusted physical dimensions, the same generator vectors.

[56] according to many fe code implementation – e.g. MSC.Marc or ABAQUS – the inhomogeneous term is allowed in spc constraints only, limiting the more general mpc kinematic constraint to the homogeneous form only; an auxiliary node whose k-th dof is interested by both the mpc and an by an inhomogeneous spc may be added to the model to circumvent such limitation.

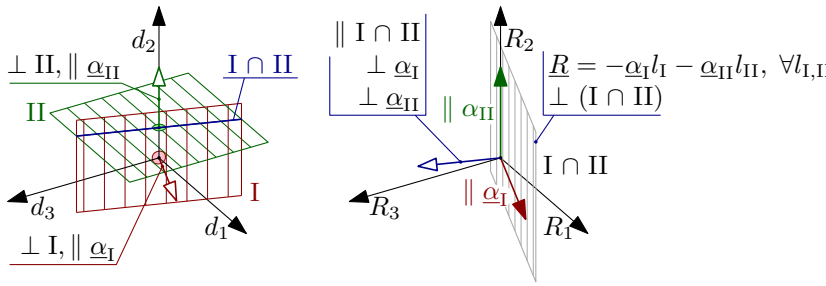

(a) configuration space (b) reaction space

Figure 2.21: Allowed system configurations and constraint reactions for the pedagogical example of Fig. 2.20. The allowed virtual displacement sets are easily derived as the homogenous counterpart of (a), and are left to the reader's imagination.

the structure $\underline{\mathrm{d}}$ dofs which may embody various kinds of kinematic relations, e.g. the pedagogic ones described above as, again,

$$\sum_i \alpha_{ji} d_i = \underline{\alpha}_j^{\top} \underline{\mathrm{d}} = \beta_j, \quad j = 1 \dots m \tag{2.125}$$

2.7.3 A first solution procedure for the constrained system

which reveals itself consistent with the Lagrange multiplier technique for constrained minimization.

Differences with respect to the alternative one that was proposed in previous courses, and which is still presented below are:

- the present one is shorter;
- it is more classical and widespread in literature;
- constraint equations are treated as, indeed, equations, and not as dof assignments; in particular the dofs are not to be partitioned into the *tied*/*retained* sets. Such a distinction is however a fact in actual implementations;
- the order of the system of equations to be solved is augmented (vs. reduced) of one unit for each added constraint; the impact on the matrix bandwidth is however analogous;

- the assembled stiffness matrix is bordered with further minors, but not otherwise manipulated;
- the basis for the reaction force vectors clearly appears from the formulation.
- the equivalence between non-zero imposed displacements and a suitable sets of external loads does *not* appear evident according to the present formulation.

A basis for the allowed constraint reactions subspace

By employing a matrix formulation, Eq. 2.125, may be directly cast as

$$\underline{\underline{\mathcal{L}}}^{\top} \underline{\mathrm{d}} = \underline{\beta} . \tag{2.126}$$

where each $\mathcal{L}_{ji}$ element of the m rows, n columns $\underline{\underline{\mathcal{L}}}^{\top}$ matrix equates the corrisponding α_{ji} coefficient, and the $\underline{\beta}$ column vector collects the m β_j inhomogeneous terms[57].

Also, the homogeneous counterpart of **??** hold for the same virtual displacements, namely

$$\underline{\underline{\mathcal{L}}}^{\top} \delta \underline{\mathrm{d}} = \underline{0} , \tag{2.127}$$

they are required to be orthogonal to the $\underline{\underline{\mathcal{L}}}$ matrix columns, but otherwise free; the linear span of those columns thus contains all and the only reaction vectors that are orthogonal (and, in particular work-orthogonal) to any feasible virtual displacement. We hence have that the variation of the m terms of a $\underline{\ell}$ column vector makes

$$\underline{\mathrm{R}} = - \underline{\underline{\mathcal{L}}} \, \underline{\ell} , \tag{2.128}$$

span all the allowed ideal constraint reaction subspace[58].

Due to their role in defining the $\underline{\underline{\mathcal{L}}}$ matrix, the α_{ji} coefficients that drive the homogeneous part of Eqs. **??** kinematic relations also rule the allowed internal and external reaction forces. In particular, for each

[57] The relation between the equivalent matrix/vector pairs ($\underline{\underline{\lambda}}$, $\underline{\mathrm{d}}$), ($\underline{\underline{\Lambda}}$, $\underline{\mathrm{d}}$) and ($\underline{\underline{\mathcal{L}}}$, $\underline{\beta}$) is here reported: XXX

[58] the inclusion of a minus sign does not really require a justification, due to the arbitrary nature of $\underline{\ell}$.

j-th tying equation a parametric constraint reaction $\underline{\mathrm{R}}^j$ is raised in the form

$$\underline{\mathrm{R}}^j = -\begin{bmatrix} \vdots \\ \alpha_{ji} \\ \vdots \end{bmatrix} \ell_j \tag{2.129}$$

to enforce the associated equation.

The overall reaction force vector $\underline{\mathrm{R}}$ is obtained as the accumulation of the $\underline{\mathrm{R}}^j$ contributions. The ℓ_j factors may be obtained from the solution of the equilibrium equations, as shown in the following.

The system of constrained equilibrium equations, and its solution

The nodal dof equilibrium equations derived by pairing i) the $\underline{\underline{\mathrm{K}}}\,\underline{\mathrm{d}}$ external forces required to keep the structure in a $\underline{\mathrm{d}}$ deformed configuration, see Eq. 2.121, ii) the actual external forces $\underline{\mathrm{F}}$ which are applied to the elements as distributed loads, see Eq. 2.124, or directly at nodes in form of concentrated loads, and iii) the reaction forces $\underline{\mathrm{R}}$ may be cast as

$$\underline{\underline{\mathrm{K}}}\,\underline{\mathrm{d}} = \underline{\mathrm{F}} + \underline{\mathrm{R}}\,. \tag{2.130}$$

Here, $\underline{\mathrm{d}}$ and $\underline{\mathrm{R}}$ are both unknown.

The Eq. 2.128 form for the reaction forces is substituted within the nodal equilibrium equations 2.130, thus obtaining the following

$$\underline{\underline{\mathrm{K}}}\,\underline{\mathrm{d}} + \underline{\underline{\mathcal{L}}}\,\underline{\ell} = \underline{\mathrm{F}}$$

under-determined system of n equations in the $n+m$ unknowns $\underline{\mathrm{d}}$ and $\underline{\ell}$. By appending the m constraint equations **??**, cardinality consistency between equation number and unknowns is restored, thus leading to the linear system of equations

$$\begin{bmatrix} \underline{\underline{\mathrm{K}}} & \underline{\underline{\mathcal{L}}} \\ \underline{\underline{\mathcal{L}}}^{\top} & \underline{\underline{0}} \end{bmatrix} \begin{bmatrix} \underline{\mathrm{d}} \\ \underline{\ell} \end{bmatrix} = \begin{bmatrix} \underline{\mathrm{F}} \\ \underline{\beta} \end{bmatrix}, \tag{2.131}$$

whose order is $n + m$.

The educated reader might recognise in 2.131 the system of equations associated to the retrieval of the stationary point in the $\underline{\mathrm{d}}\,, \underline{\ell}$

variables of the following quadratic form

$$\frac{1}{2}\,\underline{\mathrm{d}}^{\top}\,\underline{\underline{\mathrm{K}}}\,\underline{\mathrm{d}} - \underline{\mathrm{d}}^{\top}\,\underline{\mathrm{F}} + \underline{\ell}^{\top}\left(\underline{\underline{\mathcal{L}}}^{\top}\,\underline{\mathrm{d}} - \underline{\beta}\right), \tag{2.132}$$

which in turn represents – according to the Lagrange multiplier technique – the minimization of the total potential energy of a linearly elastic system

$$\frac{1}{2}\,\underline{\mathrm{d}}^{\top}\,\underline{\underline{\mathrm{K}}}\,\underline{\mathrm{d}} - \underline{\mathrm{d}}^{\top}\,\underline{\mathrm{F}}$$

i.e. the sum of i) internal strain energy, and ii) the unexerted work aka. the potential of the external forces, subject to the

$$\underline{\underline{\mathcal{L}}}^{\top}\,\underline{\mathrm{d}} - \underline{\beta} = \underline{0}$$

kinematic constraints, being $\underline{\ell}$ the vector obtained by stacking the Lagrange multipliers.

By solving the Eq. 2.131 system of linear equations, the solution vectors d^*, ℓ^* are obtained; the first directly describes the structure deformed configuration, whereas the second may be employed to derive the [generalized] reaction forces as

$$\underline{\mathrm{R}} = -\,\underline{\underline{\mathcal{L}}}\,\underline{\ell}^{*}.$$

2.7.4 An alternative constraining procedure

Tied and retained dofs

According to this alternative procedure, for each j-th constraint equation Eq. 2.7.1, one of the involved[59] dofs, e.g. the $d_k \in \underline{\mathrm{d}}$, is designated as the associated t_j *tied* one; the value of the tied dof is parametrically defined base on that equation, as in

$$d_k \equiv t_j = \sum_{i \neq k} \left(-\frac{\alpha_{ji}}{\alpha_{jk}}\right) d_i + \left(\frac{\beta_j}{\alpha_{jk}}\right), \quad j = 1 \dots m \tag{2.133}$$

Each kinematic constraint is hence treated as an assignment in the sense of computer programming, more than as a further simultaneous equation to be satisfied by the solution.

[59] i.e. $\alpha_{jk} \neq 0$

In order to avoid assignment conflicts, a given dof can't serve as tied in more than one equation; however, the assignment expression may legitimately involve dofs which act as tied for other equations, thus possibly producing a tangled dependency tree.

The designation of as suitable set of t_j, $j = 1 \dots m$ tied dofs may be discussed based on Fig. 2.22, where the quantities involved in Eqs. 2.126 are represented. In particular, each column of the $\mathcal{L}^\top$ matrix is associated to a d_i dof (and vice versa), and the tied dof selection may therefore be rationalized as the selection of m linearly independent columns amid the n of the $\underline{\underline{\mathcal{L}}}^\top$ matrix; if the k-th column is selected, the associated d_k enters the $\underline{\mathrm{t}}$ tied dof set as its j-th element[60], namely $d_k \equiv t_j$.

The dofs associated to the unselected columns are collected in the *retained* set; for each unselected h-th column, the associated $d_i \equiv r_h$ dof enters the $\underline{\mathrm{r}}$ vector as its h-th element[61].

In this way, a partitioning into *tied* and *retained* subset is defined for both the $\underline{\underline{\mathcal{L}}}^\top$ columns and the $\underline{\mathrm{d}}$ dofs.

By grouping the selected columns into a $\underline{\underline{\mathrm{A}}}$ square matrix, and the residual columns into a $(\underline{\underline{-\mathrm{B}}})$ matrix, Eqs. 2.126 may be cast as

$$\underline{\underline{\mathrm{A}}}\,\underline{\mathrm{t}} + \left(-\underline{\underline{\mathrm{B}}}\right)\underline{\mathrm{r}} = \underline{\beta} \quad \Rightarrow \quad \underline{\underline{\mathrm{A}}}\,\underline{\mathrm{t}} = \underline{\underline{\mathrm{B}}}\,\underline{\mathrm{r}} + \underline{\beta}\,,$$

we may hence explicitly define the $\underline{\mathrm{t}}$ tied dofs as a linear variation function of the $\underline{\mathrm{r}}$ retained ones, i.e.

$$\underline{\mathrm{t}} = \left[\underline{\underline{\mathrm{A}}}^{-1}\underline{\underline{\mathrm{B}}}\right]\underline{\mathrm{r}} + \left[\underline{\underline{\mathrm{A}}}^{-1}\underline{\beta}\right], \tag{2.134}$$

where the availability of the $\underline{\underline{\mathrm{A}}}^{-1}$ inverse matrix is granted based on the assumed linear independence of the selected $\underline{\underline{\mathcal{L}}}^\top$ columns. An element-wise equivalent of the former relation may be conveniently cast as

$$t_j = \underline{\mathrm{a}}_j^\top\,\underline{\underline{\mathrm{B}}}\,\underline{\mathrm{r}} + \underline{\mathrm{a}}_j^\top\,\underline{\beta}\,, \quad j = 1 \dots m \tag{2.135}$$

where $\underline{\mathrm{a}}_j^\top = \left[\underline{\underline{\mathrm{A}}}^{-1}\right]_{\mathrm{row}\,j}$ is the j-th row of the $\underline{\underline{\mathrm{A}}}^{-1}$ inverse matrix.

In most advanced fe codes the tied dof selection is left to the user's responsibility, whereas an algorithm for a robust – even if not strictly

[60] i.e. a unique relation $k \Leftrightarrow j$ is cast between the indexes k and j at which the same tied dof $t_j \equiv d_k$ is positioned within the $\underline{\mathrm{t}}$ and $\underline{\mathrm{d}}$ vectors, respectively.

[61] Again, a unique $h \Leftrightarrow i$ relation is cast between the indexes associated to the same $r_h \equiv d_i$ dof in two vectors $\underline{\mathrm{r}}$ and $\underline{\mathrm{d}}$.

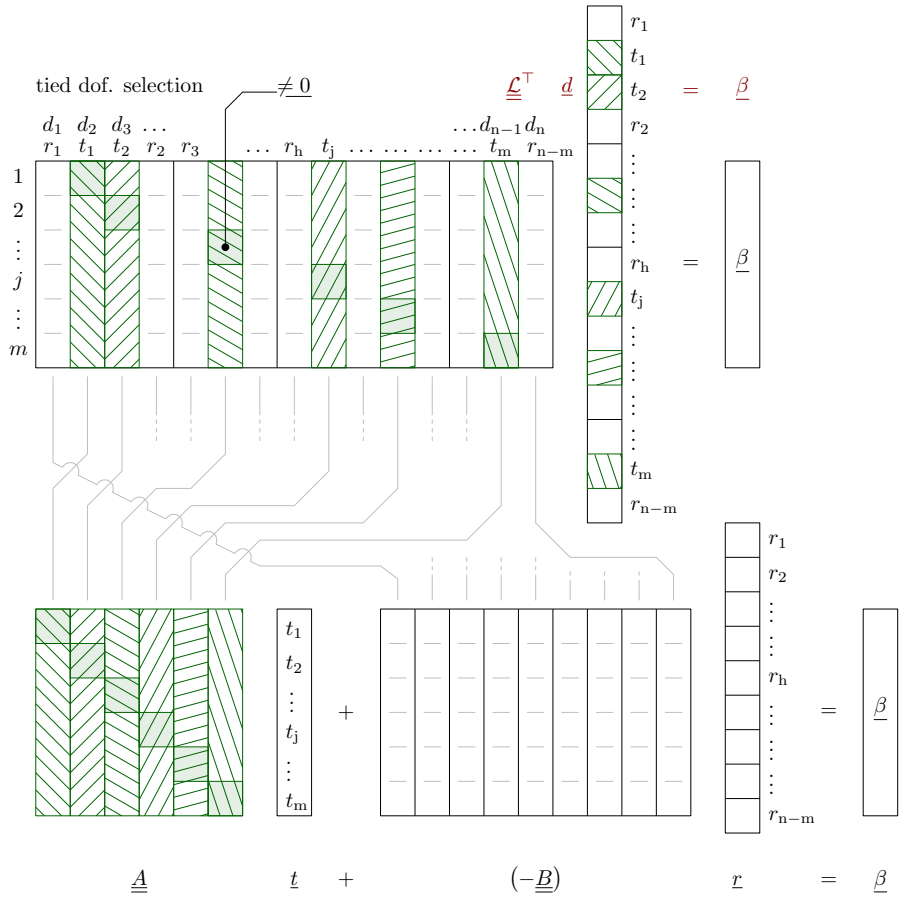

Figure 2.22: Graphical representation for the designation the tied dofs, based on the selection of m linearly independent columns within the $\underline{\underline{\mathcal{L}}}^{\top}$ matrix, which is hence partitioned in two $\underline{\underline{\mathrm{A}}}$, $\left(-\underline{\underline{\mathrm{B}}}\right)$ blocks. In the graphical representation, $m = 6$, $n = 15$, but the rationalization is of general validity.

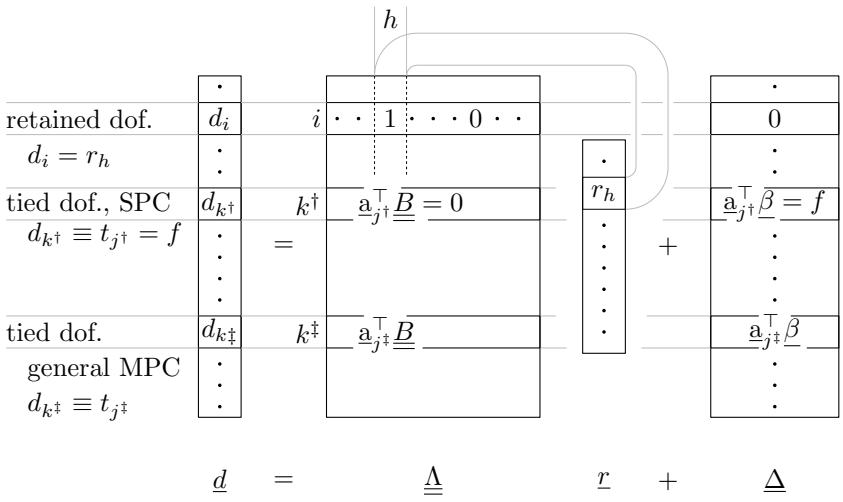

Figure 2.23: Graphical representation for the $\underline{\underline{\Lambda}}$ matrix and for the $\underline{\Delta}$ vector in Eq. 2.134; representative matrix rows are illustrated for a retained dof, and for two tied dofs, namely a fixed displacement – aka SPC – equation subcase, and the general case.

optimal – automatic selection is available in literature, see [11], [12, p.293].

Since the $\underline{\mathrm{r}}$ retained dofs do not serve as tied in any of the constraint equations, they retain a *fully independent* status and they may be effectively employed to span the subspace of *feasible* – i.e. constraint-conforming – deformed configurations.

By pairing the trivial identity relation between each r_h retained dof and its d_i counterpart in $\underline{\mathrm{d}}$, and the dependence of each tied t_j dof on the retained dofs according to Eq. 2.135, we obtain the explicit expression of the complete $\underline{\mathrm{d}}$ dof set as as a linear variation function of the retained ones only, namely

$$\underline{\mathrm{d}} = \underline{\underline{\Lambda}}\, \underline{\mathrm{r}} + \underline{\Delta}\,, \tag{2.136}$$

where the construction of the n rows, $n - m$ columns $\underline{\underline{\Lambda}}$ matrix, and of the n terms $\underline{\Delta}$ column vector is illustrated in Fig. 2.23 for a few representative rows, and it may described as follows:

- for each retained dof $d_i \equiv r_h$, the associated i-th row in $\underline{\underline{\Lambda}}$ is composed of a unit term at the h-th column, and zero elsewhere;

the associated i-th term in $\underline{\Delta}$ is also zero. In this way, the equivalence is enforced;

- for each tied dof $d_k \equiv t_j$, the associated i-th row in $\underline{\underline{\Lambda}}$, and the i-th term in $\underline{\Delta}$ house Eq. 2.135 terms, and are hence composed by the $\underline{\mathrm{a}}_j^{\top}\,\underline{\underline{\mathrm{B}}}$ row and by the $\underline{\mathrm{a}}_j^{\top}\,\underline{\beta}$ term, respectively;
- in the notable case a dof is tied based on a SPC constraint equation, i.e. $d_{k^\dagger} \equiv t_{j^\dagger} = f$, the associated $\underline{\mathrm{a}}_j^{\top}\,\underline{\underline{\mathrm{B}}}$ row in $\underline{\underline{\Lambda}}$ is null, and the associated $\underline{\mathrm{a}}_j^{\top}\,\underline{\beta}$ term in $\underline{\Delta}$ equates f, thus leading to the desired $t_{j^\dagger} = \underline{0}^{\top}\,\underline{\mathrm{r}} + a$.

Also, the virtual displacements in the neighborhood of a feasible constrained configuration are restricted to the linear combinations of the $\underline{\underline{\Lambda}}$ matrix columns $\underline{\Lambda}_h$, i.e.

$$\delta\,\underline{\mathrm{d}} \;=\; \underline{\underline{\Lambda}}\;\delta\,\underline{\mathrm{r}} \;=\; \underline{\Lambda}_1\,\delta r_1 + \underline{\Lambda}_2\,\delta r_2 + \ldots + \underline{\Lambda}_{n-m}\,\delta r_{n-m} \tag{2.137}$$

with arbitrary virtual displacement values at the retained dofs, whereas the tied ones just follow.

The ideal constraint hypothesis requires the reaction force vector $\underline{\mathrm{R}}$ to be orthogonal to a general virtual displacement, and such condition holds if and only if $\underline{\mathrm{R}}$ is orthogonal to each the $\underline{\underline{\Lambda}}$ matrix columns, i.e.

$$\left\langle \left[\underline{\underline{\Lambda}}\right]_{\mathrm{col}\;h}, \underline{\mathrm{R}} \right\rangle = 0 \quad h = 1 \ldots n-m, \tag{2.138}$$

or, equivalently,

$$\underline{\underline{\Lambda}}^{\top}\,\underline{\mathrm{R}} \;=\; \underline{0}\,. \tag{2.139}$$

The system of constrained equilibrium equations, and its solution. Alternative form.

We consider the nodal equilibrium equations as expressed in Eq. 2.130. If constraints are applied, we have

$$\underline{\underline{\mathrm{K}}}\,\left(\underline{\underline{\Lambda}}\,\underline{\mathrm{r}} + \underline{\Delta}\right) = \underline{\mathrm{F}} + \underline{\mathrm{R}} \tag{2.140}$$

and

$$\underline{\underline{\mathrm{K}}}\,\underline{\underline{\Lambda}}\,\underline{\mathrm{r}} = \left(\underline{\mathrm{F}} - \underline{\underline{\mathrm{K}}}\,\underline{\Delta}\right) + \underline{\mathrm{R}}\,, \tag{2.141}$$

where the inhomogeneous part of the constraint equations is *de facto* assimilated to a further contribution to the external loads, which may

be rationalized as the elastic nodal reactions raised when i) all the retained dof are kept fixed at their initial position, and ii) each tied dof is displaced of an amount equal to the inhomogeneous term of the tying equation.

By projecting the equations on the subspace of allowed configurations

$$\underbrace{\underline{\underline{\Lambda}}^{\top}\,\underline{\underline{K}}\,\underline{\underline{\Lambda}}}_{\underline{\underline{K}}_R}\,\underline{r} = \underbrace{\underline{\underline{\Lambda}}^{\top}\left(\underline{F} - \underline{\underline{K}}\,\underline{\Delta}\right)}_{\underline{F}_R} + \underbrace{\underline{\underline{\Lambda}}^{\top}\,\underline{R}}_{=0}, \tag{2.142}$$

the contribution of the unknown reaction forces, that are normal to such a subspace – see Eq. 2.139, vanishes.

The linear system of *constrained* nodal dof equilibrium equations is then set as

$$\underline{\underline{K}}_R\,\underline{r} = \underline{F}_R \tag{2.143}$$

and it may be solved for the retained dof vector $\underline{r}$.

Once the solution vector $\underline{r}^*$ is found in terms of displacements at retained dofs, the overall displacement vector and the unknown reaction forces may be derived as

$$\underline{d}^* = \underline{\underline{\Lambda}}\,\underline{r}^* + \underline{\Delta}\,; \tag{2.144}$$

and

$$\underline{R}^* = \underline{\underline{K}}\left(\underline{\underline{\Lambda}}\,\underline{r}^* + \underline{\Delta}\right) - \underline{F}\,. \tag{2.145}$$

2.7.5 Retrieval of element based results

Once the problem is solved in terms of the $\underline{d}^*$ structure nodal displacements, we may extract for each j-th element the associated local dofs vector as

$$\underline{d}^*_{ej} = \underline{\underline{P}}_{ej}\,\underline{d}^*. \tag{2.146}$$

We may in turn derive the strains at the reference plane, and the curvatures as

$$\underline{e} = \underline{\underline{B}}^{e}_{ej}(\xi,\eta)\,\underline{d}^*_{ej} \qquad\qquad \underline{\kappa} = \underline{\underline{B}}^{\kappa}_{ej}(\xi,\eta)\,\underline{d}^*_{ej} \tag{2.147}$$

or directly the tt, ip strain components as

$$\underline{\epsilon} = \left(\underline{\underline{B}}^{e}_{ej}(\xi,\eta) + \underline{\underline{B}}^{\kappa}_{ej}(\xi,\eta)z\right)\,\underline{d}^*_{ej}. \tag{2.148}$$

ip stresses may be then derived according to the material constitutive law, see Eq. 2.13. The oop tranverse shear strain components may be derived as

$$\underline{\gamma}_z = \underline{\underline{\mathrm{B}}}^{\gamma}_{\mathrm{e}j}(\xi,\eta)\,\underline{\mathrm{d}}^{*}_{\mathrm{e}j}. \tag{2.149}$$

All the cited quantities are customarily sampled at the gaussian integration points, and possibly extrapolated at nodes.

Chapter 3

Advanced analysis tools

3.1 Notable Multi Point Constraints

3.1.1 Rigid body link RBE2

A master (or retained, control, independent, etc.) C node is considered, whose coordinates are defined as x_C, y_C, z_C in a (typically) global reference system, along with a set of n P_i nodes whose coordinates are x_i, y_i, z_i.

A kinematic link is to be established such that the dofs – or a subset of them – associated to the P_i nodes follow the rototranslations of the C control according to the rigid body motion laws.

In the case of a fully constrained P_i node we have

$$\begin{bmatrix} u_i \\ v_i \\ w_i \\ \theta_i \\ \phi_i \\ \psi_i \end{bmatrix} = \underbrace{\begin{bmatrix} 1 & 0 & 0 & 0 & +(z_i - z_C) & -(y_i - y_C) \\ 0 & 1 & 0 & -(z_i - z_C) & 0 & +(x_i - x_C) \\ 0 & 0 & 1 & +(y_i - y_C) & -(x_i - x_C) & 0 \\ 0 & 0 & 0 & 1 & 0 & 0 \\ 0 & 0 & 0 & 0 & 1 & 0 \\ 0 & 0 & 0 & 0 & 0 & 1 \end{bmatrix}}_{\underline{\underline{\mathrm{L}}}_i} \cdot \begin{bmatrix} u_C \\ v_C \\ w_C \\ \theta_C \\ \phi_C \\ \psi_C \end{bmatrix} \tag{3.1}$$

where u, v, w (θ, ϕ, ψ) are the translation (rotation) vector components with respect to the x, y, z cartesian reference system. A subset of the above dof dependency relations may be cast to obtain a partial constraining of the P_i node; a free relative motion of such node with respect to the rigid body is allowed at the unconstrained dofs.

External actions that are applied to tied P_i dofs are reduced to the master node in form of a statically equivalent counterpart; the contributions deriving from each P_i node are finally accumulated.

3.1.2 Distributed load / averaged motion link RBE3

A *reference* C node of coordinates $\underline{\mathrm{x}}_C = (x_C, y_C, z_C)$ – which is here customarily assumed as an isolated node – is considered, along with a distribution of n *weighted* nodes P_i, q_i, whose coordinates are $\underline{\mathrm{x}}_i = (x_i, y_i, z_i)$. The nodal weight q_i is usually determined with some degree of arbitrariness, e.g. by partitioning the attached elements into nodal influence domains, and by associating to each node a weight that is proportional to the influence domain extension. Mass-referring

nomenclature is employed throughout the paragraph, although q_i are adimensional.

The G center of mass is derived for the distribution, whose coordinates are $\underline{\mathrm{x}}_G = (x_G, y_G, z_G)$, along with the overall mass $m = \sum_i q_i$ and the centroidal matrix of inertia

$$\underline{\underline{\mathrm{J}}} = \sum_i q_i \begin{bmatrix} y_{Gi}^2 + z_{Gi}^2 & -x_{Gi}\, y_{Gi} & -x_{Gi}\, z_{Gi} \\ -y_{Gi}\, x_{Gi} & z_{Gi}^2 + x_{Gi}^2 & -y_{Gi}\, z_{Gi} \\ -z_{Gi}\, x_{Gi} & -z_{Gi}\, y_{Gi} & x_{Gi}^2 + y_{Gi}^2 \end{bmatrix}, \tag{3.2}$$

where

$$\begin{bmatrix} x_{Gi} \\ y_{Gi} \\ z_{Gi} \end{bmatrix} = \underline{\mathrm{x}}_{Gi} = \underline{\mathrm{x}}_i - \underline{\mathrm{x}}_G.$$

The $\underline{\underline{\mathrm{J}}}$ matrix of inertia is assumed as nonsingular – a condition, this, that occurs if the P_i distribution involves at least three non-collinear points; its inverse may be numerically computed as $\underline{\underline{\mathrm{J}}}^{-1}$.

The RBE3 multi-dof constraint may be described based on either i) the imposed kinematic relations and ii) the nature of the associated reactions.

Starting from the latter approach, when a general load consisting of three force components $\check{U}_C, \check{V}_C, \check{W}_C$ and three moment components $\check{\Theta}_C, \check{\Phi}_C, \check{\Psi}_C$ is applied at C, it induces a suitable set of reaction forces on both C itself and on the P_i nodes, such that the C node balance gets restored – i.e. the reactions on C, namely $\underline{\mathrm{U}}_C = -\underline{\check{\mathrm{U}}}_C$, are equal and opposite to the applied loads. Since the RBE3 is an internal constraint, the overall set of reactions must be self-equilibrated, and hence the distribution of reaction forces exerted on the P_i nodes is statically equivalent to the applied load at C.

According to such observation, the RBE3 constitutes an effective tool suitable for distributing a concentrated loading on the nodes along a portion of the structure.

A crude algebraic expression for the reaction force components at

the P_i nodes may be obtained as

$$\begin{bmatrix} U_i \\ V_i \\ W_i \end{bmatrix} = q_i \left(\begin{bmatrix} a \\ b \\ c \end{bmatrix} + \begin{bmatrix} d \\ e \\ f \end{bmatrix} \wedge \underline{\mathrm{x}}_{Gi} \right) \tag{3.3}$$

$$\underbrace{\begin{bmatrix} U_i \\ V_i \\ W_i \end{bmatrix}}_{\underline{\mathrm{U}}_i} = q_i \underbrace{\begin{bmatrix} 1 & 0 & 0 & 0 & +z_{Gi} & -y_{Gi} \\ 0 & 1 & 0 & -z_{Gi} & 0 & +x_{Gi} \\ 0 & 0 & 1 & +y_{Gi} & -x_{Gi} & 0 \end{bmatrix}}_{\underline{\underline{\mathrm{S}}}_i} \underbrace{\begin{bmatrix} a \\ b \\ c \\ d \\ e \\ f \end{bmatrix}}_{\underline{\mathrm{a}}}, \tag{3.4}$$

where the $\underline{\underline{\mathrm{S}}}_i = \begin{bmatrix} \underline{\underline{\mathrm{I}}} & -[\underline{\mathrm{x}}_{Gi}]_\wedge \end{bmatrix}$ matrix is built upon the matrix multiplication form of the vector product[1], and the a, b, c, d, e, f coefficients are defined based on the static equivalence between the applied loading at C, and its distributed counterpart; in particular the system of six linear equations

$$\begin{bmatrix} \check{U}_C \\ \check{V}_C \\ \check{W}_C \end{bmatrix} = \sum_i \begin{bmatrix} U_i \\ V_i \\ W_i \end{bmatrix}, \qquad \begin{bmatrix} \check{\Theta}_C \\ \check{\Phi}_C \\ \check{\Psi}_C \end{bmatrix} = \sum_i \begin{bmatrix} x_i - x_C \\ y_i - y_C \\ z_i - z_C \end{bmatrix} \wedge \begin{bmatrix} U_i \\ V_i \\ W_i \end{bmatrix} \tag{3.5}$$

is solved for the aforementioned unknown parameters, i.e.

$$\underbrace{\sum_i q_i \begin{bmatrix} \underline{\underline{\mathrm{I}}} \\ [\underline{\mathrm{x}}_i - \underline{\mathrm{x}}_C]_\wedge \end{bmatrix} \underline{\underline{\mathrm{S}}}_i}_{\underline{\underline{\mathrm{A}}}} \underline{\mathrm{a}} = \underbrace{\begin{bmatrix} \check{U}_C \\ \check{V}_C \\ \check{W}_C \\ \check{\Theta}_C \\ \check{\Phi}_C \\ \check{\Psi}_C \end{bmatrix}}_{\underline{\check{\mathrm{U}}}_C}, \tag{3.6}$$

[1] as in

$$\underline{\mathrm{x_i}} \wedge \square = [\underline{\mathrm{x}}_i]_\wedge \cdot \square, \quad [\underline{\mathrm{x}}_i]_\wedge = \begin{bmatrix} 0 & -z_i & +y_i \\ +z_i & 0 & -x_i \\ -y_i & +x_i & 0 \end{bmatrix}$$

for a generic $\square$ column vector placeholder, see `https://en.wikipedia.org/wiki/Cross_product#Conversion_to_matrix_multiplication`

and, with nonsingular A,

$$\underline{\mathrm{a}} = \underline{\underline{\mathrm{A}}}^{-1}\, \check{\underline{\mathrm{U}}}_C \tag{3.7}$$

and finally, from Eqn. 3.5,

$$\underline{\mathrm{U_i}} = q_i \left(\underline{\underline{\mathrm{S}}}_i\, \underline{\underline{\mathrm{A}}}^{-1} \right) \check{\underline{\mathrm{U}}}_C \tag{3.8}$$

An explicit form for the inverse of the $\underline{\underline{\mathrm{A}}}$ matrix is available as

$$\underline{\underline{\mathrm{A}}}^{-1} = \underbrace{\begin{bmatrix} \frac{1}{m}\underline{\underline{\mathrm{I}}} & \underline{\underline{0}} \\ \underline{\underline{0}} & \underline{\underline{\mathrm{J}}}^{-1} \end{bmatrix}}_{\underline{\underline{\mathrm{M}}}^{-1}} \underbrace{\begin{bmatrix} \underline{\underline{\mathrm{I}}} & \underline{\underline{0}} \\ [\underline{\mathrm{x}}_C - \underline{\mathrm{x}}_G]_\wedge & \underline{\underline{\mathrm{I}}} \end{bmatrix}}_{\underline{\underline{\mathrm{L}}}_{CG}^{\top}}, \tag{3.9}$$

where $\underline{\underline{\mathrm{L}}}_{CG}^{\top}$ is the matrix that transforms the $\check{\underline{\mathrm{U}}}_C$ actions at C into statically equivalent[2] $\check{\underline{\mathrm{U}}}_G = \underline{\underline{\mathrm{L}}}_{CG}^{\top} \check{\underline{\mathrm{U}}}_C$ actions at G, and $\underline{\underline{\mathrm{M}}}^{-1}$ takes the form of the inverse of the mass matrix for a rigid body that encompass the P_i, q_i nodes, and possibly C, with handle dofs at G. The existence of the $\underline{\underline{\mathrm{A}}}^{-1}$ matrix inverse clearly depends on the assumed existence of $\underline{\underline{\mathrm{J}}}^{-1}$.

Figure 3.1 represents the distribution of reaction forces at the P_i nodes, according to Eq. 3.4.

The first contribution $\underline{\mathrm{R}}_{abc,i}$ due to the a, b and c parameters is represented in the axonometric view inset, and it results in a fractionation of the forces exerted at C, based on the nodal weights q_i. We have in fact

$$\underline{\mathrm{R}}_{abc,i} = q_i \begin{bmatrix} a \\ b \\ c \end{bmatrix} = \frac{q_i}{\sum_i q_i} \left\{ \check{U}_C, \check{V}_C, \check{W}_C \right\}; \tag{3.10}$$

based also on Eqs. 3.7,3.9; the resultant moment of this first contribution with respect to the G centroid is zero by definition.

The $\check{\Theta}_G, \check{\Phi}_G, \check{\Psi}_G$ moment components within $\check{\underline{\mathrm{U}}}_G$ must hence find representation through the further d, e, f based contributions in Eq. 3.4, namely

$$\underline{\mathrm{R}}_{d,i} + \underline{\mathrm{R}}_{e,i} + \underline{\mathrm{R}}_{f,i} = q_i \left(d \begin{bmatrix} 1 \\ 0 \\ 0 \end{bmatrix} + e \begin{bmatrix} 0 \\ 1 \\ 0 \end{bmatrix} + f \begin{bmatrix} 0 \\ 0 \\ 1 \end{bmatrix} \right) \wedge \underline{\mathrm{x}}_{Gi} \tag{3.11}$$

[2] i.e. with the addition of suitable transport moments

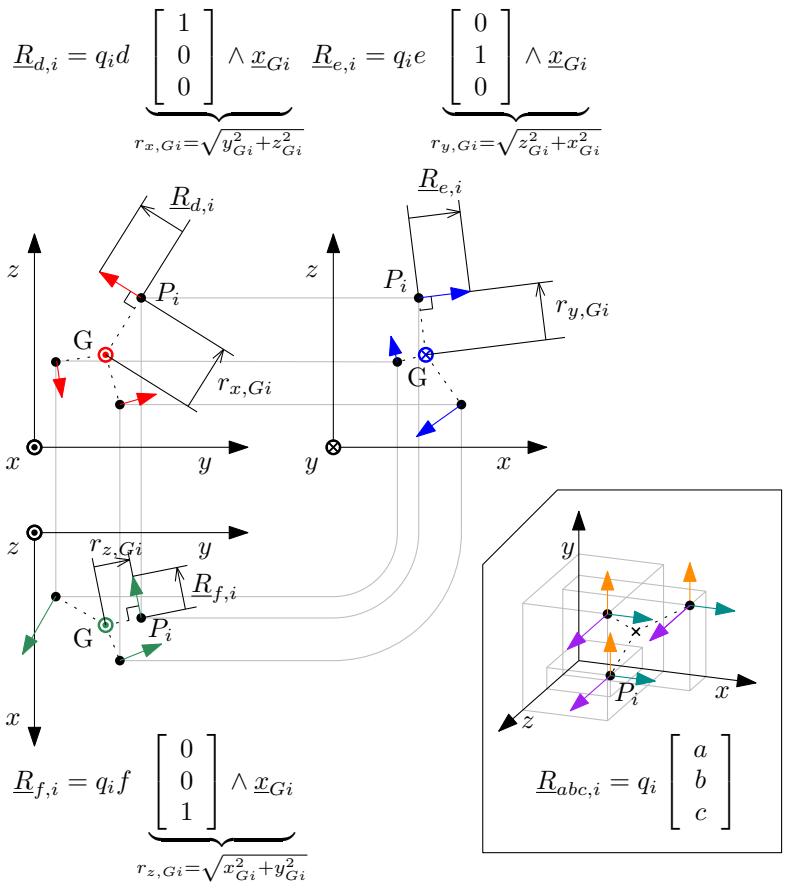

Figure 3.1: Graphical rationalization of the reactions at the P_i, q_i node distribution. In the $(yz, \perp x)$ projected view, the $\underline{\mathrm{R}}_{d,i}$ reactions at the P_i nodes associated to the d moment related parameter are plotted. The arrows are tangentially, counterclockwisely (if $d > 0$) oriented with respect to a Gx cylindrical reference system; their magnitude is proportional to the nodal weigth q_i, and to the projected distance $r_{x,Gi} = \sqrt{(y_i - y_G)^2 + (z_i - z_G)^2}$ from the centroid. The $(zx, \perp y)$, $(xy, \perp z)$ projected views analogously depict the $\underline{\mathrm{R}}_{e,i}$, $\underline{\mathrm{R}}_{f,i}$ reactions associated to the e, f moment related parameters, respectively. In the axonometric view inset, the $\underline{\mathrm{R}}_{abc,i}$ contributions due to the a, b and c force related parameters are represented. In order to point out the distance contribution, the case of uniform q_i nodal weights is considered in assigning vector lengths.

whose resultant force is zero by G centroid definition. The $\underline{\mathrm{R}}_{d,i}$ reactions are represented in the $(yz, \perp x)$ projected view of Fig. 3.1, and they consist in tangentially, counterclockwisely (if $d > 0$, and outward x) oriented forces with respect to a Gx cylindrical reference system, whose magnitude scales with i) the q_i nodal weight, with ii) the

$$r_{x,Gi} = \sqrt{(y_i - y_G)^2 + (z_i - z_G)^2}$$

projected distance from the G centroid, and, naturally, with iii) the d parameter. The $(zx, \perp y)$, $(xy, \perp z)$ projected views analogously depict the similarly characterized $\underline{\mathrm{R}}_{e,i}$, $\underline{\mathrm{R}}_{f,i}$ reactions associated to the e, f moment related parameters, respectively. Only in the case the $Gxyz$ reference system is principal of inertia[3] a simple formula for the d, e, f parameter is at hand[4], whereas in general they are retrieved by matching the $\check{\underline{\mathrm{U}}}_G$ moment components as in

$$\begin{bmatrix} d \\ e \\ f \end{bmatrix} = \underline{\underline{\mathrm{J}}}^{-1} \begin{bmatrix} \check{\Theta}_G \\ \check{\Phi}_G \\ \check{\Psi}_G \end{bmatrix} \tag{3.12}$$

see Eqs. 3.7,3.9.

By enforcing the a null virtual work cumulatively produced by i) the $\underline{\mathrm{U}}_C = -\check{\underline{\mathrm{U}}}_C$ reactions that equilibrate the external actions at C, and by ii) the $\underline{\mathrm{U}}_i$ reactions at each P_i node, i.e.

$$0 = \underline{\delta \mathrm{u}}_C^{\top} \left(-\check{\underline{\mathrm{U}}}_C \right) + \sum_i \underline{\delta \mathrm{u}}_i^{\top} \underline{\mathrm{U}}_i \tag{3.13}$$

$$= \left(-\underline{\delta \mathrm{u}}_C^{\top} + \sum_i q_i \, \underline{\delta \mathrm{u}}_i^{\top} \underline{\underline{\mathrm{S}}}_i \underline{\underline{\mathrm{A}}}^{-1} \right) \check{\underline{\mathrm{U}}}_C \tag{3.14}$$

for a general $\check{\underline{\mathrm{U}}}_C$ action at C, we obtain the six constraint equations that, by also making the customarily tied nature of the C dofs explicit, may be cast as

$$\underline{\delta \mathrm{u}}_C = \begin{bmatrix} \cdots & q_i \underline{\underline{\mathrm{A}}}^{-\top} \underline{\underline{\mathrm{S}}}_i^{\top} & \cdots \end{bmatrix} \begin{bmatrix} \vdots \\ \underline{\delta \mathrm{u}}_i \\ \vdots \end{bmatrix}, \tag{3.15}$$

[3] this condition holds e.g. in the case the P_i nodes lie on the Gxy plane, and the distribution is symmetric with respect to either the Gx or the Gy axis

[4] namely $d = \frac{\Theta_G}{J_{xx}}$, $e = \frac{\Phi_G}{J_{yy}}$, $f = \frac{\Psi_G}{J_{zz}}$, but – again – those expression only hold when $J_{xy} = J_{yz} = J_{zx} = 0$

where

$$\underline{\delta \mathrm{u}}_C^{\top} = \begin{bmatrix} \delta u_C & \delta v_C & \delta w_C & \delta \theta_C & \delta \phi_C & \delta \psi_C \end{bmatrix}$$
$$\underline{\delta \mathrm{u}}_i^{\top} = \begin{bmatrix} \delta u_i & \delta v_i & \delta w_i \end{bmatrix}$$

are the virtual generalized displacements of the C and of the P_i nodes.

Since the RBE3 constraint relations are both linear and homogeneous, Eq. 3.15 may be equally written with actual finite displacements $\{\underline{\mathrm{u}}_C, \underline{\mathrm{u}}_i\}$ in place of their $\{\underline{\delta \mathrm{u}}_C, \underline{\delta \mathrm{u}}_i\}$ virtual counterparts.

In order to rationalize the contribution of the P_i nodes motion to the C roto-translation, Eq. 3.15 may be recast as

$$\underline{\mathrm{u}}_C = \sum_i q_i \, \underline{\underline{\mathrm{A}}}^{-\top} \, \underline{\underline{\mathrm{S}}}_i^{\top} \, \underline{\mathrm{u}}_i = \cdots = \underbrace{\begin{bmatrix} \underline{\underline{\mathrm{I}}} & -[\underline{\mathrm{x}}_C - \underline{\mathrm{x}}_G]_{\wedge} \\ \underline{\underline{0}} & \underline{\underline{\mathrm{I}}} \end{bmatrix}}_{\underline{\underline{\mathrm{L}}}_{CG}} \underline{\mathrm{u}}_G \qquad (3.16)$$

where $\underline{\underline{\mathrm{L}}}_{CG}$ rigidly ties the $\underline{\mathrm{u}}_C$ motion to the

$$\underline{\mathrm{u}}_G = \begin{bmatrix} u_G & v_G & w_G & \theta_G & \phi_G & \psi_G \end{bmatrix}^{\top}$$

motion of the G centroid, whose translation is in turn assumed as the [weighted] average translation of the P_i nodes, and whose rotation is obtained from the cumulative moment of the P_i nodal displacement vectors, namely

$$\begin{bmatrix} u_G \\ v_G \\ w_G \end{bmatrix} = \frac{1}{m} \sum_i q_i \, \underline{\mathrm{u}}_i, \qquad \begin{bmatrix} \theta_G \\ \phi_G \\ \psi_G \end{bmatrix} = \underline{\underline{\mathrm{J}}}^{-1} \underbrace{\sum_i q_i \, [\underline{\mathrm{x}}_i - \underline{\mathrm{x}}_G]_{\wedge} \, \underline{\mathrm{u}}_i}_{P_i \text{ disps. moment}} .$$

If nodal velocities were used, instead of displacements, we would define the instantaneous[5] motion of G (and of C in turn) as the motion of an ideal rigid counterpart of the $C, G, (P_i, q_i)$ node set such that equivalent *linear momentum* and *angular momentum* are produced, with respect to the actual – nonrigid – motion of the (P_i, q_i) nodes.

A tentative graphical rationalization of the RBE3 kinematic relations is presented in Figure 3.2. In Fig. 3.2a, a planar P_i, q_i distribution is presented, subject to in-plane nodal motions $\underline{\mathrm{u}}_i$ (black vectors); the

[5] since the relative node positioning is allowed to vary in time

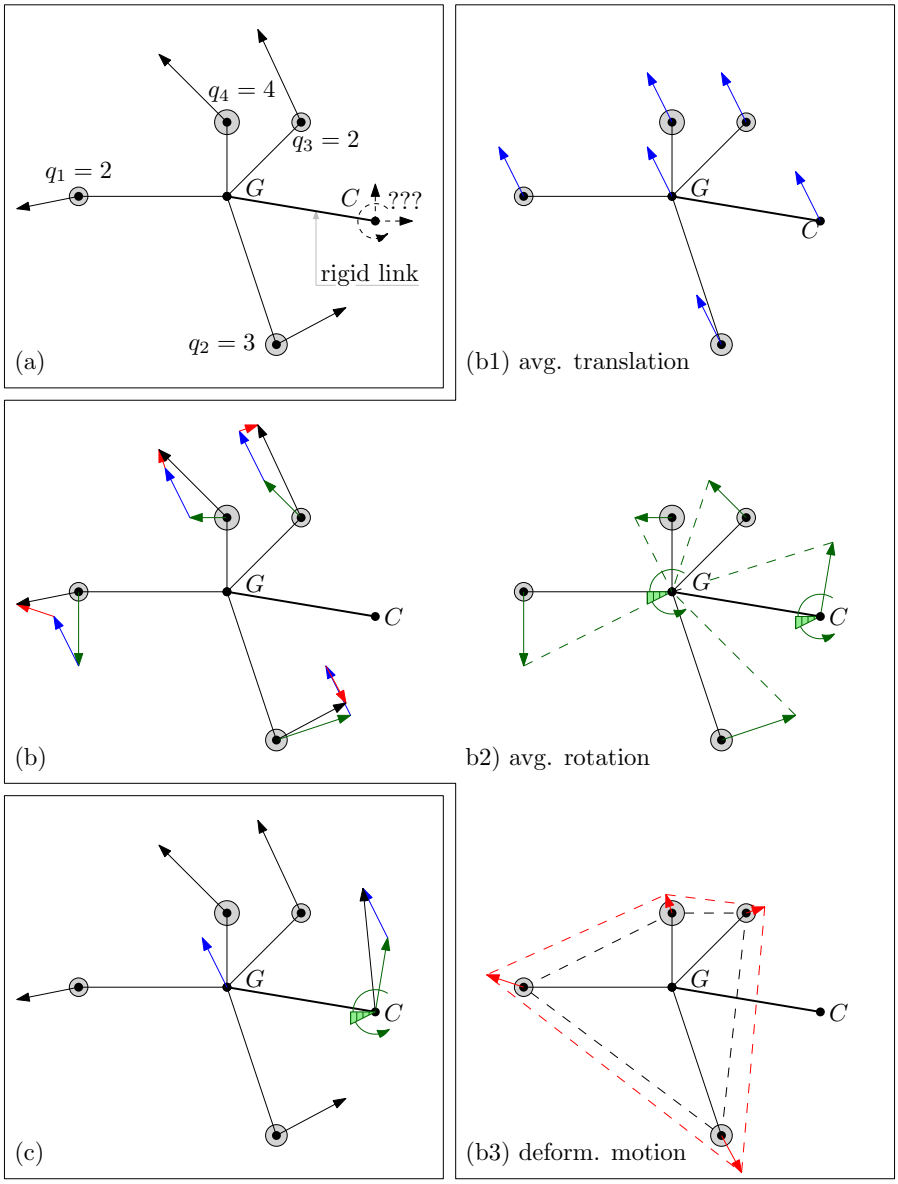

Figure 3.2: Graphical rationalization of the RBE3 kinematic relations.

$\underline{\mathrm{u}}_C$ reference node motion is currently unknown, and to be derived. In Fig. 3.2b, an average translation (Fig. 3.2b1, blue vectors), and an average rotation around G (Fig. 3.2b2, green vectors and rotation) are isolated, applied to G and then rigidly transmitted to C. By subtracting the average roto-translation from each node motion, a residual, purely deformative P_i node motion is obtained (Fig. 3.2b3, red vectors); such a motion has zero overall linear and angular moments, it is uncoupled from the motion of both the G point and the C node, and it is hence unconstrained even in the case of a possibly locked C node. Fig. 3.2c represents the obtained rototranslation for the tied C node, along with the P_i displacement field.

Again, in stark contrast to the RBE2 constraint counterpart, any motion of the P_i nodes that is null in both average translation and rotation – i.e. it is characterized by self-compensating linear and angular moment contributions, as in

$$\underline{0} = \frac{1}{m} \sum_i q_i \, \underline{\mathrm{u}}_i, \qquad\qquad \underline{0} = \sum_i q_i \left[\underline{\mathrm{x}}_i - \underline{\mathrm{x}}_G \right]_\wedge \underline{\mathrm{u}}_i$$

is completely disregarded by the constraint equations, and it is hence left free.

Finally, some variants of the presented formulation are available in actual FE solver implementations, in particular:

- a subset only of the C node dofs may be involved in the RBE3 constraint, thus deactivating some of the Eq. 3.15 identities;
- a subset only of the P_i displacement components may be involved in the RBE3 constraint; also, some rotational dofs may be also involved from selected nodes, in order to compensate for an otherwise singular $\underline{\underline{\mathrm{J}}}$ inertia matrix;
- for possibly each constraint equation, the tied nature of the involved C dof may transferred to a designated dof taken from the P_i node distribution, thus retaining the independent nature of the C dofs; it is up to the analyst to choose an alternative dof that enters the equation with a non-zero coefficient.

3.1.3 Inserts

TODO

3.1.4 Overclosure tyings

TODO

3.1.5 Inertia relief

Inertia relief[6] refers to an analysis procedure that allows unconstrained systems – or systems otherwise susceptible to stress-free motions – to be subjected to a quasi-static analysis by taking rigid body inertia forces into account.

Conventional static analysis cannot be performed for such systems since, in the absence of constraints, the stiffness matrix is singular. The structure response is measured relative to a steady state accelerating frame, whose motion is induced by the (usually nonzero) external load resultants.

The inertia relief solution procedure provides for three steps, namely i) the rigid body mode evaluation, ii) the assessment of the inertia relief loads, and iii) the solution of a supported, self-equilibrated static loadcase within the moving frame.

A set of nodal dofs is supplied, one each expected rigid body motion, whose *imposed* displacements values uniquely define the structure positioning in space; also, they may be employed in supporting the structure to untangle the stiffness matrix rank-deficiency.

The $\underline{\mathrm{t}}_l$ rigid body modes are evaluated by sequentially setting each of these *support* dof to unity, while retaining the others to zero, and solving for the constrained system of nodal equilibrium equations in the absence of further external loads. Since the tied/retained condition of the structure dofs does not vary throughout the sequence of aforementioned loadcases, comprised of the final step introduced in the following, a single $\underline{\underline{\mathrm{L}}}\,\underline{\underline{\mathrm{L}}}^{\top}$ Cholesky system matrix decomposition is required by the procedure, whose computational burden is thus not significantly increased with respect to the usual static solution.

A rigid body, steady state acceleration field is defined as the linear combination of the so defined $\underline{\mathrm{t}}_l$ rigid body modes

$$\underline{\ddot{\mathrm{d}}} = \underbrace{\begin{bmatrix} \cdots & \underline{\mathrm{t}}_l & \cdots \end{bmatrix}}_{\underline{\underline{\mathrm{T}}}} \underbrace{\begin{bmatrix} \vdots \\ \alpha_l \\ \vdots \end{bmatrix}}_{\underline{\alpha}}, \tag{3.17}$$

[6] XXX some cut and paste from the MSC.Marc vol A manual, please rewrite as required to avoid copyright infringement.

whose α_l coefficients define the modal acceleration vector $\underline{\alpha}$. Those acceleration terms are then evaluated according to the inertial equilibrium of the structure under the applied $\underline{\mathrm{F}}$ external loads, condition, this, that may be stated as

$$\underline{\underline{\mathrm{T}}}^{\top}\,\underline{\underline{\mathrm{M}}}\,\underline{\underline{\mathrm{T}}}\,\underline{\alpha} \;=\; \underline{\underline{\mathrm{T}}}^{\top}\,\underline{\mathrm{F}} \tag{3.18}$$

The projection of the equilibrium equations onto the subspace defined by the linear span of the $\underline{\mathrm{t}}_l$ rigid body mode vectors – i.e. the left multiplication of both the equation sides by the $\underline{\underline{\mathrm{T}}}^{\top}$ matrix, is solved in place of the overdetermined linear system

$$\underline{\underline{\mathrm{M}}}\,\underline{\underline{\mathrm{T}}}\,\underline{\alpha} \;=\; \underline{\mathrm{F}}\;[+\underline{\mathrm{R}}_l]$$

since the $\underline{\mathrm{R}}_l$ reaction forces associated to the rigid body constraints balance the equilibrium residual components that are orthogonal[7] to such allowed configuration subspace.

The inertia relief forces may then be quantified as $\underline{\underline{\mathrm{M}}}\,\underline{\underline{\mathrm{T}}}\,\underline{\alpha}$, and superposed to the initial external loads, thus leading to a self equilibrated loading condition in the context of the steady state accelerating frame; by employing the support dofs to establish a positioning constraint set, the elastic problem may finally be solved in the form

$$\underline{\underline{\mathrm{K}}}\,\underline{\mathrm{d}} \;=\; \underline{\mathrm{F}} \;-\; \underline{\underline{\mathrm{M}}}\,\underline{\underline{\mathrm{T}}}\,\underline{\alpha}\,, \tag{3.19}$$

The $\underline{\mathrm{d}}$ displacement components are expressed with respect to a reference frame that clings to the possibly accelerating structure through the support dofs; due to the self-equilibrated nature of the applied loads in the moving frame, reaction forces at supports are zero.

As a closing comment, the MSC.Marc solver employs a lumped definition for the system mass matrix for evaluating inertia relief forces.

[7] We note that $\underline{\underline{\mathrm{T}}}^{\top}\,\underline{\mathrm{R}}_l = \underline{0}$ is a *smooth* or *ideal* constraint condition, i.e. the $\underline{\mathrm{R}}_l$ reactions are work-orthogonal to the allowed motions.

3.1.6 Harmonic response analysis

The equilibrium equations of a multiple dof system subject to elastic, inertial and viscous actions may be stated in the general form

$$\underline{\underline{\mathrm{M}}}\,\ddot{\underline{\mathrm{d}}} + \underline{\underline{\mathrm{C}}}\,\dot{\underline{\mathrm{d}}} + \underline{\underline{\mathrm{K}}}\,\underline{\mathrm{d}} = \underline{\mathrm{f}}\,(t), \quad \underline{\mathrm{d}} = \underline{\mathrm{d}}\,(t) \tag{3.20}$$

where:

- $\underline{\mathrm{d}}\,(t)$ collects the system dofs, which vary in time;
- $\underline{\underline{\mathrm{M}}}$ is the mass matrix, which is symmetric and positive definite;
- $\underline{\underline{\mathrm{C}}}$ is the viscous damping matrix, which is symmetric and positive semidefinite;
- $\underline{\underline{\mathrm{K}}}$ is the elastic stiffness matrix, which is symmetric and positive semidefinite: complex terms may appear within the stiffness matrix to represent structural damping contributions;
- $\underline{\mathrm{f}}\,(t)$ is the vector of the external (generalized) forces;

In the customary case constraint equations are also involved in the form

$$\underline{\underline{\mathcal{L}}}^{\top}\,\underline{\mathrm{d}} = \underline{\beta}\,(t), \tag{3.21}$$

see Eq. 2.126, the $\underline{\mathrm{d}}$ system dof vector in Eq. 3.20 may be expressed in terms of the $\underline{\mathrm{r}}$ *retained* subset only, i.e.

$$\underline{\mathrm{d}}\,(t) = \underline{\underline{\Lambda}}\,\underline{\mathrm{r}}\,(t) + \underline{\Delta}\,(t), \tag{3.22}$$

see Eq. 2.136, where $\underline{\Delta}\,(t)$ includes the $\underline{\beta}\,(t)$ possibly time-varying inhomogeneous terms of the constraint equations – e.g. an imposed periodic motion at supports, as in base excitation loadcases. The Eq. 3.20 system of balance equations may hence be reduced to retained dofs only as in

$$\underline{\underline{\mathrm{M}}}_{\mathrm{R}}\,\ddot{\underline{\mathrm{r}}} + \underline{\underline{\mathrm{C}}}_{\mathrm{R}}\,\dot{\underline{\mathrm{r}}} + \underline{\underline{\mathrm{K}}}_{\mathrm{R}}\,\underline{\mathrm{r}} = \underline{\mathrm{f}}_{\mathrm{R}}(t) + \underbrace{\underline{\underline{\Lambda}}^{\top}\,\underline{\mathrm{R}}\,(t)}_{=0} \tag{3.23}$$

where $\underline{\mathrm{R}}\,(t)$ are the (ideal) constraint reactions, and

$$\left\{\underline{\underline{\mathrm{M}}}_{\mathrm{R}}, \underline{\underline{\mathrm{C}}}_{\mathrm{R}}, \underline{\underline{\mathrm{K}}}_{\mathrm{R}}\right\} = \underline{\underline{\Lambda}}^{\top}\left\{\underline{\underline{\mathrm{M}}}, \underline{\underline{\mathrm{C}}}, \underline{\underline{\mathrm{K}}}\right\}\underline{\underline{\Lambda}}$$

$$\underline{\mathrm{f}}_{\mathrm{R}}(t) = \underline{\underline{\Lambda}}^{\top}\left(\underline{\mathrm{f}}\,(t) - \underline{\underline{\mathrm{M}}}\,\ddot{\underline{\Delta}} - \underline{\underline{\mathrm{C}}}\,\dot{\underline{\Delta}} - \underline{\underline{\mathrm{K}}}\,\underline{\Delta}\right)$$

define the constraint-consistent counterparts of the dynamic system matrices, and of the load vector, see Par. 2.7.4.

In the following, however, the original Eq. 3.20 notation is naïvely maintained – i.e. the $\square_{\mathrm{R}}$ subscript is omitted, $\underline{\mathrm{d}}$ is used in place of $\underline{\mathrm{r}}$, and n refers to the $\underline{\mathrm{r}}$ (vs. $\underline{\mathrm{d}}$) cardinality – even in the presence of constraints.

The system response is assumed linear – a strong assumption, this, that hardly holds in complex structures as the automotive chassis under scrutiny. The lack of nonlinear analysis tools whose modeling and computational effort is comparable with respect to the one presented in the present section, pushes for some laxity in the linearity prerequisite check, and for the acceptance of a certain extent of error.

The applied force is assumed periodic in time, and so is the long term solution, if linearity holds. Moreover, Fourier decomposition may be applied, and there is no lack in generality in further assuming an harmonic forcing term, and hence an harmonic solution. We have

$$\underline{\mathrm{f}}\,(t) = \frac{\bar{\underline{\mathrm{f}}}\,e^{j\omega t} + \bar{\underline{\mathrm{f}}}^{\,*}e^{-j\omega t}}{2} = \mathrm{Re}(\bar{\underline{\mathrm{f}}}\,e^{j\omega t}) \tag{3.24}$$

where the asterisk superscript denotes the complex conjugate variant of the base vector. We recall that the compact notation

$$\underline{\mathrm{f}}\,(t) = \bar{\underline{\mathrm{f}}}\,e^{j\omega t} \tag{3.25}$$

extensively employed below defines a complex form for the driving force, whose real part is the portion which is physically applied to the nodes over time, i.e.

$$\mathrm{Re}(\bar{\underline{\mathrm{f}}}\,e^{j\omega t}) = \mathrm{Re}(\bar{\underline{\mathrm{f}}}\,)\cos\omega t - \mathrm{Im}(\bar{\underline{\mathrm{f}}}\,)\sin\omega t \tag{3.26}$$

This compact formalism is not rigorous but still it is effective, and hence commonly employed. Any phase difference amongst the applied nodal excitations may be described by resorting to the complex nature of the $\bar{\underline{\mathrm{f}}}$ vector terms.

In the neglection of the transient response, the harmonic tentative solution

$$\underline{\mathrm{d}}\,(t) = \bar{\underline{\mathrm{d}}}\,e^{j\omega t} \tag{3.27}$$

is substituted within Eq. 3.20, thus obtaining

$$\left(-\omega^2\,\underline{\underline{\mathrm{M}}} + j\omega\,\underline{\underline{\mathrm{C}}} + \underline{\underline{\mathrm{K}}}\right)\bar{\underline{\mathrm{d}}} = \bar{\underline{\mathrm{f}}} \tag{3.28}$$

where the $e^{j\omega t}$ time varying, generally nonzero factors are simplified away.

Expression 3.28 defines a system of linear complex equations, one each dof, in the complex unknown vector $\underline{\bar{d}}$; equivalently, each complex equation and each unknown term may be split into the associated real and imaginary parts, thus leading to a system of linear, real equations whose order is twice the number of the discretized structure dofs.

The system matrix varies with the ω parameter, and in particular its stiffness contribute $\underline{\underline{K}}$ is dominant for low ω values, whereas the $\underline{\underline{C}}, \underline{\underline{M}}$ terms acquire relevance with growing ω.

In distributed inertia systems, however, it is a misleading claim that the stiffness matrix contribution becomes negligible with high ω values, since – with the notable exception of external loads that are directly applied to concentrated masses or rigid bodies – the pulsation is unphysically high above which such behaviour arises.

Since Eqns. 3.28 are independently solved for each ω value, it constitutes no added complexity to let $\underline{\underline{M}}$, $\underline{\underline{C}}$, $\underline{\underline{K}}$ and $\underline{\bar{f}}$ vary according to the same parameter.

Finally, in the absence of the damping-related imaginary terms within the system matrix, the Eq. 3.28 problem algebraic order is led back to the bare number of system dofs; in fact, two independent real system of equations – that share a common Cholesky matrix decomposition[8] – may be cast for the real and the imaginary parts of $\underline{\bar{d}}$ and $\underline{\bar{f}}$.

3.1.7 Modal analysis

The present paragraph briefly deals with the structure's natural modes, i.e. those periodic[9] motions that are allowed according to Eq. 3.20, in the further absence of externally applied loads.

A necessary condition for a motion to endure in the absence of a driving load is the absence of dissipative phenomena; it is hence necessary to have a zero $\underline{\underline{C}}$ damping matrix, whereas the $\underline{\underline{K}}$ stiffness matrix must be free of imaginary terms. This hypothesis holding, Eq. 3.28 is reduced to the following real-term algebraic form

$$\left(-\omega^2 \underline{\underline{M}} + \underline{\underline{K}}\right) \underline{\bar{d}} = \underline{0} \tag{3.29}$$

[8] see `https://en.wikipedia.org/wiki/Cholesky_decomposition`

[9] *harmonic* in the context of linearly behaving systems

whose nontrivial solutions constitute a set of $(\omega_i^2,\, \hat{\underline{\mathrm{d}}}_i)$ *generalized* eigenvalue/eigenvector pairs, one each system dof, if eigenvalue multiplicity is taken into account.

In the context of each $(\omega_i^2,\, \hat{\underline{\mathrm{d}}}_i)$ pair, ω_i is the natural pulsation ($\omega_i = 2\pi f_i$, where f_i is the natural frequency), whereas the $\hat{\underline{\mathrm{d}}}_i$ vector of generalized displacemts is named natural mode.

The extraction of the Eq. 3.28 nontrivial solutions reduces to a *standard* eigenvalue problem is the algebraic form is left-multiplied by the mass matrix inverse, i.e.

$$\left(\underline{\underline{\mathrm{M}}}^{-1}\,\underline{\underline{\mathrm{K}}} - \omega^2\,\underline{\underline{\mathrm{I}}}\right)\,\hat{\underline{\mathrm{d}}} \;=\; \underline{0}\,; \tag{3.30}$$

the availability of solvers that specifically approach the generalized problem avoid such computationally uneconomical preliminary.

It is worth to recall that in the case of eigenvalues with non-unit multiplicity – concept, this, that is to be contextualized within the limited precision floating point arithmetics[10] – the associated eigenvectors must be considered only through their linear combination; the specific selection of the base elements for representing such a subspace (i.e., each single eigenvector) derives in fact from the unpredictable interaction between the truncation error and the inner mechanics of the numerical procedure.

Also, the eigenvectors that are associated to eigevalues of unit multiplicity are returned by the numerical solver in the misleading form of a definite vector, whereas an arbitrary (both in sign and magnitude) scaling factor has to be prepended.

In particular, any speculation which is not robust with respect to such arbitrary scaling (or combination) is of no engineering relevance, and must be avoided.

Finally, in continuous elasticity, no upper bound exists for natural frequencies; in fe discretized structure, an apparent upper bound exists, which depends on local element size[11].

A common normalizing rule for the natural modes is the one that produces a unit modal mass m_i, i.e.

$$m_i = \hat{\underline{\mathrm{d}}}_i^{\top}\,\underline{\underline{\mathrm{M}}}\,\hat{\underline{\mathrm{d}}}_i = 1 \tag{3.31}$$

[10] XXX

[11] In particular, the natural oscillation period for the highest dynamic mode is estimated with order of magnitude precision as the minimum time it takes a pressure wave to travel between two different nodes in the discretized structure.

this rule is e.g. adopted by the MSC.Marc solver in its default configuration.

The resonant behaviour of the system in correspondence with a natural frequency may be investigated by substituting the following tentative solution

$$\underline{\mathrm{x}}\,(t) = a\,\hat{\underline{\mathrm{d}}}_{\,i}\sin(\omega_i t) \tag{3.32}$$

within the dynamic equilibrium equations 3.20, with

$$f(t) = \bar{\underline{\mathrm{f}}}\,\cos(\omega_i t), \tag{3.33}$$

and thus obtaining

$$\underbrace{\left(-\omega_i^2\,\underline{\underline{\mathrm{M}}} + \underline{\underline{\mathrm{K}}}\right)\hat{\underline{\mathrm{d}}}_{\,i}}_{=\underline{0}}\,a_i\sin(\omega_i t) + \omega_i a_i\,\underline{\underline{\mathrm{C}}}\,\hat{\underline{\mathrm{d}}}_{\,i}\cos(\omega_i t) = \bar{\underline{\mathrm{f}}}\,\cos(\omega_i t). \tag{3.34}$$

By simplifying away the generally nonzero time modulating factors, and by left-multiplying both equation sides by $\hat{\underline{\mathrm{d}}}^{\,\top}$ – i.e. by projecting the equation residual along the subspace defined by the eigenvector itself, we obtain an amplitude term in the form

$$a_i = \frac{\hat{\underline{\mathrm{d}}}^{\,\top}\bar{\underline{\mathrm{f}}}}{\omega_i\,\hat{\underline{\mathrm{d}}}^{\,\top}\underline{\underline{\mathrm{C}}}\,\hat{\underline{\mathrm{d}}}_{\,i}} \tag{3.35}$$

whose singularity is prevented only a) in the presence of a damping matrix that associates nonzero and non-orthogonal viscous reactions to the motion described by the natural mode under scrutiny, or b) if the driving load is strictly orthogonal to such natural mode, i.e. it unable to perform periodic work on such a motion. The nature of the expression 3.35 numerator will be further discussed in the following paragraph.

3.1.8 Harmonic response through mode superposition

In the case the eigenvalues associated with the dynamic modes are all distinct[12], the following orthogonality conditions hold

$$\hat{\underline{\mathrm{d}}}_{\,j}^{\,\top}\,\underline{\underline{\mathrm{M}}}\,\hat{\underline{\mathrm{d}}}_{\,i} = m_i\delta_{ij} \qquad\qquad \hat{\underline{\mathrm{d}}}_{\,j}^{\,\top}\,\underline{\underline{\mathrm{K}}}\,\hat{\underline{\mathrm{d}}}_{\,i} = m_i\omega_i^2\delta_{ij} \tag{3.36}$$

[12]condition, this, that is assumed to hold; a slightly perturbed FE discretization may be effective in separating the instances of a theoretically multiple natural frequency.

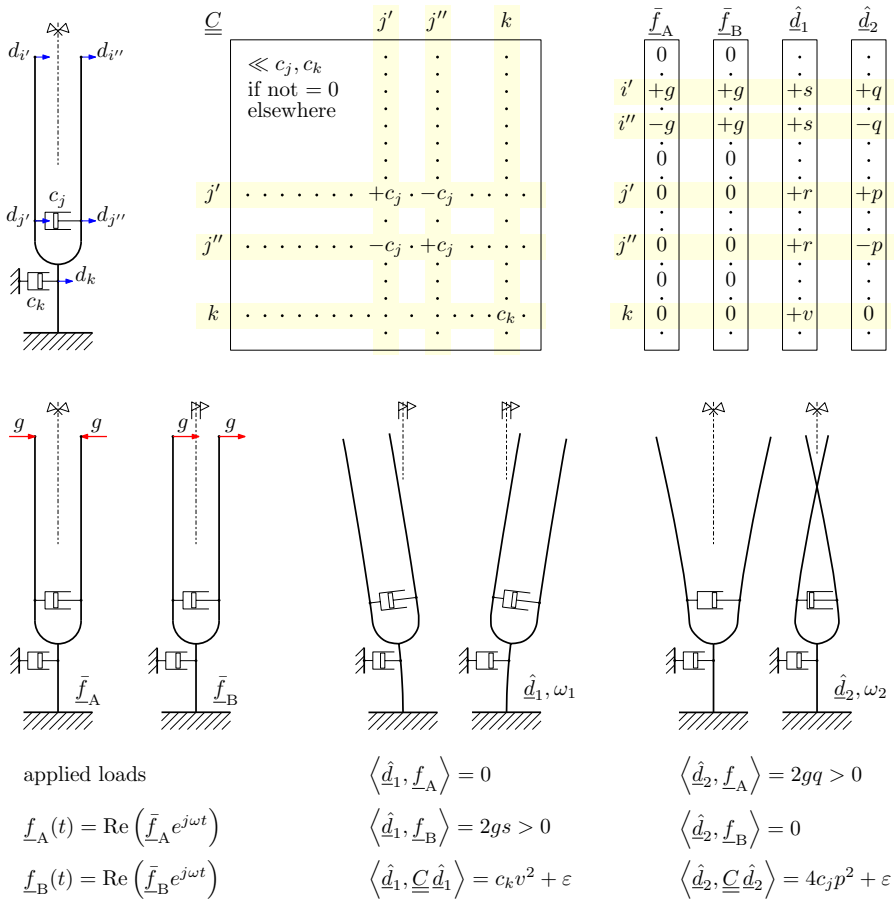

Figure 3.3: Pedagogical tuning-fork model, with a few evidenced dofs, and two picked natural modes. The c_i damper resembles the dissipative nature of the finger grip, and it rapidly damps the strongly coupled $\hat{\underline{\mathrm{d}}}_1, \omega_1$ skew-symmetric natural mode, whereas it does not interact with the second $\hat{\underline{\mathrm{d}}}_2, \omega_2$ natural mode, which is associated the nominal sound, e.g. the 440 Hz A standard pitch, which is sustained by design. The c_j damper is of a merely academic nature, instead. An outline of the involved algebraic representation of i) the $\underline{\underline{\mathrm{C}}}$ damping matrix, of ii) the natural mode vectors $\hat{\underline{\mathrm{d}}}_1$, $\hat{\underline{\mathrm{d}}}_1$, and of iii) the two distinct example load vectors $\bar{\underline{\mathrm{f}}}_{\mathrm{A}}$, $\bar{\underline{\mathrm{f}}}_{\mathrm{B}}$ are also provided, to clarify the nature of Eq. 3.35 terms. The $\underline{\underline{\mathrm{C}}}$ matrix terms besides the few which are attributable to the dampers are i) due to the material hysteretic losses, ii) they follow the $\underline{\underline{\mathrm{K}}}$ matrix sparsity pattern, and iii) even if not strictly zero, they are minimal by design.

where δ_{ij} is the Kroneker delta function, and $m_i = 1$ is the i-th modal mass, which is unitary due to the the $\hat{\underline{\mathrm{d}}}_i$ unit modal mass normalization.

It is further assumed that it is possible to describe the elastic body motion through a linear combination of a (typically narrow) subset of the dynamic natural modes. Such assumption may be rationalized in two equivalent ways: on one hand, the contribution of the neglected modes is assumed negligible, and hence ignored; on the other hand, it is imagined that a set of kinematic constraints is imposed, that rigidly impede any additional system motion with respect to the chosen set. According to this latter explanation, reaction forces will be raised that absorb any equilibrium residual term which is orthogonal with respect to the allowed displacements; the relevance of those clearly spurious nodal balance contributions may be determined by substituting the below obtained solution within the original 3.28 equations, and by checking the residuals.

The subset defined by the first m eigenvectors ($1 \leq m \ll n$) are commonly employed, whereas different assortments are possible; a control calculation perfomed with a wider base may be employed for error estimation.

By stacking those first m normalized column eigenvectors into the $\underline{\underline{\Xi}}$ matrix below,

$$\underline{\underline{\Xi}} = \left[\hat{\underline{\mathrm{d}}}_1 \quad \cdots \quad \hat{\underline{\mathrm{d}}}_l \quad \cdots \quad \hat{\underline{\mathrm{d}}}_m \right], \tag{3.37}$$

any $\bar{\underline{\mathrm{d}}}$ configuration belonging to the linear span of the selected modes may be expressed through a vector of m *modal* coordinates $\bar{\xi}_l$, as in

$$\bar{\underline{\mathrm{d}}} = \underline{\underline{\Xi}}\, \bar{\underline{\xi}} \tag{3.38}$$

.

Due to the natural modes orthogonality conditions 3.36, the $\underline{\underline{\Xi}}$ tranformation matrix diagonalizes both the mass and the stiffness matrices, since

$$\underline{\underline{\Xi}}^{\top} \underline{\underline{\mathrm{M}}}\, \underline{\underline{\Xi}} = \underline{\underline{\mathrm{I}}} \qquad \underline{\underline{\Xi}}^{\top} \underline{\underline{\mathrm{K}}}\, \underline{\underline{\Xi}} = \underline{\underline{\Omega}} = \mathrm{diag}(\omega_l^2); \tag{3.39}$$

by appling such transformation to the damping matrix, however, a dense matrix is generally obtained.

The *Rayleigh* or *proportional* damping matrix definition assumes that the latter may be passably represented as a linear combination of the mass matrix and of the stiffness matrix: in particular

$$\underline{\underline{\mathrm{C}}} = \alpha\,\underline{\underline{\mathrm{M}}} + \beta\,\underline{\underline{\mathrm{K}}} \tag{3.40}$$

where α and β are commonly named *mass* and *stiffness matrix multipliers*, respectively; according to such assumption, the damping matrix is also diagonalized by the $\underline{\underline{\Xi}}$ tranformation matrix. However, if the distributed structural damping – i.e. the losses due to the hysteric behaviour of the material and of the many frictional joints[13] – occurs at the elastic connections, and its contribution to the damping matrix is hence well correlated with a suitably scaled stiffness matrix[14], the concentrated dampers introduce a few high-magnitude matrix terms – see Fig. 3.3 example – which may unlikely be represented by the linear combination of two much less aggregated matrices – see e.g. the Fig. 2.19 final stiffness matrix, the mass matrix having an identical layout.

Equation 3.28 algebraic problem may be cast in terms of the m ξ_l modal unknowns, thus obtaining

$$\underline{\underline{\Xi}}^{\top}\left(-\omega^2\,\underline{\underline{\mathrm{M}}} + j\omega\,\underline{\underline{\mathrm{C}}} + \underline{\underline{\mathrm{K}}}\right)\underline{\underline{\Xi}}\,\bar{\underline{\xi}} = \underline{\underline{\Xi}}^{\top}\,\bar{\underline{\mathrm{f}}} \tag{3.41}$$

which reduces to the diagonal form

$$\left(-\omega^2\,\underline{\mathrm{I}} + j\omega\left(\alpha\,\underline{\mathrm{I}} + \beta\,\underline{\underline{\Omega}}\right) + \underline{\underline{\Omega}}\right)\bar{\underline{\xi}} = \underline{\underline{\Xi}}^{\top}\,\bar{\underline{\mathrm{f}}}\,, \tag{3.42}$$

or, equivalently, to the set of m independent complex equations

$$\left(-\omega^2 + j\omega\left(\alpha + \beta\omega_l^2\right) + \omega_l^2\right)\xi_l = q_l, \quad j = 1\ldots m \tag{3.43}$$

where $q_l = \left\langle \hat{\underline{\mathrm{d}}}_l, \bar{\underline{\mathrm{f}}} \right\rangle$ is the coupling factor between the external load and the l-th natural mode.

[13] e.g. riveted and bolted joints

[14] according to the usual structural damping treatise, a complex elastic modulus is employed to represent the hysteretic stress-strain relation, i.e.

$$\bar{\sigma} = E\,(1 + j\eta)\,\bar{\epsilon}, \quad \sigma(t) = \mathrm{Re}\left(\bar{\sigma}\,e^{j\omega t}\right), \quad \epsilon(t) = \mathrm{Re}\left(\bar{\epsilon}\,e^{j\omega t}\right),$$

where η is the loss factor, and E, ηE are the storage and the loss moduli, respectively. In this case, the imaginary part of the $\underline{\underline{\mathrm{K}}}$ stiffness matrix coincides with $\eta\,\underline{\underline{\mathrm{K}}}$, and its representation in terms of an equivalent $\underline{\underline{\mathrm{C}}}$ matrix for harmonic response analyses is consistent with $\alpha = 0$, $\beta = \eta/\omega$, or, equivalently $\beta = 2\zeta/\omega$ where ζ is the damping ratio.

The algebraic equation above may be interpreted as the characteristic equation of an harmonically driven single dof oscillator that exhibits the following properties:

- its mass is unity;
- its natural frequency equals that of the l-th natural mode ω_l;
- its damping ratio ζ_l is a combination of the two Rayleigh damping coefficients, i.e.
$$\zeta_l = \frac{1}{2}\left(\frac{\alpha}{\omega_l} + \beta\omega_l\right);$$
- the external load real(imaginary) term is defined as the cyclic work that the external load performs upon a system motion described as the sinusoidal (cosinusoidal) modulation in time of the l-th modal shape, divided by π.[15]

The uncoupled equations 3.43 may be solved resorting to complex division arithmetics, thus leading to the definition of the $\bar{\xi}_l$ modal amplitude and phase terms; in particular we have that the l-th modal shape is modulated in time according to the function

$$\begin{aligned}\xi_l(t) &= \mathrm{Re}(\bar{\xi}_l)\cos\omega t - \mathrm{Im}(\bar{\xi}_l)\sin\omega t \\ &= \left|\bar{\xi}_l\right|\cos\left(\omega t + \psi_l - \phi_l\right)\end{aligned}$$

whose terms are detailed in the following.

The auxiliary parameters

$$a_l = 1 - r_l^2 \qquad b_l = 2\zeta_l r_l \qquad r_l = \frac{\omega}{\omega_l}$$

are first defined; we then have the oscillation amplitude and phase terms

$$\begin{aligned}\left|\bar{\xi}_l\right| &= \frac{|\bar{q}_l|}{\omega_l^2}\frac{1}{\sqrt{a_l^2 + b_l^2}} \\ \psi_l &= \arg(\bar{q}_l) \\ \phi_l &= \arg(a_l + jb_l)\end{aligned}$$

[15] In the case of a concentrated load that act on a single dof, q_j equates the product of the load magnitude with the associated component in $\hat{\underline{\mathrm{d}}}_l$, i.e. the generalized displacement at the specific node, as shown by the FE postprocessor.

or, equivalently, the real and imaginary parts

$$\mathrm{Re}(\bar{\xi}_l) = \frac{1}{\omega_l^2} \frac{a_l \,\mathrm{Re}(\bar{q}_l) + b_l \,\mathrm{Im}(\bar{q}_l)}{a_l^2 + b_l^2}$$
$$\mathrm{Im}(\bar{\xi}_l) = \frac{1}{\omega_l^2} \frac{a_l \,\mathrm{Im}(\bar{q}_l) - b_l \,\mathrm{Re}(\bar{q}_l)}{a_l^2 + b_l^2}.$$

3.1.9 Linearized pre-buckling analysis

A few notes.

According to the linearized pre-buckling analysis, the structure is considered in an oxymoronic configuration which is both *pre-stressed* and *undeformed*.

The $\underline{\sigma}^0$ *pre-stress* condition is evaluated through a linear preliminary analysis of the structure subject to a set of applied loads, and potentially inhomogeneous constraints; both the preload and the associate stress field may be scaled by a common λ amplification factor, and the structure behaviour is parametrically examined with varying λ.

The displacement and rotation fields associated this preliminary analysis are not however retained in the subsequent step, in contrast to the pre-stress; such looseness is commonly justified based on the assumed smallness of such deflections.

For each element of the structure, the stiffness matrix is derived by a) taking into account the contribution of the $\underline{\sigma}^0$ pre-stress to the internal virtual work, and b) by employing a second order, nonlinear, *large rotation* formulation for the $\underline{\underline{\mathrm{B}}}$ matrix that derives the strain tensor from nodal dofs. Details are here omitted[16], and only the following placeholder formula for the internal virtual work is proposed

$$\begin{aligned}
\delta U_{\mathrm{i}} &= \iiint_V \delta\,\underline{\epsilon}^{\top}\left(\lambda\,\underline{\sigma}_0 + \underline{\underline{\mathrm{D}}}\,\underline{\epsilon}\right) dV \\
&= \iiint_V \left[\underline{\underline{\mathrm{B}}}\,(\underline{\mathrm{d}})\delta\,\underline{\mathrm{d}}\right]^{\top}\left(\lambda\,\underline{\sigma}_0 + \underline{\underline{\mathrm{D}}}\,\underline{\underline{\mathrm{B}}}\,(\underline{\mathrm{d}})\,\underline{\mathrm{d}}\right) dV \\
&= \dots \\
&= \delta\,\underline{\mathrm{d}}\,\left(\left(\underline{\underline{\mathrm{K}}}^{\mathrm{M}}_{\mathrm{ej}} + \lambda\,\underline{\underline{\mathrm{K}}}^{\mathrm{G}}_{\mathrm{ej}}\right)\,\underline{\mathrm{d}} + \mathrm{o}\,(\underline{\mathrm{d}})\right).
\end{aligned}$$

where a λ amplification factor for the $\underline{\sigma}^0$ pre-stress, and for the first order derived quantities, is added as preparatory for the further treatise.

The resulting element stiffness matrix is obtained as the sum of two distinct contributions; the first contribution $\underline{\underline{\mathrm{K}}}^{\mathrm{M}}_{\mathrm{ej}}$ is named *material* stiffness matrix and, in the absence of large element reorientation in space, it coincides with the customary definition of element stiffness

[16] see e.g. reference [13]

matrix. The second contribution $\lambda \underline{\underline{\mathrm{K}}}^{\mathrm{G}}_{\mathrm{ej}}$ is named *geometric* stiffness matrix and it embodies the corrective terms due to the interaction of the pre-stress with the rotations; such term is invariant with the material properties, and it scales with the pre-stress itself, i.e. with the λ amplification factor. This second contribution embodies the *stress stiffening* and *stress softening* effects.

Both the two terms are obtained by relying on the initial coordinates of the element nodes, thus effectively neglecting the preload-induced deflections.

The elemental material and geometric stiffness matrix are then assembled into their global counterparts, and contraints are applied that are consistent[17] with the ones employed in deriving the pre-stress.

The following relation is thus obtained in the neighborhood of a λ-scaled, pre-stressed configuration

$$\left(\underline{\underline{\mathrm{K}}}^{\mathrm{M}} + \lambda \underline{\underline{\mathrm{K}}}^{\mathrm{G}} \right) \underline{\delta \mathrm{d}} = \underline{\delta \mathrm{F}} \tag{3.44}$$

that relates a small variation in the externally applied actions $\delta \underline{\mathrm{F}}$ with the required adjustments in the structure configuration $\delta \underline{\mathrm{d}}$ for the sake of equilibrium; the cumulative $\underline{\underline{\mathrm{K}}}^{\mathrm{m}} + \lambda \underline{\underline{\mathrm{K}}}^{\mathrm{g}}$ term is named *tangent* stiffness matrix upon its role in locally orienting the equilibrium path.

Of a particular interest is the case of a nonzero variation in configuration for which equilibrium is preserved in the absence of external load variation; such condition is a prerequisite for a bifurcation of the equilibrium path. We have in particular an homogenous system of equations

$$\left(\underline{\underline{\mathrm{K}}}^{\mathrm{M}} + \lambda_i \underline{\underline{\mathrm{K}}}^{\mathrm{G}} \right) \underline{\delta \hat{\mathrm{d}}}_i = 0 \tag{3.45}$$

whose nontrivial solutions are in form of generalized[18] eigenpairs $(\lambda_i, \delta \underline{\hat{\mathrm{d}}}_i)$, with λ_i values that zero the determinant of the tangent stiffness matrix,

[17] not stricty equal in theory, since some variations are allowed with respect in particular positioning and symmetry constraints. FE packages may however limit such theoretically allowed redefinition of constraints.

[18] an equivalent, standard

$$\left(\underline{\underline{\mathrm{A}}} - \eta_i \underline{\underline{\mathrm{I}}} \right) \underline{\mathrm{v}}_i = \underline{0}$$

eigenproblem may be defined with

$$\underline{\underline{\mathrm{A}}} = \left[\underline{\underline{\mathrm{K}}}^{\mathrm{M}} \right]^{-1} \underline{\underline{\mathrm{K}}}^{\mathrm{G}}, \quad \lambda_i = -1/\eta_i, \quad \underline{\mathrm{v}}_i = \delta \underline{\hat{\mathrm{d}}}_i.$$

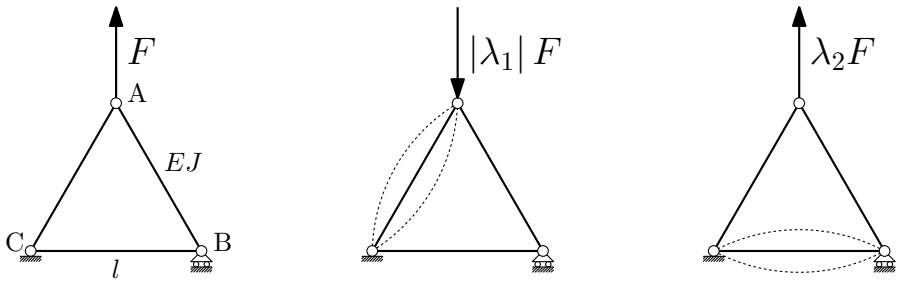

$N_{AB} = N_{CA} = +\frac{F}{\sqrt{3}}$
$N_{BC} = -\frac{F}{2\sqrt{3}}$
$N_{\mathrm{crit},i} = -\frac{\pi^2 i^2 EJ}{l^2}$

$\lambda_1 = -\frac{\pi^2 EJ}{l^2}\frac{\sqrt{3}}{F}$
moltepl. 2
minimum λ_i in absolute value

$\lambda_2 = +\frac{\pi^2 EJ}{l^2}\frac{2\sqrt{3}}{F}$
minimum $\lambda_i > 0$

Figure 3.4: In the case the load that induces the pre-stress state is subject to inversion, the minimum amplification factor in modulus is to be considered. On the other hand, if a load inversion may be excluded, the minimum among the positive amplification factors is to be considered.

and are hence named *critical* pre-stress (or preload, or load) amplification factor.

In correspondence of critical λ_i values, the elastic reactions are unable to restrain an arbitrary scaled $\delta\,\hat{\underline{\mathrm{d}}}_i$ perturbation of the structure configuration, and the related variation in stress/strain values, thus obtaining a *indifferent equilibrium* condition.

3.2 Newton-Raphson Algorithm for Nonlinear Systems of Equations

3.2.1 Basic iteration

Let's consider the nonlinear system of n equations

$$\underline{\mathrm{r}}\,(\,\underline{\mathrm{u}}\,) = \underline{0} \tag{3.46}$$

in the n unknown components of the $\underline{\mathrm{u}}$ vector, where – with reference to structural FE applications, $\underline{\mathrm{r}}\,(\,\underline{\mathrm{u}}\,)$ represents the equilibrium balance residual at each dof, expressed as the

$$\underline{\mathrm{r}}\,(\,\underline{\mathrm{u}}\,) = \underline{\mathrm{G}}\,(\,\underline{\mathrm{u}}\,) - \underline{\mathrm{f}}\,(\,\underline{\mathrm{u}}\,)$$

difference between the $\underline{\mathrm{G}}\,(\,\underline{\mathrm{u}}\,)$ actions required to keep the structure in the $\underline{\mathrm{u}}$ deformed configuration[19], and the $\underline{\mathrm{f}}\,(\,\underline{\mathrm{u}}\,)$ external actions in the same configuration; external actions are allowed to vary with the deflection, as e.g. in the notable cases of centrifugal forces, or membrane pressurization[20].

The current treatise holds in the presence of kinematic constraints, by interpreting $\underline{\mathrm{u}}$ as the *retained* dof vector, with constraint-consistent $\underline{\mathrm{G}}$ and $\underline{\mathrm{f}}$ vectors, see Par. 2.7.4.

The N-R method is built upon the first-order Taylor series expansion of the equation 3.46, in the neighborhood of an i-th iterated point $\underline{\mathrm{u}}^{\,i}$, namely

$$\underline{\mathrm{r}}\,(\,\underline{\mathrm{u}}^{\,*}) = \underline{\mathrm{r}}\,\left(\underline{\mathrm{u}}^{\,i}\right) + \underline{\underline{\mathrm{J}}}_{r}\left(\underline{\mathrm{u}}^{\mathrm{i}}\right)\cdot\left(\underline{\mathrm{u}}^{\,*} - \underline{\mathrm{u}}^{\,i}\right) + o\left(\underline{\mathrm{u}}^{\,*} - \underline{\mathrm{u}}^{\,i}\right) = \underline{0}\,. \tag{3.47}$$

In the above expression[21]

$$\left[\underline{\underline{\mathrm{J}}}_{r}\left(\underline{\mathrm{u}}^{\,i}\right)\right]_{l,m} = \left[\underline{\underline{\mathrm{J}}}_{r}^{\,i}\right]_{l,m} = \left.\frac{\partial r_l}{\partial u_m}\right|_{\underline{\mathrm{u}}=\underline{\mathrm{u}}^{\,i}}, \quad l,m = 1\ldots n \tag{3.48}$$

[19]The $\underline{\mathrm{G}}$ vector contains the nodal action components necessary to maintain the structure in equilibrium in the deformation state associated with the nodal displacement vector $\underline{\mathrm{u}}$, *i.e.* the the nodal action components required to balance to the elastic reactions of the structure constrained in the deformed state $\underline{\mathrm{u}}$. In the particular case of a linear elastic system $\underline{\mathrm{G}}\,(\,\underline{\mathrm{u}}\,) = \underline{\underline{\mathrm{K}}}\,\underline{\mathrm{u}}$, with K stiffness matrix.

[20]the element surface area and its orientation may vary in fact with inflation

[21]here, $[A]_{i,j}$ is the element at the i-th row, j-th column of the A matrix

is the Jacobian of the residual r function, as evaluated at the point $\underline{\mathrm{u}}^{\,i}$, while $\underline{\mathrm{u}}^{\,*}$ is the unknown exact solution. From the r function defition we also have

$$\underline{\underline{\mathrm{J}}}_r^{\,i} = \underline{\underline{\mathrm{J}}}_G^{\,i} - \underline{\underline{\mathrm{J}}}_f^{\,i} \tag{3.49}$$

where

$$\left[\underline{\underline{\mathrm{J}}}_G^{\,i}\right]_{l,m} = \left.\frac{\partial G_l}{\partial u_m}\right|_{\underline{\mathrm{u}}=\underline{\mathrm{u}}^{\,i}}, \quad \left[\underline{\underline{\mathrm{J}}}_f^{\,i}\right]_{l,m} = \left.\frac{\partial f_l}{\partial u_m}\right|_{\underline{\mathrm{u}}=\underline{\mathrm{u}}^{\,i}}, \quad l,m = 1\ldots n \tag{3.50}$$

which reduces to $\underline{\underline{\mathrm{J}}}_r^{\,i} = \underline{\underline{\mathrm{J}}}_G^{\,i}$ in the notable case $\underline{\mathrm{f}}$ is invariant with deflection[22]. By naïvely neglecting the further order term, the identity 3.47 is no longer verified; however, by replacing the exact solution $\underline{\mathrm{u}}^{\,*}$ with a less pretentious next iteration term $\underline{\mathrm{u}}^{\,i+1}$, the form

$$\underbrace{\underline{\underline{\mathrm{J}}}_r^{\,i}}_{\underline{\underline{\mathrm{K}}}^{\,i}} \underbrace{\left(\underline{\mathrm{u}}^{\,i+1} - \underline{\mathrm{u}}^{\,i}\right)}_{\underline{\Delta\mathrm{u}}^{\,i\to i+1}} = \underbrace{-\,\underline{\mathrm{r}}\left(\underline{\mathrm{u}}^{\,i}\right)}_{\underline{\Delta\mathrm{r}}^{\,i\to i+1}} \tag{3.51}$$

is obtained, in which the $\underline{\underline{\mathrm{J}}}_r^{\,i}$ Jacobian matrix correlates a $\underline{\Delta\mathrm{u}}^{\,i\to i+1}$ deformed configuration adjustment with the $\underline{\Delta\mathrm{r}}^{\,i\to i+1}$ desired variation of the residuals[23] which is expected to produce, thus clarifying its nature of *tangent stiffness matrix*, $\underline{\underline{\mathrm{K}}}^{\,i}$, in the neighborhood of the $\underline{\mathrm{u}}^{\,i}$ deformed configuration.

If we assume that the $\underline{\underline{\mathrm{J}}}_r^{\,i}$ matrix is non-singular, we can rewrite Eq. 3.51 as the step of an iterative adjustment procedure

$$\underline{\mathrm{u}}^{\,i+1} = \underline{\mathrm{u}}^{\,i} - \underline{\underline{\mathrm{J}}}_r^{\,i} \backslash \underline{\mathrm{r}}\left(\underline{\mathrm{u}}^{\,i}\right) \tag{3.52}$$

where the $\underline{\underline{\mathrm{A}}} \backslash \underline{\mathrm{b}}$ notation indicates the solution of a linear system of equation whose coefficient matrix is $\underline{\underline{\mathrm{A}}}$, and known term vector $\underline{\mathrm{b}}$.

Finally, given an initial guess vector $\underline{\mathrm{u}}^{\,0}$, the 3.52 defines a sequence that *may or may not* converge to the exact solution $\underline{\mathrm{u}}^{\,*}$; with the exclusion of pathologically flawed edge cases, convergence occurs if the $\underline{\mathrm{u}}^{\,0}$ initial guess is near enough to fall within the (mostly unknown) basin of attraction of $\underline{\mathrm{u}}^{\,*}$.

[22] $\underline{\mathrm{f}}$ may still vary in time, see below.

[23] for the current configuration $\underline{\mathrm{u}}^{\,i}$, the residuals are in excess of $+\underline{\mathrm{r}}\left(\underline{\mathrm{u}}^{\,i}\right)$ with respect to the desired zero value, and such $\underline{\Delta\mathrm{r}}^{\,i\to i+1} = -\,\underline{\mathrm{r}}\left(\underline{\mathrm{u}}^{\,i}\right)$ is expected to be compensatory

Since we need to eventually stop the 3.52 iterations, we need to define a convergence criterion – i.e. a criterion for the acceptance of the $\underline{\mathrm{u}}^{i+1}$ current iteration results. Typically, two criteria are available:

- residual (dof balance) based convergence criterion: iteration is stopped when $\left|\underline{\mathrm{r}}\left(\underline{\mathrm{u}}^{i+1}\right)\right| \leq \epsilon_r$, being ϵ_r the allowed (absolute) error on the residuals;
- unknowns (dof values, usually *displacements* in the FEM specific case): iteration is stopped when $\left|\underline{\mathrm{u}}^{i+1} - \underline{\mathrm{u}}^{i}\right| \leq \epsilon_u$, being ϵ_u the allowed (absolute) error on the unknowns. This latter method requires at least two iterations for the comparison[24], even in the linear system case.

The implementation of *relative* tolerance values for both residuals and unknowns is generally desirable, but it requires the identification of suitable absolute value reference magnitudes for forces and displacements. The determination of the allowable tolerances is a crucial aspect of nonlinear analysis, since the quest for excessive precision unnecessarily increases computation times, while loose tolerances may lead to inaccurate solutions.

3.2.2 Graphical rationalizaton for the Newton-Raphson iteration

1d case, see Fig. 3.5. 2d case, see Fig. 3.6a and Fig. 3.6b.
TODO.

3.2.3 A continuation method based on the evolution in time from an initially undeformed configuration

TODO.

[24] apart the unlikely case of exact initial guess, i.e. $\left|\underline{\mathrm{u}}^{0} - \underline{\mathrm{u}}^{*}\right| \leq \epsilon_u$

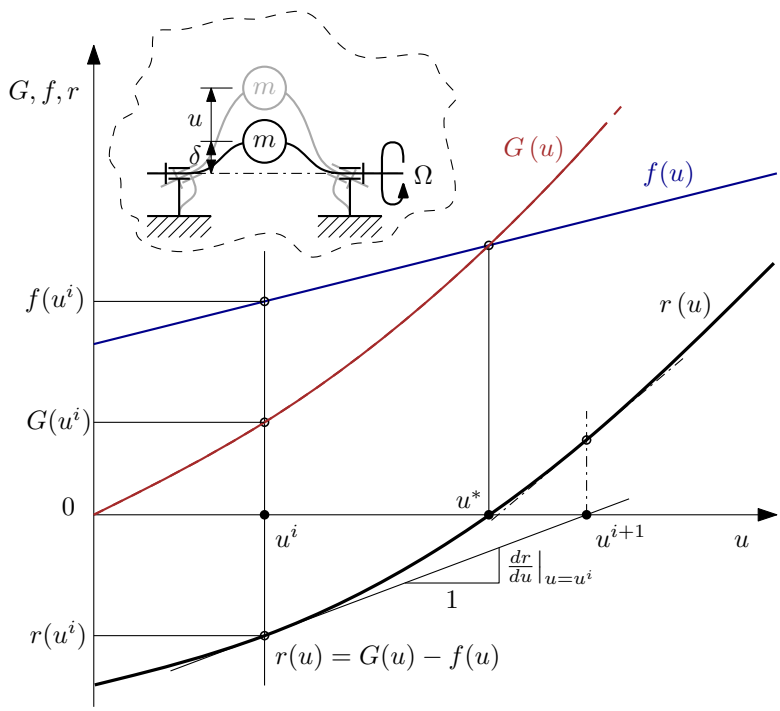

Figure 3.5: Graphical rationalization for the Newton algorithm, $n = 1$ case

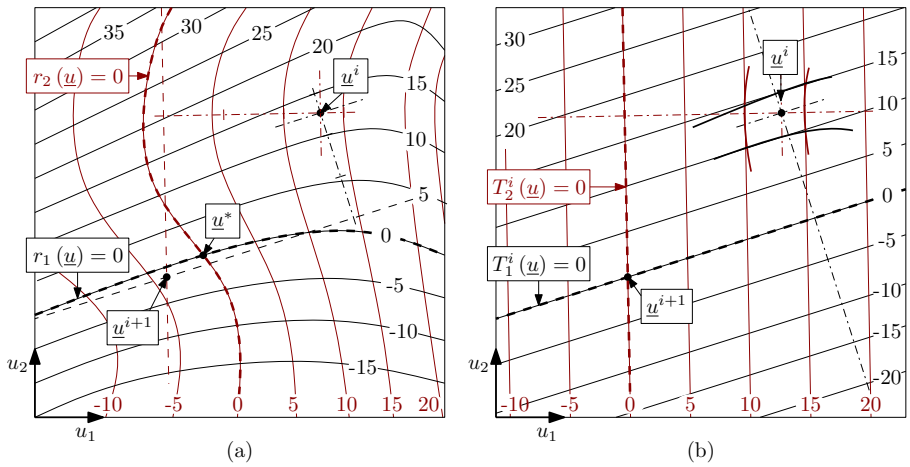

Figure 3.6: Graphical rationalization for the Newton-Raphson algorithm, $n = 2$ case

Bibliography

[1] A. E. H. Love, *A treatise on the mathematical theory of elasticity.* Cambridge university press, 2013.

[2] S. Timoshenko and J. Goodier, *Theory of Elasticity.* McGraw-Hill book Company, 1951.

[3] S. Vlachoutsis, "Shear correction factors for plates and shells," *International Journal for Numerical Methods in Engineering*, vol. 33, no. 7, pp. 1537–1552, 1992.

[4] T. Chow, "On the propagation of flexural waves in an orthotropic laminated plate and its response to an impulsive load," *Journal of Composite Materials*, vol. 5, no. 3, pp. 306–319, 1971.

[5] V. Birman and C. W. Bert, "On the choice of shear correction factor in sandwich structures," *Journal of Sandwich Structures & Materials*, vol. 4, no. 1, pp. 83–95, 2002.

[6] C. Hua, "An inverse transformation for quadrilateral isoparametric elements: analysis and application," *Finite elements in analysis and design*, vol. 7, no. 2, pp. 159–166, 1990.

[7] B. M. Irons and A. Razzaque, "Experience with the patch test for convergence of finite elements," in *The mathematical foundations of the finite element method with applications to partial differential equations*, pp. 557–587, Elsevier, 1972.

[8] C. Militello and C. A. Felippa, "The individual element test revisited," in *The finite element method in the 1990's*, pp. 554–564, Springer, 1991.

[9] R. MacNeal, *Finite Elements*. CRC Press, 1993.

[10] T. J. Hughes and T. Tezduyar, "Finite elements based upon Mindlin plate theory with particular reference to the four-node bilinear isoparametric element," *Journal of applied mechanics*, vol. 48, no. 3, pp. 587–596, 1981.

[11] B. W. Lewis and M. Kane, "Svd subset selectionn," 2014.

[12] G. H. Golub and C. F. Van Loan, *Matrix computations*. JHU press, 2013.

[13] J. Oden, "Calculation of geometric stiffness matrices for complex structures.," *AIAA Journal*, vol. 4, no. 8, pp. 1480–1482, 1966.